



HAL
open science

Novel electrokinetic and analytical approaches for isolation and detection of extracellular vesicles

Marco Morani

► **To cite this version:**

Marco Morani. Novel electrokinetic and analytical approaches for isolation and detection of extracellular vesicles. Analytical chemistry. Université Paris-Saclay, 2022. English. NNT : 2022UPASF021 . tel-03642494

HAL Id: tel-03642494

<https://theses.hal.science/tel-03642494v1>

Submitted on 15 Apr 2022

HAL is a multi-disciplinary open access archive for the deposit and dissemination of scientific research documents, whether they are published or not. The documents may come from teaching and research institutions in France or abroad, or from public or private research centers.

L'archive ouverte pluridisciplinaire **HAL**, est destinée au dépôt et à la diffusion de documents scientifiques de niveau recherche, publiés ou non, émanant des établissements d'enseignement et de recherche français ou étrangers, des laboratoires publics ou privés.

Novel electrokinetic and analytical approaches for isolation and detection of extracellular vesicles

*Nouvelles approches électrocinétiques et analytiques pour l'isolement et la
détection des vésicules extracellulaires*

Thèse de doctorat de l'université Paris-Saclay

École doctorale n°571 : sciences chimiques : molécules, matériaux, instrumentation et
biosystèmes (2MIB)

Spécialité de doctorat : Chimie

Graduate School : Chimie. Référent : Faculté des Sciences d'Orsay

Thèse préparée dans l'unité de recherche **IGPS (Université Paris-Saclay, CNRS)**, sous
la direction de **Myriam TAVERNA**, Professeure, le co-encadrement de **Thanh Duc
MAI**, Maître de conférences

Thèse soutenue à Châtenay-Malabry, le 24 mars 2022, par

Marco MORANI

Composition du Jury

| | |
|---|----------------------------|
| Bruno LE PIOUFLE Professeur, Université Paris-Saclay (CNRS FR3242) | Président |
| Anne VARENNE Professeure, i-CLeHS, Chimie ParisTech | Rapporteuse & Examinatrice |
| Céline ELIE-CAILLE Maîtresse de conférences (HDR), Univ. Bourgogne (UMR 6174- CNRS) | Rapporteuse & Examinatrice |
| Guillaume VAN NIEL Directeur de recherche, Université de Paris (INSERM 1266) | Examineur |
| Myriam TAVERNA Professeure, Université Paris-Saclay (UMR CNRS 8612) | Directrice de thèse |

Titre : Nouvelles approches électrocinétiques et analytiques pour l'isolement et la détection des vésicules extracellulaires

Mots clés : Vésicules Extracellulaires, Méthodes de séparations Électrocinétiques, Microfluidique, Billes Magnétiques, Électrophorèse Capillaire, Biomarqueur

Résumé : Les vésicules extracellulaires (EVs) sont d'importants messagers intercellulaires qui peuvent être exploités comme biomarqueurs pronostiques ou diagnostiques. Cependant, isoler, enrichir et caractériser les EVs à partir de fluides biologiques reste un défi. L'objectif de la thèse est de développer de nouvelles approches analytiques pour l'isolement et la détection des EVs, et l'analyse de protéines internes.

Dans un premier temps, nous présentons une nouvelle méthode d'électrophorèse capillaire (CE), couplée à une détection fluorescente induite par laser (LIF) pour l'identification et la quantification des EVs. Ensuite, l'analyse de dispersion de Taylor (TDA) a été étudiée pour déterminer la taille des EVs.

Enfin, nous présentons une nouvelle approche pour l'isolement des EVs à l'aide de polyéthylène glycol (PEG) pour précipiter les EVs à la surface de billes magnétiques. Pour améliorer les performances, nous avons transféré cette méthode dans un système microfluidique de gouttes.

Title: Novel electrokinetic and analytical approaches for isolation and detection of extracellular vesicles

Keywords: Extracellular Vesicles, Electrokinetic separation techniques, Microfluidic, Magnetic Beads, Capillary Electrophoresis, Biomarker

Abstract: Extracellular vesicles (EVs) are important intercellular messengers that may be exploited as prognostic or diagnostic biomarkers. However, owing to technical limitations in purifying and assessing EV subpopulations, knowledge on individual EVs is still in its infancy. The goal of the thesis is therefore to develop novel analytical approaches for EVs isolation and detection, and analysis of internal and targeted proteins.

First, we present a new capillary electrophoresis (CE), method coupled with laser-induced fluorescent (LIF) detection for identification and quantification of EVs after their purification. Then, Taylor dispersion analysis (TDA) was investigated to determine the size of isolated EVs.

Finally, we present a novel approach for the isolation of EVs using polyethylene glycol (PEG) to precipitate EVs on the surface of magnetic beads. To improve the performance, we further translated this method into a droplet microfluidic protocol using a purpose-made droplet platform.

Résumé de la thèse en français

Les vésicules extracellulaires (EVs) sont une famille de particules délimitées par une double couche phospholipidique et sécrétées par tous types de cellules. Les EVs transportent des protéines, lipides, acides nucléiques vers des cellules cibles et sont donc des acteurs clés de la communication intercellulaire dans des conditions normales ou pathologiques. Par conséquent, le potentiel des EVs à fournir des biomarqueurs moléculaires pronostiques ou diagnostiques de pathologies attire une attention croissante ces dernières années. L'isolement et l'enrichissement des EVs à partir de fluides biologiques reste un préalable difficile avant d'explorer les EVs. L'ultracentrifugation est la méthode la plus utilisée dans toutes les applications sur les EVs. Cependant, cette technique présente de nombreux inconvénients. En conséquence, des technologies pouvant extraire et garantir la pureté et l'intégrité des EVs isolées de manière reproductible sont toujours recherchées. De plus, pour fournir des informations physicochimiques et biologiques suffisantes sur les EVs isolées, de nombreuses techniques complémentaires doivent être mises en œuvre. Bien que robustes et efficaces, la plupart des plates-formes analytiques fournissent des informations sur la population des EVs dans son ensemble, masquant l'hétérogénéité des populations. L'objectif de la thèse a été de développer de nouvelles approches analytiques pour l'extraction et la détection d'EVs intactes, et l'analyse de protéines internes et ciblées d'EVs pouvant servir de futurs biomarqueurs de maladies. La première partie expérimentale du projet de thèse est dédiée au développement de méthodes basées sur l'électrophorèse capillaire (CE) pour analyser des EVs ou des protéines. Pour la première fois, nous présentons la CE couplée à la détection par fluorescence induite par laser (LIF) pour l'identification et la quantification des EVs. Cette méthode repose sur un marquage fluorescent des membranes des EV par clivage enzymatique intravésiculaire d'un précurseur. Ce marquage n'affecte ni la taille moyenne ni la distribution de charge des vésicules, indiquant qu'elles ont été préservées. Pour y parvenir des électrolytes moins classiques ont été utilisés comme tampon de séparation. Ces électrolytes, qui contiennent de grosses molécules faiblement chargées à des concentrations extrêmement élevées, ont permis d'éviter/minimiser l'adsorption des EVs sur la paroi du capillaire en silice et la lyse des EVs lors de l'électrophorèse. Pour éviter l'agrégation des EVs, une substitution de tampon des échantillons analysés a été effectuée pour diminuer la conductivité de la matrice d'échantillon. La CE-LIF a ainsi permis de différencier des EVs d'origine variée (sérum, plasma, lait) ou obtenues par différentes méthodes d'isolement et de vérifier leur qualité. Comme alternative à la DLS ou à la NTA, nous avons également exploré l'intérêt de la dispersion de Taylor (TDA-UV et TDA-LIF) pour estimer la taille des EVs isolées. Il s'agit de la première preuve de concept de l'applicabilité de la TDA à ce type de nanoparticules. La deuxième partie du travail a consisté à développer une technique pour l'isolement des EVs à partir de fluides biologiques reposant sur l'utilisation de billes magnétiques dans une plate-forme de gouttelettes microfluidique. Grâce à des EVs de haute qualité et bien caractérisées, isolées à partir de lait bovin, nous avons pu évaluer les performances d'extraction des EVs. Le polyéthylène glycol (PEG), un polymère d'exclusion d'eau a été utilisé pour précipiter des EVs à la surface des billes magnétiques. Par rapport au format d'extraction en tube, une nette augmentation du taux de récupération (jusqu'à 50 %) est obtenue avec une réduction des quantités d'échantillons et de réactifs (x10) et du temps d'extraction (x3). En conclusion, ces recherches contribuent au développement de méthodes innovantes, fiables et compactes pour la séparation, la purification et la caractérisation des EVs.

Acknowledgements

First of all, I would like to thank my thesis director, Professor Myriam Taverna, for welcoming me to her laboratory, but also for her great availability, her attentive listening and her undeniable scientific rigour. Thank you for your valuable advice, both scientifically and personally, and thank you for giving me the opportunity to present my work at several international conferences. A big thank you also to my thesis co-supervisor, Doctor Duc Thanh Mai, for his advice and the more global vision of the project that he was able to bring me during these three years, for his great listening, his availability but also for his unfailing optimism. Thanks to your extensive scientific knowledge and skills, I was able to learn and evolve on a daily basis within the laboratory. It was a great pleasure to be able to discuss with you both on scientific subjects and on life in general.

I would like to thank Professor Anne Varenne, Doctor Céline Elie-Caille, Professor Guillaume Van Niel and Professor Bruno Le Pioufle who do me the honor of being members of my thesis jury. I would also like to thank Doctor Christophe Junot for agreeing to be the external member of my thesis committee and for advising me throughout this project.

I also wanted to express my thanks to Doctor Zuzana Krupova and Doctor Pierre Defrenaix with whom we had the chance to collaborate during these three years of thesis. Thank you for your availability but also for your precious advice to carry out my thesis project. I also thank you for always providing us with high-quality extracellular vesicle samples for our experiments. This thesis project was able to progress in large part thanks to you.

I would like to thank Professor Hervé Cottet and Doctor Joseph Chamieh for their invaluable assistance with Taylor dispersion analysis. You have been a great help to us over the last few months of manipulations and we could not have gone this far in the project without you.

I would also like to thank Professor Marja-Liisa Riekkola and Doctor Evgen Multia for their collaboration and for their precious extracellular vesicles samples they extracted from human plasma using their novel immunoaffinity chromatography.

Thank you also to the PNAS (Proteins and Nanotechnology in Analytical Sciences) team members: Professor Claire Smadja and Professor Thuy Tran. It has been an honor to spend these three years with you, both scientifically and personally. Your teachings have been very influential in my life.

I would also like to thank Marie-Claude, Sylvie Z., Patricia, Fatiah, Maria and Orane for their daily logistical assistance. Thank you for your promptness and assistance. Thank you very much for the several cake sessions and other goodies.

I would also like to thank the old and new doctoral students as well as the interns I had the chance to meet during my thesis: Corentin, Jeanne, Cédric, Seray, Etienne, Ayoub, Balazs, Emmanuel, Gregory, Camille, Clara, Lucile, Théo, Van Thanh and Bin.

Special thanks to Doctor Coralie Ruel who introduced me to the PNAS team during my 6 months of Erasmus even before I started my thesis and for his training on capillary electrophoresis, you have helped me save valuable time. It was a real pleasure to work with you.

A special thank you to Doctors Emilie and Minh, with whom I had the chance to share my office at the start of my thesis. Every day, I laughed a lot thanks to you and all your good jokes.

Thanks to Sylvie Liu, for being my personal French teacher when I arrived, for all the discussions we had, thank you for all the good times we shared in the laboratory and thank you for your good mood. You helped me a lot on a daily basis, and I wish you all the best for your new adventure.

Many thanks to Joanie and Cecile, with whom I shared my office at the end of my thesis. I laughed a lot by your side, and I really appreciated all the moments we spent together in the laboratory but also outside. Thank you for letting me also decorate our office with some Italian flags (just a few) to celebrate the victory of the European Championship. I wish you much success in your thesis. You have become friends outside the lab, and I know that we will continue to see each other in the future.

Thank you to all my friends for staying close despite the distance: Bale, Lori, Fra, Ale, Ciccio, Fabio, Signo, Teo C., Teo D., Agui. Thank you for always being there for me even though my time in Italy has been more than limited over the last three years. Thanks also to my friends I met in Paris: Dome, Delia, Fede, Needhi, Ste, Romane, Fra, Edo. I've always spent amazing weekends or weeks of vacation with you, and I'm certain that will continue.

Thanks to Anja for your presence by my side, your encouragement and your daily support.

Infine, vorrei fare un enorme ringraziamento ai miei genitori e alla mia sorellona. Grazie per avermi permesso di evolvere liberamente fino a questo dottorato e per avermi dato fiducia. Grazie per il vostro supporto. Tutto questo è stato possibile grazie a voi.

Curriculum Vitae

Education:

- **Single-cycle Master** Pharmacy and Industrial Pharmacy at Università degli Studi di Milano (SEP 2012 - JUL 2018)
- **PhD** in Analytical Chemistry at the Faculty of Sciences of Orsay, University of Paris-Saclay (2018-2021)

Oral communication:

- *“A novel Capillary electrophoresis method to identify and quantify exosomes from bio fluids”*; International Symposium on Electroseparation and Liquid Phase-Separation Techniques (ITP 2019); Université Paul Sabatier-Toulouse (1-4 Sep 2019)
- *“A novel Capillary electrophoresis method to identify and quantify Extracellular Vesicle (EVs)”*; Journée Scientifique: groupes CE & FFF de l’Afsep: complémentarité des méthodes électrocinétiques capillaires et de fractionnement flux force (1 July 2021)
- *“New Magnetic Bead-based Strategies for Extracellular Vesicle Isolation: Towards Microfluidic Droplet Operation”*; International Symposium on Microscale Separations and Bioanalysis (MSB 2021); Virtual edition (12-15 July 2021)

Posters:

- *“Towards a novel Capillary electrophoresis method for identification and quantification of purified exosomes from bio fluids”*; International Symposium on Electroseparation and Liquid Phase-Separation Techniques (ITP); Université Paul Sabatier-Toulouse (1-4 Sep 2019)
- *“Towards novel strategies for isolation of extracellular vesicles: performance evaluation with a new characterization tool by CE-LIF”*; International Symposium on Microscale Separations and Bioanalysis (MSB 2020) ; Virtual edition (27-30 Sep 2020)

Publications:

- Morani M, Taverna M, Mai TD, A fresh look into background electrolyte selection for capillary electrophoresis-laser induced fluorescence of peptides and proteins. (2019) *Electrophoresis*. 2019 Sep;40(18-19):2618-2624. <https://doi.org/10.1002/elps.201900084>
- Morani M, Mai TD, Krupova Z, Defrenaix P, Multia E, Riekkola ML, Taverna M, Electrokinetic characterization of extracellular vesicles with capillary electrophoresis: A new tool for their identification and quantification. (2020) *Analytica Chimica Acta*, 1128, 42-51. <https://doi.org/10.1016/j.aca.2020.06.073>
- Morani M, Mai TD, Krupova Z, van Niel G, Defrenaix P, Taverna M. (2021). Recent electrokinetic strategies for isolation, enrichment and separation of extracellular vesicles. (2021) *TrAC Trends in Analytical Chemistry*, 116179. <https://doi.org/10.1016/j.trac.2021.116179>

List of abbreviations

AAB: 4-aminoazobenzene

AF4: Asymmetric flow field-flow fractionation

AFM: Atomic Force Microscopy

ALIX: Apoptosis-Linked gene 2-Interacting protein X

ALK: anaplastic lymphoma kinase

APCs: antigen presenting cells

AsFIFFFF: Asymmetrical flow field-flow fractionation

ATPase: adenosine triphosphatase

ATPS: Aqueous two phase system

A β : amyloid beta

BGE: Background electrolyte

CE: Capillary Electrophoresis

CFDA-SE: 5-(and-6)-Carboxyfluorescein diacetate succinimidyl ester

cIEF: Isoelectric focusing capillary

CSF: Cerebrospinal fluid

CVC: current-voltage characteristic

CZE: Capillary Zone Electrophoresis

DCs: dendritic cells

DLD: Deterministic lateral displacement

DLS: Dynamic Light Scattering

DNA: deoxyribonucleic acid

EGFR: epidermal growth factor receptor

ELISA: Enzyme-Linked Immunosorbent Assay

EM: Electron microscopy

EML4: Echinoderm microtubule-associated protein-like 4

EOF: Electroosmotic flow

ESCRT: Endosomal Sorting Complex Required for Transport

EVs: Extracellular vesicles

FASI: Field-amplified sample injection

FASS: Field amplified sample stacking

FFF: Flow field-flow fractionation

FSC: Forward Scatter

FSEV: French Society of Extracellular Vesicles

GCE: Capillary gel electrophoresis

GO/PDA: graphene oxide and polydopamine

HPLC: High-performance liquid chromatography

HSP: heat shock proteins

ILVs: intraluminal vesicles

IS: Ionic Strength

ISEV: International Society for Extracellular Vesicles

ISF-BGE: Inorganic-species-free BGE

ITP: Isotachopheresis

LAMP-3: lysosomal-associated membrane protein 3

LAMTOR 1: late endosomal / lysosomal adaptor, MAPK and mTOR activator 1

LC-MS/MS: Liquid chromatography-tandem mass spectrometry

LE: leading electrolyte

LIF: Laser induced fluorescence detection

LVSS: Large volume sample stacking

MAGEA3/6: Melanoma-associated antigen 3

MALS: multi-angle light scattering

MB: Magnetic beads

MEKC: Electrokinetic chromatography

MFG-E8: lactadherin/milk-fat globule epidermal growth factor-like factor 8

MHC-II: Class II Major Histocompatibility Complex

miRNA: microRNA

MISEV: minimal information for studies of extracellular vesicles

mRNA: messenger ribonucleic acid
MS: Mass spectrometry
MSC: Mesenchymal stem cell
MVBs: multivesicular bodies
NAs: Nuclei acids
NA-Seq: Nucleic acid sequencing
NPs: Nanoparticles
NTA: Nanoparticle Tracking Analysis
PC: phosphatidylcholine
PCR: Polymerase Chain Reaction
PD-L1: Programmed death-ligand 1
PE: phosphatidyl-ethanolamine
PEG: Polyethylene glycol
PEO: poly-(oxyethylene)
PFP: platelet-free plasma
PI: phosphatidylinositol
PI3P: Phosphinositol-3 phosphate
PLL: Poly-L-lysine
PS: phosphatidylserine
PSA: prostate-specific antigen
RT-PCR: Real-time fluorescence techniques
SEC: Size exclusion chromatography
SEM: Scanning electron microscopy
SM: sphingomyelin
SPR: Surface plasmon resonance
SSC: Side Scatter
TAS: Thermophoretic aptasensor
TDA: Taylor dispersion analysis
TE: terminating electrolyte
TEI: Total Exosome Isolation

TEM: Transmission Electron Microscopy

TFF: Tangential flow filtration

TGF- β 1: Transforming growth factor beta 1

TI: Trypsin inhibitor

Tim 4: T cell immunoglobulin and mucin domain protein 4

TMV: Tobacco mosaic virus

TRPS: Tunable resistive pulse sensing

TSG 101: Tumor Susceptibility Gene 101 protein

UC: Ultracentrifugation

UF: Ultrafiltration

UV: Ultraviolet

VFC: Vesicle Flow Cytometer

VPS4: Vacuolar Protein Sorting-associated protein 4

WB: Western blot

β -CD: β -cyclodextrin

Contents

| | |
|---|-----------|
| Contents | 15 |
| General introduction | 18 |
| BIBLIOGRAPHY | 21 |
| Chapter I: Extracellular vesicles | 22 |
| I.1. General aspects | 22 |
| I.1.1. Historical background | 22 |
| I.1.2. Nomenclature and classification | 24 |
| I.1.2.1. Biogenesis of Exosomes | 24 |
| I.1.2.2. Biogenesis of Microvesicles | 27 |
| I.2. EV composition | 28 |
| I.2.1. Lipids | 28 |
| I.2.2. Proteins | 28 |
| I.2.3. Nucleic acids | 30 |
| I.3. Extracellular vesicles: new sources of human health information? | 31 |
| I.3.1. Biological role | 31 |
| I.3.2. Pathological role | 31 |
| I.3.3. EVs as a source of promising biomarkers | 32 |
| I.3.4. Therapeutic potential of EVs | 36 |
| I.4. Concluding remarks | 37 |
| Chapter II: Current methods for EVs isolation and characterization | 39 |
| II.1. EVs extraction and isolation | 39 |
| II.1.1. Ultracentrifugation (UC) | 39 |
| II.1.1.1. Differential ultracentrifugation | 40 |
| II.1.1.2. Density gradient ultracentrifugation | 41 |
| II.1.2. Ultrafiltration (UF) | 42 |
| II.1.3. Size-exclusion chromatography (SEC) | 43 |
| II.1.4. Polymer-based precipitation | 45 |
| II.1.5. Immunoaffinity capture-based methods | 45 |
| II.1.6. Asymmetric flow field-flow fractionation (A4F) | 47 |
| II.1.7. Concluding remarks | 48 |
| II.2. EVs analysis and characterization | 49 |
| II.2.1. Physical characterization | 50 |
| II.2.1.1. Dynamic Light scattering (DLS) | 50 |
| II.2.1.2. Nanoparticle tracking analysis (NTA) | 50 |
| II.2.1.3. Tunable resistive pulse sensing (TRPS) | 51 |
| II.2.1.4. Flow cytometry | 52 |
| II.2.1.5. Electron microscopy (EM) | 54 |
| II.2.1.6. Atomic force microscopy (AFM) | 55 |

| | |
|--|-----------|
| II.2.1.7. Surface Plasmon Resonance (SPR) | 56 |
| II.2.2. Molecular characterization | 57 |
| II.2.2.1. Western blot (WB) and ELISA | 57 |
| II.2.2.2. Mass spectrometry (MS) | 58 |
| II.2.2.3. Nucleic acid analysis | 58 |
| II.2.3. Concluding remarks | 59 |
| Chapter III: Emerging methods for EVs isolation, analysis and detection | 60 |
| III.3. Microfluidic-based technologies | 60 |
| III.1.1. Immunoaffinity-based microfluidics for EV isolation | 60 |
| III.1.2. Label-free microfluidic strategies for EV isolation | 63 |
| III.1.2.1. Microfluidic filtration | 63 |
| III.1.2.2. Viscoelastic-flow sorting | 64 |
| III.1.2.3. Deterministic lateral displacement (DLD) | 65 |
| III.1.2.4. Acoustic separation | 66 |
| III.1.2.5. Thermophoresis technology | 67 |
| III.2. Electrokinetic-based technologies | 68 |
| PAPER 1 | 70 |
| III.3. Concluding remarks | 83 |
| Objective of the thesis | 85 |
| EXPERIMENTAL PART | 89 |
| Chapter IV: Development of novel methods for analysis of intact EVs and specific intravesicular proteins with capillary electrophoresis | 90 |
| IV.1. Introduction | 90 |
| IV.2. Principle of capillary electrophoresis (CE) | 92 |
| IV.2.1. Electroosmotic flow (EOF) | 94 |
| IV.2.2. Electrophoretic mobility (μ_{ep}) | 95 |
| IV.3. "Inorganic-species-free" BGE (ISF BGE) for capillary electrophoresis-laser induced fluorescence (CE-LIF) performance improvement | 97 |
| PAPER 2 | 99 |
| IV.4. CE-LIF method development to study the electrokinetic distribution of EVs | 106 |
| PAPER 3 | 109 |
| IV.5. Development of in-line electrokinetic preconcentration prior to CE-LIF separation of EVs | 134 |
| IV.5.1. Large volume sample stacking (LVSS) with polarity switching of EVs | 135 |
| IV.2. Online Preconcentration in Capillaries by Multiple LVSS of EVs | 139 |
| IV.3. Concluding remarks | 142 |
| IV.6. Size-based characterization of EVs by Taylor Dispersion Analysis (TDA) | 143 |
| IV.6.1. Principle of Taylor Dispersion Analysis (TDA) | 144 |
| IV.6.2. From diffusion to size determination: experimental considerations | 146 |
| IV.6.3. CE procedure | 148 |
| IV.6.4. Results | 149 |
| IV.6.4.1. TDA-UV and TDA-LIF of bovine milk derived EVs | 149 |
| IV.6.4.2. TDA-UV and TDA-LIF of human plasma derived EVs | 151 |

| | |
|--|---------------------------------------|
| IV.6.5. Concluding remarks | 153 |
| Chapter V: New micro-sized method for the isolation of EVs | 155 |
| V.1. Introduction | 155 |
| V.2. Principle of microfluidic droplets and their combination with MB | 157 |
| V.2.1. General statements on Droplet Microfluidics | 157 |
| V.2.2. Magnetic beads as cargos: principle and theory | 158 |
| V.3. Capture and Elution of EVs from commercial immuno-based beads | 161 |
| V.3.1. Introduction of preliminary in-tube experiments | 161 |
| V.3.2. Preliminary in-tube experiments to select MB capture and elution conditions | 162 |
| V.4. Alternative MB-based strategies to extract EVs | 165 |
| V.4.1. Recent alternative MB-based methods to extract intact EVs: a brief revision of the literature | 166 |
| V.4.2. Development of a microfluidic droplet platform with an antibody-free magnetic-bead-based strategy for high through-put and efficient EVs isolation (submitted to Talanta) | 169 |
| PAPER 4 | 169 |
| Conclusion and perspectives | 213 |
| References | 217 |
| APPENDIX | 232 |
| Table A: Representative table showing a selection of completed and ongoing clinical trials with the term “exosome” (from http://clinicaltrials.gov , November 2021). | 233 |
| Table B: Representative table showing a selection of completed and ongoing clinical trials with the term “extracellular vesicle” (from http://clinicaltrials.gov , November 2021). | 242 |
| Résumé de la thèse en français | 4 |
| Summary of the thesis in English | Errore. Il segnalibro non è definito. |

General introduction

Extracellular vesicles (EVs) are a family of heterogeneous lipid bilayer-delimited particles secreted into the extracellular space by all types of cells and thus found in various human body's physiological fluids (plasma, saliva, urine, cerebrospinal fluid, etc.). Circulating EVs may transport proteins, lipids, and nucleic acids that mirror the producing cells; therefore they can reflect a broad spectrum of biological activities, both normal and pathological. Consequently, open up new possibilities for noninvasive liquid biopsy. Several characteristics make them particularly interesting in clinical diagnosis, including their high concentration in biological fluids in comparison to circulating tumor cells (of the order of 10^{10}) and their stability, which distinguishes them from other soluble RNA-type biomarkers, for example [1]. Finally, because of their inherent biological properties, EVs may be engineered with a specific active component as well as therapeutic and vectorization properties. Furthermore, in recent years, they have emerged not just as novel potential drug delivery vehicles, but also for their intrinsic therapeutic properties, particularly in the context of regenerative medicine [2].

Nevertheless, the isolation and enrichment of EVs from biological fluids remains a difficult prerequisite before exploring EVs. Ultracentrifugation is the most used method in all EV applications. However, this technique presents many drawbacks. As a result, developing EVs separation or extraction technologies that may guarantee EV purity and integrity in a repeatable way is still in great demand. Furthermore, EVs are quite heterogeneous, with a certain heterogeneity in structure and molecular content resulting in distinct EV subpopulations. For this reason, numerous complementary approaches must be used to provide adequate physical and biological information on the isolated EVs. A good approach should fulfill all of the requirements for EV profiling, including the capacity to distinguish between various subpopulations and to maintain EV integrity throughout analysis. Faced with this limitation, the International Society for Extracellular Vesicles (ISEV) has brought together researchers from diverse backgrounds to give recommendations in order to homogenize existing protocols for isolation and characterization of EVs as well as foster the development of new reproducible and standardized methods [3].

In this context, microfluidic systems are particularly attractive for enhancing the isolation performance of EVs, in part because new mechanisms may be applied and be more efficient in a microfluidic format. Microfluidic devices aimed to reduce the time required for the processing of EV samples by making the

isolation system portable, efficient, and simple to use. One part of the present microfluidic-based systems for EVs isolation is based on the use of capture molecules (e.g., antibodies) capable of binding specific markers (called Labels here), that are either (i) constantly found surface proteins (like CD63) or specific ones that are overexpressed during development of tumors for instance (like EpCAM). These approaches ensure labeled EV separation purity, but they need to be enhanced for greater throughput and targeting numerous EV populations with different labels. Alternative approaches focusing on the physical properties (e.g., particle size and electric charge) of EVs, also in combination with the use of external forces such as hydrodynamic force, electric field, or acoustic field have been developed to allow isolation without the use of labels (label-free) [4]. Despite significant advances in label-free isolation, existing microfluidic technologies are limited in their ability to separate certain EV subpopulations and remove undesirable components such as aggregating proteins and lipoproteins. Among the various microfluidics technologies, an interesting but unexplored option for EV isolation is Droplet-based Microfluidics, which is broadly defined as the science and technology of generating and manipulating micro to femtoliter microreactors (droplets). This enables constant sample and reagent compartmentalization while reducing contamination risks with the surrounding environment. In particular, Droplet-based microfluidic devices utilizing magnetic beads (MB) as solid support have already been demonstrated for the extraction and purification of different kind of target analytes (such as proteins, nucleic acids and viruses) from complex matrices, but they have not yet been demonstrated for the isolation of EVs.

In parallel, capillary electrophoresis (CE), which may be defined broadly as a micro technique allowing the migration and therefore the separation of charged compounds in solution under an electric field, is a separation and quantitative technique which format could be compatible with the microdroplet volume produced in a microfluidic droplet system. This technique is capable of analyzing small molecules as well as particles, virus and bacteria but was not yet explored for intact EVs analysis when I started my thesis. While electric field have been used to sort and drive EVs in different microdevices, capillary electrophoresis to assess EVs or discriminate EV subtypes based on electrophoretic migration was never reported. Moreover, Taylor dispersion analysis (TDA), which uses pressure rather than an electric field to determine the hydrodynamic radius from the observed peak dispersion, makes CE equipment especially appealing for profiling the distribution and quality of isolated EV populations.

The objective of this thesis is therefore to combine a microfluidic droplet technology that can allow the extraction of specific EVs or whole EVs present in a biological sample, with multiple capillary

electrophoresis modes for analysis of intact EVs, which would result in a new automated device, potentially reproducible and standardizable, for EVs users.

The **first chapter** presents an overview on EVs, their biogenesis and molecular composition, their biological and pathological role in order to emphasize their diagnostic potential for monitoring human health as well as carriers or delivery nano systems for therapeutic applications. **Chapter II** presents an overview of the different conventional techniques currently available for isolating and characterizing EVs and their associated limits. The **third chapter** focuses on the advantages of emerging methods applied to EVs including microfluidic-based technologies and in particular electrokinetically driven methods for isolation, enrichment and characterization of EVs. The objectives of the thesis are detailed at the end of this chapter.

The experimental part of the manuscript is divided into two chapters that describe the two main strategies that have been investigated to achieve the objective of our project.

The **fourth chapter** focuses rather on the development of innovative methods all based on the technique of CE for characterizing intact EVs and also specific intravesicular proteins. Its multiple modes of separation and analysis and the possibility to run analyses under voltage or pressure allowed to investigate several different approaches, e.g., Capillary zone electrophoresis method coupled with laser induced fluorescence detection (CE-LIF) for analyzing intact EVs or the internal protein content of them, and Taylor dispersion analysis (TDA) for size estimation of isolated intact EVs. Additionally, strategies for in-capillary sample preconcentration of EVs are discussed in order to improve the sensitivity of conventional LIF detection.

The **fifth chapter** presents the development of the first module of the platform relying on a microfluidic droplet system by integration of magnetic beads for EVs manipulation and handling, during the multistep sample treatment. Different kind of magnetic beads-based approached are compared using already purified EVs samples before transferring the protocol to droplet system and applying it to more complex biofluids (e.g., pony serum and plasma).

Bibliography

Chapter I: Extracellular vesicles

EVs are a family of cell-derived membrane vesicles which can transport their cargo to target cells acting as mediators of key functions in numerous patho-physiological conditions. However, their properties were not readily known when they were first observed more than 50 years ago. Throughout these years of studies and discoveries, their role has been increasingly clarified and a wide terminology has been proposed to identify or class EVs. As a result, the scientific field of EVs required harmonization. EVs can be narrowly classified into two major groups: exosomes and microvesicles. The difference between these vesicles lies in their biogenesis, size, content, and functions. Despite their great potential for pathology diagnosis or treatment, the use of exosomes in the clinic is currently limited due to a lack of standardization of separation, isolation and analysis or characterization methods. Misuse of terminology is common in the literature due to the difficulty of distinguishing exosomes from microvesicles. As a result, the word exosome is frequently used to refer to a heterogeneous sample comprising exosomes and microvesicles. Unless otherwise specified, the term EV will refer to exosomes and microvesicles throughout this thesis.

In this chapter I will briefly present the extracellular vesicles, their physical and biochemical characteristics, their physiological roles, their implications in various pathologies as well as the recent advances of EV-based therapies, before detailing current and developing methods for EVs isolation and analysis or characterization

I.1. General aspects

I.1.1. Historical background

As often reported by researchers working on EVs, the early evidence for the existence of EVs have been firstly reported in 1946 by Chargaff and West [5] when they described the presence of a precipitable factor in platelet-free plasma (PFP) that can accelerate the generation of thrombin. These results showed, for the first time, the presence of factors other than platelets, which were responsible for blood clotting. Subsequently, in 1967, Wolf et al [6], with the help of electron microscopy, similarly observed small lipid-rich particles released from platelets with procoagulant activity, referring to them as "platelet dust". The term "extracellular vesicle" was first used in 1971 by Aaronson [7] for EVs released from *Ochromonas Danica*, a flagellated alga.

In 1981, Trams [8] was the first to use the term "exosomes" to describe a large panel of vesicles ranging in size from 40 nm to 1 μ m that were released from cultured cells.

However, a turning point arrived in 1983, when the two groups of Stahl and Johnstone reported almost simultaneously that transferrin receptors associated with small vesicles of around 50 nm were released by reticulocytes into the extracellular space [9] [10]. Later in 1987, Johnstone discovered that such release took place through the endosomal route with formation of intraluminal vesicles (ILVs) in the endosome, followed by fusion of MVBs with the plasma membrane and extracellular release of these ILVs [11]. This time, the term “exosomes” previously coined by Trams, was used to describe these ILVs. A decade later, interest in vesicles increased in the field of immunology. A breakthrough article appeared in 1996, when Raposo’s team demonstrated that B lymphocytes release exosomes expressing the Class II Major Histocompatibility Complex (MHC-II) and thus, induce a response in T cells [12].

In 2007, Valadi and his colleagues reignited the interest in research on EVs by demonstrating for the first time the presence of messenger ribonucleic acids (mRNA) and microRNAs (miRNA) in the exosomes isolated from murine and human mast cells, recognizing them as cell-cell communication mediators [13]. Over the last decade, the number of studies on EVs has increased significantly, as shown by the number of publications per year (Fig.1), found with the key words “extracellular vesicles” in Web of Science database.

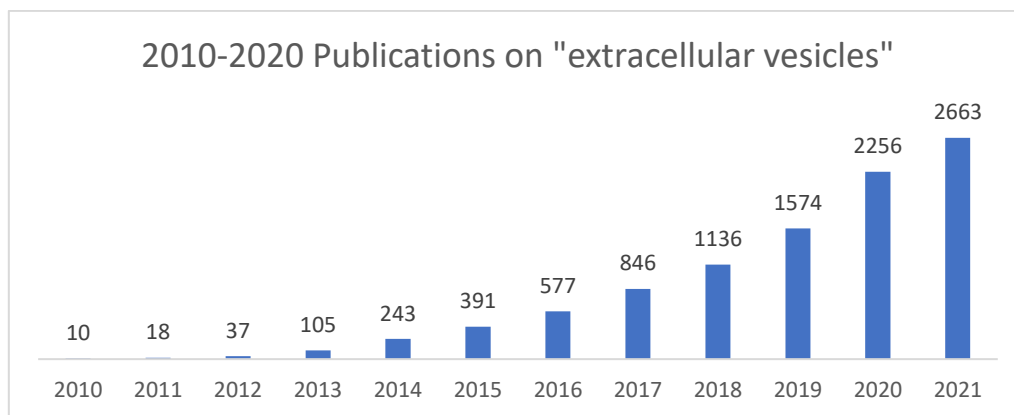


Figure 1 : Evolution of the number of publications dealing with EVs between 2010 and 2021. The graph shows the number of publications with the term "extracellular vesicles" in the title, between 2010 and 2021 (October), obtained from the entire Web of Science (WoS) database.

The first meeting bringing together EVs scientists was held in Montreal (Canada) in 2005. Six years later, in 2011, an international conference on EVs was organized at the Institut Curie in Paris, France. In the same year, the International Society for Extracellular Vesicles (ISEV, <https://www.isev.org/>) was established, aiming at standardizing the field, and this also led to the creation of the Journal of

Extracellular Vesicles (JEV). Currently, the society has over 1500 members, but a plenty of national EV societies have also been formed. The French Society of Extracellular Vesicles (FSEV, <https://www.fsev.fr/>) was officially founded on April 21, 2018.

I.1.2. Nomenclature and classification

Over the years, the nomenclature for extracellular vesicles has become highly muddled. The accumulated data show that content, size, and membrane composition of the EVs are highly heterogeneous and complex, depending on the pathophysiological state of the origin cell. Several terms have been used to describe vesicles released by cells. Vesicles have been named after the cells or tissues from where they are released. Thus, terms like oncosomes, for EVs released by cancer cells [14] [15]; prostasomes, for those released by prostate epithelial cells [16] [17] or dexosomes, for those released by dendritic cells (DCs) [18] have been employed. When nomenclature is based on the mechanism of generation, terms like exosomes (endosomal vesicles) [19], ectosomes (vesicles from membrane budding) [20], or apoptotic bodies (vesicles formed following cell death) [21] have been also used. Alternatively, depending on their biological role, we can find terms like calcifying matrix vesicles [22], tolerosomes [23] or argosomes [24]. Although specific characteristics have been proposed for each EVs subpopulation, at present there is still no specific identification of each subgroup that is widely accepted and it remains a matter of debate [25-27]. For such reason, according to the Minimal Information for Studies of Extracellular Vesicles (MISEV) guidelines from ISEV, authors are recommended to use "extracellular vesicle" as an umbrella term to represent all types of cell-secreted vesicles, except if authors may identify remarkable markers that are reliable within their experimental system [28]. However, the most commonly used terminology is based on two key criteria: the mode of biogenesis and the biochemical markers. Then, EVs can be narrowly classified into two major groups: exosomes and microvesicles which exhibit moreover, size differences.

I.1.2.1. Biogenesis of Exosomes

Exosomes are vesicles surrounded by a lipid bilayer, having a size between 30 and 100 nm, even though they can reach 150 nm according to some authors [29, 30], and density ranging from 1.13 to 1.19 g/mL [31]. Exosomes are produced via the endosomal pathway. They are first generated as intraluminal vesicles (ILVs) in the lumen of early endosomes, which mature into late endosomes, forming multivesicular bodies (MVBs). Before being secreted, exosomes go through a "sorting" step.

Indeed, they are either degraded in the lysosome or sent to the plasma membrane to be secreted in the extracellular medium [32]. The causes that determine the fate of these multivesicular bodies are not yet known, but it seems that cholesterol levels in MVBs play a role. Actually, some studies have shown that cholesterol-rich vesicles are secreted, whereas cholesterol-poor vesicles are degraded by the lysosome [33].

The ESCRT machinery (Endosomal Sorting Complex Required for Transport) is the most well-studied pathway for inducing the formation of ILVs and subsequently of MVBs [34, 35]. ESCRT is a complex composed of four sub-complexes (0, I, II and III) and other associated proteins such as VPS4 (Vacuolar Protein Sorting-associated protein 4), ALIX (Apoptosis-Linked gene 2-Interacting protein X), TSG 101 (Tumor Susceptibility Gene 101 protein) and ATPase (adenosine triphosphatase), playing a crucial role in the transport of ubiquitinated proteins to endosomes and the formation of MVBs. ESCRT-0 is recruited at the endosomal membrane boundary by interacting with the phospholipid PI3P (Phosphatidylinositol-3 phosphate) present in the endosome membrane. ESCRT-0 recruits ESCRT-I and together they group the ubiquitinated cargoes into microdomains. ESCRT-I recruits ESCRT-II and starts creating invagination of the membrane. Finally, ESCRT-I/II in turn recruits ESCRT-III which is involved in the detachment of the formed vesicle. ESCRT-III is then dissociated and recycled by the action of ATPase VPS4 (Fig. 2).

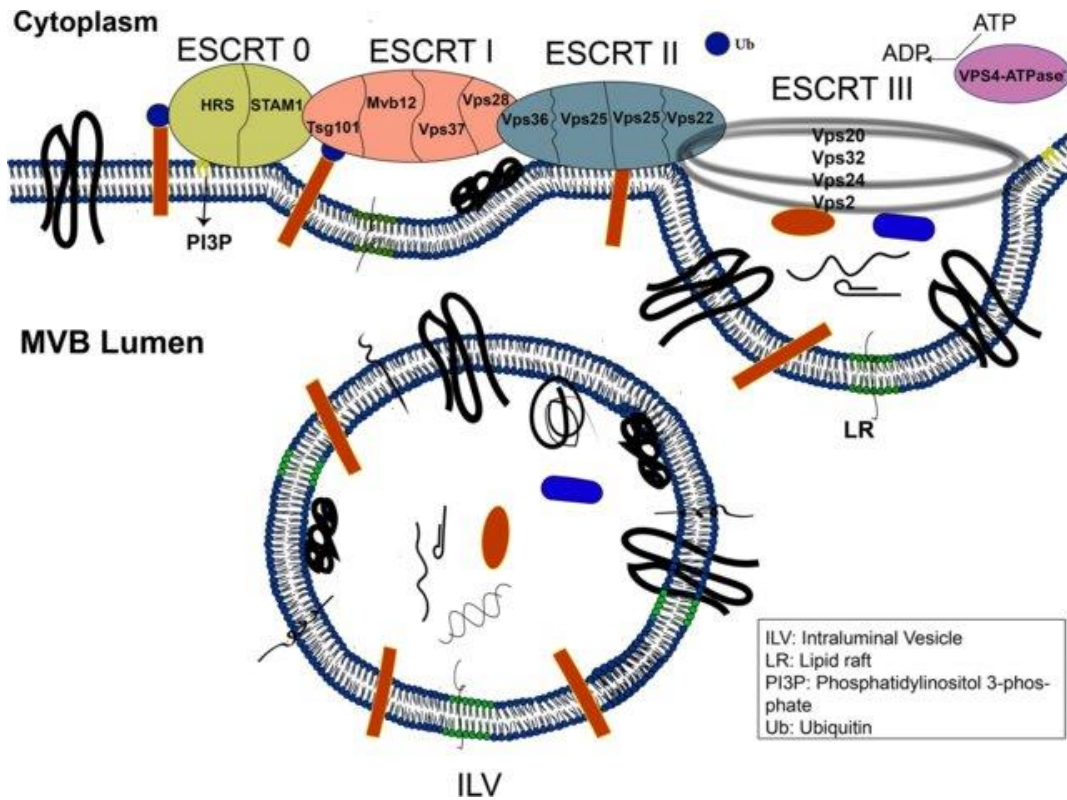


Figure 2: Representation of the ESCRT complex. ESCRT machinery is first set up by the ESCRT-0 complex. This complex can divide proteins into microdomains and interact with the ESCRT-I complex's TSG101 subunit, which, in turn, recruits ESCRT-II subunits. The inner budding of the ILVs into the lumen of the MVBs is then triggered by ESCRT-I and ESCRT-II. ESCRT-I and ESCRT-II initiate the inward budding of the ILVs into lumen of the MVBs. Subsequently, ESCRT-III subunits bind to the neck of the early ILVs and cleavage them into free vesicles. Reprinted from [36].

The biogenesis of exosomes can also occur in an ESCRT-independent pathway which involves the formation of lipid rafts, in which sphingomyelin is transformed into ceramide under the action of sphingomyelinase [37]. These ceramide-rich domains cause invagination of the endosome membrane and the generation of intraluminal vesicles.

Along with this mechanism of exosome biogenesis, exosomes can be formed by direct budding from domains of the plasma membrane enriched in endosomal and exosomal proteins, called “endosome-like domains” [38]. On the other hand, actin-myosin binding has been shown to play a role in the formation of MVBs and the biogenesis of exosomes [39]. However, more evidence is needed to support exosome biogenesis at the plasma membrane.

From these observations, we can therefore note that the exact mechanism responsible for the formation and release of exosomes remains discussed in the literature, and it seems that the presence

of different mechanisms of exosome biogenesis depends on the type of cell and / or intracellular conditions.

I.1.2.2. Biogenesis of Microvesicles

Microvesicles are delimited by a lipid bilayer as well, but their size range from 100 to 1000 nm, and their density is less than 1.10 g/mL [40]. They are produced as a result of direct outward blebbing and pinching of the cell membrane, following activation of cells by various physicochemical stimuli. The exact mechanism of formation and release are still not fully understood, but it seems that it involves redistribution of membrane lipids and the use of contractile machinery located at the level of the plasma membrane like actin and microtubules, as well as molecular motors like kinesis and myosins [30]. In general, a stimulus in the cell causes an increase in the intracellular concentration of calcium which inhibits the aminophospholipid translocase and activates the scramblase, resulting in the loss of lipid asymmetry. All these events lead to membrane budding and the release of microvesicles exposing phosphatidylserine (PS) on their outer leaflet (Fig. 3) [41].

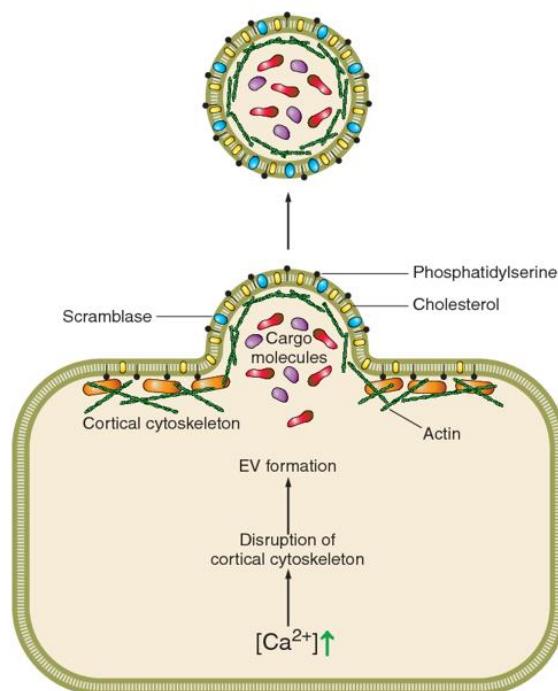


Figure 3: Mechanism of microvesicles biogenesis from plasma membrane of cells. Reprinted from [41].

I.2. EV composition

EVs are composed by a lipid bilayer that encloses a variety of soluble or membrane proteins, lipids, metabolites, and nucleic acids. Numerous studies on the lipidome, proteome and transcriptome of EVs have been conducted and the results have been compiled in web-based catalogues such as ExoCarta (<http://exocarta.org>) and Vesiclepedia (<http://microvesicles.org>) which are constantly updated with the help of the scientific community. According to these findings, the type of the EV content is largely related on the donor cell and its physiological or pathological status.

I.2.1. Lipids

EVs are mainly composed of phosphatidylserine (PS), phosphatidyl-ethanolamine (PE), sphingomyelin (SM), phosphatidylinositol (PI), phosphatidylcholine (PC), cholesterol and ceramides [42-45]. It is well established that exosomes exhibit greater rigidity than the plasma membranes of cells. This rigidity would be the result of a pH-dependent mechanism. Indeed, the membrane rigidity of exosomes increases between pH 5 and 7 [46]. This finding could explain why a lower pH such as those of the tumor microenvironment enhances cellular absorption of EVs [47]. The increased acidity makes the membranes of EVs more fluid thereby promoting their fusion with cell plasma membranes. Finally, the greater rigidity of EV membranes comes from their high content of sphingomyelin, desaturated lipids, and cholesterol [48, 49] which might contribute to their resistance to degradation and, as a result, their stability as carriers of different biomolecules through bodily fluids [50, 51]. Consistently, exosomes have been shown to be more resistant to detergent treatments than microvesicles, indicating a greater membrane lipid order [52]. Furthermore, EVs' high cholesterol and sphingomyelin content might lead to apoptosis of receptor cells [53, 54]. Indeed, synthesized nanoparticles imitating the lipid content of EVs decrease the survival of pancreatic tumor cells [55]. On the other hand, such synthetic exosome-like nanoparticles induced the activation of the survival pathway in a different human pancreatic tumoral cell line [56]. Taken together, these data show that lipids not only convey stability and structural rigidity to the vesicular membrane, but also take part in cellular signaling pathways [57].

I.2.2. Proteins

Proteins are important components of EV cargo, and their expression is frequently employed for characterization purposes. Other than being used as a quality control tool, they can be used to detect

exogenous or disease-specific proteins. Although proteins can be typical of different EVs, they cannot be considered real specific markers of the various types of EVs. In this context, the ISEV provided the minimal experimental requirements for the definition of EVs. The specific categories of proteins to consider for EV characterization are listed in the table 3 from the Minimal Information for Studies of Extracellular Vesicles 2018 (MISEV2018) guidelines [3]. EVs proteins include proteins of endosomal and cytosolic origin (annexins, ALIX, TSG101, flotillins) [58], tetraspanins (CD9, CD63, CD81) that are among the most prevalent membrane proteins on EVs and are often utilized to characterize them [59, 60], heat shock proteins (HSP70, HSP90) [11, 61] and cytoskeletal ones (tubulin, actin). These molecules are generally present in EVs regardless of their cellular origin (Fig. 4). However, there are proteins found in relatively low proportions in EVs that are negative markers of EVs: when compared to cell lysate. This is the case, for example, of calnexin [30]. EVs also contain cell-type specific proteins like MHC class II on antigen presenting cells (APCs)-derived vesicles [12]. Likewise, milk fat globule-epidermal growth factor 8 (MFG-E8), also known as lactadherin, is present only in EVs originating from immature dendritic cells [62]. These observations highlight the specificity of formation of these vesicles. Furthermore, EVs include glycosylated proteins that play an important role in cellular targeting of EVs and their interactions [63-65]. Indeed, the protein profile of EVs reveals the presence of many glycan binding proteins that control which cells would be targeted by EVs and how [40]. For example, glypican-1, a heparan sulfate-containing cell surface proteoglycan is implicated in exosome docking [66]. P-selectin (CD62p) present on the surface of EVs produced by activated platelets permits EVs' attachment to target cells [67]. Therefore, the protein composition of EVs influences their roles, adhesion capacities and cell targeting.

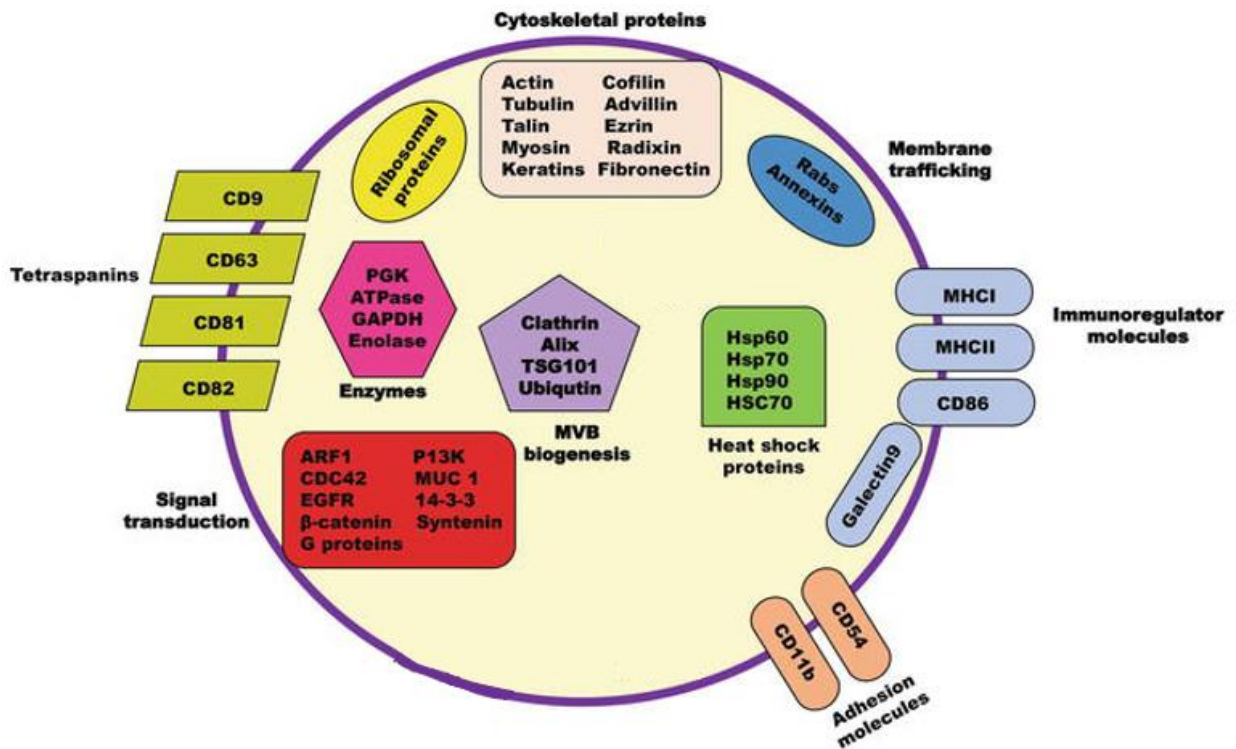


Figure 4: A graphical illustration of common proteins found in EVs. The molecules depicted here are classified according to their function or protein class: Cytoskeletal proteins, Membrane trafficking proteins, Immunoregulator molecules, Adhesion molecules, Signal transduction molecules and Tetraspanins. Readapted from [68].

1.2.3. Nucleic acids

Significant advancements in the characterization of EVs have revealed that they can also transport nucleic acids. The majority of studies have described RNA, including mRNA and miRNA which are often smaller in size than the RNA found in cells [13, 69]. Aside from transporting RNA, the presence of deoxyribonucleic acid (DNA) in EVs has been less studied and is still a matter of debate as DNA might be considered a contaminant from improper isolation [70, 71]. Therefore, further research is required to determine whether DNA is present and, if so, what its real significance in EVs is. The RNA content of EVs varies depending on the cell type. For instance, EVs produced by certain cancer cells contain more RNA than those produced by healthy cells [72]. The RNA content of EVs reflects the RNA content of the parent cell, suggesting that RNA molecules are selectively integrated into EVs. However, the mechanism involved in the selection of RNA to be transferred in EVs has not yet been explained. Furthermore, it has been shown that the extracellular miRNAs encapsulated inside the EVs can be transferred to the recipient cells, altering their gene expression and mediating their functional effects [73, 74].

I.3. Extracellular vesicles: new sources of human health information?

Initially, EVs were thought to be membrane detritus with little biological significance. However, Raposo et al. demonstrated in 1996 that these vesicles might trigger the adaptive immune response [12]. Thereafter, several articles have established the relevance of EVs in intercellular communication via the transfer of proteins, lipids, and nucleic acids. The use of EVs for pathology diagnosis or therapy is extremely promising due to their unique biological characteristics and endogenous source. As a result, interest in these vesicles grows year after year. In this section, I will briefly discuss the significance of EVs in the maintenance of normal physiology, as well as their potential clinical use for new perspectives in medicine, both diagnostically and therapeutically.

I.3.1. Biological role

The biological functions of EVs differ depending on the cell type from which they are derived, and hence on what they carry. In fact, they can operate as a signaling complex, delivering membrane receptors and other proteins to target cells, or altering their phenotypic via horizontal genetic information transfer. Inflammation and immunological response, intercellular communication, cell survival, angiogenesis, coagulation and waste disposal represent the major biological activities reported on EVs [75]. An implication in stem cell biology and different aspects of early development have also been confirmed quite recently [76]. Despite these findings, several physiological functions of EVs remain unclear due to the difficulties in investigating endogenous vesicles in vivo. However, significant attempts have been undertaken to develop in vivo models to better understand EV physiology [77].

I.3.2. Pathological role

EVs play an important and complex role also in some pathologies. The role of EVs in cancer biology has been widely investigated. Cancer cells are able to release EVs that promote tumor growth by boosting angiogenesis [78]. They can promote invasive growth of the tumor mass by degrading the extracellular matrix [79], and carry oncogenes that induce the transformation of the phenotype of the target cells, favoring metastasis formation [80]. Moreover, cancer EVs protect cancer cells by allowing them to evade apoptosis and develop resistance to chemotherapy [81, 82], and finally they have the ability to escape the immune system [83].

Beyond tumors, EVs have also been linked to the spread of neurological disorders. In Alzheimer's disease, EVs carrying amyloid beta (A β), the toxic protein responsible for the formation of amyloid plaques, as well as hyperphosphorylated protein Tau, were shown to promote their deposition in several areas of the brain and to hijack the secretory endosomal pathway in the recipient neurons [84, 85]. Similarly, α -synuclein monomers, oligomers and fibrils can be found in the lumen as well as on the surface of EVs, contributing to the progression of Parkinson's disease [86]. Other studies have shown that EVs have a role in the development of infectious diseases by increasing the movement of receptors, virulence factors, and genetic material across cells, resulting in pathogen spread and harmful effects [87, 88].

1.3.3. EVs as a source of promising biomarkers

A biomarker is defined as “a characteristic that is objectively measured and evaluated as an indicator of normal biological processes, pathogenic processes, or pharmacological responses to therapeutic intervention” [89]. The use of a biomarker therefore offers information about a patient's medical status, allowing for more precise diagnosis and prognosis, as well as assessing the success and compatibility of therapeutic treatments. As a result, it must be pathological specific, i.e. capable of identifying only patients presenting a given disease, as well as sensitive, i.e. capable of detecting as many ill patients as possible. A biomarker must also be robust (show a link between the biomarker and the physiopathology of the disease) and ideally predictive (the biomarker must be correlated with the severity of the pathology) [90]. When a diagnostic test is based on a biomarker assay, a cut-off value is established. This is the value used to classify subjects as either healthy or sick. With the growing evidence that EVs contain a biologically active cargo that reflects the pathophysiological state of the parent cell, their potential use as a source of biomarkers in the identification of diseases in a non-invasive manner has increased significantly.

Many EVs studies focused on their application in identifying different cancers at their earliest stages and understanding their progression [91-96]. Exploiting EVs' content has resulted in the identification of different potential biomarkers. Table 1 provides a list of relevant biomarkers from EVs found in different biological fluids, which have been investigated in individuals with different pathologies. It is interesting to note that EVs are currently being explored mostly in cancerology and neurology. In addition, it can be noted that the EVs markers used are, in most cases, genetic material and more particularly microRNAs.

Table 1 : Biomarkers from EVs used in the diagnosis of different pathologies.

| Pathology | Biofluids | Identified biomarker | References |
|---------------------|--|---|------------|
| Ovarian cancer | Ascitic fluid | HNRHPU, U2AF2 | [97] |
| | | TGM2 and U2AF1 | [98] |
| | Urine | miR-30a-5p | [99] |
| | Plasma | TGF- β 1 et MAGE3/6 | [100] |
| | | Claudin-4 | [101] |
| Serum | miR-21, miR-141, miR-200a, miR200c, miR-200b, miR-203, miR-205 and miR-214 | [91] | |
| Blood | miR-21 | [102] | |
| Prostate cancer | Urine | TM256,LAMTOR1 | [103] |
| | | PCA3, TMPRSS2:ERG and SPDEF | [104] |
| | | miR-196a-5p, miR-501-3p, miR-141 and miR375; miR-107 and miR-574-3p | [105, 106] |
| | Plasma | miR-1290 and miR-375 | [107] |
| Lung cancer | Saliva | IQGAP, MUC5B, BPIFA1 and CRNN | [108] |
| | Serum | miR-1247-3p | [109] |
| | Urine | LRG1 | [110] |
| Glioblastoma | Serum | EGFRvIII (mRNA) | [111] |
| | CSF | miR-21 | [112] |
| Alzheimer's disease | Blood | A β 42, pT181-tau, | [113] |
| | | pS396-tau, total-tau | |
| | | IRS-1 | [114] |
| | | miR-193b | [115] |

| | | | |
|-------------------------------|--------------------|---------------------------------|-------|
| Parkinson's disease | Plasma | α -synuclein | [116] |
| | Saliva | α -synuclein | [117] |
| Amyotrophic lateral sclerosis | CSF, plasma, serum | TDP-43, NfL, phospho-NfH | [118] |
| Multiple sclerosis | Serum | hsa-miR-122-5p, hsa-miR-196b-5p | [119] |

EVs are also involved in metabolic, cardiovascular and renal disorders, making them possible biomarkers of other diseases [120-123]. The ClinicalTrials.gov database was utilized to summarize information on ongoing and completed clinical studies that employed EVs for diagnosis purposes. 75 clinical studies were found using the keyword "exosome" (see table A in the appendix). Whereas, using "extracellular vesicle", only 20 additional ones were obtained (see table B in the appendix). The majority of these studies are conducted cancer, respiratory tract, urogenital and gastrointestinal diseases diagnosis. Among these 95 studies, 61 are in recruiting phase, 8 are ongoing and 26 have been completed.

However, only a small number of patents have been submitted, and some of them have resulted in the first commercially viable diagnostic based on EVs. At the beginning of 2016, Exosome Diagnostics, Inc. of Cambridge (now part of Bio-Techne), introduced the first CLIA-validated exosome-based clinical liquid biopsy test, the ExoDx Lung (ALK), to detect the echinoderm microtubule-associated protein-like 4 (EML4)-anaplastic lymphoma kinase (ALK) fusion transcripts in the plasma of lung cancer patients [124]. Last year, Bio-Techne's Exosome Diagnostics launched ExoDx™ Prostate Test At-Home Collection Kit, a urine-based test that assists both physicians and their patients with determining if a prostate biopsy is needed when patient has an ambiguous prostate-specific antigen (PSA) test result (see Fig. 5). In 2019, Avalon GloboCare developed the world's first saliva-based exosomal microRNA biomarker, miR-185, as a dual diagnostic and therapeutic target for oral cancer. Exosomics (Siena, Italy) also provides RNA and DNA extraction kits from intravesicular contents for liquid biopsy and cancer screening. A few milliliters of plasma are collected for the isolation of EVs by two different methods. The "SeleCTEV" technology captures EVs by an affinity method with peptides while the "SoRTEV" system captures them by beads coated with specific antibodies against surface antigens. Exosomics also markets analytical assays, based on ELISA or PCR (Polymerase Chain Reaction) type platforms. Caris Life Sciences (Dallas, USA) has also developed an immunocapture method called "Carisome" that allows for the capture of EVs from blood onto coated beads and the detection of specific fluorescently

tagged surface proteins. A preliminary test based on a blood sample is now available for the diagnosis of prostate cancer and offers higher sensitivity and specificity than the currently used prostate-specific antigen (PSA) test. Finally, Exosome Sciences (San Diego, USA) is developing an ELLSA (Enzyme-Linked Lectin-Specific Assay) test to isolate biomarkers such as TauSome, a non-invasive marker of chronic traumatic encephalopathy from a blood sample.

However, transitioning from basic research to clinical validation and industrial manufacturing is still challenging. The primary issue is the lack of standardization of EV isolation procedures. This has an effect on the repeatability of the results, as well as the identification and confirmation of the discovered biomarkers. Beside the purification protocols, the procedure utilized to collect the biological fluid containing the EVs, as well as the storage conditions, can also have an impact on the quality and purity of the isolated EVs and therefore on biomarker identification. Indeed, they can alter the protein content of isolated vesicles, but they can also cause EV aggregation. As a result, the diagnostic test's performance is affected [125]. Moreover, it is critical to identify specific subtypes of EVs because distinct vesicles might have diverse biological effects. Several molecules transported by EVs have therefore been identified as potential biomarkers, but further studies are required before they can be used to diagnose diseases.

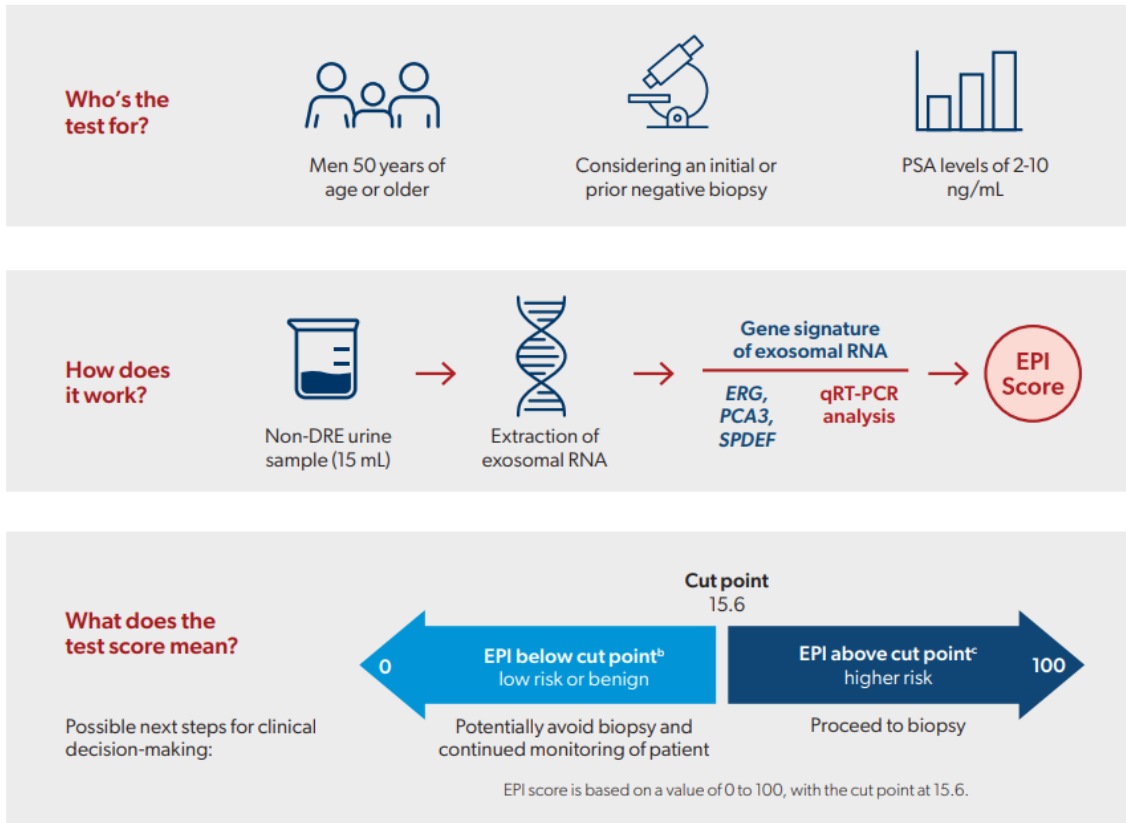


Figure 5: A graphical illustration of ExoDx Prostate Test (EPI) workflow. RNA is isolated from urine exosomes to examine the expression of three genes (PCA3, ERG, and SPDEF) linked to high-grade, aggressive prostate cancer. The RNA expression levels of these three genes are then included into an equally weighted proprietary algorithm and a personalized risk score. Reprinted from (<https://www.urologytimes.com/view/the-role-of-the-exodx-prostate-test-in-early-detection-of-prostate-cancer>)

1.3.4. Therapeutic potential of EVs

Considering that EVs have an inherent biological impact that modifies the phenotypic of the receiving cell, the scientific community is increasingly trying to exploit EVs for therapeutic purposes. One area where EVs have found application is regenerative medicine. The objective of regenerative therapy has always been to find stem cells that can be safely transplanted into a patient and successfully repair the injured organ, freeing it from the difficulties of the immune response. Mesenchymal stem cell (MSC)-derived vesicles are an example of how EVs may be used. Mesenchymal stem cells are multipotent adult stem cells capable of differentiating into many cell types such as osteoblasts, chondrocytes, myocytes and adipocytes. Due to their properties, numerous studies have been carried out on the intravenous administration of MSCs in order to treat various pathologies. However, researchers have revealed that the therapeutic activity of MSCs is mainly attributed to their secretome, including EVs

[126]. As a result, MSC-derived EVs have been investigated as potential therapeutic agents with regenerative properties, including protective effects in models of myocardial ischemia [127, 128], chronic myocardial infarction [129], liver injury [130], neural injury [131] and chronic wounds [132]. Furthermore, MSC-derived EVs are being studied for a variety of inflammatory diseases due to their immunomodulatory characteristics. Several papers discuss also the use of EVs in cancer therapy [133]. These vesicles have several advantages: they have no tumorigenic potential since they cannot replicate unlike cells they are easy to handle and they can be sterilized by filtration [134].

EVs have also been exploited as vehicles to deliver small molecules and drugs. Because of their small size, EVs can avoid clearance by the mononuclear phagocyte system, extending the circulation time required for passive targeting of cancer cells and inflamed tissues. EVs can also penetrate biological barriers like the blood-brain barrier, making them useful for drug delivery to the central nervous system. Finally, because EVs are endogenous biological vesicles with great biocompatibility, they are well tolerated [135]. Although the preclinical results are intriguing, a few clinical trials on EVs have been used for therapy to date [136].

However, the use of EVs in the treatment of pathologies brings also several drawbacks. A large number of EVs is required for the treatment of a single patient. This implies that a high number of cells are required, followed by the ability to separate EVs in accordance with acceptable laboratory procedures.

EVs have also been explored as a platform for vaccination, by delivering disease-associated antigens [137]. This fundamental approach was evaluated *in vitro* with EVs loaded with the viral spike S protein against the SARS-CoV-2 coronavirus, offering insight into the possible use of EVs for SARS-CoV-2 vaccination [138].

I.4. Concluding remarks

As mentioned in the preceding paragraphs, EVs are very promising biological objects for diagnostic and therapeutic purposes. However, scientific interest in EVs is still relatively new, and current research presents several hurdles. Different aspects must be optimized in order to increase the knowledge on the functions of EVs and their potential. The nomenclature of EVs must be standardized to clarify the different types of EVs, which are very complex to identify with precision. The biogenesis of EVs must therefore be better understood. Additionally, current isolation and quantification protocols are not considered fully robust, therefore new techniques need to be implemented and standardized. These techniques must also be developed in such a way that they enable for the isolation of distinct EV subpopulations. To get pure EV samples and offer a thorough investigation of the exosomal signature,

robust isolation and characterization approaches are required. The next section discusses isolation and characterization approaches, as well as developing technologies to address the limits of existing methods.

Chapter II: Current methods for EVs isolation and characterization

II.1. EVs extraction and isolation

The interest in EVs has resulted in the development of several isolation and purification techniques from various culture media and biological fluids. EVs investigation/exploration is being hampered by a lack of uniformity in the techniques for isolating, storing, and measuring or characterizing these vesicles. The data obtained by the different research groups which employ different isolation protocols or even techniques are often contradictory, limiting the use of these vesicles for diagnosis or therapeutic monitoring. A high yield of extraction and a good repeatability of EV purification/isolation procedure are a prerequisite before investigating deeper EVs for health application. It is also mandatory to maintain their integrity and stability and to avoid contamination by other vesicles or cell components (purity) during these isolations. Only by meeting all these criteria of high yield, high purity, high reproducibility we will be able to get representative batches of the whole EV population and prevent unacceptable batch-to-batch fluctuations. When dealing with such vesicles, however, a number of technical considerations must be considered, including their small sizes, their fragility, as well as their propensity to aggregate or lyse. Since the separation of EV subpopulations from each other is still very complicated with existing techniques and reported works, the terms exosomes and extracellular vesicles will be used interchangeably throughout the rest of this chapter. In this section, we will go through the most common macroscopic techniques reported for preparing and isolating EVs, presenting for each of them their advantages and disadvantages. It will be addressed the many aspects of distinct techniques, including separation efficiency, EV yield and the qualities of isolated EVs.

II.1.1 Ultracentrifugation (UC)

According to a global survey of techniques used for EV isolation made in 2016 and submitted to all ISEV members, ultracentrifugation is the most widely used primary isolation method (> 80 % of respondents) [139]. When a heterogeneous suspension is subjected to centrifugal force, the particles it contains sediment according to their density, size and shape. There are 2 types of ultracentrifugation-based techniques (Fig. 6), differential ultracentrifugation and density gradient ultracentrifugation. Figure 4 highlights the major centrifugation and ultracentrifugation steps; however, specific

parameters such as rotation speed and centrifugation duration must be adjusted according to the rotor in use and starting sample viscosity.

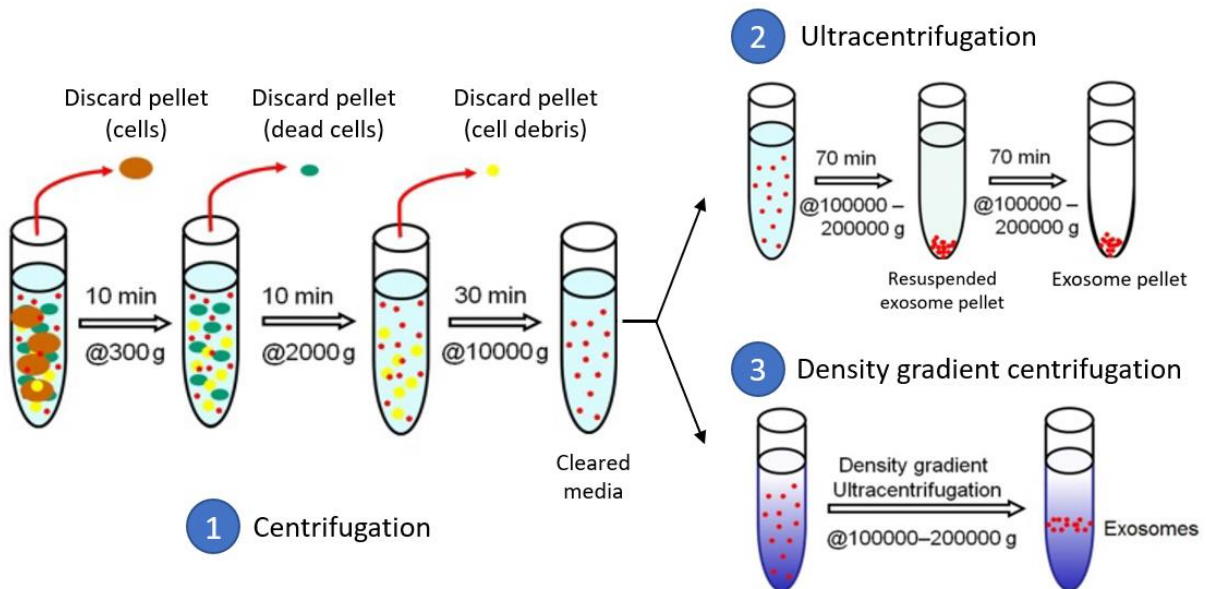


Figure 6: Ultracentrifugation-based isolation methods used for EVs. (1) First successive rounds of centrifugation are intended to pellet consecutively cells (alive and dead) and debris. EVs are then separated and enriched using either several cycles of centrifugation (2) or after prolonged centrifugation in a gradient medium (3). Readapted from [140].

II.1.1.1. Differential ultracentrifugation

Differential centrifugation consists in applying several cycles of centrifugation at different acceleration and duration. Théry et al proposed the approach shown in figure 7 for the isolation of exosomes. First, to eliminate dead cells and cellular debris, the culture supernatant or biological fluid containing the exosomes is centrifuged at 300xg and again at 2,000xg. After that, the supernatant is centrifuged at 10,000xg to eliminate bigger vesicles, then the supernatant is centrifuged at 100,000xg for at least 1 hour. This protocol and variation of it (centrifuge time, speeds) have been extensively utilized by different teams. A rinse procedure is recommended to remove any potential protein aggregate that may have co-precipitated with EVs. Exosomes are typically washed in a PBS solution before being centrifuged at 100,000xg. Although this approach is widely used, it is still highly reliant on the viscosity of the medium. As a result, differential ultracentrifugation is less efficient when dealing with viscous

samples like serum and plasma [141]. This method offers however several advantages. Indeed, this approach is quite simple to use because it requires minimal technical skill and does not necessitate pre-processing of the samples. However, we must keep in mind that it is time consuming, impurities (such as lipoproteins, aggregates, microparticles, MVs etc.) may still be present, and EVs can cluster together or deteriorate, resulting in artefacts during analysis [142].

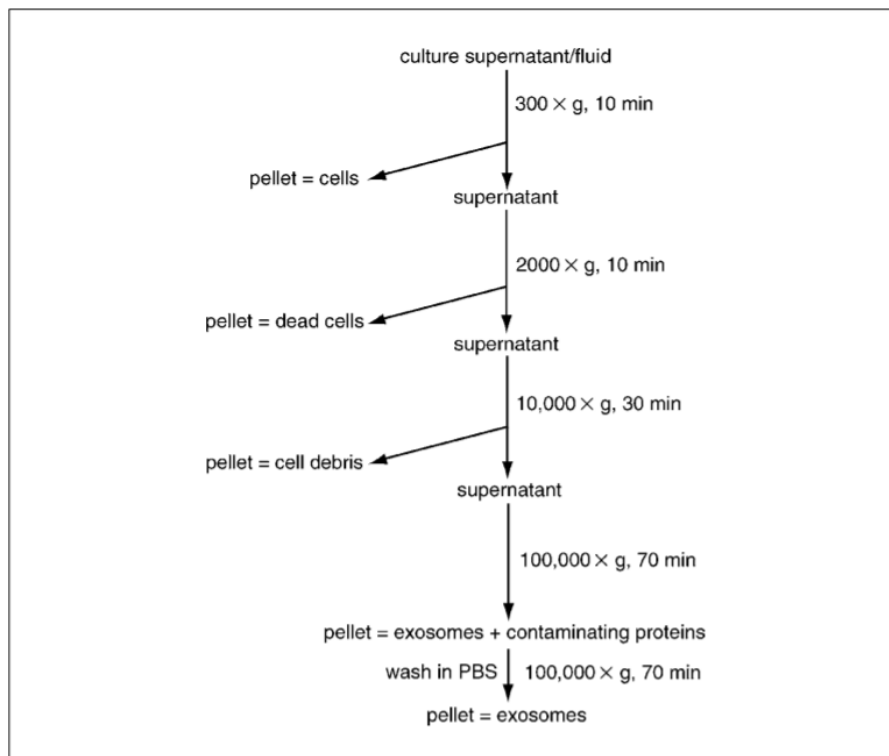


Figure 7: Workflow for the differential ultracentrifugation-based exosome purification method. Pellets (cells, dead cells, and cell debris) are eliminated after the first three centrifugations, and the supernatant is kept for the following step. After the two 100,000 g centrifugations, the pellets (exosomes + contaminating proteins, exosomes) are preserved, while the supernatants are discarded. Reprinted from [143].

II.1.1.2. Density gradient ultracentrifugation

Density gradient centrifugation is a technique for isolating EVs based on the size, mass and density of the vesicles. The vesicles are ultracentrifuged at high speed (at least 100,000g) in a tube containing a concentration gradient of one molecule, usually a sucrose or iodixanol (Optiprep) gradient. Several investigations have shown that iodixanol is better than sucrose for density gradients because it can generate isosmotic solutions at varying densities while preserving vesicle size and structure [144]. The

various molecules sediment over the gradient and coalesce at their distinct densities during centrifugation. As a result, the exosomes will not settle at the bottom of the tube, but rather in a single zone based on their density, which ranges between 1.13 and 1.21 g/mL. The exosomes must next be washed using ultracentrifugation to remove the molecule from the gradient. This approach is well recognized for allowing the separation of subcellular components like mitochondria, peroxisomes, and endosomes, and it is considered as one of the finest ways for EV isolation [145]. However, since the densities of several types of EVs and other chemical components in the sample overlap, this approach cannot reliably separate a single type of EV [146, 147]. As demonstrated, a double sucrose cushion comprising two layers containing 1 and 2 mol/L sucrose in D₂O may effectively reduce non-EV protein contamination of the target fraction [148, 149]. This process, however, results in significant EV losses and low yields, is complicated, time consuming (up to 2 days), and costly [150, 151]. This variation of ultracentrifugation technology produces EV fractions of better purity; nonetheless, as with conventional ultracentrifugation, it needs high-volume sampling, making it unsuitable for low-volume clinical samples.

II.1.2. Ultrafiltration (UF)

Ultrafiltration may be used to separate EVs from their biological fluid based on their size and molecular weight utilizing semi-permeable membranes coupled with small centrifugation cycles [152, 153]. In comparison to ultracentrifugation procedures, ultrafiltration is quicker and do not require specific equipment. The molecular weight cut-off (MWCO) ranges from 10 to 100 kDa for ultrafiltration, and the most often utilized membrane is regenerated cellulose with a 100 kDa pore size [154]. Vergauwen et al., on the other hand, revealed that regenerated cellulose membranes with pore sizes of 10 kDa recovered the most EVs, whereas other tested filters recovered less than 40%, when using plasma, urine, and EV-spiked PBS [155].

Tangential flow filtration (TFF), also known as cross-flow filtration, is a more advantageous alternative ultrafiltration technique to classical centrifugal one, in which the fluid flows directly through the membrane, resulting in cake formation that clogs the pores and, as a result, EV loss [156]. In TFF EV-containing fluids moves tangentially over the membrane and smaller molecules which pass through the membrane are eliminated, whereas bigger molecules, like EVs, stay above membrane and are recirculated and concentrated (Fig. 8).

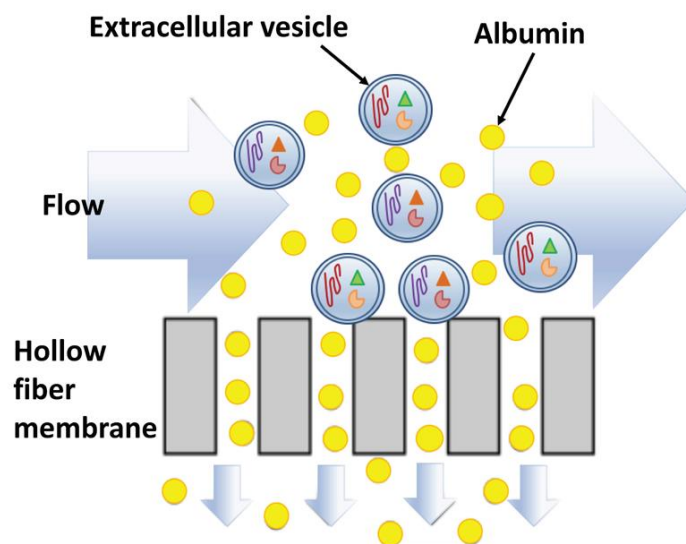


Figure 8: Schematic representation of TFF. Biological fluids travel over the ultrafiltration membrane. Smaller molecules pass through the membrane while larger molecules, such as EVs, remain on the membrane. Reprinted from [156].

Busatto et al. reported that TFF resulted in a one to two orders of magnitude improvement in EV recovery per million cultivated cells ($\sim 10^{10}$ EVs/ 10^6 cells vs 10^8 EVs/ 10^6 cells) and improved batch-to-batch repeatability when compared to ultracentrifugation. Albumin removal was also superior by a factor of 40 [156]. Sequential centrifugal ultrafiltration may also fractionate EVs. In the procedure reported by Xu et al., two EV subtypes were identified from a human colon cancer cell line by using consecutive hydrophilic polyvinylidene difluoride membranes with 0.65, 0.45, 0.22, and 0.1 μm pores [157]. Finally, while ultrafiltration alone may be adequate for EV separation in certain circumstances, combined to other methods (such as size exclusion chromatography), it may bring extra purity and selectivity [158-160].

II.1.3. Size-exclusion chromatography (SEC)

Using size exclusion chromatography (SEC), EVs can be separated from biological fluid based on their hydrodynamic diameter. First, the material is centrifuged to eliminate dead cells and debris that might clog the column. The medium is then pushed through a column packed with porous spherical polymer beads whose pores have a specific calibrated size (Fig. 9). Larger particles, such as EVs, elute first because they cannot penetrate the pores and hence flow around the resin. Particles smaller than the isolation range penetrate the pores and elute later. Cross-linked agarose beads (commercially known

as Sepharose® (CL-2B and CL-4B) and Sephacryl® S-400) are the most often utilized stationary phase materials [154].

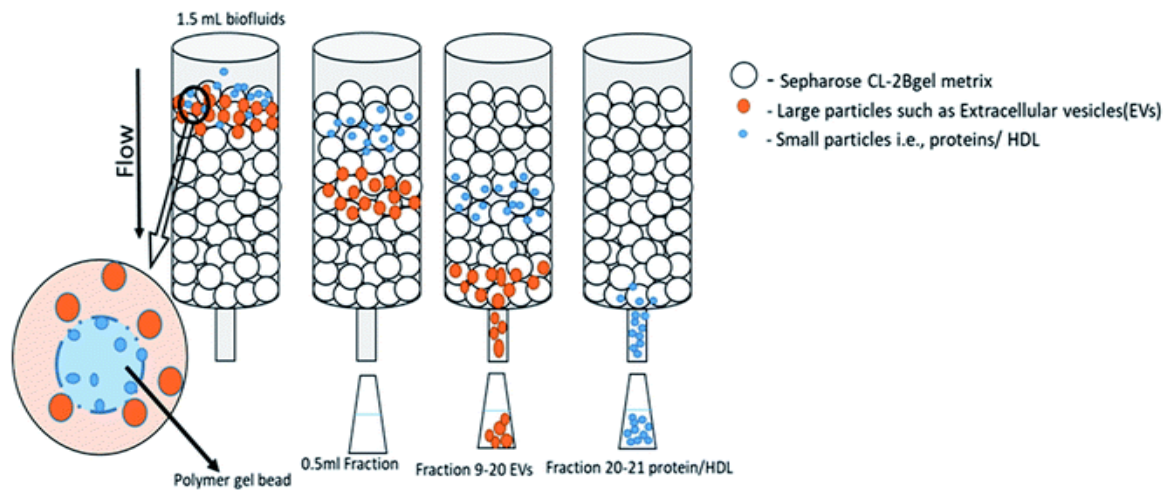


Figure 9: Schematic representation of size-exclusion chromatography principle. From a heterogeneous sample comprising EVs and other molecules, the small contaminating molecules, such as protein aggregates, seep into the pores and are eluted later, whilst EVs are eluted in the early fractions. Reprinted from [161].

Recently, Izon™ released chromatography columns called qEV Original, which are available in two isolation ranges (35 nm and 70 nm). The 70 nm qEV columns have an optimum recovery of particles from 70 nm to 1000 nm, while the newer 35 nm ones have an optimum recovery range of 35 nm to 350 nm. Takov et al. recently evaluated ultracentrifugation and qEV using rat plasma and found that SEC achieves a greater particle yield based on the estimation of the concentration of two EVs markers (CD81 and HSP70) than ultracentrifugation (ultracentrifugation yield was barely a fourth of the EVs-containing SEC fraction yield). However, the SEC-derived EVs exhibited much worse purity, resulting in a 30 times higher concentration of a lipoprotein marker (APOB) compared to ultracentrifugation samples [162]. Purity was increased by using two Sepharose SEC columns with identical stacking volumes but differing column lengths (56 mm and 222 mm). While EV particle size distribution and yields were the same, protein and immunoglobulin contamination was reduced by 90% [163]. It is worth noting that SEC protects more EV functionality and integrity thanks to the use of gentle mobile phases like PBS. In this thesis we have principally worked on EVs provided by Excilone, which employs qEV columns to isolate EVs from pony plasma / serum and human plasma. Paper 3 in Chapter IV.4. will go into further depth.

II.1.4. Polymer-based precipitation

Isolation of EVs by precipitation is a preferred solution for users with limited technological resources in the laboratory. Water excluding polymer, mostly polyethylene glycol (PEG), have recently been employed to provide an affordable and efficient alternative for EV isolation. Numerous commercial exosome isolation kits are now available, such as ExoQuick (System Biosciences), Total Exosome Isolation (TEI) Reagent (Life Technologies), ExoPrep (HansaBioMed) and Exosome Purification Kit (Norgen Biotek), for EVs isolation from plasma, serum, cerebrospinal fluid and cell culture medium. These commercial reagents generally reduce the hydration of EVs (and therefore their solubility) to cause their precipitation. Next, the precipitated EVs can be isolated easily and reproducibly with low centrifugal forces, avoiding long ultracentrifugation. PEG with molecular weights ranging from 6000 to 20000 Da are commonly used in existing polymer-based EVs precipitation techniques [164-167]. From a technical point of view, PEG-based technique is relatively simple to use, quick and do not require special equipment. PEG demonstrated 10 times higher yield than ultracentrifugation starting from 2 mL of human serum volume (4×10^{10} particles/mL with PEG) [164]. However, its main disadvantage is the co-precipitation of non-vesicular components and the presence of polymers in the final solution [144]. Polymer-based precipitation of EVs is therefore limited if it is not coupled with more resolving techniques. The aqueous two phase system (ATPS) has been shown to isolate EVs with higher purity. Once the sample has been thoroughly mixed with the ATPS solution containing PEG and dextran, the mixture is centrifuged [168]. The EVs then migrate to the dextran phase, which has surface characteristics that are more favorable to EVs. However, because EVs are recovered in a dextran-containing solution that may interfere with standard analytical methods like Western Blotting or RNA separation, further washing steps are required to decrease the amount of dextran in the final suspension [168, 169].

II.1.5. Immunoaffinity capture-based methods

Immunocapture is the most specific and effective approach to isolate EVs [170]. In contrast to previous techniques based on physical properties, the affinity-based technique are based on EVs capture using antibodies against EV surface proteins, which are often covalently linked to magnetic beads. The most widely utilized antibodies target tetraspanin proteins often found on exosome and EV surfaces, including CD9, CD63, and CD81 [60], resulting in kits made by companies like ThermoFisher, Miltenyi Biotec, and Abcam (Fig. 10A). Immunoaffinity chromatography using monolithic materials have been reported as an alternative to magnetic beads to isolate EVs [171, 172]. In particular, Multia et al. established a technique using monolithic disks functionalized anti-CD 61 (specific for platelet-derived

EVs) and anti-CD-9 to isolate EVs from human plasma within 30 minutes (Fig. 10B) [172]. For automated separation and fractionation of EV subpopulations, immunoaffinity chromatography was further coupled online with asymmetrical flow field-flow fractionation (AsFIFFFF) [173].

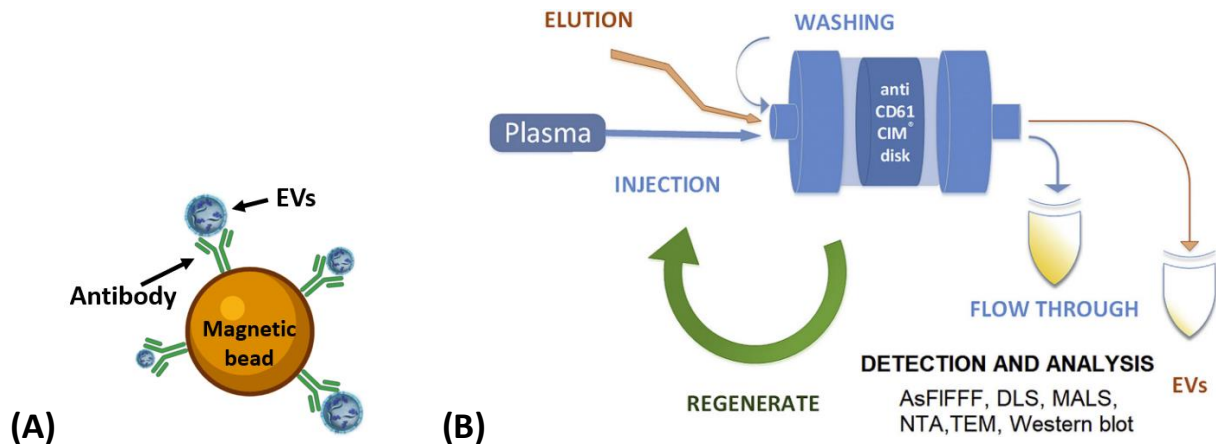


Figure 10: Schematic representation of (A) magnetic bead-based capture with specific antibody against EVs and (B) whole EV separation technique from plasma using the anti-CD61 disk developed by Multia 2019. Diluted human plasma samples are percolated through monolithic disk columns. The enriched EVs are eluted with either ammonium hydroxide (pH 11.3) or carbonate-bicarbonate (pH 11.3). Reprinted from [172].

Affinity-based approaches have the advantage of being rapid, simple, and compatible with laboratory practice. However, one of the major drawbacks is that it could only capture EVs expressing a given specific antigen, potentially excluding other EVs subpopulations concurrently present in a biofluid. Moreover, the sample volume must be small, and it must first be enriched in EVs through ultracentrifugation or ultrafiltration. Furthermore, the strong antibody-antigen affinity may be a limiting factor that prevents the release of pure EVs for further applications. Only a few works on capture and eventual elution of EVs on magnetic beads have been reported. Zhang et al., for example, used magnetic beads coated with CD63-specific DNA aptamers to extract EV from human plasma [174]. The researchers showed non-destructive EV release from aptamers by inserting a complementary sequence that hybridizes with the aptamer, resulting in the aptamer breaking and the release of intact EVs. Song et al. attached two high affinity DNA aptamers specific for CD63 proteins onto magnetic beads and proved that the CD63 aptamers could capture and subsequently release EVs using a simple 0.5 M NaCl elution step [175]. Brambilla et al. exploited DNA-directed antibody immobilization on magnetic beads to facilitate the intact release of vesicles by using DNase I's endonuclease activity

[176]. Nakai et al. used magnetic beads coated with Tim4, a transmembrane protein that binds phosphatidylserine on EVs [177]. Because Tim4-phosphatidylserine binding is Ca²⁺-dependent, intact EVs could be released by adding a chelating buffer. Cai et al. attached anti-CD63 antibodies to superparamagnetic nanoparticles through β -cyclodextrin (β -CD) and 4-aminoazobenzene (AAB) host guest interactions. α -CD was used to elute EVs from the nanoparticles [178]. It was shown that the particle-to-protein ratio of captured EVs using this approach was eight times greater ($8.8 \pm 1.3 \times 10^9$) than that of UC and more than twice as high as that of PEG-based precipitation. Although these procedures effectively release intact EVs, they may have an effect on their physicochemical qualities since they will bear the antibody used to capture them on their surface.

II.1.6. Asymmetric flow field-flow fractionation (A4F)

Another size-based fractionation technique for EV separation is flow field-flow fractionation (FFF), with asymmetrical flow field-flow fractionation (AsFIFFF or AF4). It comprises a small channel with a diameter ranging from 5 to 500 μm and a permeable membrane at the bottom (accumulation wall). The sample is carried along the channel by a laminar flow to detectors. To accomplish size-based fractionation, a perpendicular cross flow to the parabolic one is used to separate EVs on the accumulation wall (Fig. 11).

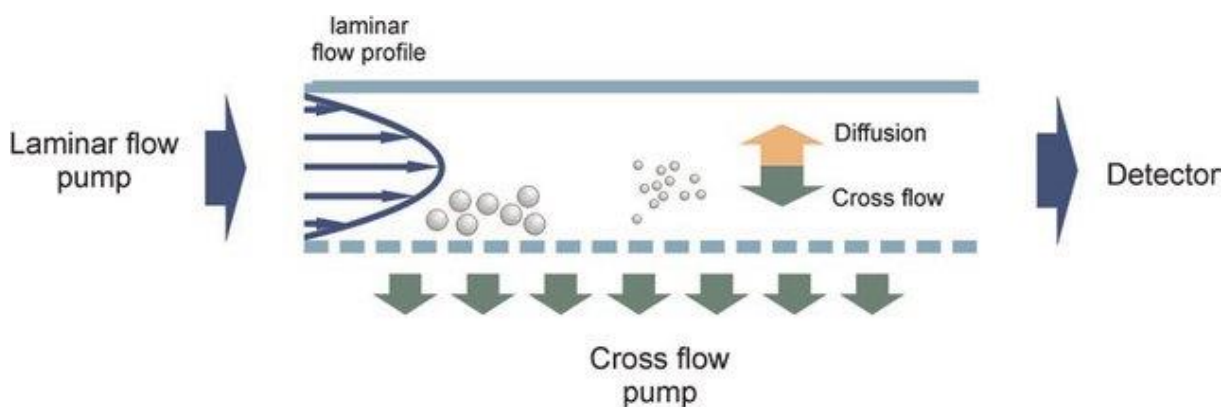


Figure 11: Schematic representation of Asymmetrical flow field-flow fractionation (AsFIFFF) principle. Reprinted from [179].

Then, due to their greater diffusion coefficient, small particles remain far from the accumulation bottom, while larger particles accumulate near to the wall. As a result, the parabolic flow profile transports small particles first, followed by bigger ones, contrary to SEC, which elutes larger particles first. This technique has the advantage of being compatible with several type of detectors that can even be placed in series, such as ultraviolet (UV), multi-angle light scattering (MALS), and

refractometer, providing information on EV size distribution, size morphology and aggregation or agglomeration states. EV subpopulations can also be collected for further studies when combined with a fraction collector. AsFIFFF has proven particularly significant in the separation of EV subpopulations, culminating in the separation of a novel EV subpopulation known as exomeres (~35 nm) (see Fig. 12) [180, 181].

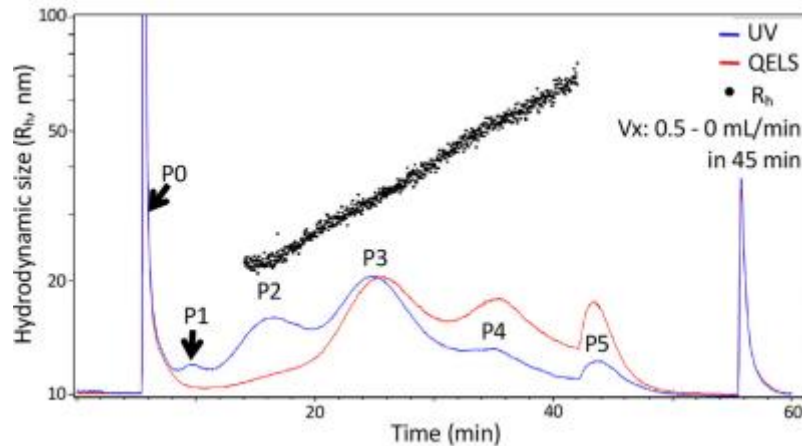


Figure 12: AF4 fractograms of EVs from cultured murine melanoma cell line. Three major peaks (P2, P3 and P4) represented the exomeres and two exosome subsets (small exosomes (Exo-S) and large exosomes (Exo-L) respectively. P0 is the void peak. P5 is due to larger microparticles. Reprinted from [181].

However, AsFIFFF has several disadvantages, which explains why it is not widely used. Indeed, this technique cannot separate particle with the same hydrodynamic radius but having different morphology, surface molecules or other physical properties, its resolution is not high. Only little amounts of sample can be injected to minimize self-association and overloading effects. Furthermore, fractionated EVs collected by AsFIFFF are largely diluted and may necessitate a further pre-concentration step.

II.1.7. Concluding remarks

If many isolation techniques based on different mechanisms are already, none of the above-mentioned EV isolation techniques can combine effectiveness, specificity, good reproducibility and high yield and purity. The choice of one method is mostly determined by the analysis that will be used following the isolation of the vesicles as well as the availability of the necessary equipment.

In conclusion to this presentation on EV isolation strategies, a table comparing the most commonly used procedures is included in our review paper 1 in subchapter III.2. of this thesis (Table 1).

Ultracentrifugation remains the reference method of isolation despite the vesicular pellet is often contaminated with aggregated proteins and lipoproteins, and high-speed centrifugation may cause EV mechanical damage. When the column is commercial, size exclusion chromatography is relatively fast; nevertheless, the available phases are not yet sufficiently resolutive to remove lipoproteins, which have a retention time similar to that of EVs. Polymer-based precipitation using commercial kits is unquestionably the approach with the lowest EV purity. Immunocapture can be used to isolate subpopulations of EVs depending on the marker targeted by the beads. However, the strength of antibody-antigen binding makes dissociation difficult, limiting EV recovery for other uses or analyses. Because different approaches and technologies have benefits and drawbacks and distinct principles for EV isolation, combination of two techniques, like UC with UF or SEC, or even more sophisticated combination of three different methods (UF, SEC, and AsFIFFF), have been recently proposed to reach EV purity while preserving their integrity in a straightforward and high-throughput manner. Among the other new approaches are microfluidic-based tools for fast and efficient EV processing, which will be discussed in depth in Chapter III.. Towards this direction, one development of my thesis was toward a novel method for isolating EVs from pre-purified and biofluid samples using microfluidic droplets.

II.2. EVs analysis and characterization

EVs must be characterized once they have been isolated. This step verifies that the isolated vesicles are EVs, as well as that the population is homogenous and that the vesicles have not been lysed or aggregated. Today, isolated vesicles are often subjected to two distinct kinds of investigation: physical and chemical/biochemical/compositional analysis. Physical analysis provides information on the size and/or concentration of particles. Chemical/biochemical/compositional analysis provides information on the separated vesicles' contents. According to a recent study conducted by Gardiner et al. [139], the most commonly used techniques to study EVs are: Western-blot, particle size measurement techniques (nanoparticle tracking analysis (NTA), tunable resistive pulse sensing TRPS, and dynamic light scattering (DLS)), electron microscopy, and flow cytometry, which represents the gold standard because it is used by nearly 40% of laboratories. There are currently no uniform rules for performing EV characterization. However, in 2018, the International Society for Extracellular Vesicles (ISEV) published a guide to help research teams characterizing EVs [28]. As a result, the following are the primary recommendations:

- Provide an analysis of the protein composition of the EV preparation. The identification and relative quantification of several proteins (at least three) is required since no specific marker for the presence of EVs has been established so far.

- Characterize the heterogeneity of the EV population using at least two distinct methods, in particular techniques for assessing size distributions that must be compared to microscopic observations.
- After demonstrating the function of vesicular proteins or particular RNA species, it is crucial to confirm that these components are derived from EVs and are not co-isolated soluble molecules.

In this section, we will discuss the most often used approaches, as well as their benefits and drawbacks.

II.2.1. Physical characterization

II.2.1.1. Dynamic Light scattering (DLS)

Dynamic light scattering (DLS) is a quite simple technique to determine the size of the particles in a sample ranging from nm to μm size. The vesicles in suspension are subjected to a random Brownian motion whereby small particles move faster than larger ones. A light beam passing through the suspension causes the scattering of laser light at different intensities. The analysis of these intensity fluctuations gives the velocity of the Brownian motion and hence the particle size using the Stokes-Einstein equation. In the case of a polydisperse population, such as EVs, the size distribution is strongly influenced by the large particles, since the intensity of scattered light increases with particle size [182]. Therefore DLS is more effective technique for measuring monodisperse sample [183]. The evolution of the size distribution towards a higher diameter range for the EV populations was observed by Van der Pol et al. [184]. This bias can even render small vesicles undetectable. This is why a preliminary preparation of the samples of EVs aiming to split them into subpopulations is necessary if one wishes to use the DLS.

II.2.1.2. Nanoparticle tracking analysis (NTA)

Nanoparticle tracking analysis (NTA) is a more recent technology that has recently gained popularity. Like DLS, it is based on light scattering and the Brownian motion of suspended vesicles, but this approach allows for individual monitoring of all nanoparticles present in the medium. The sample is loaded in a chamber through which a light beam pass. When moving particles cross the path of the beam, they scatter light. By live tracking the mean squared displacement of a single particle using an optical microscope coupled to a camera, hydrodynamic diameters (D_h) can be determined using the Stokes-Einstein equation (Fig. 13A). As a result, NTA is more suited to measure the size of particles in a polydisperse sample. The non-symmetric profile of the size distribution in Figure 13B, for example, clearly suggests that the examined solution comprises a heterogeneous population of particles [183].

Furthermore, it provides quantitative information because it is possible to know the concentration, namely the number of particles per milliliter present in the population examined. NTA gives information on the size distribution of vesicles between 50nm and 1µm, and the ideal particle concentration is advised to be in the range of 2×10^8 to 2×10^9 EVs/mL [185].

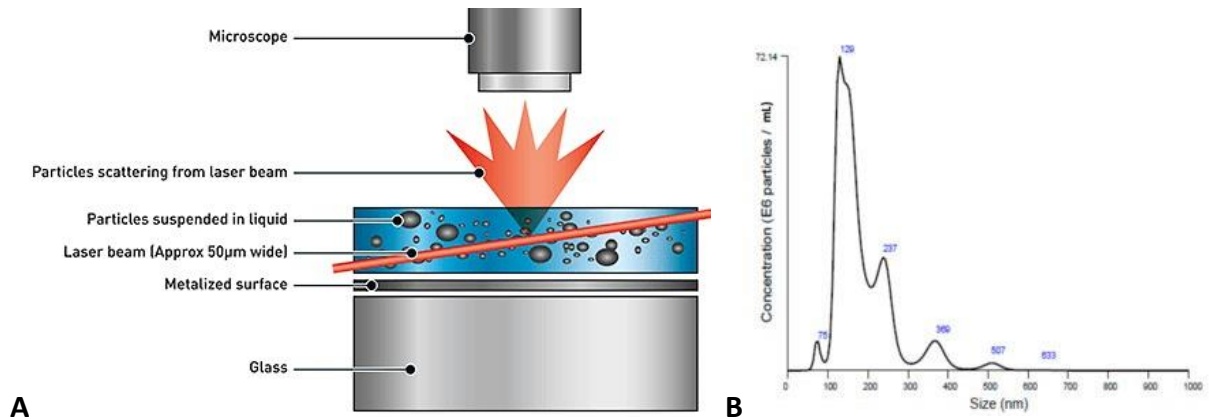


Figure 13 : (A) Scheme of NTA measurement set-up. (<https://www.azonano.com/>). (B) NTA results of EVs released by tumor cells of the gastric cancer cell line GC1401. Reprinted from [183].

If necessary, a fluorescence mode (F-NTA) is also available for the detection of antigens present on EVs surface using specific antibodies coupled to a fluorochrome. This can be particularly interesting in applications involving the characterization of vesicular subtypes or when looking for phenotypic changes in EVs passing from a physiological state to a pathological state [186]. The benefit of using this NTA technique is that the sample can be recovered, the analysis is performed in liquid media with no EV morphological changes. The sample preparation is easy and fast. However, this particle counter-based technique cannot discriminate extracellular vesicles from aggregated proteins. Accurate quantitative measurement may be a challenge that require, sample dilution, camera detection threshold, and focus to be precisely optimized.

II.2.1.3. Tunable resistive pulse sensing (TRPS)

Tunable resistive pulse sensing (TRPS) may be used instead of NTA to determine the concentration and size distribution of EVs. It is based on measuring the electrical resistance generated by the passage of individual EVs through a pore within an insulating membrane (Fig. 14).

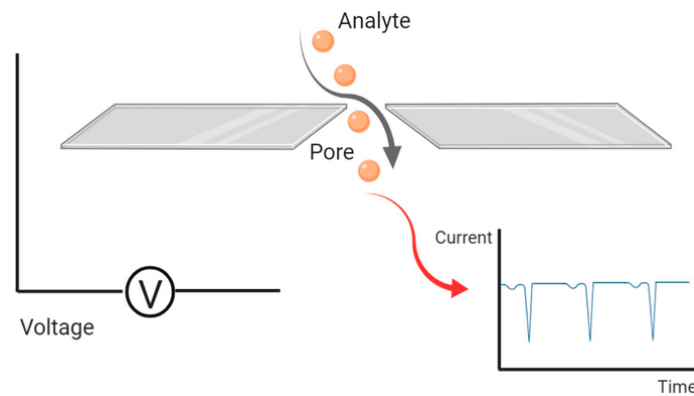


Figure 14: Schematic representation of tunable resistive pulse sensing (TRPS) measurement set-up. Reprinted from [187].

This membrane separates two chambers, each of which contains a single electrode immersed in an electrolyte solution. In this configuration, an ionic current flow between the two chambers, and each particle passing through this pore generates a resistivity peak which amplitude is proportional to the particle's size, while the blockade rate is related to the concentration. In order to measure a polydisperse population of EVs, several pores must be cascaded with different detection limits. Maas et al. demonstrated the influence of pore size on the measured particle concentrations [188]. Depending on their pore size, TRPS instruments can measure particles from 50 nm to 10 μm [189] and recent developments have shown further improvements in measurement stability and sensitivity [190], although lower detection limit are still needed in order to analyze all sizes of EVs. The main problem with using TRPS to characterize EVs is the risk of many particles passing through the pore at the same time (which are identified as a single large particle), and the risk of pore clogging or protein adhesion on the pore surface. Izon Science Ltd was the first company to market the qNano instrument, a bench-top device enabling TRPS application in practice [191]. Thanks to stretchable pores in polyurethane membrane, this equipment can characterize particles ranging in size from 40 nm to 10 μm . TRPS and NTA were recently compared by Akers et al. [192], showing that the NTA detected more EVs smaller than 150 nm, while the TRPS system was more efficient in detecting large EVs.

II.2.1.4. Flow cytometry

Flow cytometry has always been regarded as a robust technique for characterizing cells or micrometric entities. This method employs a laser beam in front of which the EVs pass one by one. The light scattered by the EVs which is proportional to particle size is measured by the flow cytometer. Axial (Forward Scatter or FSC) and orthogonal light scattering (Side Scatter or SSC) light are available, the latter being more sensitive. The principle is shown schematically in Figure 15.

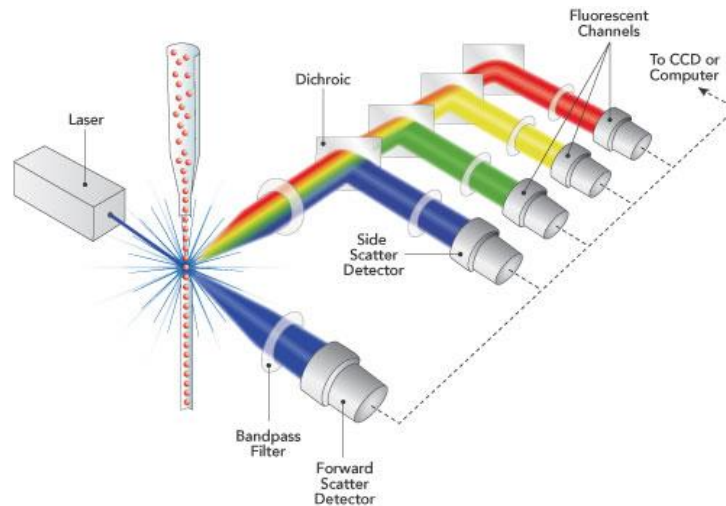


Figure 15 : Schematic representation of flow cytometry system. Reprinted from <https://www.semrock.com/flow-cytometry.aspx>

Most FCM cannot detect particles below 200nm. The EVs can be labeled with different fluorescent ligands, lipophilic fluorophores, or EV specific fluorescent antibodies allowing to identify, in addition to the size, their phenotype and their cellular origin. It is indeed possible to analyze the expression levels of specific surface markers like CD9, CD63, CD81 of EVs. Koliha et al. described an original flow cytometry platform based on multiplexed beads for the analysis of different EV subpopulations [193]. Beads coated with a maximum of 39 capture antibodies were used to form a bead-EVs complex making analysis by flow cytometry possible. However, it is impossible to distinguish EVs from labeled protein aggregates [194]. Recently, Stoner et al. proposed a new high-sensitivity flow called Vesicle Flow Cytometer (VFC) to specifically increase the fluorescent signal associated with EVs [195]. A comparative study showed that the VFC, however, had two to three times fewer EVs than the NTA and the TRPS, perhaps because this system makes it possible to exclude protein aggregates or other particles of similar size [192]. Apogee Flow Systems (Northwood, UK) currently sells a microflow cytometer dedicated to the identification of nanometric particles such as EVs or protein aggregates. A comparative study showed that conventional flow cytometry gave EV concentrations 300 times lower than the comparative analyzes by NTA and TRPS. In parallel, the dedicated Apogee A50 Micro cytometer gave an underestimation by a factor of fifteen of the concentration of EVs . However, as with TRPS, overlapping signals can occur when multiple vesicles are contained in the detection volume concurrently [196]. As a result, the particle concentration range that may be employed to identify individual EVs is limited to between 10^7 and 10^{10} particles/mL [197]. Flow cytometry is still one of the

most used approaches because of its flexibility, but it needs specific equipment, which raises costs and limits accessibility [198].

II.2.1.5. Electron microscopy (EM)

Images of EVs with a resolution of 1 angstrom (\AA) may be obtained using electron microscopy (EM). EVs have a distorted cup-shaped morphology, similar to that of a red blood cell (Fig. 16). The images are obtained either by transmission of the electron beam through the sample (transmission electron microscopy, TEM) or by inelastic scattering of the electron beam on the surface of the sample (scanning electron microscopy, SEM). Because of its higher resolution, TEM is the most often used EM method for characterizing EVs. As EM observations are performed under vacuum, EVs must first be chemically fixed and dehydrated to be observed. The most common sample preparation protocol consists of depositing a drop of liquid sample on the grid, fixing it by chemical treatment with paraformaldehyde [150] or glutaraldehyde [199] and then dehydrating it (Fig. 16A). Sometimes, these chemical treatments are responsible for artifacts on the morphology and size of EVs. Cryogenic freezing, preceding the EM observations, is a preparation technique that is increasingly being used to replace the chemical fixing procedures (cryo-TEM) [199]. However, changes in the size and natural structure of the vesicles may still occur in cryo-TEM owing to the thickness of ice (typically a few hundred nanometers), which can compress the vesicles together. However, changes in the size and natural structure of the vesicles may still occur in cryo-TEM owing to the thickness of ice (typically a few hundred nanometers), which can compress bigger vesicles and make them appear larger. Moreover, the strong intensity of the electron beam can be responsible for damage caused to the EVs [200] (Fig. 16B). However, at the moment, cryo-TEM is the most powerful method for analyzing the morphology of EVs. Finally, TEM may be integrated with immunodetection utilizing antibodies linked to gold particles to detect subpopulations of EVs, as reported by Melo et al. who specifically imaged EVs from breast cancer cells expressing the CD9 protein on their surface [201].

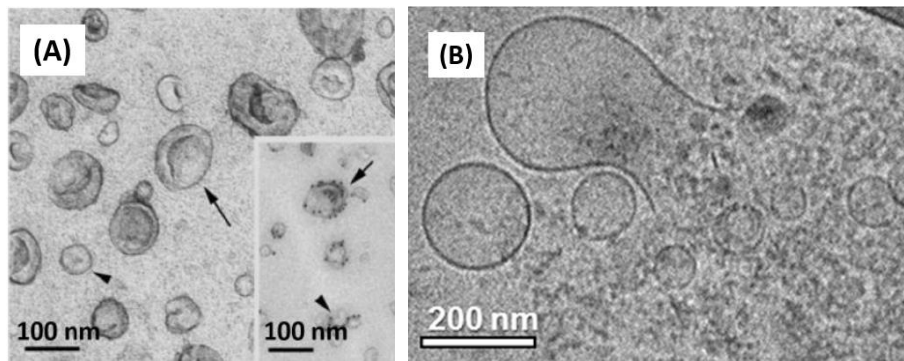


Figure 16: (A) TEM observations of the cup-shaped structure of EVs after chemical fixation. Magnification: Labeling of exosomal MHC class II surface antigens with 10 nm gold particles. Reprinted from [199]. (B) TEM observations of EVs after cryogenic fixation and rupture of the vesicle membrane. Reprinted from [200].

II.2.1.6. Atomic force microscopy (AFM)

Another approach for viewing the surface of EVs and consequently analyzing their morphology is atomic force microscopy (AFM) [202, 203]. It enables the visualization of EVs with nanometric resolution whether they are deposited on a flat surface, in a specific way (captured by specific ligands) or non-specifically (adsorption), in a liquid medium, at atmospheric pressure, and without sample preparation or labeling. AFM is based on the employment of a flexible cantilever with a tip that scans the surface of the sample to produce a topographic picture of the surface (Fig. 17).

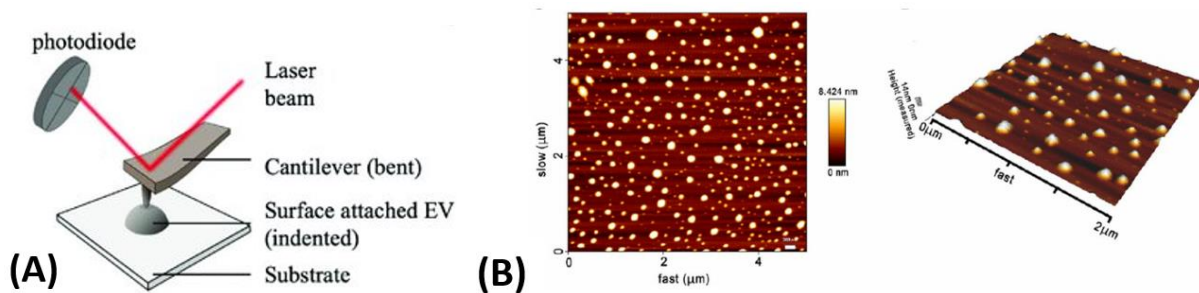


Figure 17 : (A) Schematic representation of the AFM setup. AFM involves the interaction of a cantilever with the sample, and the reflected laser beam is monitored by a photodiode. Reprinted from [204]. (B) AFM image of salivary exosomes from healthy individuals. Reprinted from [205].

Typically, AFM imaging uses mica surfaces coated with antibodies specific to EV surface biomarkers, allowing subpopulation detection [206]. Because the fixation and dehydration processes in the preparation technique might alter the morphology of EVs, the liquid phase is preferred over air for AFM characterization of EVs [207]. The AFM is used to obtain two types of information: the first is

about the topography of the reflected surface, and the second is about the detected structure's local stiffness and adhesion characteristics. However, AFM cannot give quantitative data on EVs. Furthermore, the shape of the EVs can vary when they attach to the surface, causing the vesicles to flatten.

II.2.1.7. Surface Plasmon Resonance (SPR)

Surface plasmon resonance (SPR) is a sensing technique that enables quick, label-free characterization of EVs. It is an optical transduction method frequently used to examine interactions between molecules on the surface of a metal chip (gold or silver). SPR is an approach for quantitatively recognizing biological species in real time by detecting the change in local refractive index caused by contact at the sensor surface. Another benefit of SPR detection is that different ligands can be tested on the same surface at the same time. Zhu et al. reported that six different antibodies were used to detect the EVs (anti-CD9, anti-CD63, anti-CD81, anti-CD41b, anti-EpCAM, anti-E-cadherin) [208]. In recent years, considerable progress has been made in the production and use of plasmonic nanostructures that enhance sensitivity. Im et al. developed a novel platform called nanoplasmonic exosome (nPLEX) sensor, based on transmission SPR through periodic nanohole arrays of 200 nm in diameter, each functionalized with antibodies to identify a molecular signature to detect ovarian-cancer exosomes. This nPLEX platform has 10^4 times the sensitivity of western blot and 10^2 times that of ELISA [98]. In addition to SPR, localized Surface Plasmon Resonance (LSPR), reliant on the use of metal nanoparticles floating in solution or micro- and nano-fabricated metallic structures including gratings, nanopillars, and surface enhanced Raman spectroscopy (SERS), which combines Raman spectroscopy's excellent chemical specificity with exceptional sensitivity achieved by plasmon-assisted scattering of molecules on or near metal nanostructures have been applied to characterize EVs [209]. Other nano-plasmonic devices have been developed, including the one described by Liang et al. [210]. By functionalizing a microarray with anti-CD81 antibodies, EVs were captured and then detected using anti-CD63 and anti-CD9 antibodies coupled to easily identifiable gold nanospheres and nanorods, as shown in Figure 18. This combination produced a local plasmon effect that improved the sensitivity and specificity of EV detection. This technique has been demonstrated on EVs derived from pancreatic cancer and has outperformed ELISA tests in terms of LOD, requiring only 1 μ L of biological sample and 5 hours of analysis, making this device a promising diagnostic tool. This device is now being developed for commercial use.

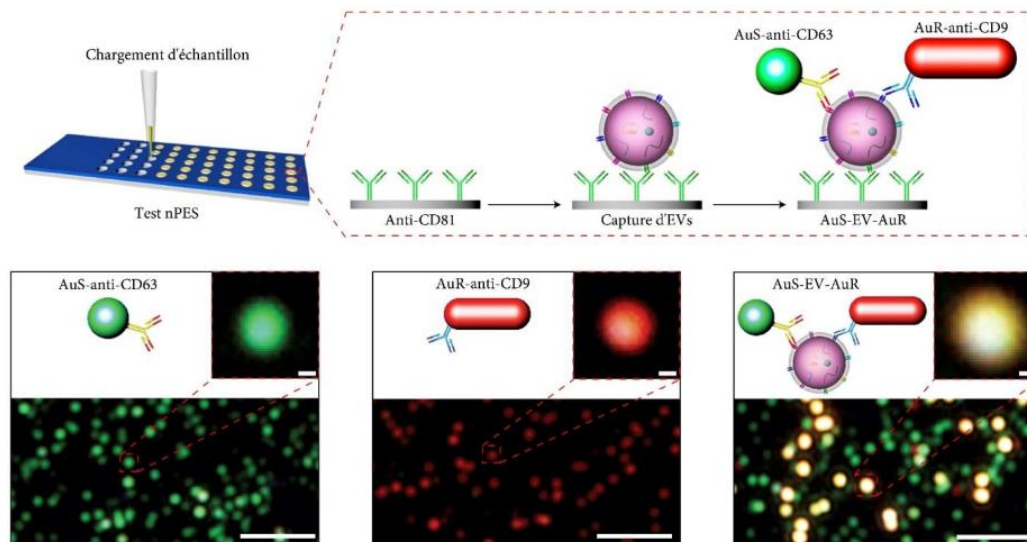


Figure 18: Capture and detection of EVs on the surface of a nanoplasmon-enhanced scattering (nPES) device using antibodies directed against the three tetraspanins. The signal is amplified when the CD63 and CD9 proteins are present on the EVs (yellow signal). Scale bars: main images, 2 μm ; magnified images, 100 nm. Reprinted from [210].

II.2.2. Molecular characterization

II.2.2.1. Western blot (WB) and ELISA

Western blot (WB) is a biochemical method for detecting particular proteins in a sample containing different proteins. WB is frequently used to verify the expression of EV-associated proteins (e.g. CD9, CD81, CD63, Alix, Tsg101) and the lack of contaminating proteins (e.g. Calnexin, Albumin, Fibronectin) in isolated samples [28]. Following EV lysis, the proteins are separated by gel electrophoresis (generally SDS-PAGE) and transferred onto a membrane (often nitrocellulose) before being revealed by specific antibodies. Because contaminating proteins cannot be differentiated from exosomal proteins, WB necessitates meticulous previous purification of EVs. This is why WB identification of the proteins on the surface of the EVs is required but not sufficient to verify the existence of the vesicles in the sample. In addition, the considerable quantity of EVs used in this type of analysis and the duration of manipulation (2 days) do not allow considering the WB as a routine characterization.

Enzyme-Linked Immunosorbent Assay (ELISA) can also be used to analyze specific proteins under different configurations: direct, indirect, in a sandwich, or via competition. The sandwich configuration is often used for EVs. Isolated EVs are captured by an antibody immobilized on a solid support allowing additional washing procedures to remove non-EV-associated proteins. A second antibody that

recognizes trapped EVs is then employed [171]. The use of the ELISA test as a reference for the development of EV detection technologies has been widely demonstrated [210, 211].

Commercial ELISA kits are available, such as ExoElisa-ULTRA (System Biosciences) and Exo-TEST (HansaBioMed) which are designed for the detection of EVs using particular tetraspanin probes (CD9, CD81 ...).

In terms of detection limit and outcomes, the two approaches presented here are similar. They are mostly determined by the efficacy and specificity of the used antibodies. ELISA is quicker and seems to be more suited for routine use. However, it is still difficult to find specific antibodies for each subcategory of EVs. Moreover, the ELISA does not directly measure the number of vesicles in the sample and does not give any information on the physical characteristics (size and morphology) of the EVs.

II.2.2.2. Mass spectrometry (MS)

The protein composition of EVs may be also investigated using liquid chromatography-tandem mass spectrometry (LC-MS/MS). The proteins of the isolated EVs are digested enzymatically and the peptides are then separated using liquid chromatography and ionized before being analyzed by mass spectrometry. Several steps and parameters in this process have a significant impact on the proteome profile of EVs. In addition to efficient EV purification by selecting a good technique to minimize contamination by non-vesicular proteins, the choice of mass analysis and the performance of the mass spectrometer used are also very important. Because mass spectrometry analyzes peptide fragments, identification, quantification, and proper validation of the peptides produced are required. The relevance of proteomic data is determined not only by the stringency of the filters used, but also by the databases consulted during the raw data analysis. Indeed, not all of the databases are updated on a regular basis. Although mass spectrometry necessitates substantial data preparation and processing time, it may enable high throughput, quantitative, and comparative proteomic analyses of EVs. Mass spectrometry has been used to characterize thousands of vesicular proteins [212], which have been compiled in databases such as EVpedia [213], ExoCarta [214] and Vesiclepedia [215]. In addition, other MS-based workflows have been conducted to investigate the lipid and phospholipid content of EVs [216, 217].

II.2.2.3. Nucleic acid analysis

In addition to proteins, EVs include several types of RNAs (messenger RNAs, microRNAs and small non-coding RNAs). The amounts of RNA in biofluids are relatively low, 20–50 ng/mL of total plasma and 5

ng/mL of EV-associated RNA, and numerous approaches have been used to measure and identify distinct types of extracellular RNA in EVs [218, 219]. Conventional nucleic acid extraction and analysis methods have been utilized successfully to establish a solid foundation for our understanding of EV nucleic acids. This analysis consists of the extraction of vesicular RNA using cell-like techniques, followed by conversion to DNA, amplification, and sequencing. A target sequence can be amplified selectively using polymerase chain reaction (PCR) and identified using end-point electrophoresis or real-time fluorescence techniques (RT-PCR) [220]. With a rising interest in using EV nucleic acids as non-invasive diagnostic markers, new biosensor technologies have been developed to allow for more efficient and faster extraction and analysis. Taller et al. developed an ion exchange nano sensor. It consists of two microfluidic systems connected in series. The first enables EV lysis through surface acoustic vibrations. The second uses an ion exchange nanomembrane to detect RNA. By applying an electric current across the membrane, anions are forced through the membrane, resulting in a corresponding current-voltage characteristic (CVC) recorded across the membrane. By functionalizing the membrane surface with capturing oligonucleotide probes, changes in CVC measures may be sensitively and quantitatively detected.

II.2.3. Concluding remarks

In conclusion, each of the approaches presented has advantages but also limits, and none of these techniques allows us to assess simultaneously the concentration, size, and biochemical properties of EVs. A comparison table of the most frequently used procedures for EV characterization is presented in our review paper 1 in subchapter III.2. of this thesis (Table 2). At the present, there is an agreement that multiple of these methodologies should be used in order to obtain an accurate and complete characterization of EVs. Moreover, the most appropriate analysis method for studying EVs must meet several conditions:

- Ensure an analysis of EVs directly in their raw sample or with the minimum possible pre-analytical interventions.
- Enable the biochemical and physical characterization of EVs
- Give access to a quantification / assay of EVs.
- Characterize the vesicles on an individual scale.
- Ensure reproducibility and make automation possible

However, because of their small size, heterogeneity, the presence of contaminants, and the low sensitivity of existing methods, EV characterization remains a challenge.

Chapter III: Emerging methods for EVs isolation, analysis and detection

III.3. Microfluidic-based technologies

In recent years, researchers have developed numerous microfluidic systems for the isolation, detection and analysis of EVs, utilizing both physical and biological characteristics of EVs at the microscale level. Microfluidics has enormous potential by reducing sample volume, cost, and reagent consumption, completing reactions faster, and running multiple assays in small devices at the same time. Additionally, microfluidic systems, on the other hand, are especially appealing for improving the isolation performance of EVs, in part because novel processes may be used and are more efficient in a microfluidic format. In this part, several representative examples of microfluidic-based devices are given, which are categorized into two primary approaches: affinity-based (label-based) and label-free isolation methods.

III.1.1. Immunoaffinity-based microfluidics for EV isolation

Like the widely used immunoaffinity-based EVs separation approach described above, the immuno-microfluidic-based EV separation devices employ antibodies to recognize specific EVs markers. This may be done by covering the inner wall of the micro-channels with antibodies or employing magnetic beads coated with antibodies inside the microfluidic system [221]. Chen et al. pioneered the use of microfluidic affinity methods to extract EVs from human serum or cell culture media using anti-CD63-coated microchannels. Furthermore, the researchers were able to recover RNA by adding a lysis solution to the collected EVs on the microchannel surface and flushing with air, demonstrating the method's potential for cancer diagnostics. [222]. Many microfluidic immuno-affinity systems have been developed since then to enhance interactions between EVs and antibodies and they can be divided into two main types: those with an internal surface covered with antibodies and those that use capture beads. Table 2 lists the main immunoaffinity-based microfluidic approaches.

Table 2 : Immunoaffinity-based microfluidic platforms for isolation of EVs referenced in the literature from 2010.

| Method | Sample | Volume (μL) | Recovery yield (%) | Ref |
|--|---------------|-----------------|--------------------|-------|
| Micro-channels coated with anti-CD63 | Serum | 400 | 42 - 94 | [222] |
| Mica surface coated with anti-CD41 | Plasma | 150 | Not communicated | [223] |
| ExoChip: multi-channel coated with anti-CD63 | Serum | 400 | Not communicated | [224] |
| Capture via functionalized electrodes (CD9, HER2) | Serum | 500 | Not communicated | [225] |
| Filter paper coated with anti-CD63 antibodies and annexin V | Serum | 72 | Not communicated | [226] |
| Microchannel to mix with magnetic beads conjugated with anti-EpCAM, IGF-1R, CA125, CD9, CD63, CD81 | Plasma | 30 | Not communicated | [227] |
| surface plasmon resonance platform (nPLEX) functionalized with anti-CD63 | Ascetic fluid | 150 | Not communicated | [98] |
| RInSE: anti-EpCAM coated polystyrene beads | Plasma | Continuous flow | Not communicated | [228] |
| iMER: magnetic microbeads coated with anti-EGFR | Serum | 100 | > 93 | [229] |
| ExoSearch: micro-sized magnetic beads coated with anti-CD9 | Plasma | 20 | 72 | [230] |
| Nano-IMEX: Y-shaped micro rods coated with anti-CD81 | Plasma | 20 | Not communicated | [231] |
| Functionalized SPR chip with anti-CD9 and/or anti-CD63 | Serum | 250 | Not communicated | [232] |

| | | | | |
|--|--------|-----|------------------|-------|
| On-chip immunocapture with anti-CD63 | Plasma | 900 | Not communicated | [233] |
| Herringbone grooved surface coated with anti-CD9 or EpCAM | Serum | 100 | 60 | [234] |
| ^{EV} HB-Chip: herringbone microfluidic device with antibody cocktail anti-EGFR, EGFRvIII, podoplanin, and PDGFR | Plasma | 90 | 59 | [235] |
| ExoPCD-chip: magnetic beads coated with Tim4 | Serum | 30 | 68.5 | [236] |

Here, we provide two examples to demonstrate the two alternative methods (Fig. 19).

The higher the microchannel's surface area, the more antibodies may be immobilized on the surface, resulting in a higher EVs isolation recovery rate. When Zhang et al. came up with this concept, they decided to utilize graphene oxide and polydopamine (GO/PDA) to create a larger nanoporous structure and greater surface area to immobilize more anti-CD81 antibodies and so capture more EVs (Fig. 19A) [231]. This device, known as nano-IMEX, exhibited on-chip measurement of ovarian cancer-derived exosomes with a plasma sample volume of 2 μ L and a LOD 10^3 -fold greater than benchtop chemiluminescence ELISA.

Functionalized beads are easier to manipulate than the functionalized microchannels mentioned earlier. For a typical example, Zhao et al. recently developed a microfluidic chip, called ExoSearch, that allows continuous isolation of EVs using immunomagnetic beads [230]. The chip consists of a Y-shaped injector and a serpentine fluidic mixer that allows the incubation of three probing antibodies (against CA-125, antiCD-24, and anti EpCAM) labeled with various fluorescent dyes (Fig. 19B). This technique was capable of quantifying ovarian cancer-derived exosomes in patient plasma samples with a LOD of 750 particles per μ L, a sample volume of 20 μ L, and a 40-minute processing period.

Although immunoaffinity-based EV isolation has been proven to be simple and efficient, these techniques may only capture EVs expressing a particular antigen, possibly ignoring other EV subpopulations present in a biofluid. Furthermore, the binding's high antibody-antigen affinity, which is difficult to break, may be a limiting factor that prevents the release of pure EVs for later usage.

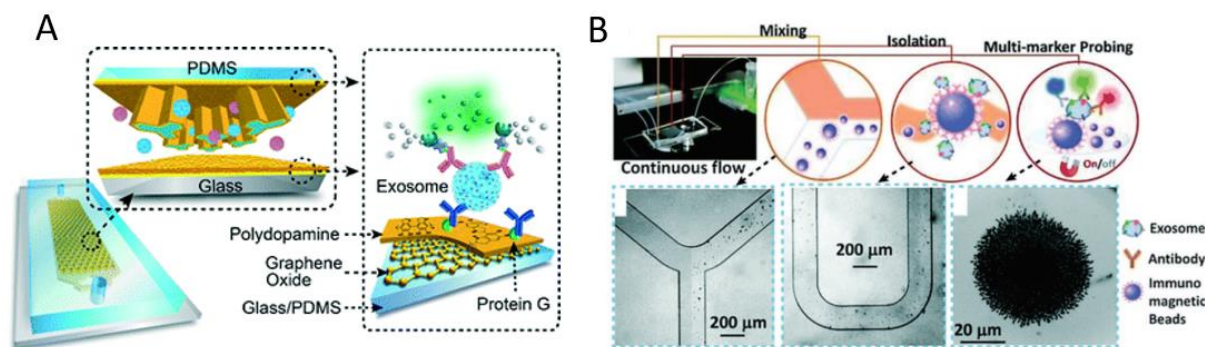


Figure 19 : Examples of immunoaffinity-based microfluidic approaches for EVs isolation. (A) Schematic of the nano-IMEX platform. The surface of the microchannel and micro posts were coated with graphene oxide and polydopamine to capture EVs using anti-CD81 antibody immobilized on protein G. Isolated EVs were then detected using ELISA. Reprinted from [231]. (B) Schematic workflow of the ExoSearch platform continuous mixing, separation, and in-situ, multiplexed detection of EVs. Reprinted from [230].

III.1.2. Label-free microfluidic strategies for EV isolation

Many label-free microfluidic approaches for EV isolation have been developed [237, 238]. They can be divided into two broad categories: active and passive modes. Passive techniques depend mostly on vesicle intrinsic properties (e.g. size or electrical properties). On the contrary, active separation techniques rely on the interaction of intact vesicles with an external force field. Different typical examples of passive techniques are given below. Typically, electrical fields and magnetic fields can be used to manipulate EVs. Readers can refer to section III.2. of this chapter to have some examples of these passive technologies. For exhaustive view of all passive and active strategies, readers can glean from recent reviews [221, 237, 238].

III.1.2.1. Microfluidic filtration

Isolation based on size is an appealing method for separating EVs from big cellular detritus. Several microfluidic filter methods have been designed to separate EVs from big cellular detritus and protein aggregates. For example, exosome complete isolation chip (ExoTIC) developed by Liu et al. is made up of several plastic layers and nanoporous filter membranes with different pore sizes [239] (Fig. 20).

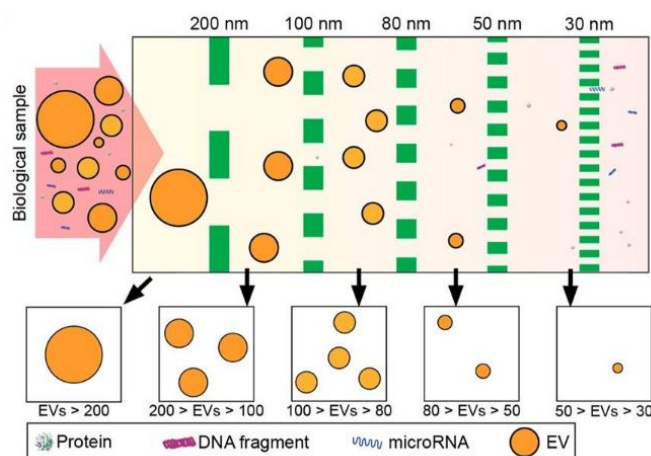


Figure 20 : ExoTIC's scheme. The modular components, which have pore diameters of 200, 100, 50, and 30 nm, are linked in series to separate exosomes of various sizes. Reprinted from [239].

The trapping process was relatively fast (~10 min), with a higher yield than ultracentrifugation. However, the device's recovery performance was shown to decrease with greater sample volumes, most likely due to saturation effects (around 10^{10} EVs/mL from 500 μ L of human plasma)

III.1.2.2. Viscoelastic-flow sorting

When particles of different sizes move through channels in a viscoelastic medium, they migrate in a size-dependent way due to the effect of elastic lift. Viscoelastic fluids are non-Newtonian fluids that show nonlinear viscosity and elasticity under the effect of shear stress. The impact of viscoelastic flow sorting is determined by the viscoelastic medium. For example, Liu et al. used poly-(oxyethylene) (PEO) as the separation medium and found that exosomes smaller than 200 nm were moved by elastic lift forces along the microchannel sidewalls, but bigger vesicles tend to migrate towards the channel midline (Fig. 21). The authors demonstrated a high separation purity (>90%) and higher recovery (>80%) of exosomes than that of ultracentrifugation (5–25%) from cell culture media [240]. Later, to increase separation efficiency and recovery, they employed λ -DNA as a viscoelastic medium and an aptamer-mediated method to fractionate three distinct EV subtypes (30-200 nm, 200-1000 nm and >1000 nm) [241].

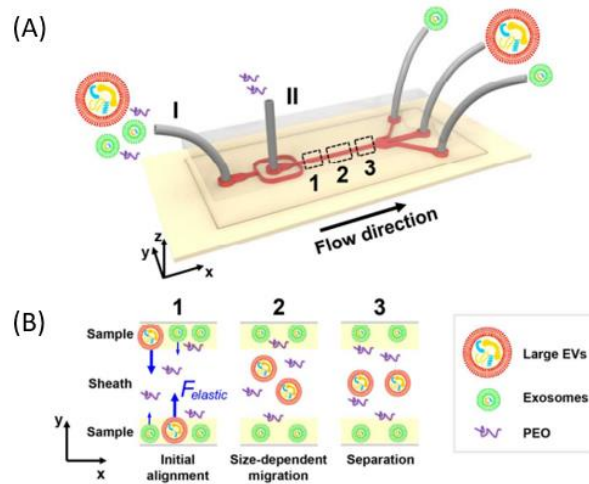


Figure 21 : (A) Schematic of a viscoelastic separation of exosome from large EVs. (B) Separation mechanism in viscoelastic microfluidics. The sheath fluid aligns the sample fluid along the sidewalls. Exosomes and large EVs are driven toward the microchannel centerline by elastic lift forces caused by fluid viscoelasticity, resulting in their size-dependent separation. Reprinted from [240].

III.1.2.3. Deterministic lateral displacement (DLD)

DLD is a passive microfluidic separation approach that employs a gradient of nano-pillar arrays placed within microfluidic channels to geometrically define the critical diameter (D_c). The particle separation concept in a DLD chip is that the flow path of particles bigger than the D_c is altered while the path of smaller particles remains unchanged. Inspired by the DLD technology introduced by Huang et al. in 2004 [242], Santana et al. developed a device to extract exosomes from a heterogeneous EV sample pre-purified from cell culture media [243]. In another paper, Wunsch et al. showed the enrichment and separation of EVs with diameters down to 20 nm at the nanoscale using DLD (Nano-DLD) which yielded rates of $10^4 - 10^6$ particles per minute. [244] (Fig. 22).

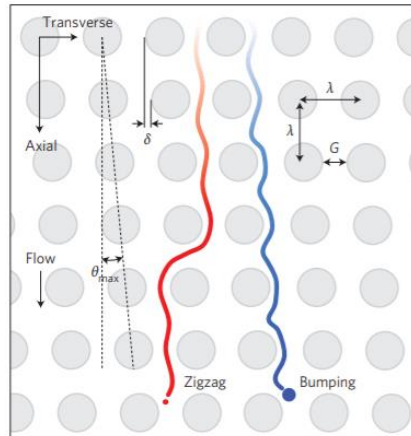


Figure 22 : Schematic representation of the nano-DLD device which is in the form of a matrix formed by a network of pillars spaced from 25 to 235 nm and a maximum migration angle $\theta_{max} = 5.7^\circ$. Trajectories for particles with a particle diameter (DP) less than the nominal critical diameter (D_c) follow laminar flow in zigzag mode (red), while larger ones with $DP \geq D_c$ follow a deviation θ_{max} in a bumping mode (blue). Reprinted from [244].

However, the device requires high pressure due to the dense structure of the network and the restricted experimental time. In fact, the device can function for more than 2 hours before the accumulation of particles at the interface of the input pillar obstructs it and prevents substantial data acquisition.

III.1.2.4. Acoustic separation

Acoustics technique enables a contact-free manipulation of particles on microfluidic devices. This approach employs ultrasonic waves to provide differential acoustic stress on particles in order to separate them depending on size and density. Based on this concept, Lee et al. employed acoustic waves to separate EVs from cell culture media [245]. The device consists of a pair of interdigital transducers to generate a standing surface acoustic wave. Particles in the acoustic region experience radial pressure and migrate. Larger vesicles move faster because the acoustic force is proportional to the volume of the vesicle. Wu et al. described an integrated acoustofluidic device that included a microscale cell-removal module, which eliminates bigger blood components [246] (Fig. 23). In an automated way, this platform was able to isolate EVs directly from undiluted blood samples with both high purity (98.4%) and efficient recovery (82.4%).

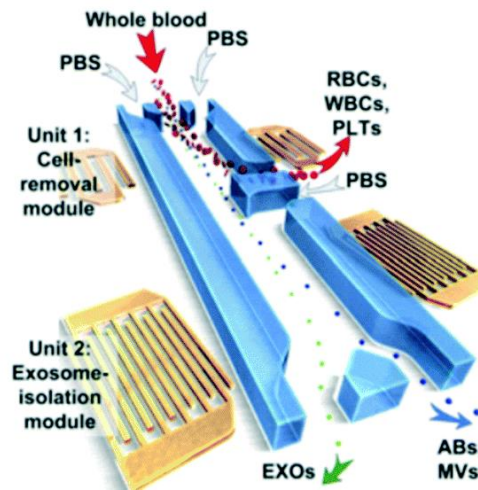


Figure 23 : Schematic of the acoustofluidic module for separation of EVs from whole blood. The cell-removal module removes red blood cells (RBCs), white blood cells (WBCs), and platelets (PLTs), and the EVs-isolation module separates them. Reprinted from [246].

The development of acoustics-based techniques is still in its early stages, but it offers tremendous promise for future applications requiring quick and high-resolution sorting of undamaged EVs. However, biological fluids include several components with comparable size and acoustic properties to EVs, making acoustic separation difficult.

III.1.2.5. Thermophoresis technology

Thermophoresis is a phenomenon observed in mobile particle mixture in which various particle types respond differently to the force induced by a temperature gradient. Liu et al. were the first to use thermophoresis to create a thermophoretic aptasensor (TAS) to combine thermophoretic enrichment and aptamer-based fluorescence labeling to achieve effective EVs profiling [247]. They created a high-temperature zone using a microfluidic system that can be heated by a laser (Fig. 24).

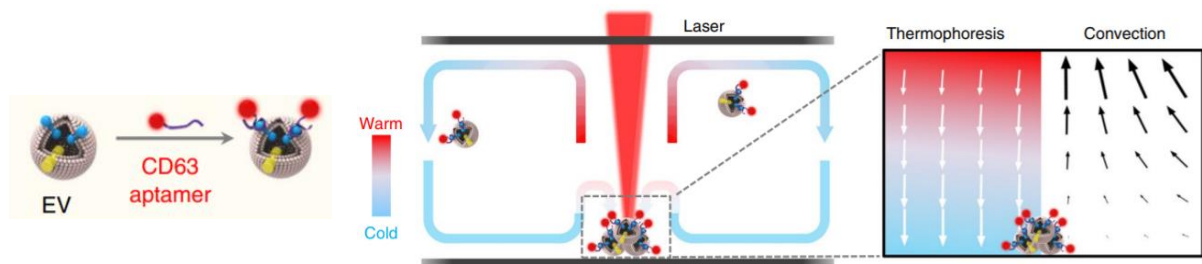


Figure 24 : Schematic illustration of the thermophoretic mechanism of accumulation of EVs. Reprinted from [247].

The high charge aptamers had a substantial thermophoretic impact. This technique was able to enrich the aptamer bounded EVs in a matter of minutes while also demonstrating device economy due to the low cost of aptamer production and ease of device manufacturing. The thermophoretic aptasensor was then utilized by the same team to profile cancer-associated protein markers from plasma EVs and forecast the progression of metastatic breast cancer [248]. Recently, Yang et al. also reported PD-L1 (programmed death-ligand 1) aptamer to recognize exosomal PD-L1 indicating significant potential as non-invasive tests for early cancer screening [249].

Microfluidic systems can combine the advantages of portability, cheap cost, small sample volume, high throughput, and high sensitivity into a single device. Despite these benefits, microfluidic devices for EV application are still uncommon. This is due to the numerous difficulties in microfluidic control and microfabrication encountered while creating integrated systems capable of multistep processes. Researchers have given more an interest in the immuno-affinity technique because of its high specificity thanks to antibody-antigen interaction and wide range of potential applications. These techniques, however, depend substantially on the development of antibodies, which must be both specific to the target of interest and non-interfering with the downstream analysis. Furthermore, not only is it difficult to find specific antibodies for each specific analyte, but it is also necessary to thoroughly investigate the stability of the antibodies and the reusability of the device. Finally, the binding of antibodies to EVs' surface may adversely impact the biological properties of EVs. In parallel to immune-capture based approaches, other techniques focusing on the physical features of EVs have been developed to explore EVs separation. However, passive size-based approaches such as membrane filtration have a low selection resolution. Although active approaches have the potential to alleviate this issue, it is yet unclear if the fields induced have any effect on the characteristics of the EVs. New developing microfluidics-based EV analysis technologies are expected to play an increasingly essential role in basic EV research as well as clinical cancer diagnosis, prognosis, and tailored therapy.

III.2. Electrokinetic-based technologies

The ability of an electric field to isolate and control EVs has recently been used as a contactless particle sorting process in various microdevices. Indeed, when suspended in a neutral medium, EVs have a negative surface charge [250]; thus, negatively charged EVs may migrate at different velocity based on their size, charge, and shape when a voltage is applied. This approach may be used to isolate EVs (for example, through a selective membrane) from other species (e.g. proteins, cell membrane debris) or

to separate EVs via a microchannel (capillary or microchip) (see Fig. 25 for schematic example). The following paper ([Morani et al., Trends in Analytical Chemistry, 2021](#) [251]) provides a comprehensive review of electrokinetic-based methodologies for EV isolation, separation, and quantification up to 2020. In this paper, we discussed several instrumental and methodological advancements for such aims, as well as their advantages and disadvantages.

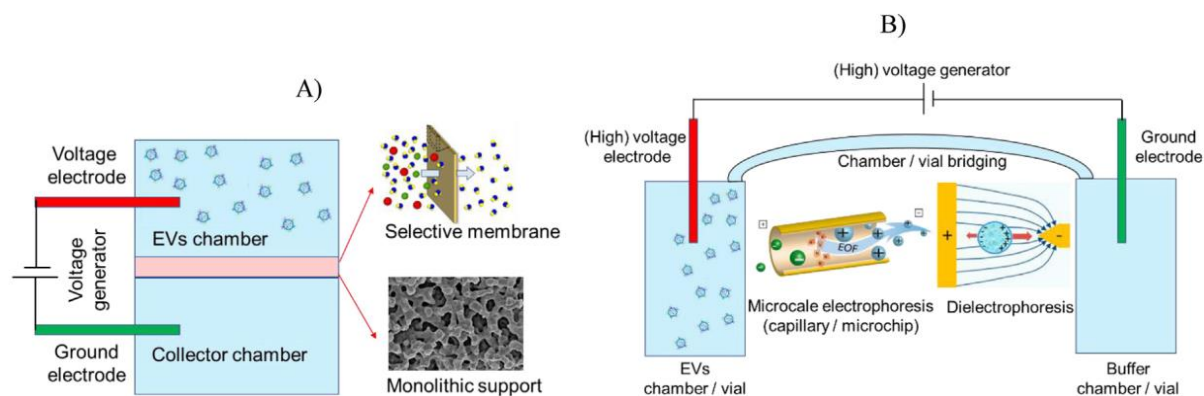


Figure 25 : Electrokinetically driven techniques for (A) EV isolation through a selective membrane or monolithic support; and (B) EV separation and characterization employing either non-uniform (dielectrophoresis) or uniform electric fields (for microscale electrophoresis). Reprinted from [251].

Our pioneer work relying on Capillary electrophoresis (CE) for analyzing and characterizing EVs, as well as possibly distinguishing EV subtypes based on electrophoretic migration, is also presented at a glance. This early study on EV characterization using electromigration method show the field's promise for CE. Standard CE characteristics including automation, little sample consumption and quick analysis represent the main advantages of this approach. However, attention should be paid to the selection of different parameters (e.g. sample injection plug length, electric field strength and Background electrolyte (BGE) composition) that might impact the overall CE analysis. These technical considerations will be discussed in further detail in Chapter IV.

It is worth noting that after this review paper was published, some other recent works have been communicated on the use of CE approach to analyze and quantify EVs; these are discussed further below.



Contents lists available at ScienceDirect

Trends in Analytical Chemistry

journal homepage: www.elsevier.com/locate/trac

Recent electrokinetic strategies for isolation, enrichment and separation of extracellular vesicles



Marco Morani ^a, Thanh Duc Mai ^a, Zuzana Krupova ^b, Guillaume van Niel ^{c, d},
Pierre Defreinaix ^b, Myriam Taverna ^{a, e, *}

^a Université Paris-Saclay, CNRS, Institut Galien Paris-Saclay, Protein and Nanotechnology in Analytical Science (PNAS), 92296, Châtenay-Malabry, France

^b Excilone - 6, Rue Blaise Pascal, Parc Euclide, 78990, Elancourt, France

^c Université de Paris, Institute of Psychiatry and Neuroscience of Paris (IPNP), INSERM U1266, "Endosomal Dynamic in Neuropathies", F-75014, Paris, France

^d GHU PARIS Psychiatrie & Neurosciences, F-75014, Paris, France

^e Institut Universitaire de France (IUF), France

ARTICLE INFO

Article history:

Available online 11 January 2021

Keywords:

Capillary electrophoresis
Electrokinetic approaches
Extracellular vesicles
Exosomes
Isolation

ABSTRACT

Extracellular vesicles (EVs) are a family of cell-derived membrane vesicles that are present in almost all body fluids. EVs have gained significant interest over the last decades as mediators of key functions in numerous patho-physiological condition (clearance, signalling, trophic support, cargo delivery) and as potential prognostic or diagnostic biomarkers. The endogenous delivery capacities of these nanometric entities also hold a high potential as engineered drug nanocarriers for clinical and pharmaceutical applications, especially for targeted therapies. Nevertheless, knowledge about the features of individual EVs (composition, physical and chemical characteristics) is still at the infancy because of the technical challenges to purify and analyze the various subpopulations of EVs. In this review, a comprehensive overview of electrokinetically driven methods for isolation, enrichment and characterization of EVs is presented. This review covers new trends of analytical science (over 7 years up till 2020), serving for high-quality EVs production, isolation, analysis and quality control, which are expected to provide powerful and complementary alternatives to the conventional and recently emerged approaches such as microfluidics. We critically discuss here the pros and cons of the different instrumental and methodological developments for electrokinetic strategies applied to EVs.

© 2021 Elsevier B.V. All rights reserved.

1. Introduction

Extracellular vesicles (EVs) cover a family of heterogeneous particles delimited by a phospholipid bilayer and secreted by all types of cells, with a size ranging from around 30 nm up to a few micrometers. Based on existing knowledge of their biogenesis, EVs can be narrowly classified into two major groups: exosomes and microvesicles (see Fig. 1 for EVs formation and secretion). However, these generic terms might mean different things depending on the research field [1]. For such reason, as endorsed by International Society of Extracellular Vesicles, "extracellular vesicles" is used as an umbrella term to represent all types of cell-secreted vesicles [2].

* Corresponding author. Université Paris-Saclay, CNRS, Institut Galien Paris-Saclay, Protein and Nanotechnology in Analytical Science (PNAS), 92296, Châtenay-Malabry, France.

E-mail address: myriam.taverna@u-psud.fr (M. Taverna).

It is now well established that EVs are implicated in a wide range of physiological processes, such as immune response, tissue repair, inflammation and neuronal functions [3–5], as well as in different pathological processes, like diabetes, liver disease, neurodegenerative diseases and cancer progression [6–8]. As EVs and their composition reflects the patho-physiological state of their producing cells, they provide a new source of biomarkers for diagnostic and prognostic applications [9–12]. Their capacities to deliver encapsulated materials in a targeted way open new avenues to harness them as biocompatible drug nanovesicles in targeted therapies [13–16]. Depending on their cellular origin and state, EVs are highly miscellaneous in size, cargo and membrane composition [17]. Even though the past decades have witnessed an exponential development in the field of EVs, there is still a lack of widely accepted specific markers to characterize the different subpopulations of EVs. Moreover, guidelines for isolation, enrichment and separation of EVs samples are still facing difficulties to properly exclude contaminants and separate EV subpopulations. In this

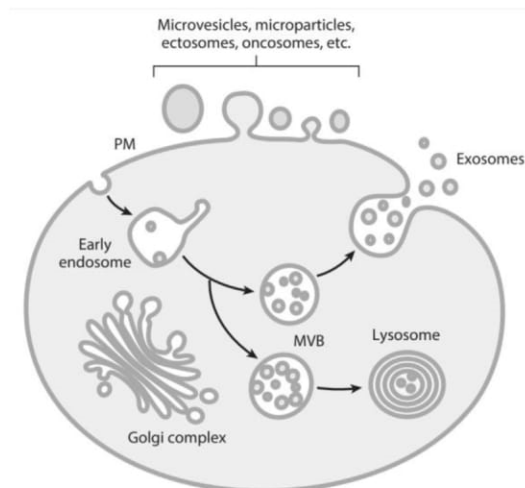


Fig. 1. Schematic representation of the different types of membrane vesicles released by cells, either by direct budding from the plasma membrane (PM) or by fusion of internal multivesicular compartments (MVB) with the PM. Reprinted from Ref. [89] with permission. Copyright (2014) Annual Reviews.

context, further investigations are required to improve isolation, enrichment and separation of extracellular vesicles in order to fully understand their intrinsic properties and to confirm their great potential in clinical applications.

EV isolation and enrichment is a prerequisite before their clinical use as diagnostic biomarker. A sufficiently high yield and good reproducibility of EVs purification/isolation process is required to get a representative batch of the whole EVs population and avoid unacceptably high batch-to-batch variations with evident failure at identification and validation of relevant biomarkers for instance. During the last years, many reviews have been dedicated to summarize and compare different technologies for isolation of EVs [18–26]. The traditional methods used for EV isolation exploit a variety of EVs properties, such as their density, shape, size, specific interaction with solvents and surface proteins (see Table 1 for comparison of the most commonly used EV isolation methods). Typical batch-wise isolation techniques include ultracentrifugation (UC), gradient ultracentrifugation, ultrafiltration, polymer co-precipitation, size-exclusion liquid chromatography (SEC), field flow fractionation and immunoaffinity. Among them, ultracentrifugation

is the most widely used primary isolation method across all EVs applications (>80%) [27]. However, this approach has many disadvantages such as bulky and expensive equipment, time-consuming procedure, contamination by protein aggregates and other particles, as well as high-volume sampling. A comparison study on EVs isolation yields from human serum achieved with some of these conventional methods revealed the highest numbers of total isolated EVs for polymer-based precipitation and size-exclusion chromatography methods (i.e. 5.6×10^{10} and 4.2×10^{10} particles/mL according to NTA analysis, respectively) [28]. These were followed by ultracentrifugation and density gradient ultracentrifugation approaches that led to the obtention of EVs concentrations of between 3.8×10^9 and 9.5×10^9 particles/mL [28]. In parallel, microfluidic technologies have been recently exploited for EVs isolation, making use of both physical and biochemical properties of EVs at microscale level. Microfluidics offers a tremendous potential by minimizing the sample volume, cost and reagent consumption, performing the reactions faster and conducting multiple assays in small devices simultaneously. These microfluidic systems bring also new functionalities and employ a wide range of EVs isolation approaches such as microporous filtration, immunoaffinity, trapping on nanowires, together with the use of acoustic, electrophoretic and electromagnetic sorting mechanisms [18,19,29–33].

Once EVs isolation has been achieved, it is also extremely challenging to verify the identity of EVs and monitor their quantity and quality. Until now, EVs characterization by multiple and complementary techniques has to be carried out to evaluate the performance of the isolation methods and to give an insight into the EV nature [21,22,34,35]. Microscopy-based methods (transmission electron microscopy TEM, atomic force microscopy AFM), dynamic light scattering (DLS), nanoparticle tracking analysis (NTA), single EV analysis (SEA) method and tuneable resistive pulse sensing (TRPS) are among the most widely used to measure the physical characteristics of EVs. These methods and their inherent advantages and drawbacks for EVs detection/characterization are summarized in Table 2. Besides these techniques, conventional protein analysis techniques, such as Western blotting, enzyme-linked immunosorbent assay (ELISA) and mass spectrometry (MS), provide high-throughput mapping of EVs' membrane and intra-vesicular proteins. EVs also contain nucleic acids which can be successfully examined by conventional extractions such as phenol-based method and spin column techniques. This led to the development of DNA/RNA-detection-based analysis tools for EVs, notably polymerase chain reaction

Table 1
Summary of the most commonly used EVs isolation techniques and their advantages/disadvantages.

| Method | Advantages | Disadvantages |
|-------------------------------|---|---|
| Ultracentrifugation | <ul style="list-style-type: none"> • Most commonly used • High purity by density gradient centrifugation | <ul style="list-style-type: none"> • High equipment cost • Time consuming • Large sample volume needed • Potential vesicle aggregation and mechanical damage • Low yield |
| Ultrafiltration | <ul style="list-style-type: none"> • Low equipment cost • Quick and simple • Possibility of processing many samples simultaneously | <ul style="list-style-type: none"> • Possible loss of vesicles due to clogging • Potential vesicle deterioration and deformation |
| Polymer-based precipitation | <ul style="list-style-type: none"> • Low cost • No special equipment required • High yield | <ul style="list-style-type: none"> • Co-precipitation of protein aggregates and polymeric contaminants • Low purity |
| Size-exclusion chromatography | <ul style="list-style-type: none"> • Keep native structure of vesicles • High purity • Good reproducibility | <ul style="list-style-type: none"> • Required clean-up steps • Limitation on sample volume • Long run time |
| Immunoaffinity capture | <ul style="list-style-type: none"> • High purity • High efficiency for specific EV subtypes | <ul style="list-style-type: none"> • Specific columns required • High reagent cost • Extra step for elution may damage EVs' native structure • Antibody cross-reactivity • Low yield |

Table 2
Summary of commonly used EVs characterization techniques and their advantages/disadvantages.

| Method | Advantages | Disadvantages |
|---|---|--|
| Transmission electron microscopy (TEM) | <ul style="list-style-type: none"> • Direct assessment of morphology and size • Powerful magnification and resolution | <ul style="list-style-type: none"> • Laborious sample preparation • Time consuming • Expensive equipment |
| Dynamic light scattering (DLS) | <ul style="list-style-type: none"> • Fast • No need for sample preparation | <ul style="list-style-type: none"> • Inaccurate with polydisperse and size-heterogeneous samples |
| Nanoparticle tracking analysis (NTA) | <ul style="list-style-type: none"> • Ability to analyze normal and fluorescent samples • Approximate particle counts | <ul style="list-style-type: none"> • Contamination caused by diluents during the preparation of samples |
| Flow cytometry | <ul style="list-style-type: none"> • Single EV molecular characterization • Quantitative and qualitative | <ul style="list-style-type: none"> • Results are operator-dependent • Detection limit is flow dependent • Aggregates or debris can give false results • Technical expertise required |
| Tuneable resistive pulse sensing (TRPS) | <ul style="list-style-type: none"> • Particle by particle measurement of size and charge | <ul style="list-style-type: none"> • Difficult to select the correct nanopore setup • Possible pore clogging • Less reproducible |

with real-time fluorescence measurements (RT-PCR) or more recent technologies such as Droplet PCR, Ion-Exchange Nanodetector and localized surface plasmon resonance (LSPR) based assay [21]. Among all conventional methods used for EV characterization, Western blotting (74%), single particle tracking (72%, mainly with NTA) and electron microscopy (60%) are among the most widely used [27]. Microfluidic-based technologies have also evolved in the field of EV detection, in which capture and characterization of EVs are combined in one integrated platform [29,31,32,36]. These emerging approaches are expected to provide fast and sensitive measurement with little sample consumption.

In a related context, EVs have been considered as nanoparticles (NPs) since they are within the same size range. Among analytical methods commonly used for NP characterization, electrokinetic approaches have emerged as simple and powerful techniques that are complementary to other spectroscopic, microscopic and optical ones, providing supplementary information on NPs' electrophoretic mobility, ζ -potential, particle size and biomolecular interactions [37–40]. Indeed, microscale electrophoresis relying on electrophoretic migrations of charged species under a high electric field, with its notable advantages of high separation efficiency, limited consumption of sample/chemicals and high potential for miniaturization and integration, has been widely used for high-resolution separation, isolation as well as preconcentration of NPs. With a similar viewpoint, electrokinetic strategies are expected to provide a powerful tool/alternative to conventional methods for EVs production, analysis and quality control. By application of a (high) voltage, the negatively charged EVs can migrate at different mobilities according to their size, charge and shape. The electroosmotic flow (EOF), which is the bulk liquid motion normally occurred under a high voltage over a charged support, typically silica capillaries possessing negative surface charges, can also be used to tune the apparent mobilities of EVs. This mechanism can be exploited for either i) isolation of EVs (via a selective membrane for instance) from other untargeted entities (e.g. proteins, cell membrane debris) or ii) separation of EVs over a microchannel (capillary or microchip) (see Fig. 2 for schematic illustration). Both non-uniform electric fields (for dielectrophoresis) and uniform ones (for microscale electrophoresis), as well as different variants of electrophoresis (for instance isotachopheresis, capillary zone electrophoresis etc.) can be used for these purposes. While both electrokinetic separation and isolation techniques rely on an electrical field to drive EVs, the migration pattern and geometric design of the system would determine the respective

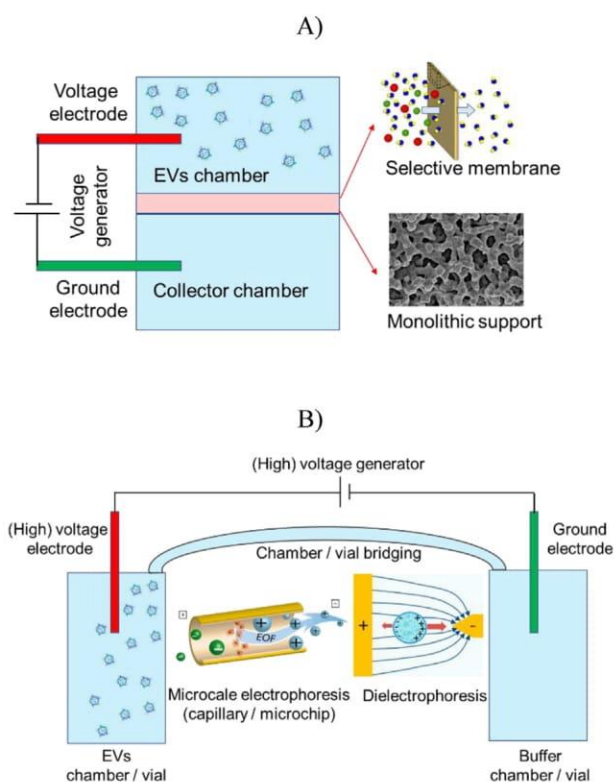


Fig. 2. Schematic drawings for electrokinetically driven methods for (A) EVs isolation; and (B) EVs separation and characterization.

purpose (typically micro-bored channels for EVs microscale separation and chambers separated by membranes or porous supports for EVs isolation). Normally, high electrical fields (more than 300 V/cm) are required for the former whereas lower ones are employed for the latter. Herein, we report on the first comprehensive overview of different electrokinetic strategies for isolation, separation and quantification of EVs. These strategies that exploit the electrokinetic migration of EVs are expected to possess advantages over conventional approaches in term of high resolution for EVs separation, high purity for EVs isolation, high potential for miniaturization and integration, as well as high versatility (i.e. EVs isolation, separation and characterization using an electrical field). Different instrumental and methodological developments for such purposes

as well as their positive features and limitations are discussed. There have been almost 35 research articles on this topic, with more than one-third released in the last two years (2019–2020), confirming the recent interest of our research community in this emerging approach to provide a reliable and accurate tool for purifying, characterizing and quantifying EVs.

2. A glance at EVs characteristics

It is widely accepted that the EVs size, contents and membrane composition are highly heterogeneous [5]. This heterogeneity relates partially to their origin and the patho-physiological state of the producing cells and will impact their different functionalities [41,42]. Yet this heterogeneity is also dependent on various other factors. EVs indeed can vary widely in terms of their composition and may carry specific sets of proteins, lipids or RNA species that then determine their fate and functions [5,43]. While the accumulating data in the past few years indicated that all EVs possess a negative surface charge due to their negatively charged phospholipid membrane, EVs from different origins may exhibit different zeta potentials, varying from -10 to -40 mV [25]. The EVs concentrations also vary significantly from one biofluid to another, from the range of 107 particles/mL for cerebrospinal fluid (CSF) up to 108–109 particles/mL for plasma and blood [25]. In addition, the number of EVs released also changes depending on the physiological state of the parent cell and the microenvironment conditions [44]. Similar to the behavior of cells, EVs are capable of responding to changes in the microenvironment that surrounds them, resulting in EVs shape, size and zeta potential variations in different buffer conditions [44,45]. Zijlstra and Di Vizio recently provided evidence that the heterogeneity of EVs is not only driven by size variation, but also defined by their diverse proteomic profiles, N-Glycosylation patterns, lipidic, RNA and DNA profiles [46]. All these data therefore suggest that while at first sight both EVs and NPs were thought to share similar size and charge characteristics, a deeper investigation revealed that EVs are much more complex than NPs and may behave differently from NPs under an electric field [47].

Lysis and/or characteristic modification of EVs can also occur, requiring a careful and restricted selection of suspension buffer composition and ionic strength during isolation and analysis [48–50]. This suggests that numerous parameters must be considered when handling the EVs, and high attention must be paid to maintain the native properties of EVs during isolation, purification, characterization and quantification. It is well known that the dependency of NPs' electrophoretic mobilities on their size, charge, charge-to-size ratio and shape can be determined only under very specific conditions [51–54]. Various parameters, notably background electrolyte (BGE) ionic strength, pH and composition as well as applied electric fields were found to have impacts on NPs' electrophoretic mobilities [55]. The situation is even more constrained for EVs. The fact that EVs from different origins probably have different shapes and also different proteins/biomolecules on their surface and that they are prone to lysis or shape-deformed renders it very difficult to establish rules for the sole dependency of EVs electrophoretic migration behavior on charge and/or size-based parameters. The application of a high electric field, as suggested by Jones et al. and d'Orlyé et al. when dealing with NPs [52,56], may not be applicable for EVs because it would provoke EVs lysis. With the present state of the art of EV purification technologies, it is still not readily possible to obtain EVs with very low degree of polydispersity and narrow size distribution [47], whereas this is already possible for NPs synthesis. All these features imply that the solid background already acquired for NPs should be used with care when applying to EVs, and consideration of the difference

between EVs' and NPs' behaviors should be taken into account when developing electrokinetic strategies for EVs production and characterization.

3. Electrokinetic isolation and enrichment of EVs

The utility of an electric field to isolate and manipulate EVs has been recently exploited as contact-free particle sorting mechanism within different developed microdevices. A summary of electrokinetic approaches for EVs isolation and enrichment is shown in Table 3. The electrophoretic sorting of EVs is based on different electric field intensity and charge-to-mass ratios of the EVs, without the need of pumps or other moving parts. Some of the devices presented here have proved the advantage of electrophoresis in EVs isolation via a filtration mode. In this sense, Davies et al. demonstrated direct isolation of EVs from mouse's whole blood [57]. In this system, they designed a porous polymer monolith in the center of an open cross flow channel to act as a membrane filter. This nano-pored monolithic membrane, playing the role of a size exclusion filter, was prepared *in situ* and was integrated into a poly (methyl methacrylate) micro-system. To render the monolithic membrane compatible with the extraction of vesicles, pore size was tuned to fit EVs sizes by changing the ratio of porogenic solvent to monomer solution. Then, direct current (DC) electrophoresis with a bias voltage of 10 V (corresponding to an electric field of 6.25 V/cm) was activated with the electric field applied perpendicular to the flow direction to propel the EVs across the membrane and drive them in the opposite direction to the positively charged interfering large debris and proteins, thus avoiding the clogging that occurred when simple pressure-driven mode is employed (see Fig. 3 for comparison between pressure-driven and electrokinetically-driven EVs isolation). In this configuration, sample and collection streams were performed at a relatively high flowrate (2 μ L/min) to prevent larger particles and cells in the bulk stream from retaining onto the membrane. EVs extraction from 240 μ L of blood could be completed within 2 h using this system. A 10-fold better purity of isolated EVs (approaching the purity offered by ultracentrifugation) was achieved when compared to that obtained with the pressure-driven mode. Moreover, the electrophoresis mode demonstrated the capacity to remove most of the soluble proteins from mouse blood, similarly to conventional ultracentrifugation. Nevertheless, the EVs recovery with this electrokinetic mode was unsatisfactory, with only 2% of EVs recovered. In another microdevice isolation system, Cho et al. applied a higher electric field across a porous dialysis membrane with an appropriate pore size (30 nm) to selectively capture EVs on the membrane from mouse blood plasma while facilitating protein migration through the membrane [58]. In this isolation system, two electrodes and two membranes between electrodes are juxtaposed. Three flow channels were arranged between electrodes and membranes, one for sample solution, one for cathodic buffer, and the other for anodic buffer. EVs and other particles (e.g., proteins) move horizontally in the sample flow confined between the membranes, and simultaneously migrate vertically under the applied voltage. As EVs and most of the proteins in the plasma (e.g., albumin) have negative surface charges, they move toward the anode and encounter the membrane, whereas particles with neutral or positive charges (e.g., histidine, lysine, non-polar lipids) move with the sample flow or are driven toward the cathode by electrostatic attraction. When the negatively charged particles arrive at the membrane pores, only small species (i.e., proteins) can pass through the membrane to enter the buffer channel and are consequently flushed out. In contrast, particles >30 nm (i.e., EVs) accumulate on the membrane, and the attached EVs are then washed and collected by pipetting with phosphate buffered saline (PBS). The membrane can be regenerated after each

Table 3
Electrokinetic strategies for isolation and enrichment of EVs.

| EV isolation approach | Sample type | Recovery yield (%) | Isolation throughput ($\mu\text{L}/\text{min}$) | Isolated size (nm) | Ref |
|--|--|--------------------|---|--------------------|------|
| Electrophoresis-driven filtration | Mouse whole blood | 1.5 | 2 | 150 | [57] |
| Electrophoretic isolation on porous membrane | Mouse plasma | 65 | 20 | ~10 - 400 | [58] |
| Ion-depletion zone | Cell culture filtered EVs | 98 | 1 | not communicated | [59] |
| Ion concentration polarization (ICP)-based gel electrophoresis | Cell culture supernatant, blood serum | 60–80 | 2.5–3.5 | ≤ 150 | [61] |
| Ion concentration polarization (ICP)-based electrokinetic concentrator | Cell culture supernatant | not communicated | 1 | ~50 - 75 | [62] |
| alternating current electrohydrodynamic (ac-EHD) induced nanoshearing | Exosome pellets from breast and prostate cancer cell lines | not communicated | not communicated | 30–350 | [63] |

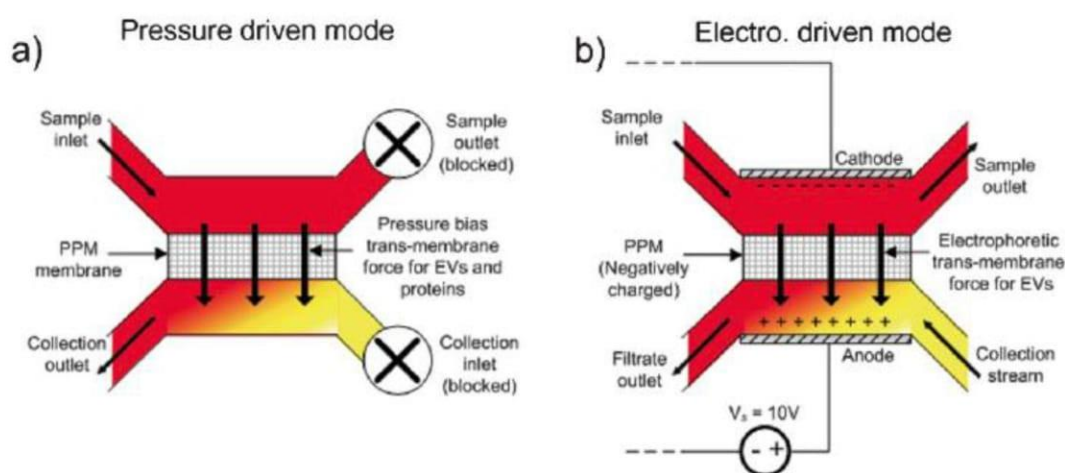


Fig. 3. (a) Schematic drawing of pressure-driven filtration procedure. Inlet pressure bias drives particles through the membrane into the collection chamber. After injection of the blood sample, the filtrate is collected by injecting one chamber volume of PBS through the collection inlet to eject the permeated EVs. "X" indicates an outlet blocked by sealing the attached plastic tubing. (b) Schematic of electrophoresis-driven filtration. Bias voltage is applied across the porous polymer monolith (PPM) membrane so that negatively charged vesicles experience a transmembrane driving force. Filtration is performed under syringe pump driven flow. 10 V is applied over an electrode separation distance of 1.5 cm for an electric field strength of 6.7 V/cm. Reprinted from Ref. [57] with permission. Copyright (2012) RSC.

EVs collection for repeated use. Based on NTA measurements, this method permitted a 65% EVs recovery rate in approximately 30 min. According to RNA analysis and characteristic EV protein (CD63), this device led to less impurities than commercial polyethylene glycol (PEG) precipitation method (84% vs 68%, respectively). However, EVs isolated using this technique were less pure than those isolated by conventional ultracentrifugation (98%).

In a related context, Mogi et al. proposed in 2018 the use of an electrical filtration device utilizing an ion-depletion zone in a microchannel to concentrate EVs from the culture media of four types of cell lines [59]. The approach is called ion concentration polarization (ICP). Readers can refer to a recent review for the theoretical background and extended applications of this electrokinetic concentration mode on chips utilizing ICP [60]. The ion-depletion zone, from which all positively and negatively charged particles are excluded, was generated by applying a voltage between two microchannels, i.e. main and ground (GND) channels, bridged by a cation-exchange membrane. The application of a voltage caused cations around the bridged area of the high-voltage side in the main channel to be drawn into the low-voltage zone of the GND one, resulting in an increase in the anions' amount relative to the cations' one. This led to an instantaneous expulsion of anions by electrostatic repulsion to re-establish the electro-neutral situation, thereby forming an ion-depletion zone. As long as the

electrostatic force required to generate the ion-depletion zone is still stronger than the driving force needed to move particles into the zone, the ion-depletion zone works as an intangible barrier to prevent any charged particles from entering in this zone. As a result, any negatively charged particles (more specifically EVs) passing through this zone by a pressure-driven flow are pushed away to the other side of the microchannel for preconcentration/collection (see Fig. 4). They demonstrated that the ion-depletion zone method caused less damage to EVs when compared to standard ultracentrifugation isolation process. The EV recovery yields achieved for ICP and ultracentrifugation isolation were 98% and 57%, respectively. Further evidence is of course needed to certify the potential of the former for EVs concentration and separation from clinical samples. Interestingly, the ion depletion feature was also exploited in the same year by Marczak et al. These authors designed a different electrophoresis assisted device for EVs isolation that uses a cation-selective membrane to produce a transverse local electric field [61]. Under this electric field, the EVs pumped with a syringe into the microchip were carried into a perpendicular channel containing agarose gel, which filtered undesirable cell debris, and finally got concentrated near the membrane surface. When tested with cell culture media and blood sample spiked with EVs isolated with a commercial kit, this device was able to isolate between 60% and 80% of the incoming EVs within 20 min. This

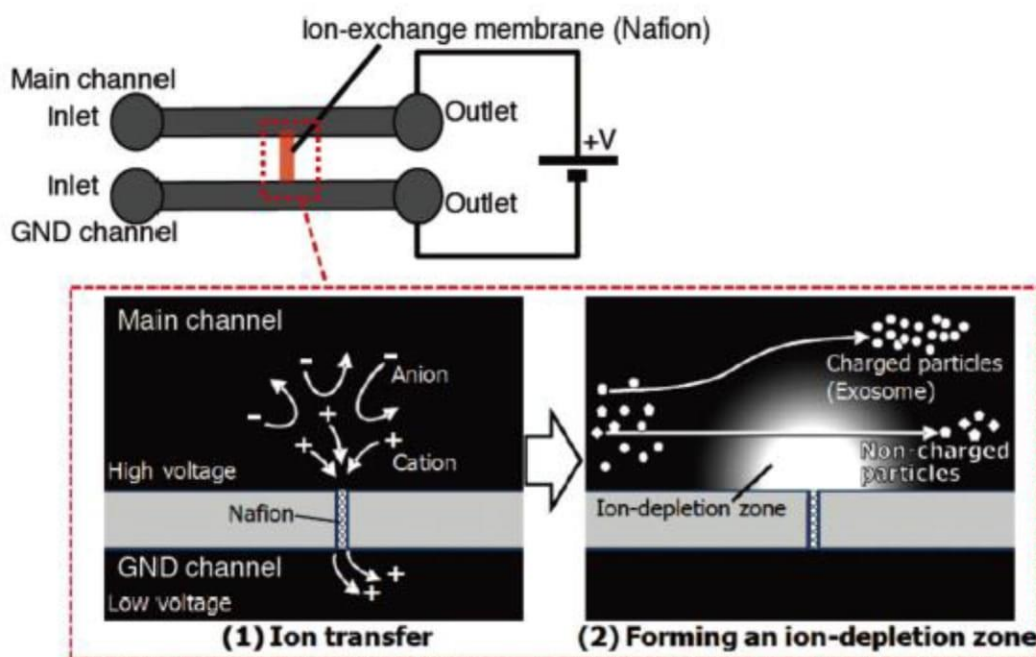


Fig. 4. Schematic drawing of the generation of an ion-depletion zone for EVs preconcentration. An ion-depletion zone is formed by applying a voltage between two microchannels bridged by an ion-exchange membrane. (1) Cations that are drawn into and anions are pushed away from the edge of the Nafion membrane on the high-voltage side by an electrostatic force. (2) The generated ion-depletion zone is used as an intangible barrier against the entry of charged particles. A Nafion pattern intersects the Main and the GND channels. The inlet and outlet ports of the channels are in contact with the electrodes to apply an electric potential difference between the two microchannels. Reprinted from Ref. [59] with permission. Copyright (2018) JSAC.

system demonstrated a superior recovery yield compared to the conventional techniques of ultracentrifugation (6%) and polymer-based precipitation (ExoQuick, 30%). Furthermore, the use of negatively charged membranes allowed prevention of membrane pore clogging by repelling the exosomes, whereas the utilization of the external ion concentration polarization phenomenon enriched these target entities. Later, Cheung et al. exploited the use of ion-selective membranes as well, by printing them directly on a PMDS microchannel [62]. This system incurred surface binding-based or passive trapping mechanism near the conductive polymer membrane, allowing to simultaneously preconcentrate and capture EVs. The buffer solution was loaded into the cathodic reservoir and allowed to flow through the channel, whereas the EV sample was loaded into the anodic reservoir. Once the voltage was applied (electric field of 45 V/cm), the flow generated by the electroosmotic flow (EOF) pushed the EVs towards the cathode reservoir in front of the printed membrane. This ICP-based electrokinetic concentrator was demonstrated to preconcentrate and capture EVs from human breast cancer cell lines by increasing the EVs concentration by ~ 100 -fold within 30 min. The limit of detection achieved was 5×10^7 particles/mL, which is better by two orders of magnitude than those obtained with a microfluidic approach without ICP. Their fabrication strategy that decoupled the ion-selective membrane from the substrate allowed the flexibility of either using an antibody-immobilized substrate to increase the EVs capture specificity or a glass substrate with passive microtraps to capture EVs in a highly efficient manner. However, once again, the EVs samples tested with this system came from batches extracted using a commercial kit. Direct application of this device to untreated clinical samples has yet to be demonstrated.

Diverted from DC electrophoresis driven mechanism, a nonuniform electric field was combined with immunoaffinity strategy for isolation of EVs [63]. Vaidyanathan et al. developed a microfluidic device containing a long array of asymmetric

functionalized electrode pairs within three individual microfluidic channels. The use of an alternating current across the electrodes generated flow vortices that both increased collisions between target EVs and functionalized electrodes and reduced nonspecific adsorption of weakly bound molecules from the electrode surface. Detection and quantification of EVs spiked in PBS and breast cancer patient serum were performed both visually and via absorbance measurements from colorimetric solutions. A 3-fold enhancement in detection sensitivity compared to a pressure-driven system (via a syringe pump) was reported. On the other hand, considering that it is closer to an immunoaffinity based method, it could only capture EVs expressing a given specific antigen, potentially excluding other EVs subpopulations concurrently present in a biofluid.

At a glance, electrokinetic strategies exhibit relatively higher EVs recovery yields (varying between 60 and 98%, depending on the working principle) compared to those obtained with conventional precipitation (30%) and ultracentrifugation (6–57%, depending on testing conditions). Better purities are also achieved with electrokinetic approaches. Among all approaches presented, the electrophoretic isolation on porous membranes and ICP-based gel electrophoresis offered the highest EV isolation yield, which is far superior than those of conventional methods. This technique [61], however, may come with a penalty of large size distribution up to 400 nm. On the other hand, much narrower size distribution was achieved with the ICP system [59], but further tests using clinical samples need to be performed in terms of EVs recovery and purity compared to conventional approaches. Note that a fair and systematic comparison of EVs isolation performances between electrokinetic strategies, microfluidic ones and the established methods (i.e. ultracentrifugation, polymer precipitation, membrane filtration, size exclusion chromatography SEC and membrane affinity) could not be made at the actual stage, as electrokinetic and microfluidic approaches are still under development and considered as emerging trends. They are therefore not included yet in

different systematic performance evaluation/comparison studies. To have a rough estimation, readers can nevertheless glean to a recent study by Tian et al. for information on the EVs isolation performance of different established methods [64]. Starting from a same platelet-free plasma sample, ultracentrifugation is first ranked for the purity of isolated EVs (78%), followed by SEC (28%) and polymer precipitation (5–18%). On the contrary, the yields provided by polymer precipitation kits (83–89%) are much higher than those obtained with SEC (65%) and ultracentrifugation (2%). The presence of electrokinetic strategies in such comparison study is expected soon to appear.

4. Electrokinetic separation and quantification of EVs

4.1. Dielectrophoresis of EVs

The reported electrokinetic strategies for separation and quantification of EVs are summarized in Table 4. Dielectrophoresis (DEP) was the first approach developed for such purpose. DEP is the motion mechanism of an electrically polarizable particle that occurs in the presence of a non-uniform electric field [65]. Upon generation of a non-uniform electric field, the movement of charged particles driven by the dielectric force depends on their size and dielectric properties, the electrical properties of the suspending solution as well as the frequency and intensity of the applied electric field. DEP was employed to manipulate EVs after successful application with microparticles, nanoparticles and cells [66–68]. The DEP separation force generated by the alternating current electrokinetic (ACE) microarray chip device was first demonstrated in 2017 by Ibsen et al. for rapid isolation and recovery of glioblastoma EVs spiked in human plasma in less than 30 min [69]. The setup of this system is illustrated in Fig. 5. On the ACE chip, the EVs were attracted to the high-field regions around the microelectrode edges, while cells or larger particles in the samples were concentrated into the DEP low-field areas between the microelectrodes. The attracted EVs were either observed under SEM and detected by fluorescent staining after washing away the excess plasma or eluted from the chip and collected for further analysis. Nevertheless, protein aggregates and other cellular debris were undesirably collected as well. The same ACE procedure was then applied for capture and analysis of EVs from whole blood, plasma and serum of pancreatic ductal adenocarcinoma (PDAC) patients [70]. Two EV associated proteins of interest, glypican-1 and CD63, were subsequently detected and measured using immunofluorescence-based methods to distinguish between PDAC patients from healthy controls with 99% sensitivity and 82% specificity. However, it was not clear whether the high levels of glypican-1 and CD63 were caused by elevated protein-to-exosome ratio or increased number of exosomes. In another study, Shi et al. reported a dielectrophoretic approach to design an insulator-based dielectrophoresis (iDEP) to capture EVs at the proximity of a glass nanopipette tip using a DC field [71]. The instrumental setup is shown in Fig. 6, in which a nanopipette was inserted into the opening of a chamber and connected with platinum electrodes. This device was based on the application of negative voltage polarity at the base of the pipette and induction of a strong non-uniform electric field that created a DEP force near the pipette region. The EVs trapping was controlled by three dominant forces including dielectrophoretic, electrophoretic and electroosmotic ones. The separation performance was first confirmed with fluorescence intensity measurements using fluorescently labelled artificial liposomes in PBS solution to simulate EVs capture. The separation capability of this iDEP device was further demonstrated in an extended setup connecting four micropipettes in parallel on a single chip, to carry out the extraction of EVs within 20 min from

200 μ L of undiluted human plasma, serum or saliva [72]. According to NTA results, this method showed two orders of magnitude greater yields when compared to the differential centrifugation method, with a particle size distribution ranging from 50 nm to 150 nm covering most of the small and large EV subpopulations. This yield improvement came with a penalty of larger initial sample volumes needed. Ayala-Mar et al. then designed another direct current–insulator-based dielectrophoretic (DC-iDEP) system not only for EVs capture but also for EVs separation and collection based on their size [73,74]. This device is composed of a micro-channel having two different electrically insulating post sections, each with different gap space (15 μ m and 10 μ m). Adjacent to these two sections, side channels with recovery reservoirs are arranged to allow collection of the separated sample. When DC voltages are applied, the EVs are dragged by the EOF across the main channel. As a result, large EVs are captured in the first post array, while smaller size EVs are trapped in the second post array. DLS measurements of two recovered fractions demonstrated successful separation of two different EV sizes of approximately 120 nm and 75 nm in only 20 s. Furthermore, such a tool was able to concentrate and separate EVs from previously extracted EV samples. Chen et al. then gave an account of the development of a fast DEP method to isolate EVs with higher yield (>87%) and higher purity than conventional ultracentrifugation from plasma [75]. This DEP chip consisted of interdigitated electrodes covered with poly-HEMA hydrogel to reduce their degradation by the contact with high conductivity samples. Under positive DEP force, the EVs were successfully attracted and concentrated near the edges of the microelectrodes. The DEP step was followed by *in situ* lysis of EVs for identification of miRNAs levels in lung cancer patients. In addition, the authors demonstrated with DEP chips the possibility of *in situ* siRNA loading by electroporation of EVs that could be exploited for drug delivery and/or gene therapy. To conclude this section, the dielectrophoretic-based methods presented here demonstrate label-free, rapid and high-throughput separation of EVs. However, in our opinion, only few devices proved to be able to concentrate and separate EVs from complex biological mixtures. Pre-treatment of biological samples was always needed as forefront of these DEP approaches. Integration of upstream sample processing to downstream DEP-based separation of EVs should be envisaged and constitutes probably attractive perspectives to improve the performance of these systems in the future.

4.2. Microscale electrophoresis of EVs

During the past decade, microscale electrophoresis has been explored to provide analysis and characterization of EVs and potentially distinguish EV subtypes based on their electrophoretic migration in a microchannel under a high intensity electric field. The first electrokinetic approach coupled with light-scattering-based detection was reported in 2013 by Ichiki's group for tracking EVs and obtaining their zeta potential, using an on-chip microcapillary electrophoresis (μ CE) system coupled with a laser dark-field microscope [76–79]. A typical setup is shown in Fig. 7. This μ CE consisted in a microfluidic channel in which EVs flow under application of DC voltage and afterwards they are tracked thanks to a laser dark-field microscope. This system enabled individual EVs visualization in a dark field by detecting the scattered laser light and their zeta potential was deduced from the measured electrophoretic mobility, revealing a strong correlation between the EVs zeta potential and their cells of origin. Furthermore, the authors developed an on-chip immunoelectrophoresis method to profile the protein expression of individual EVs, detecting their shifts in the electrophoretic velocity which resulted from the binding of EVs to specific antibody markers. This system was

Table 4
Electrokinetic strategies for separation and quantification of EVs.

| EV analysis approach | Sample type | Detection limit | Calibration range | Operation time | Isolated size (nm) | Concentration (particles/mL) | Ref |
|---|--|--|---|--|---|---|---------|
| Alternating current electrokinetic (ACE) microarray chip | glioblastoma EVs purified from cell culture and spiked in human plasma | not communicated | not communicated | <30 min | -50–150 (UC) | -1–10 × 10 ⁹ (loaded into the system) | [69] |
| Alternating current electrokinetic (ACE) microarray chip | EVs from whole blood, plasma and serum of pancreatic ductal adenocarcinoma (PDAC) patients | not communicated | not communicated | <30 min | -20 - 500 | not communicated | [70] |
| Nanopipette insulator-based dielectrophoresis (iDEP) device | EVs extracted from plasma of healthy donors and resuspended in PBS | not communicated | not communicated | ~2 min (only for entrapment) | not communicated | not communicated | [71] |
| Nanopipette insulator-based dielectrophoresis (iDEP) device (four pipettes in parallel) | EVs from undiluted human plasma, serum and saliva | not communicated | not communicated | 20 min (10 min entrapment and 10 min collection) | 50–150 | 1.01 × 10 ¹² (detected after isolation) | [72] |
| Direct current–insulator-based dielectrophoretic (DC-iDEP) system | EVs purified from human breast adenocarcinoma cells | not communicated | not communicated | 20 s (for entrapment and separation) | -75 (section 2); -120 (section 1) | 2.1 × 10 ¹⁰ (loaded into the system) | [73,74] |
| Dielectrophoresis (DEP) chip | EVs isolated from plasma of lung cancer patients | not communicated | not communicated | 30 min | -50 - 250 | 7.13 ± 0.86 × 10 ¹⁰ (detected after isolation) | [75] |
| On-chip microcapillary electrophoresis (μCE) coupled with a laser dark-field microscope | EVs extracted from six types of human cell | not communicated | not communicated | not communicated | not communicated | not communicated | [76] |
| On-chip microcapillary electrophoresis (μCE) coupled with a laser dark-field microscope | EVs extracted from normal and cancer prostate cells | not communicated | not communicated | not communicated | not communicated | not communicated | [77] |
| On-chip microcapillary electrophoresis (μCE) coupled with a laser dark-field microscope + immunoelectrophoresis | EVs collected from culture supernatant of human breast cancer cells and from mouse blood | not communicated | not communicated | not communicated | -50–450 (UC) | 1.19 × 10 ¹² (loaded into the system) | [78] |
| Capillary electrophoresis (CE) coupled with UV–visible detector | EVs isolated from human urine | not communicated | not communicated | ~4 h (separation) | 80–120 (low density EVs); 40–100 (heavy density EVs) (Sucrose gradient UC) | not communicated | [80] |
| Capillary electrophoresis (CE) coupled with UV–visible detector | EVs isolated from <i>Pectobacterium betavascularum</i> strain | protein concentration down to 0.17 mg/mL | not communicated | <15 min (separation) | <200 (differential centrifugation + filtration) | not communicated | [81] |
| Capillary electrophoresis coupled with laser-induced fluorescent (LIF) detection | EVs isolated from bovine milk, pony plasma/serum and human plasma | 8 × 10 ⁹ EVs/mL | 1.22 × 10 ¹⁰ to 1.20 × 10 ¹¹ EVs/mL | <30 min (separation) | <200 (sucrose gradient UC, size exclusion chromatography, monolithic affinity chromatography) | not communicated | [47] |
| Cyclical electrical field flow fractionation (Cy-EI-FFF) | EVs purified from human melanoma cells | not communicated | not communicated | not communicated | -120 (radius) (differential centrifugation) | not communicated | [45] |
| Capacitance-voltage measurements | EVs isolated from human embryonic kidney cell line and small cell lung cancer cell line | not communicated | not communicated | 10 min | 90–110 (ExoQuick-TC kit) | >1 × 10 ⁶ | [83] |

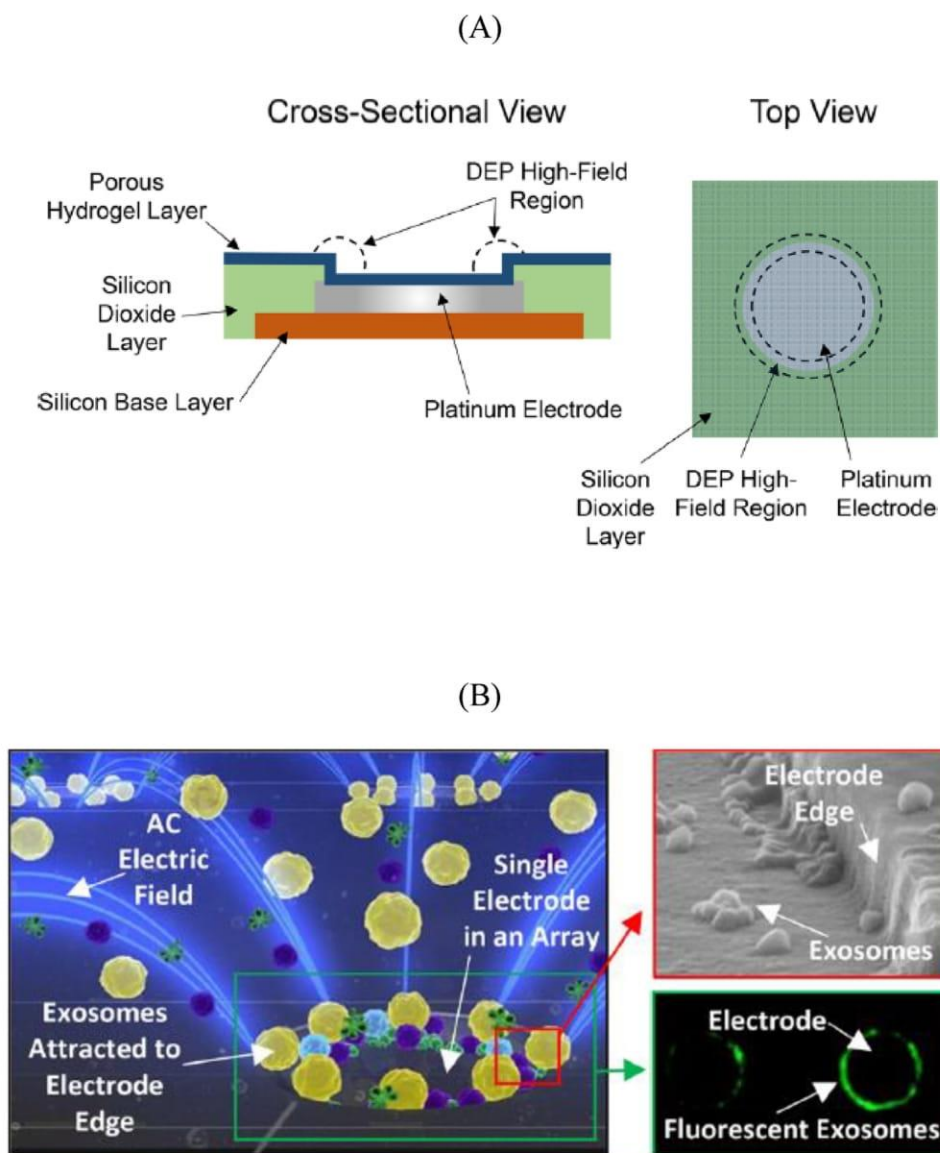


Fig. 5. Schematic drawing (A) as well as simulated and captured photos (B) of the microelectrode array chip showing the cross-sectional and top views of a single electrode. Over 1000 electrodes can be set in a single device. The DEP high-field regions where particles are collected are shown within the dotted lines. The darker color of the silicon dioxide layer and electrode in the top view represents the overlying transparent porous hydrogel layer. Reprinted from Ref. [69] with permission. Copyright (2017) ACS.

expected to be a valuable tool for sensitive profiling of EVs of tumor origin and therefore for early cancer diagnosis. Nevertheless, specific purpose-made instrumentation and manual operation are required for this new application, hindering its high throughput potential.

Diverted from the microchip setup, Lan et al. reported the first result of a capillary electrophoresis (CE) method applied for urinary EVs [80]. The authors investigated the potential of CE for separation of two kinds of EVs exhibiting different densities and obtained by sucrose gradient ultracentrifugation. However, it was not clear if the peaks detected from the CE analysis of low- and high-density EVs were either a result of different EVs size or different charge characteristics related to their different origins. No concrete information could be withdrawn from this work, due to (at least partially) the non-optimized conditions employed for CE analysis of EVs. More recently, two capillary electrophoresis methods have been proposed for the identification and quantification of EVs after their isolation. Piotrowska et al. demonstrated a CE-UV method for

qualitative and quantitative analysis of bacterial EVs [81]. To maintain EVs stability during CE analysis under electric field, the authors employed large buffering counter-ions. Thanks to this configuration, they obtained satisfactory separation of EVs from other non-target entities/molecules without any sample pretreatment in about 15 min, using the optimized BGE composed of 50 mM 1,3-Bis(tris (hydroxymethyl)methylamino)propane (BTP) and 75 mM glycine (pH 9.5) and application of an electric field of 333 V/cm. This method coupled with UV detection at 200 and 230 nm enabled the identification and quantification of EVs in the samples featuring protein concentration down to 0.17 mg/mL. Although this method enabled to quantify the number of vesicles in isolates, the linear correlation achieved was far from optimal ($R^2 = 0.81$) due to the presence of co-isolated impurities and the lack of a standard for method validation. Furthermore, the ability of this CE-UV method to separate and distinguish EVs from different origins was not investigated. In a parallel work, Morani et al. proposed a CE method with a laser-induced fluorescent (LIF) detection

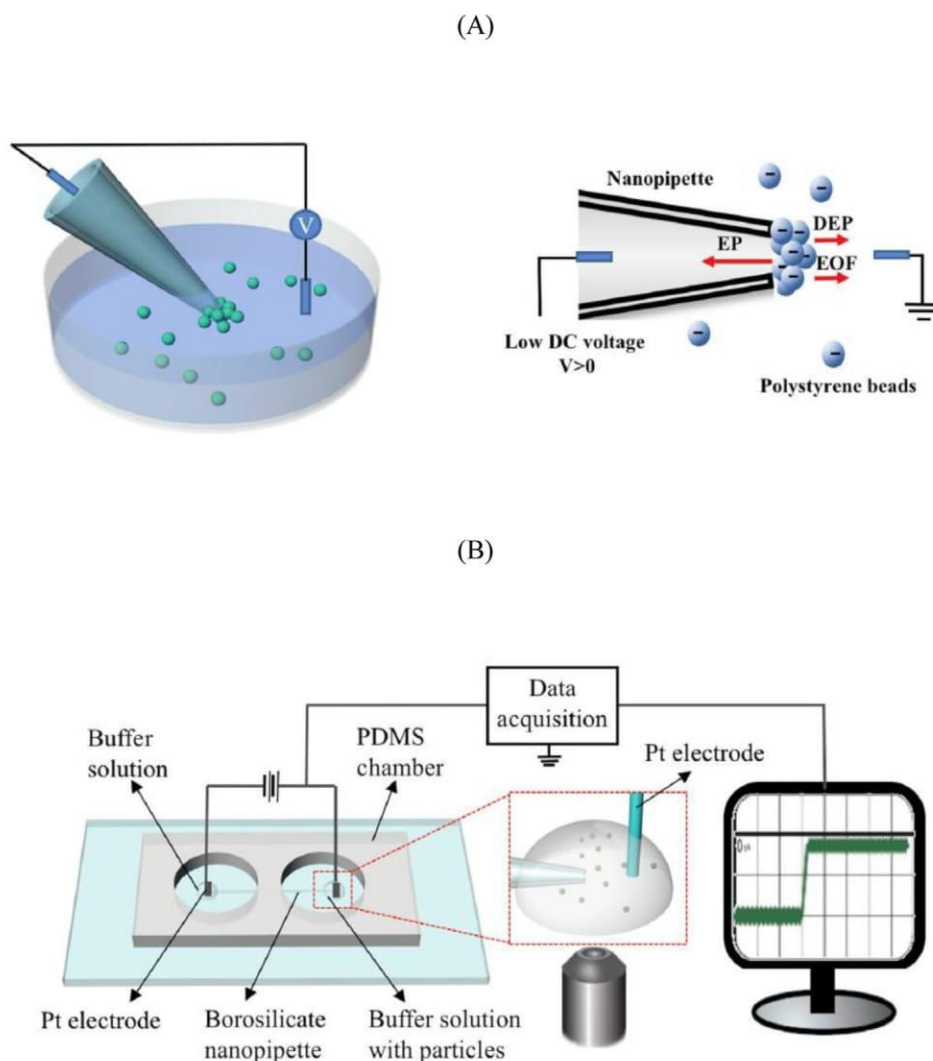


Fig. 6. (A) Schematic drawing of the nanopipette DEP device for entrapment of the particles suspended in the solution. (B) The overall setup. The ionic current across the pipette and the trajectory of the particles were simultaneously recorded. DEP stands for dielectrophoresis; EP and EOF stand for electrophoresis and electroosmotic flow, respectively. Reprinted from Ref. [71] with permission. Copyright (2018) Nature.

for the electrokinetic profiling of EVs from different sources (animal and human fluids) [47]. In this approach, EVs were first rendered fluorescent via an intra-membrane labeling. The CE-LIF separation of labelled EVs from the residual fluorophore was performed under an electric field of 500 V/cm. A new BGE was proposed for such purpose, employing large and weakly charged molecules (i.e. Tris (hydroxymethyl)aminomethane and N-Cyclohexyl-2-aminoethanesulfonic acid) at extremely high concentrations to avoid/minimize adsorption of EVs onto the silica capillary wall and lysis of EVs during electrophoresis. To avoid aggregation of EVs, buffer substitution of the analyzed samples was performed to avoid the high conductivity of the PBS matrix of the samples. A protocol overview and a typical electropherogram are shown in Fig. 8. Unlike UV detection, LIF detection offered better sensitivity achieving a detection limit of approximately 8×10^9 EVs/mL (i.e. 5-fold better than the CE-UV approach) that is sufficient for this method to be used for quality control of EVs batches isolated with different conventional EV isolation techniques. Despite the additional fluorescent labelling step to render the EVs detectable with a LIF detection, no morphology modifications of EVs were produced according to DLS and NTA data. This CE-LIF method allowed to reveal different profiles and electrophoretic mobilities for isolated

EVs from different origins. However, further characterization study is needed to prove whether such differences are size-dependent or due to different surface composition. Different from the intra-membrane labelling strategy for CE-LIF of EVs, Tani and Kaneta have very recently proposed an alternative for LIF-based quantification of exosomes, using indirect capillary electrophoresis immunoassay (CEIA) of exosomal membrane protein, CD63 [82]. In this method, reactions between the exosomes and a fluorescently labelled anti-CD63 antibody were optimized to form a CD63 complex localized on the surface of exosomes, followed by removal of the exosome-antibody complex by centrifugation prior to CE-LIF analysis of the supernatant containing the free fluorescent antibody. The diminution of peak areas was proportional to the increase in EVs' amount when the initial fluorescent antibody's concentration was kept constant. Thus, the concentration of the exosomal membrane's CD63 could then be estimated based on the slope of the linear relationship. This "indirect" method that measures the concentration of the fluorescent antibody allows straightforward quantification of exosomes without possible interference of unwanted peaks. Nevertheless, no information on the electrokinetic profile reflecting the size/charge distribution and eventual presence of EVs subpopulations can be provided this way.

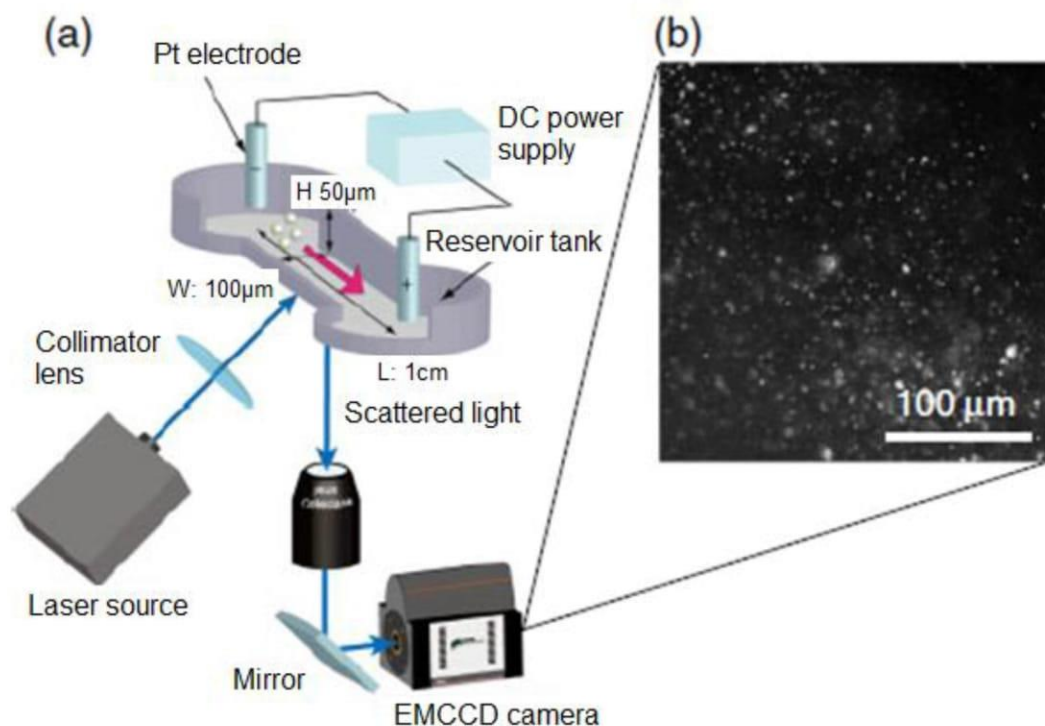


Fig. 7. (a) Schematic drawing of the on-chip μ CE system with a laser dark-field microscope. The system consists of a μ CE chip, a pair of platinum electrodes, a DC power supply, a laser source, an inverted microscope, and an EM-CCD camera. The μ CE chip equipped with a microfluidic channel with small reservoir tanks on both ends and the platinum electrodes were mounted on the inverted microscope. (b) Dark-field image of exosomes. Reprinted from Ref. [76] with permission. Copyright (2013) IOPScience.

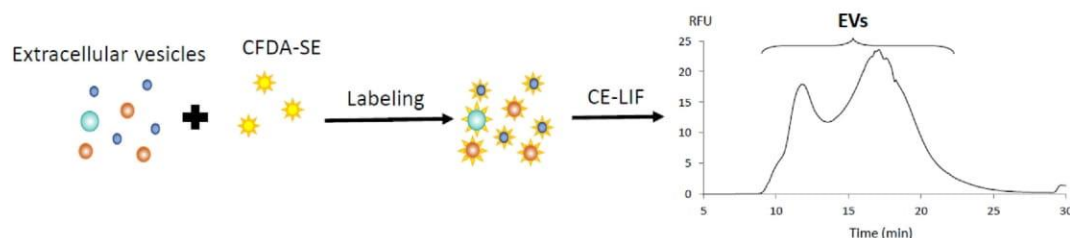


Fig. 8. Work flow of the CE-LIF method for separation and quantification of fluorescent EVs via intra-membrane labelling approach. CFDA-SE: 5-(and-6)-Carboxyfluorescein diacetate succinimidyl ester dye. Reprinted from Ref. [47] with permission. Copyright (2020) Elsevier.

Detection bias can also occur if membrane debris are co-present in the EVs sample.

4.3. Other related techniques

In addition to the electrokinetic strategies listed above, other techniques have also been investigated. Petersen et al., for instance, presented a cyclical electric field flow fractionation (Cy-EI-FFF) approach to separate EVs based on their size and charge [45]. Basically, application of an AC voltage produces a strong electric field perpendicular to the direction of flow, which enables EVs separation within a channel, due to their different electrophoretic mobilities. This strategy showed changes in electrophoretic mobilities when similarly sized polystyrene particles, melanoma exosomes sourced from a common human A375 melanoma cell line or synthetic liposome-based exosome mimetics were substituted in different buffers (i.e. deionized water, PBS, trehalose and isopropyl alcohol) having different salt concentrations. Therefore, EVs could be separated depending on their different charge in different buffers. In another work, Al Ahmad et al. reported an electrical detection and quantification of EVs via

capacitance-voltage measurements [83]. The authors compared three types of EVs and demonstrated the identification of EVs according to their corresponding self-capacitance. However, the employed equipment in this work enabled only to estimate the EVs count. This could be overcome in the future by implementation of more precise micro/nano-based capacitance analysers. Recently, Akbarinejad proposed a new approach relying on a low electric field and an electrochemically switchable substrate for the fast, selective, nondestructive, and efficient capture and release of EVs [84]. In this system, using gold-sulfur (Au-S) covalent bonding, the electrospun substrates were functionalized with SH-terminated aptamer probes that are selective to EV surface proteins. The specific aptamer-EV interactions allows efficient capture of EVs and easy removal of the nonspecifically bound material through washing steps. The trapped EVs were then released into fresh PBS at a high efficiency (>92%) by applying a potential of -1.2 V for 5 min for cathodic cleavage of the Au-S bond. This approach was demonstrated for capture, enrichment and release of EVs derived from primary human dermal fibroblast (HDFa) and breast cancer (MCF-7) cell lines with low nonspecific adsorption.

A high resolution particle-to-particle measurement technique, developed by Trau et al. for nanoparticle characterization [85,86] and commercialized under a trade name of qNano – Izon Science [87], has recently been adapted for measurements of EVs' size, volume and surface charge. This elastic pore sensor, employing the tunable resistive pulse sensing (TRPS) principle is composed of conically shaped, size-tunable pores that are fabricated by puncturing a polyurethane thermoplastic membrane with a tungsten needle. Stretching or relaxing the elastic membrane allow the dimensions of the conical pore to be tuned to the size range of the target particles. When a voltage is applied across the conical pore, its shape results in a resistance gradient. TRPS measures nanoparticles suspended in electrolytes on a particle-by-particle basis as they pass through a nanopore. Sample particles are driven through the nanopore via a combination of pressure and voltage. Each particle causes a resistive pulse or "blockade" signal that is detected and measured. The blockade magnitude is directly proportional to the volume of each particle. The blockade duration is dependent on the velocity and surface charge of the particle, and blockade frequency is used to determine particle concentration. Applications of this technology have been extended recently to measure physicochemical parameters (size, concentration and charge) of EVs and nanomedicines with high precision.

When positioning the electrokinetic and related strategies for EVs analysis together with other commonly used methods, the electrokinetic ones would have the advantage of high resolution. Nevertheless, they are still mostly at research stage and require for most of them further improvement of measurement reproducibility. To bring a fair view to readers, the limitations of other established techniques are also mentioned, including limited resolution and sensitivity for NTA and DLS, low throughput for TEM and limited multi-parameter capability for flow cytometer. Depending on the measurement requirements and available infrastructure, a single instrument or a combination of techniques is generally used to zoom into target EVs. Electrokinetic and related strategies, while still needing to further mature in the near future, could be included in the list of the methods of choice for this purpose.

5. Conclusion remarks and perspectives

The potential of EVs as a source of prognostic or diagnostic biomarkers but also as drug nanocarriers or gene therapy tools has attracted significant attention over the recent years. However, many technical challenges should be taken into account when dealing with such vesicles, notably their high heterogeneity, their small sizes, their fragility and also the tendency to aggregate or lyse. To date, ultracentrifugation (highest EV purity, lowest EV yield), commercial kits of polymer precipitation (highest EV yield, lowest EV purity) and SEC (compromise between purity and yield) are still the methods of choice for EVs isolation. For EV analysis, NTA, DLS, flow cytometry and TEM are the most widely used techniques. Electrokinetic strategies, together with microfluidic ones, bring not only new functionalities but also more possibilities of integration. They constitute an emerging trend that is expected soon to be ranked among the list of preferred methods for EVs isolation and analysis.

As reviewed here, there are different electrokinetically driven methods for isolation, preconcentration and separation of EVs. Most of them are still at the stage of research development (with an exception for TRPS). Application of such strategies on clinical samples and systematic comparison of their performances to those of established techniques still need to be investigated. Although some of electrokinetic approaches demonstrated their ability to distinguish subpopulation of EVs, results are highly variable

according to how samples are handled or collected, storage conditions and on the measurement itself. Further improvement of the measurement reproducibility and precision is prerequisite. Although the current electrokinetic methods are unable to fully combine purification, enrichment, separation and detection of EVs, they are individually capable of carrying out these steps quite efficiently as discrete modules. Thus, we expect in the future the emergence of integrated electrokinetic systems into a single platform to perform all these steps from highly complex biofluids. This is indeed a positive feature (i.e. performing EVs isolation and analysis with a high degree of automation, integration and ease of use) that electrokinetic strategies can address and make them afterwards superior to more conventional methods. All these developments require however the use of high-quality EV standards with narrow size distribution and homogeneous population to reduce discrepancies and enable unbiased devices comparison. The generation of recombinant EVs as a biological reference may open the door for well-characterized EV standards [88], and should be used as the starting material for further development of electrokinetic strategies for EVs isolation and analysis.

Declaration of Competing Interest

The authors declare that they have no known competing financial interests or personal relationships that could have appeared to influence the work reported in this paper.

Acknowledgement

This work has been financially supported by the Institut Universitaire de France (for M. Taverna, senior member). The doctoral scholarship for Marco Morani was supported by the doctoral school 2MIB (Sciences Chimiques: Molécules, Matériaux, Instrumentation et Biosystèmes) – University Paris Saclay.

References

- [1] K.W. Witwer, C. Théry, J. Extracell. Vesicles 8 (2019) 1648167.
- [2] C. Théry, K.W. Witwer, E. Aikawa, et al., J. Extracell. Vesicles 7 (2018) 43.
- [3] M. Yanez-Mo, P.R.M. Sijlander, Z. Andreu, et al., J. Extracell. Vesicles 4 (2015) 60.
- [4] N. Iraci, T. Leonardi, F. Gessler, B. Vega, S. Pluchino, Int. J. Mol. Sci. 17 (2016) 32.
- [5] G. van Niel, G. D'Angelo, G. Raposo, Nat. Rev. Mol. Cell Biol. 19 (2018) 213.
- [6] A. Latifkar, R.A. Cerione, M.A. Antonyak, Biochem. Soc. Trans. 46 (2018) 1137.
- [7] A. Latifkar, Y.H. Hur, J.C. Sanchez, R.A. Cerione, M.A. Antonyak, J. Cell Sci. 132 (2019) 9.
- [8] A. Becker, B.K. Thakur, J.M. Weiss, H.S. Kim, H. Peinado, D. Lyden, Canc. Cell 30 (2016) 836.
- [9] R.E. Lane, D. Korbie, M.M. Hill, M. Trau, Clin. Transl. Med. 7 (2018) 11.
- [10] H.C. Bu, D.G. He, X.X. He, K.M. Wang, Chembiochem 20 (2019) 451.
- [11] J. Howitt, A.F. Hill, J. Biol. Chem. 291 (2016) 26589.
- [12] M.H. Rashed, E. Bayraktar, G.K. Helal, M.F. Abd-Allah, P. Amero, A. Chavez-Reyes, C. Rodriguez-Aguayo, Int. J. Mol. Sci. 18 (2017) 25.
- [13] R.C. Lai, R.W.Y. Yeo, K.H. Tan, S.K. Lim, Biotechnol. Adv. 31 (2013) 543.
- [14] M.J. Haney, N.L. Klyachko, Y.L. Zhaoa, R. Gupta, E.G. Plotnikova, Z.J. He, T. Patel, A. Piroyan, M. Sokolsky, A.V. Kabanov, E.V. Batrakova, J. Contr. Release 207 (2015) 18.
- [15] F. Menay, L. Herschlik, J. De Toro, F. Cocozza, R. Tscalian, M.J. Gravisaco, M.P. Di Sciullo, A. Vendrell, C.I. Waldner, C. Mongini, Front. Immunol. 8 (2017) 14.
- [16] Y. Wang, Y.R. Zhang, G. Cai, Q. Li, Int. J. Nanomed. 15 (2020) 4257.
- [17] D.S. Choi, D.K. Kim, Y.K. Kim, Y.S. Cho, Proteomics 13 (2013) 1554.
- [18] X.X. Yang, C. Sun, L. Wang, X.L. Guo, J. Contr. Release 308 (2019) 119.
- [19] D. Yang, W. Zhang, H. Zhang, F. Zhang, L. Chen, L. Ma, L.M. Larcher, S. Chen, N. Liu, Q. Zhao, P.H.L. Tran, C. Chen, R.N. Veedu, T. Wang, Theranostics 10 (2020) 3684.
- [20] B.Y. Chen, C.W.H. Sung, C.C. Chen, C.M. Cheng, D.P.C. Lin, C.T. Huang, M.Y. Hsu, Clin. Chim. Acta 493 (2019) 14.
- [21] H.L. Shao, H. Im, C.M. Castro, X. Breakefield, R. Weissleder, H.H. Lee, Chem. Rev. 118 (2018) 1917.
- [22] W.S. Wang, J. Luo, S.T. Wang, Adv. Healthcare Mater. 7 (2018).
- [23] P. Li, M. Kaslan, S.H. Lee, J. Yao, Z.Q. Gao, Theranostics 7 (2017) 789.

- [24] M.Y. Konoshenko, E.A. Lekchnov, A.V. Vlassov, P.P. Laktionov, *BioMed Res. Int.* (2018) 27.
- [25] T.S. Martins, J. Catita, I.M. Rosa, O. Silva, A.G. Henriques, *PLoS One* 13 (2018).
- [26] M.I. Ramirez, M.G. Amorim, C. Gadelha, I. Milic, J.A. Welsh, V.M. Freitas, M. Nawaz, N. Akbar, Y. Couch, L. Makin, F. Cooke, A.L. Vettore, P.X. Batista, R. Freezor, J.A. Pezuk, L. Rosa-Fernandes, A.C.O. Carreira, A. Devitt, L. Jacobs, I.T. Silva, G. Coakley, D.N. Nunes, D. Carter, G. Palmisano, E. Dias-Neto, *Nanoscale* 10 (2018) 881.
- [27] C. Gardiner, D. Di Vizio, S. Sahoo, C. Thery, K.W. Witwer, M. Wauben, A.F. Hill, *J. Extracell. Vesicles* 5 (2016).
- [28] K. Brennan, K. Martin, S. FitzGerald, J. O'Sullivan, Y. Wu, A. Blanco, C. Richardson, M. Mc Gee, *Sci. Rep.* 10 (2020) 1.
- [29] S. Gholizadeh, M.S. Draz, M. Zarghooni, A. Sanati-Nezhad, S. Ghavami, H. Shafiee, M. Akbari, *Biosens. Bioelectron.* 91 (2017) 588.
- [30] W.T. Su, H.J. Li, W.W. Chen, J.H. Qin, *Trac. Trends Anal. Chem.* 118 (2019) 686.
- [31] Y. Jia, Z.H. Ni, H. Sun, C. Wang, *Ieee Access* 7 (2019) 45080.
- [32] S.J. Lin, Z.X. Yu, D. Chen, Z.G. Wang, J.M. Miao, Q.C. Li, D.Y. Zhang, J. Song, D.X. Cui, *Small* 16 (2020).
- [33] A. Liga, A.D.B. Vliegthart, W. Oosthuyzen, J.W. Dear, M. Kersaudy-Kerhoas, *Lab Chip* 15 (2015) 2388.
- [34] U. Erdbrugger, J. Lannigan, *Cytometry Part A* 89A (2016) 123.
- [35] R. Szataneck, M. Baj-Krzyworzeka, J. Zimoch, M. Lekka, M. Siedlar, J. Baran, *Int. J. Mol. Sci.* 18 (2017).
- [36] J.C. Contreras-Naranjo, H.J. Wu, V.M. Ugaz, *Lab Chip* 17 (2017) 3558.
- [37] L. Trapiella-Alfonso, G. Ramirez-Garcia, F. d'Orlye, A. Varenne, *Trac. Trends Anal. Chem.* 84 (2016) 121.
- [38] M.N. Alves, M. Miro, M.C. Breadmore, M. Macka, *Trac. Trends Anal. Chem.* 114 (2019) 89.
- [39] S. Dziomba, K. Ciura, M. Dawid, *J. Chromatogr. A* 1606 (2019).
- [40] T.K. Mudalige, H. Qu, D. Van Haute, S.M. Ansar, S.W. Linder, *Trac. Trends Anal. Chem.* 106 (2018) 202.
- [41] S. Gill, R. Catchpole, P. Forterre, *FEMS Microbiol. Rev.* 43 (2019) 273.
- [42] J. Kowal, G. Arras, M. Colombo, M. Jouve, J.P. Morath, B. Primald-Bengtson, F. Dingli, D. Loew, M. Tkach, C. Thery, *PNAS* 113 (2016) E968.
- [43] L. Margolis, Y. Sadovskiy, *PLoS Biol.* 17 (2019) 12.
- [44] I. Parolini, C. Federici, C. Raggi, L. Lugini, S. Palleschi, A. De Milito, C. Coscia, E. Iessi, M. Logozzi, A. Molinari, M. Colone, M. Tatti, M. Sargiacomo, S. Fais, *J. Biol. Chem.* 284 (2009) 34211.
- [45] K.E. Petersen, F. Shiri, T. White, G.T. Bardi, H. Sant, B.K. Gale, J.L. Hood, *Anal. Chem.* 90 (2018) 12783.
- [46] A. Zijlstra, D. Di Vizio, *Nat. Cell Biol.* 20 (2018) 228.
- [47] M. Morani, T.D. Mai, Z. Krupova, P. Defrenaix, E. Multia, M.-L. Riekkola, M. Taverna, *Anal. Chim. Acta* 1128 (1 September 2020) 42–51.
- [48] V.S. Chernyshev, R. Rachamadugu, Y.H. Tseng, D.M. Belnap, Y.L. Jia, K.J. Branch, A.E. Butterfield, L.F. Pease, P.S. Bernard, M. Skliar, *Anal. Bioanal. Chem.* 407 (2015) 3285.
- [49] J.H. Deng, Z.J. Li, Z.X. Wang, J. Feng, X.J. Huang, Z.M. Zeng, *Microsc. Microanal.* 26 (2020) 310.
- [50] F. Cao, Y. Gao, Q. Chu, Q. Wu, L. Zhao, T. Lan, L. Zhao, *Electrophoresis* (2019) 7.
- [51] F. d'Orlye, A. Varenne, P. Gareil, *Electrophoresis* 29 (2008) 3768.
- [52] F. d'Orlye, A. Varenne, T. Georgelin, J.M. Siaugue, B. Teste, S. Descroix, P. Gareil, *Electrophoresis* 30 (2009) 2572.
- [53] F.K. Liu, F.H. Ko, P.W. Huang, C.H. Wu, T.C. Chu, *J. Chromatogr. A* 1062 (2005) 139.
- [54] N.G. Vanifatova, B.Y. Spivakov, J. Mattusch, U. Franck, R. Wennrich, *Talanta* 66 (2005) 605.
- [55] U. Pyell, *Electrophoresis* 31 (2010) 814.
- [56] H.K. Jones, N.E. Ballou, *Anal. Chem.* 62 (1990) 2484.
- [57] R.T. Davies, J. Kim, S.C. Jang, E.J. Choi, Y.S. Gho, J. Park, *Lab Chip* 12 (2012) 5202.
- [58] S. Cho, W. Jo, Y. Heo, J.Y. Kang, R. Kwak, J. Park, *Sens. Actuators, B* 233 (2016) 289.
- [59] K. Mogi, K. Hayashida, T. Yamamoto, *Anal. Sci.* 34 (2018) 875.
- [60] J. Kim, S. Sahloul, A. Orozaliev, V.Q. Do, V.S. Pham, D. Martins, X. Wei, R. Levicky, Y.A. Song, *IEEE Nanotechnol. Mag.* 14 (2020) 18.
- [61] S. Marczak, K. Richards, Z. Ramshani, E. Smith, S. Senapati, R. Hill, D.B. Go, H.C. Chang, *Electrophoresis* 39 (2018) 2029.
- [62] L.S. Cheung, S. Sahloul, A. Orozaliev, Y.A. Song, *Micromachines* 9 (2018) 12.
- [63] R. Vaidyanathan, M. Naghibosadat, S. Rauf, D. Korbie, L.G. Carrascosa, M.J.A. Shiddiky, M. Trau, *Anal. Chem.* 86 (2014) 11125.
- [64] Y. Tian, M.F. Gong, Y.Y. Hu, H.S. Liu, W.Q. Zhang, M.M. Zhang, X.X. Hu, D. Aubert, S.B. Zhu, L. Wu, X.M. Yan, *J. Extracell. Vesicles* 9 (2020).
- [65] H.A. Pohl, *J. Appl. Phys.* 22 (1951) 869.
- [66] R. Pethig, *Biomicrofluidics* 4 (2010) 35.
- [67] A. Kuzyk, *Electrophoresis* 32 (2011) 2307.
- [68] C. Qian, H.B. Huang, L.G. Chen, X.P. Li, Z.B. Ge, T. Chen, Z. Yang, L.N. Sun, *Int. J. Mol. Sci.* 15 (2014) 18281.
- [69] S.D. Ibsen, J. Wright, J.M. Lewis, S. Kim, S.Y. Ko, J. Ong, S. Manouchehri, A. Vyas, J. Akers, C.C. Chen, B.S. Carter, S.C. Esener, M.J. Heller, *ACS Nano* 11 (2017) 6641.
- [70] J.M. Lewis, A.D. Vyas, Y.Q. Qiu, K.S. Messer, R. White, M.J. Heller, *ACS Nano* 12 (2018) 3311.
- [71] L.L. Shi, A. Rana, L. Esfandiari, *Sci. Rep.* 8 (2018) 12.
- [72] L.L. Shi, D. Kuhnell, V.J. Borra, S.M. Langevin, T. Nakamura, L. Esfandiari, *Lab Chip* 19 (2019) 3726.
- [73] S. Ayala-Mar, R.C. Gallo-Villanueva, J. Gonzalez-Valdez, *Mat. Today Proc.* 13 (2019) 332.
- [74] S. Ayala-Mar, V.H. Perez-Gonzalez, M.A. Mata-Gomez, R.C. Gallo-Villanueva, J. Gonzalez-Valdez, *Anal. Chem.* 91 (2019) 14975.
- [75] J.G. Chen, Y.C. Xu, X. Wang, D.C. Liu, F. Yang, X.R. Zhu, Y. Lu, W.L. Xing, *Lab on a Chip* 19 (2019) 432.
- [76] K. Kato, M. Kobayashi, N. Hanamura, T. Akagi, N. Kosaka, T. Ochiya, T. Ichiki, *Jpn. J. Appl. Phys.* 52 (2013) 4.
- [77] T. Akagi, K. Kato, N. Hanamura, M. Kobayashi, T. Ichiki, *Jpn. J. Appl. Phys.* 53 (2014).
- [78] T. Akagi, K. Kato, M. Kobayashi, N. Kosaka, T. Ochiya, T. Ichiki, *PLoS One* 10 (2015), e0123603.
- [79] T. Akagi, T. Ichiki, in: W.P. Kuo, S. Jia (Editors), *Microcapillary Chip-Based Extracellular Vesicle Profiling System*, Humana Press Inc., Totowa, 2017, p. 209.
- [80] T. Lan, X. Xi, Q. Chu, L. Zhao, A. Chen, J.J. Lu, F. Wang, W. Zhang, *Electrophoresis* 39 (2018) 2316.
- [81] M. Piotrowska, K. Ciura, M. Zalewska, M. Dawid, B. Correia, P. Sawicka, B. Lewczuk, J. Kasprzyk, L. Sola, W. Piekoszewski, B. Wielgomas, K. Waleron, S. Dziomba, *J. Chromatogr. A* (2020) 461047.
- [82] Y. Tani, T. Kaneta, *J. Chromatogr. A* 1629 (2020) 461513.
- [83] M. Al Ahmad, *Ieee Access* 6 (2018) 22817.
- [84] A. Akbarinejad, C.L. Hisey, D. Brewster, J. Ashraf, V. Chang, S. Sabet, Y. Nursalim, V. Lucarelli, C. Blenkinsop, L. Chamley, D. Barker, D.E. Williams, C.W. Evans, J. Travas-Sejdic, *ACS Appl. Mater. Interfaces* 12 (2020) 39005.
- [85] R. Vogel, G. Willmott, D. Kozak, G.S. Roberts, W. Anderson, L. Groenewegen, B. Glossop, A. Barnett, A. Turner, M. Trau, *Anal. Chem.* 83 (2011) 3499.
- [86] D. Kozak, W. Anderson, R. Vogel, S. Chen, F. Antaw, M. Trau, *ACS Nano* 6 (2012) 6990.
- [87] qNano, Izon, 2020. <https://store.izon.com/collections/instruments/products/qnano-gold>.
- [88] E. Geurickx, J. Tulkens, B. Dhondt, J.V. Deun, L. Lippens, G. Vergauwen, E. Heyrmar, D. De Sutter, K. Gevaert, F. Impens, I. Miinalainen, P.J. Van Bockstal, T. De Beer, M.H.M. Wauben, E.N.M. Nolte-t-Hoen, K. Bloch, J.V. Swinnen, E. van der Pol, R. Nieuwland, G. Braems, N. Callewaert, P. Mestdagh, J. Vandesompele, H. Denys, S. Eyckerman, O. De Wever, A. Hendrix, *Nat. Commun.* 10 (2019).
- [89] M. Colombo, G. Raposo, C. Thery, in: R. Schekman, R. Lehmann (Editors), *Biogenesis, Secretion, and Intercellular Interactions of Exosomes and Other Extracellular Vesicles*, 2014, p. 255.

In early 2021, El Ouahabi et al. developed a CE-ultraviolet diode array (CE-UV-DAD) method for the characterization of EVs isolated from human serum samples [252]. After EV isolation by polyethylene glycol (PEG) precipitation, the authors obtained characteristic electrophoretic multiwavelength profile of the EV preparation thanks to the addition of low concentration of hydroxypropyl cellulose to background electrolyte (BGE) to reduce the adsorption of the EVs to the ionized silanol groups of the inner capillary wall. However, a conclusion on the reason behind the different components detected in the electrophoretic fingerprints cannot be made. More recently, Dou et al. used CE with laser-induced fluorescence (LIF) detection to determine the quantity of RNA amount per EV and the concentration of EVs [253]. After isolation from cancer cells, a fluorogenic dye binding to DNA and RNA was employed to stain both intravesicular and free nuclei acids (NAs). The EVs and free NAs were subject to electrophoresis and separated into two distinct zones. After EVs lysis by SDS, the peak indicating the EV percentage disappeared, and the peak representing NAs increased. This increment represented the total quantity of intravesicular NAs released from EVs. This method offered good sensitivity achieving a detection limit of approximately 10^6 EVs/mL. However, this method did not provide any electrokinetic information on intact EVs profile.

III.3. Concluding remarks

Microfluidic systems can combine the advantages of portability, cheap cost, small sample volume, high throughput, and high sensitivity into a single device. Despite these benefits, microfluidic devices for EV application are still uncommon. This is due to the numerous difficulties in microfluidic control and microfabrication encountered while creating integrated systems capable of multistep processes. Researchers have given more an interest in the immuno-affinity technique because of its high specificity thanks to antibody-antigen interaction and wide range of potential applications. These techniques, however, depend substantially on the development of antibodies, which must be both specific to the target of interest and non-interfering with the downstream analysis. Furthermore, not only is it difficult to find specific antibodies for each specific analyte, but it is also necessary to thoroughly investigate the stability of the antibodies and the reusability of the device. Finally, the binding of antibodies to EVs' surface may adversely impact the biological properties of EVs. In parallel to immune-capture based approaches, other techniques focusing on the physical features of EVs have been developed to explore EVs separation. However, passive size-based approaches such as membrane filtration have a low selection resolution. Although, active approaches have the potential to alleviate this issue. Among them, we have emphasized how an external electrical field has been employed for EV isolation, enrichment, and characterisation. Although electrokinetic strategies are not

yet capable of fully integrating EV isolation and characterization into a single system, they can do it rather successfully as distinct modules.

Objective of the thesis

As previously stated in the preceding bibliography chapters, purification of EVs from biological fluids with good yields and reproducibility, and production of pure EVs to be used for diagnostic and pharmaceutical purposes remains a key challenge. This is mainly due to the technological difficulties to isolate and characterize such nanometric vesicles. Standardized approaches for accurately quantifying isolated EVs or characterize them in-depth, from biological fluids are currently required for clinical applications. The difficulties that must be overcome for the creation of diagnostic tools based on EVs are significant. It is necessary to standardize and simplify the isolation of EVs from undiluted biological fluids, to detect and quantify all relevant EV biomarkers with high sensitivity and specificity, and finally to passively collect intact vesicles in order to study their structural and biophysical properties in more detail in parallel with proteomic and genomic analysis [254].

In all EV applications, ultracentrifugation is considered the gold standard for their isolation. However, this method has several downsides, including lengthy processes, contamination of EV populations by protein aggregates and other particles, membrane damage, and significant loss of EVs. As a result, developing EVs isolation approaches that may guarantee EV purity and integrity in a repeatable and high-throughput way are still in great demand. Microfluidic systems look especially appealing in this context because they bring new functionalities and new mechanisms to sort or isolate EVs together with a capacity to reduce sample volume, costs, and reagent usage, speed up processes, and run several experiments in small devices at the same time.

Furthermore, the great heterogeneity of EV populations in terms of size and protein content complicates not only their isolation but also their physical and biochemical characterisation. Indeed, various complementary techniques must be carried out to ensure adequate physical and biological information are provided from the isolated EVs or that the extracted population is pure and has expected characteristics. Thus, new EV analysis methods or techniques are still searched to guarantee consistent EV purity and integrity.

In this regard, the goal of the thesis is to create a unique integrated analytical platform able to:

- allow effective extraction of EVs from biological fluids
- profile the distribution and quality of isolated of EV populations
- separate precise EV subpopulations

- extract specific intravesicular proteins of EVs that might be relevant as biomarkers in future diagnosis application and quantify or analyse them.

To achieve these objectives, different methodologies/techniques were developed throughout the course of this thesis with the purpose of ensuring the smooth progression toward the conception of the integrated analytical platform dedicated to EVs. The first panel of investigated methods relies on capillary electrophoresis (CE) which separates charged substances in solution under an electric field and has previously been reported for assessing the physical properties of nanoparticles such as their ζ -potential, surface charge density, particle radius, and size distribution. All the results of these developments are gathered in chapter IV.. The second category of techniques explored the capture and intact release of EVs using both immunoaffinity bead-based kits that utilize specific antibodies against EVs surface proteins and antibody-free magnetic beads that take advantage of their physical features rather. After refining the batchwise technique, it was converted to a microfluidic droplet procedure. Chapter V. compiles all of the outcomes of these advancements.

Faced with the challenge of isolating better EVs, the area of microfluidics as a tool for biological sample preparation is expanding. In order to develop the first module of the platform dedicated to EVs isolation, among all branches of microfluidics, we paid our particular attention to microfluidic droplets. Droplet-based microfluidics, which consists in manipulating discrete volumes of fluids in an immiscible phase, was chosen to ensure consistent compartmentalization of sample and reagents while simultaneously reducing both the amount of liquid required for analysis and the risk of contamination with the surrounding environment through the use of droplets. Microfluidic droplet systems with magnetic beads as solid support for extracting and purifying target analytes from complex matrices, in particular by using magnetic tweezers technology to transfer the magnetic beads from one droplet to another, have been demonstrated as promising biological sample preparation devices. Traditionally, EVs have been extracted using magnetic beads coated with specific antibodies against EV surface proteins. However, after isolation, such commercial kits, which are more often used for further EVs downstream lysis and analysis, do not provide any effective elution option for recovering intact EVs. In order to overcome this problem, we investigated different antibody-free magnetic beads strategy for capturing and eluting of EVs and in particular different surface chemistries of magnetic beads surface able to retain EVs. These developments relied on a microfluidic droplet technology already available in our laboratory. Furthermore, droplet microfluidics was only reported twice during the course of my thesis for immunoassay-based EV detection and never for high performance and high throughput isolation of EVs.

To develop the platform, we had then to combine the microfluidic collection of EVs to a characterization technique capable of distinguishing and detecting the different EV subpopulations as well as profiling the quality of isolated EVs. To facilitate an easier integration to the little amount of volume generated by the droplet module, we chose CE as it appears to be quite powerful and unexplored option to address this challenge either to analyze intact EVs or specific intravesicular proteins. Furthermore, CE provides several options for efficient analyte preconcentration and, thanks to its varied modes/mechanisms of performing separation and analyses under voltage or pressure, may be tuned to give complementary analytical modes. For the first time, we thus explored one mode of CE: Capillary Zone Electrophoresis (CZE) for profiling intact EVs but also for intravesicular protein analysis. Since conventional DLS and NTA for EVs size measurements are very sensitive to the presence of aggregates, Taylor dispersion analysis (TDA) which has emerged as a promising approach due to its ability to attain size scales ranging from molecule to nanoparticle was also explored for the first time for intact EVs size characterization. TDA can indeed be performed with a conventional CE. This CE-TDA-based characterization module was anticipated to be in the future either directly hyphenated to the isolation module (Droplet-TDA) or on-line to the CZE method, already hyphenated to the isolation module (Droplet-CZE-TDA). A summary scheme of the thesis project is presented below (Fig. 25)

Combining a micro-sized instrument for the controlled capture and release of EVs through magnetic beads with a promising methodology for electrokinetic profiling of EVs and intravesicular proteins, as well as EV size characterisation using CE technology, looks to be an attractive strategy to pursue as an innovative and promising project in terms of diagnosis application.

For the realization of this platform, another thesis project led by Théo Lienard—Mayor (Institut Galien Paris Saclay), aims to develop the instrumentation components, which will require i) a droplet-interfaced capillary electrophoresis (Digital CE) and ii) a system to interface the microfluidic droplet module to digital CE.

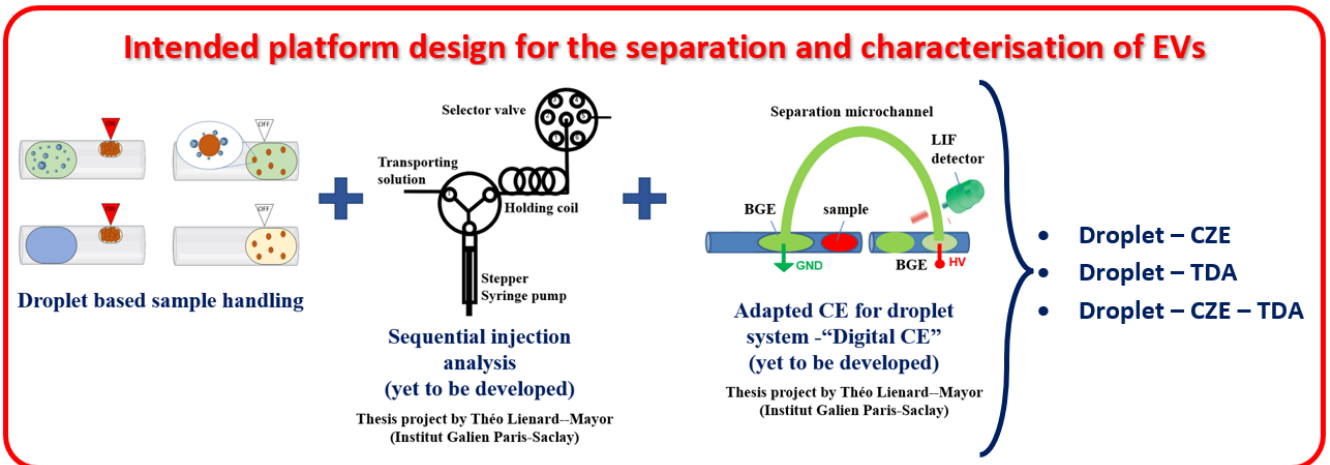
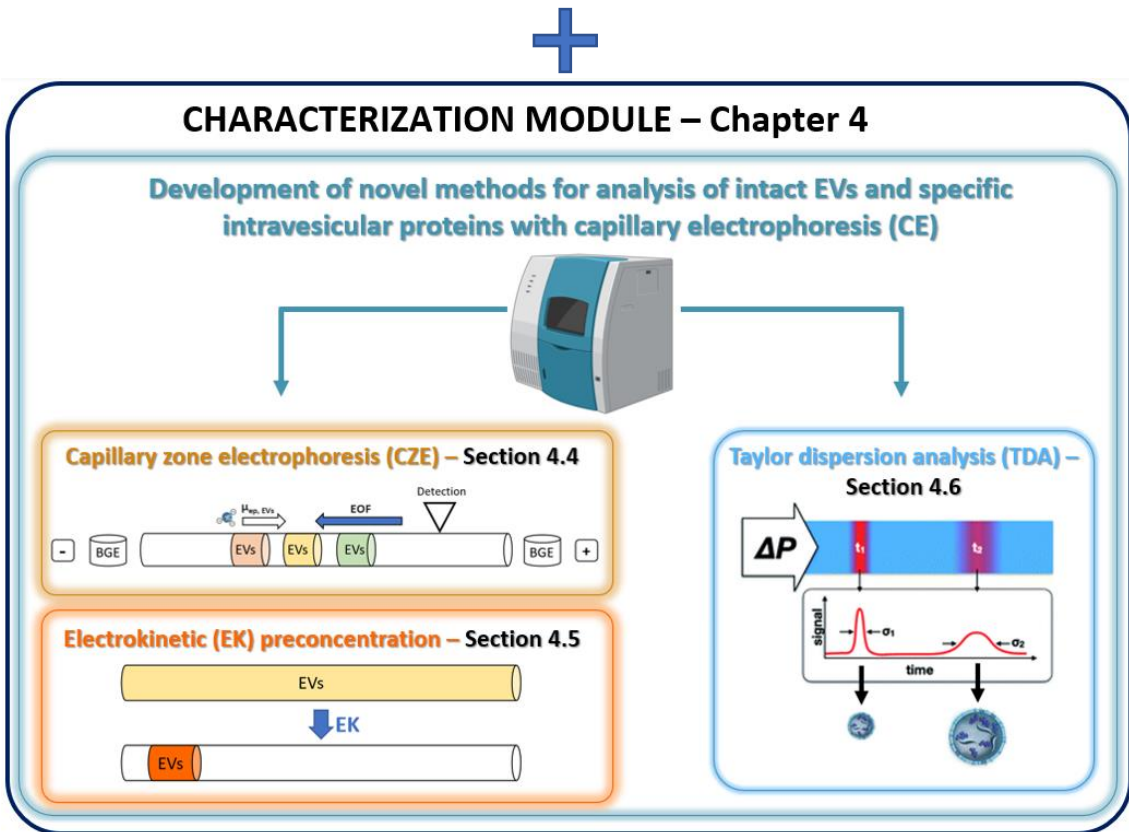
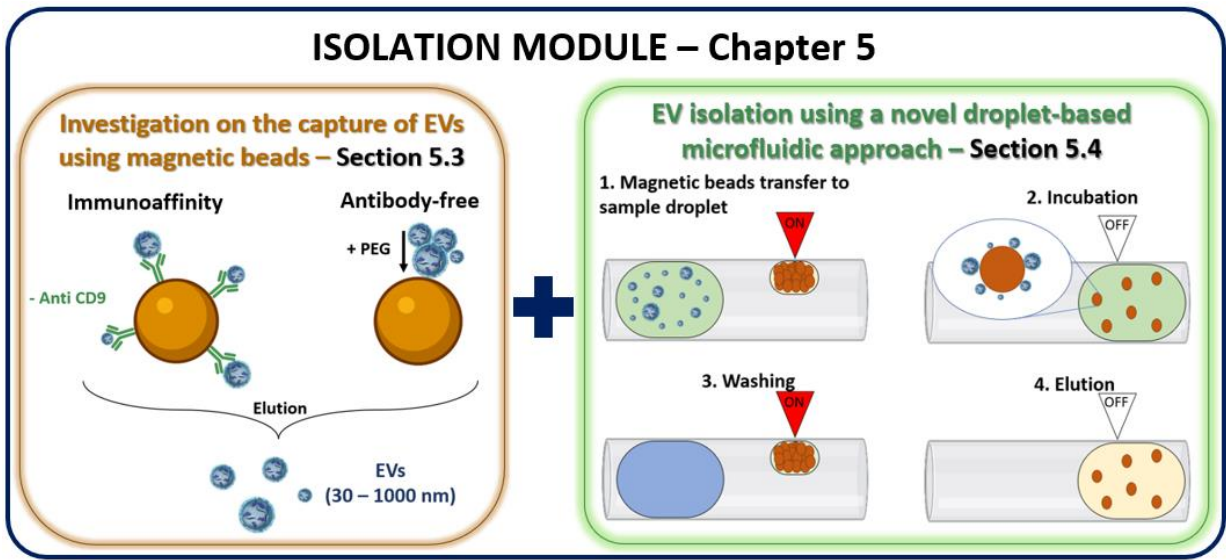


Figure 25: Schematic representation of the thesis project and on the two modules I focused on during my thesis

Experimental part

Chapter IV: Development of novel methods for analysis of intact EVs and specific intravesicular proteins with capillary electrophoresis

IV.1. Introduction

EVs have been recognized as important mediators for cellular communication. These lipid vesicles, physiologically secreted by the cells, show great heterogeneity both in size and in molecular content. It has been proven before that protein alterations, exhibited on their surfaces or in their content, may reflect the state and the nature of the generating cells. As a result, EVs are regarded as suitable source of biomarkers in a variety of diseases. Given the focus placed on liquid biopsy in recent years, this characteristic offers up new avenues for EV clinical applications. However, since none of the EV isolation procedures discussed above can combine repeatability, high yield, and high purity, the quality and concentration of isolated EVs must be validated before target intravesicular molecules can be evaluated for diagnostic and prognostic purposes. That is why, studies which investigate the potential of EVs as biomarkers are restricted by the characterization tools currently available, and one of the challenges of this thesis is to contribute to the creation of an appropriate technology or approach. Our analytical platform is indeed intended to allow effective extraction of EVs from biological fluids not only for intracellular protein analysis, but also for characterization of isolated EVs through differentiation of EV subpopulations, as well as to ensure their quality through the detection of potential contaminants.

One challenge with intact EV analysis is related to their very small size, the polydispersity of the EV population, the low refractive index of EVs, and the presence of protein aggregates and other particles contaminants in most isolated EVs samples. Single particle tracking (72%, mostly with NTA) and electron microscopy (60%) are the most often utilized traditional techniques for intact EV analysis [139]. Although robust and effective, they present some disadvantages that have been discussed in the bibliography section. A good approach should be able to identify and characterize EVs reliably and quickly, while also satisfying all of the requirements for EV phenotyping, such as the capacity to distinguish between various size sub-populations and potential contaminants, as well as maintaining EV integrity throughout analysis. In order to separate such close bioentities, the use of a separative analytical method with great resolving power is essential.

CE is an analytical method for the separation and quantification of a wide range of compounds, which can be described in general as the movement of charged substances in solution using an applied

voltage. The narrow tubes (generally between 20 and 100 μm in diameter) that are employed in CE contribute to the high resolution of the method. The use of narrow capillary tubes has the benefit of reducing lateral diffusion effects as well as reducing Joule heating effect upon application of a high voltage, and thus band-broadening. Compared to high-performance liquid chromatography (HPLC), CE does not suffer from band-broadening and wider peaks due to the parabolic velocity profile, as the liquid's velocity through the CE capillary is flat and uniform across the tube. Moreover, the use of CE silica capillaries without packing materials simplifies instrument design and generate less fluidic resistance than packed columns as in HPLC. Additionally, in our project, where we aim to develop a downstream separation approach to be subsequently integrated to the forefront droplet platform for EVs isolation (which will be discussed in the next chapter), CE is the separation approach that is most compatible to the limited sample volumes generated by the droplet platform. For all these reasons, CE was chosen as an intriguing and never explored option for potentially analysing EVs and their subpopulations as well as for a quality control of isolated EVs. In parallel, thanks to the ease with which Taylor dispersion analysis (TDA) can be set up on a commercial CE device by applying pressure to the capillary's inlet rather than an electric field, and the ability to determine the size of ultra-small NPs ($< 5 \text{ nm}$), we found it interesting to test the possibility to perform TDA either directly after EVs isolation or for subsequent coupling of CZE-TDA in the same capillary, allowing for the determination of the hydrodynamic radius of each sample zone previously separated by CE. Indeed, when I started my thesis, no work reported the use of CE for the identification and quantification of EVs after their isolation. During the course of my thesis, only another CE-based method [255] was disclosed on bacterial EVs and shortly before the publication of our research. In this work authors did not propose to separate and distinguish EVs from different origins. In our hands, laser induced Fluorescence (LIF) detection was investigated rather than UV, to bring more specificity in the obtained profiles but also sensitivity. As CE is already considered as a powerful techniques for protein analysis [256, 257], we aimed to use it also for potential analysis of specific intravesicular proteins. We used LIF for both objectives in order to get high sensitivity in both the proteins and EVs that were analyzed. However, proteins must be fluorescently labelled; the most common strategy to label proteins is via their cysteine and amino groups [258]. Then, being the first group to explore CE on EVs, I had to figure out how to avoid EV lysis and prevent the formation of EV aggregates under high voltages. At the same time, attention had to be paid on possible EV adsorption to the silica capillary wall that could result in some resolution loss. Moreover, even though LIF is still one of the most sensitive and selective detection methods in CE, various protein biomarkers may be visualized at low amounts in an EVs sample [259]. In addition, EVs concentration after extraction from complex biofluids may be very low and vary significantly among biofluids, ranging from 10^7 particles/mL for cerebrospinal fluid (CSF) to

10^8 - 10^9 particles/mL for plasma and blood [260]. As a result, we investigated several ways to overcome these difficulties and in particular to try to gain sensitivity. The first one relied on the use of new BGEs and the another on investigating electrokinetic preconcentration techniques which are based on differences in the analyte migration velocity across discontinuous solution interfaces. The analytes dissolved in a different sample matrix than the BGE are accumulated (stacked) at the boundary of the two solutions.

The first part of this experimental chapter IV., which is dedicated to all investigated strategies relying on CE, will briefly present the fundamentals and some theoretical aspects of CE. The second part will present our achievements in improving the performance of CE-LIF in terms of stacking preconcentration and separation resolution of fluorescently labelled proteins and peptides. In the third part, our first achievements in establishing a solid background for the electrokinetic profiling of EVs is presented. In the fourth section, effective strategies for in-capillary sample preconcentration for EVs are explored in order to further increase the sensitivity of regular LIF detection. Finally, the TDA applicability to EVs was explored for precise size evaluation and our preliminary and encouraging results are presented in the last section of this chapter.

IV.2. Principle of capillary electrophoresis (CE)

EVs have been shown to be high in negatively charged phosphatidylserine [261, 262]. As a result, by applying a voltage, negatively charged EVs may migrate at varying velocities depending on their size, charge, and shape. In chapter III. of the bibliographic part of this thesis, I highlighted how this mechanism has lately been exploited, most notably as a particle sorting method in various microdevices to separate and drive the EVs. However, when I began my thesis, no publication had mentioned the possibility of using CE to analyze EVs or distinguish EV subtypes based on their electrophoretic migration. During the course of my thesis, four CE methods for analyzing and quantifying EVs have been disclosed [252, 253, 255, 263]. However, only two of these have been proposed for the investigation of intact EVs. Before investigating the power of CE to address two of our aims (i) develop a CE approach capable of assessing intact EVs after their isolation in order to deliver information on the diverse subpopulations of EVs and (ii) assess their protein internal content, which may be employed as biomarkers in the future once validated; this first part is intended to provide the fundamentals of electrophoretic migration and some theoretical aspects of CE, which will be necessary in order to better understand the achievements achieved and show the potential for CE in the area of EVs.

Typically, in CE (see Fig. 26) performed with voltage application, the sample is injected into a capillary filled with the background electrolyte (BGE) serving as the separation medium and then a high voltage is applied over two ends of the capillary (immersed in a BGE containing reservoir) to trigger the separation of target molecules. On-capillary detection via an optical window created directly on the capillary contributes to the great efficiency found in CE because the separation continues to occur while analytes pass through the detection window, and there is no broadening of the zone due to dead volume, as otherwise encountered in post-column detection.

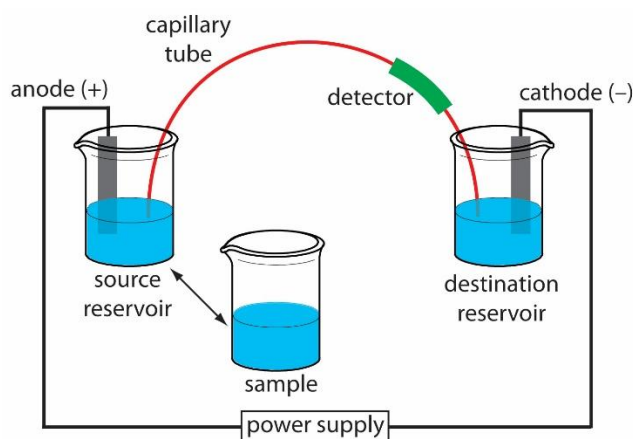


Figure 26: Schematic representation of the instrumentation used in CE.

By far the most prevalent kind of detection is UV-visible. In many circumstances, this option is insufficient in terms of detection sensitivity and selectivity to fulfill the analytical criteria. In CE, LIF detection is the most sensitive on-column detection mode. This is why it was prevalently used in this thesis.

Like HPLC, CE entails many separation modes which are based on different separation mechanisms, such as capillary zone electrophoresis (CZE), electrokinetic chromatography (MEKC), capillary gel electrophoresis (GCE) and isoelectric focusing capillary (cIEF) [264]. CZE is one mode of CE that separates analytes, and particles according to their charge-to-size ratio under a high electrical field and often in the presence of an electroosmotic flow generated by the silica wall of the capillary. We selected CZE over other modes because of its simplicity and benefits, including complete automation of detection and identification (sample loading, separation, and detection are all computer programmed and therefore standardized) and higher resolution. The movement of molecules during the CZE separation is the result of two phenomena: the electroosmosis and the electromigration of

analytes. The theory behind these two electromigration mechanism which are involved in CZE separation is reminded in the following part.

IV.2.1. Electroosmotic flow (EOF)

The fused silica capillaries that are typically used for separations have ionizable silanol groups (Si-OH) which are negatively charged (SiO⁻) when the pH of the BGE filled inside the capillary is superior to 3.0 (see Fig. 27) [265].

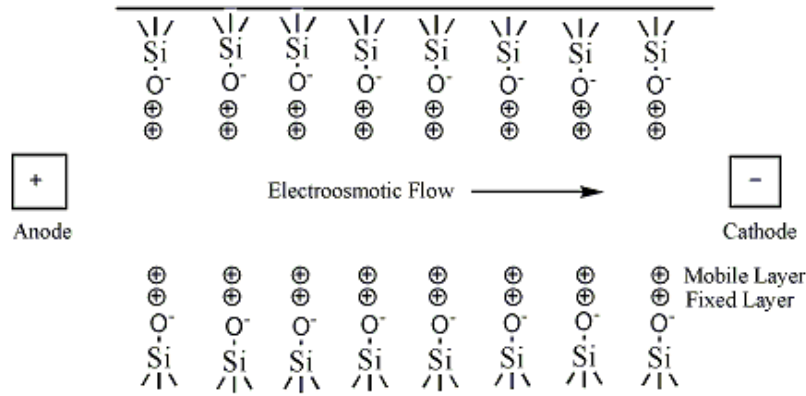


Figure 27: Electroosmotic flow of positive ions through the capillary with negative charged walls.

The negatively-charged wall attracts cations of the buffer, creating an electrical double layer. It is composed of one fixed and compact layer and one diffuse layer in which cations are more mobile and move along the capillary toward the cathode. This double layer can be characterized by the value of its surface potential, called Zeta (ζ) potential (in V). This potential is described according to equation 1, and depends on the thickness of the double layer, the charge density of the capillary internal surface, and the electrolyte parameters:

$$\zeta = \frac{\delta \cdot \sigma}{\epsilon_r \cdot \epsilon_0} \text{ avec } \delta = \sqrt{\frac{\epsilon_r \cdot \epsilon_0 \cdot R \cdot T}{2 \cdot I \cdot F^2}} \quad (1)$$

Where δ is the thickness of the double layer (m), σ the density of surface charges of the capillary (C.m⁻²), ϵ_r the dielectric constant of the electrolyte, ϵ_0 the permittivity of the vacuum (8,85.10⁻¹² C² .N⁻¹.m⁻²), R the ideal gas constant (8.325 J.mol⁻¹.K⁻¹), T the temperature (K), I the ionic strength of the electrolyte and F the Faraday constant (96500 C.mol⁻¹).

Under the action of an electric field, the cations of the diffuse layer are attracted to the cathode, while the cations of the compact layer are retained by strong electrostatic interactions binding them to

silanol groups. This movement of the outer layer, which causes all the compounds present in the electrolyte to move toward the cathode, is called the electroosmotic flow (EOF). This displacement has a flat profile, unlike pressure separations which have a parabolic velocity one (liquid chromatography) that limits diffusion during separations and allows CE to achieve high efficiencies. The electroosmotic flow, can be characterized according to equation 2 by the electroosmotic velocity v_{eo} ($m \cdot s^{-1}$), dependent on the electroosmotic mobility μ_{eo} ($m^2 \cdot V^{-1} \cdot s^{-1}$) and the applied electric field E ($V \cdot cm^{-1}$):

$$v_{eo} = \mu_{eo} \cdot E = -\frac{\epsilon_r \cdot \epsilon_0 \cdot \zeta}{\eta} \cdot E \quad (2)$$

Where η corresponds to the viscosity of the medium (Pa.s). The electroosmotic mobility depends on the medium (composition, pH, ionic strength, viscosity of the BGE) as well as the surface chemistry and nature of the capillary. Note here that it is possible to modify this surface by specific treatments, such as covering with polymers modifying the surface properties.

IV.2.2. Electrophoretic mobility (μ_{ep})

Electrophoretic mobility corresponds to the displacement of a charged species under an electric field [266]. This species will be attracted towards the electrode of polarity opposite to its charge at the velocity v_{ep} ($m \cdot s^{-1}$), dependent on the electrophoretic mobility of the species μ_{ep} ($m^2 \cdot V^{-1} \cdot cm^{-1}$) and on the electric field applied E ($V \cdot cm^{-1}$) described in equation 3:

$$v_{ep} = \mu_{ep} \cdot E \quad (3)$$

The electrophoretic mobility is specific to each compound and the physicochemical properties of the electrolyte. In case of infinite dilution, the electrophoretic mobility μ_{ep} of a species is dependent on its hydrodynamic radius R_h as well as on its charge q , therefore more generally on its charge density (equation 4). At equal charge, for example, a small cation will move faster than a large one.

$$\mu_{ep} = \frac{q}{6 \cdot \pi \cdot r_h \cdot \eta} \quad (4)$$

CZE is one of the most frequent and simplest of the CE modes and is often used for the study and separation of a wide variety of compounds, including proteins and NPs. The migration of the species to be separated under the effect of the electric field is governed by their charge density. The higher this density, the faster the species will be attracted towards the electrode of opposite polarity. In the case of the analysis of peptides and proteins having ionizable groups, the pH of the electrolyte therefore plays a major role since it determine the charge state of the peptide/protein according to

titration curve. At the same time the pH impacts the electroosmotic mobility. The EOF is substantially bigger at high pH, where the silanol groups are largely deprotonated, than at low pH, when they get protonated. Thus, at high pH, the EOF may be excessively strong, resulting in species elution before separation. In CZE, the migration of a species is characterized by its apparent mobility μ_{app} , the sum of electroosmotic mobility and electrophoretic mobility [267] practically measured using Eq5.

$$\mu_{app} = \mu_{eo} + \mu_{ep} = \frac{L \cdot l}{V \cdot t_m} \quad (5)$$

Where L is the total length of the capillary (cm), l the length to the detector (cm), V the applied voltage (V) and t_m the migration time of the species (s). Figure 28 shows the direction and intensity of mobility of each type of species during separation. Note that it will only be possible to detect an anion if the electroosmotic mobility is greater in absolute value than its electrophoretic mobility and that neutral compounds or particles cannot be easily discriminated from each other.

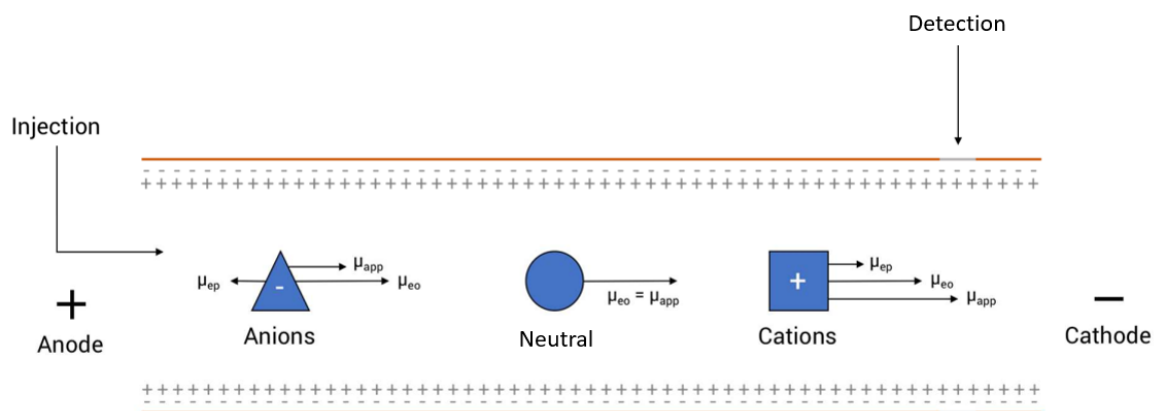


Figure 28 : Principle of separation in capillary zone electrophoresis.

However, electrophoretic methods have some drawbacks. Adsorption onto the walls of fused silica capillaries owing to electrostatic or hydrophobic interactions is a well-known limitation in CZE protein analysis. Protein adsorption causes poor repeatability, lower detector response, decreased resolution and separation efficiency. Similar to proteins, the problem with EVs may be exacerbated by the presence of various amine functionalities present on EVs membrane proteins which can interact with negatively charged silanol groups on the capillary surface. Another issue of CE is its poor detection sensitivity due to small sample injection volumes (some nL ranges in CZE mode) and limited detection pathlengths across the capillary section when working with optical detection modes, which may be troublesome when working with biological materials such as EVs or their protein contents at low concentrations. In the following section, I will present a strategy based on the selection of appropriate

BGE to overcome these issues as well as the results achieved for CE-LIF analysis of proteins and, subsequently, EVs.

IV.3. “Inorganic-species-free” BGE (ISF BGE) for capillary electrophoresis-laser induced fluorescence (CE-LIF) performance improvement

In this thesis project and for all CE-based developments, LIF detection was preferred over commonly used UV detection because of its higher sensitivity and selectivity for the detection of target analytes, which is especially crucial for achieving our final goal to analyze and investigate intravesicular molecules (mostly proteins) in the pM range. The detection sensitivity for target proteins, is heavily dependent on their amino acid composition, and in part on the intrinsic fluorescence of tryptophan, tyrosine, and phenylalanine. As these amino acids with intrinsic fluorescence are most often not abundant in a protein sequence, proteins and peptides must be labeled with a fluorescent tag to allow for sufficient sensitivity of detection. Depending on the desired applications, there are many markers that can be used to derive proteins [258]. The choice of a fluorophore to label target proteins/peptides is normally based on its extinction coefficient, emission efficiency, excitation/emission wavelengths, as well as the functional group present on the protein for covalent attachment. The most popular technique is to target cysteine and amine groups with direct chemical labelling. Cysteines provide the most flexibility in terms of labeling position. Lysine residues or N-terminal amines may be labeled using amine-reactive conjugates. Labeling a particular protein which bears multiple target residues, on the other hand, results in a number of distinct labelled protein species, each with a different number of tags and consequently a varied electrophoretic mobility. As a result, it is critical that the CE conditions employed should ensure efficient separation of bound and non-bound labeled reagents (i.e., tagged target proteins and residual fluorophores in our particular case) as well as simultaneous analysis of several proteins and their possible multiple tagged species. We chose rather to reinvestigate BGE compositions to achieve this goal. Indeed, BGEs for CE-LIF separation are often derived from those optimized for CE-UV separation, and little attention has been devoted to the development of proper BGEs for CE-LIF. Based on this logic, we investigated a new BGE selection strategy to improve the performance of CE-LIF in terms of stacking preconcentration and separation resolution of fluorescently labeled proteins and peptides. Beta amyloid peptide ($A\beta$ 1–42) and trypsin inhibitor (TI) were utilized as model of peptides and proteins, respectively, for this study. Following that, to assess the resolution enhancement, we worked on ovalbumin, which may be tagged at several spots and to varied degrees and is also a more complex protein, being glycosylated and so existing as a mixture of glycoforms. Actually, one of the long-term goals of this thesis was to bring new information and also to possibly

reveal interesting post-translational modifications of specific glycoproteins contained within EVs extracted from CSF and serum for diagnostic purpose. Although this experiment was unable to be carried out due to time constraints for the thesis, the data reported in the following paper ([Morani et al., Electrophoresis, 2019](#) [268]) highlighted the difficulties when dealing with multi-tagged proteins that could be assimilated to intravesicular proteins.

Marco Morani
Myriam Taverna* 
Thanh Duc Mai

Institut Galien Paris Sud, UMR
8612, Protein and
Nanotechnology in Analytical
Science (PNAS), CNRS, Univ.
Paris-SudUniv. Paris-Saclay,
Châtenay-Malabry, France

Received February 5, 2019
Revised May 14, 2019
Accepted May 18, 2019

Research Article

A fresh look into background electrolyte selection for capillary electrophoresis-laser induced fluorescence of peptides and proteins

This study reports a reinvestigation of background electrolyte selection strategy for performance improvement in CE-LIF of peptides and proteins. This strategy is based on the employment of high concentrations of organic species in BGE possessing high buffer capacity and low specific conductivity in order to ensure excellent stacking preconcentration and separation resolution of fluorescently tagged peptides and proteins. Unlike universal UV detection, the use of such BGEs at high concentrations does not lead to degradation of LIF detection signals at the working excitation and emission wavelengths. At the same buffer ionic strength, pH and electric field, an “inorganic-species-free” BGE (or ISF BGE) for CE-LIF of fluorescently labeled beta amyloid peptide A β 1–42 (a model analyte) offered a signal intensity and peak efficiency at least three-times higher than those obtained with a conventional BGE normally used for CE-LIF, while producing an electric current twice lower. Good peak performance (in terms of height and shape) was maintained when using ISF BGEs even with samples prepared in high-conductivity phosphate buffer saline matrix. The advantageous features of such BGEs used at high concentrations over conventional ones in terms of high separation resolution, improved signal intensities, tuning of EOF magnitudes and minimization of protein adsorption on an uncoated fused silica capillary are demonstrated using Alexa-488-labelled trypsin inhibitor. Such BGE selection approach was applied for investigation of separation performance for CE-LIF of ovalbumin labelled with different fluorophores.

Keywords:

Background electrolyte optimization / Capillary electrophoresis / LIF detection / Peptides and proteins
DOI 10.1002/elps.201900084

1 Introduction

CE is a particularly adapted technique for proteins and peptides analysis due to its high separation resolution, low consumption of samples and reagents, and high throughput. To increase sensitivity of detection of target proteins and peptides, especially in the context of biomarker quantification (down to nM ranges) from biological matrices, LIF detection is in many cases preferable to the universal UV detection. Deep UV-LIF detection is one interesting option that does

not require protein/peptide derivatization [1]. Its widespread use however is limited by the low availability and high cost of powerful laser sources at the UV wavelengths. In addition, the detection sensitivity is much dependent on the intrinsic fluorescence of tryptophan, tyrosine, and phenylalanine in the target proteins or peptides. It is also interfered by the presence of other molecules in the matrix that absorb the excitation UV wavelength. A more conventional approach that often offers higher sensitivity is the labeling of proteins/peptides with fluorophores prior to CE-LIF [1]. In this direction so far, strategies to ensure a good CE-LIF sensitivity for proteins and peptides analyses mainly focus on sample treatment (i.e. optimization of fluorescent tagging of the target analytes, removal of unwanted matrices), and instrumental improvement (i.e. excitation source and wavelength, optical filtration, and signal conversion) (see [2–4] and references listed therein). On the other hand, little attention has been paid to the proper selection of BGEs to improve the separation resolution and

Correspondence: Dr. Thanh Duc Mai, Institut Galien Paris Sud, UMR 8612, Protein and Nanotechnology in Analytical Science (PNAS), CNRS, Univ. Paris-Sud, Univ. Paris-Saclay, 5 rue Jean Baptiste Clément, 92290 Châtenay-Malabry, France
E-mail: thanh-duc.mai@u-psud.fr

Abbreviations: C⁴D, contactless conductivity detection; FP, Fluoprobe; IS, ionic strength; ISF, inorganic species free; TI, trypsin inhibitor

*Additional corresponding author: Professor Myriam Taverna
E-mail: myriam.taverna@u-psud.fr

stacking effect that results in enhanced detection sensitivity. Indeed, BGEs for CE-LIF are often 'borrowed' from those optimized for CE-UV separation. A list of frequently used BGEs for CE-LIF of proteins and peptides was established by de Kort et al. [5]. These BGEs are either composed of inorganic species (typically NaOH/phosphate and NaOH/borate buffers) or contain inorganic acids/bases (HCl or NaOH for pH adjustment) which possess negligible or no UV absorbing features. Due to the high mobility of these inorganic ions, high concentrations are precluded to avoid Joule heating effect.

In another context, zwitterionic organic BGEs with high buffering capacity and low electric conductivity were proposed sometimes to improve CE separation resolutions and shorten analysis time under very high electric field strength [6–9]. Thanks to the very low Joule heating, these BGEs allow application of very high electrical fields up to several thousands of volts per cm without rupture of the electric current during CE nor peak broadening or distortion. Nevertheless, relatively low BGE concentrations had to be used for CE-UV due to (i) UV absorption of organic species in such BGEs, leading to unwanted high background signals and (ii) presence of system peaks [10–12]. Employment of very high concentrations of such BGEs to favor excellent stacking and preconcentration of analytes prior to CE separation has not been trivial with UV detection.

On the other hand, zwitterionic or organic BGEs at high concentrations have been applied successfully for CE separations of non-UV absorbing compounds, using (capacitively coupled) contactless conductivity detection (C^4D) [13,14]. Unlike UV detection, the detection sensitivity in this case is not degraded by the C^4D background signal. To the best of our knowledge, until now this type of buffer has not been investigated for CE-LIF purposes, in particular for CE-LIF of derivatized peptides and proteins. With a similar rationality to the case of C^4D , CE-LIF signals of derivatized proteins and peptides are expected to be little (if not) influenced by the BGEs composed of organic species, as they do not produce residual signals at the working excitation wavelength (normally in the visible range such as 488 nm and 532 nm). This drove us to re-investigate BGE selection using organic species at high concentrations to improve the separation and stacking performance for CE-LIF of fluorescently tagged peptides/proteins. For this purpose, fluorescently labeled beta amyloid peptide A β 1–42 and trypsin inhibitor (TI) were used as the model peptide and protein, respectively. We compared the sensitivity and separation performance obtained with conventional and inorganic-species-free BGEs (ISF BGEs) for CE-LIF of tagged A β 1–42. The tuning of EOF magnitudes, elimination of Joule heating effect and minimization of protein adsorption on the capillary wall were investigated with Alexa-488 labelled TI. To evaluate the resolution improvement, we worked on ovalbumin that may be tagged on different sites and with different degrees. Different fluorescent dyes possessing various electrophoretic mobilities were used to optimize the separation between the tagged ovalbumin

and the residual fluorophore within an uncoated fused silica capillary.

2 Materials and methods

2.1 Chemicals and reagents

Amyloid beta peptide A β 1–42 was purchased from Anaspec (Fremont, CA, USA). Trypsin inhibitor from Soybean, Alexa Fluor[®] 488 Conjugate (TI-Alexa 488) was obtained from Thermo Fisher Scientific (Waltham, MA, USA). Albumin from chicken egg white (ovalbumin) was purchased from Sigma Aldrich (St. Louis, MO, USA). Ammonium bicarbonate, boric acid, 2-(Cyclohexylamino)ethanesulfonic acid (CHES), dimethyl sulfoxide (DMSO, 99.9% purity), L-Histidine, 4-(4-Methoxybenzylamino)-7-nitro-2,1,3-benzoxadiazole, phosphate buffered saline (PBS 10x), sodium dodecyl sulfate (SDS, 98.5%), 2-((2-Hydroxy-1,1-bis(hydroxymethyl)ethyl)amino)ethanesulfonic acid, Tris, Tris(2-carboxyethyl)phosphine were all obtained from Sigma Aldrich. Sodium hydroxide (1 M), hydrochloric (1 M) and citric acid were obtained from VWR (Fontenay-sous-Bois, France). Sodium phosphatemonobasic (NaH_2PO_4) and disodium phosphate dibasic (Na_2HPO_4) were purchased from Thermo Fisher scientific. All buffers were prepared with deionized water. The Fluoprobe-488 NHS ester (FP-488-NHS), Fluoprobe 488 maleimide (FP-488-Maleimide), and Fluorescein-X5-Maleimide were obtained from Interchim (Montluçon, France). The Alexa Fluor[™] 488 C5 Maleimide (Alexa-488-Maleimide) was purchased from Thermo Fisher Scientific. The CF[™] 488A maleimide (CF-488-Maleimide) was purchased from Sigma Aldrich. All dyes were dissolved in DMSO to obtain aliquots of 10 mg/mL which were then stored at -20°C in the darkness.

2.2 Apparatus and material

The studies were performed with a PA 800 Plus system (Sciex Separation, Brea, CA) equipped with a solid-state laser induced fluorescence detector ($\lambda_{\text{excitation}}$: 488 nm, $\lambda_{\text{emission}}$: 520 nm) purchased from Integrated Optics (Art. No. 40A-48A-52A-64A-14-DM-PT, distributed by Acal BFi, Evry, France). Uncoated capillaries were purchased from CM Scientific (Silsden, UK). Data acquisition and instrument control were carried out using Karat 8.0 software (Sciex Separation, Brea, CA). Deionized water used in all experiments was purified using a Direct-Q3 UV purification system (Millipore, Milford, MA, USA). Conductivity and pH values of buffer solutions and samples were acquired with a SevenCompact pH meter (Mettler Toledo, Schwerzenbach, Switzerland). Preparation of BGE and buffer ionic strength (IS) calculations were based on simulations with the computer program PhoeBus (Analis, Suarlée, Belgium).

Table 1. Properties of the investigated native peptide and proteins

| Analyte | pI | Molecular weight (Da) | Number of potential derivatization sites | Reagent used for fluorescent labeling |
|--|-----|-----------------------|---|--|
| Amyloid beta peptide A β 1–42 | 5.5 | 4514 | Three amino groups (two lysine and one terminal NH ₂) | FluoProbe 488 NHS |
| Trypsin inhibitor from Soybean | 4.6 | 21 000 | From three to six amino groups | Alexa Fluor [®] 488 |
| Albumin from chicken egg white (ovalbumin) | 4.5 | 42 700 | Six cysteine groups | Fluorescein-488, Alexa-488, FP-488, CF-488 |

2.3 Methods

2.3.1 Fluorescent labelling of peptide and proteins

The properties of the investigated native peptide and proteins are shown in Table 1. The fluorescently labelled A β 1–42 was prepared using the Fluoroprobe 488 dye and according to the labelling and filtering protocol developed previously in our group [15]. Ovalbumin was chosen as a model protein and was labelled with different fluorescent dyes. Reduction was performed prior to labelling by incubating 50 μ M of ovalbumin with 140 μ M Tris(2-carboxyethyl)phosphine prepared in phosphate buffer (pH 7.4, IS 20 mM) over 2 h at room temperature. The protein was then incubated with a fluorophore (i.e. FP-488-maleimide, Alexa-488-maleimide, CF-488-maleimide, or Fluorescein-X5-maleimide) at a fluorophore/protein molar ratio of 2 at room temperature for 2 h in the dark.

2.3.2 CE-LIF of labelled peptide and proteins and EOF measurement

The working capillary (i.d. of 50 μ m, effective length (L_{eff}) of 50.2 cm, and total length (L_{tot}) of 60.2 cm) was pre-conditioned (using a pressure of 25 psi at the capillary inlet) with the following sequence: water for 10 min, 1 M NaOH for 10 min, 1 M HCl for 10 min, and then water for 10 min. The rinsing between two analyses was carried out with SDS 50 mM for 5 min, 1 M NaOH for 5 min, deionized water for 5 min, and finally the running BGE for 5 min using a pressure of 30 psi. A plug of sample was hydrodynamically injected from the inlet end by applying a pressure of 0.5 psi for 10 s. The separation was carried out under 30 kV at 25°C and the samples were maintained at 5°C with the sample storage module of the PA 800 Plus equipment. 4-(4-methoxybenzylamino)-7-nitro-2,1,3-benzoxadiazole, with its neutral charge and fluorescent property [16], was used as an EOF marker for CE-LIF at the working excitation wavelength of 488 nm. The marker was dissolved with a DMSO:CH₃OH (1:1) solution to a concentration of 20 mM, and then further diluted to 2 mM in BGE before use.

3 Results and discussion

3.1 ISF BGEs versus BGEs conventionally used for CE-LIF

In this study, the term “inorganic-species-free” BGEs (or ISF BGEs) was used to indicate buffers composed of zwitterionic and/or organic species without any inorganic ion in their compositions. The term ‘conventional BGEs’ was used for those containing at least one inorganic ion. For CE-LIF analyses of derivatized proteins and peptides, conventional BGEs composed of inorganic species (typically phosphate and borate with pH adjusted with HCl or NaOH), ‘borrowed’ from CE-UV, are generally employed. Indeed, those BGEs contain little or no UV-absorbing species that are detrimental to UV detection. While the performance in terms of peak height and resolution was not degraded when working with low-conductivity samples, it is not the case when the sample matrix becomes much more conductive. This situation is demonstrated in Fig. 1A where fluorescently labelled A β 1–42 prepared in PBS 1X was analysed with CE-LIF using different conventional BGEs at different pH values (from 6.0–9.7). The first two peaks in the electropherograms are the residual fluorophore whereas the third one corresponds to the tagged A β 1–42 which is negatively charged and pushed by the EOF towards the detection end. BGEs with pH above 7.0 allowed the tagged A β 1–42 to be detected whereas no peak of this peptide was observed even after 1 h at pH 7.0 or 6.0 due to decreased EOF. At a fixed IS of 20 mM, these conventional BGEs produced current intensities of 16–20 μ A under an electrical field of 333 V/cm. The peaks of A β 1–42 were relatively small, becoming more broadened and retarded when decreasing the pH of the BGE. On the other hand, these problems were alleviated, at any investigated pH, when these BGEs were replaced with ISF ones, i.e., His/2-((2-Hydroxy-1,1-bis(hydroxymethyl)ethyl)amino)ethanesulfonic acid and Tris/CHES (see Fig. 1B). The peak of A β 1–42 became sharper and higher, thanks to a pronounced difference of the ionic density between the ISF BGE and sample zones. The stacking preconcentration strategy indeed was based on a significant increase of the ionic density in the BGE zone without incurring unwanted current increase and Joule

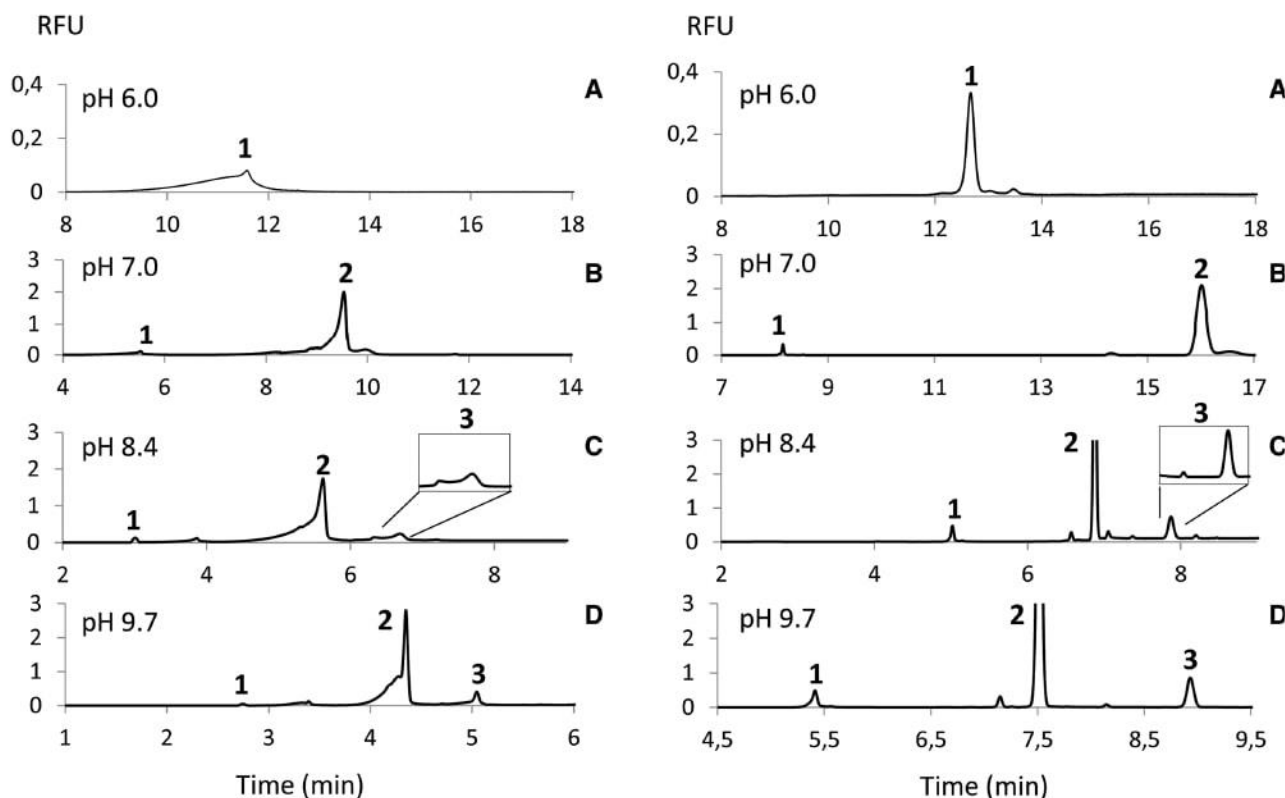


Figure 1. Electropherograms for the CE-LIF of the fluorescently tagged A β 1–42 (40 nM in PBS 1X) using conventional BGEs (panel 1) and ISF BGEs (panel 2). Peaks 1 and 2 are from the fluorophore and peak 3 is for A β 1–42. Conventional BGEs (IS 20 mM) were composed of (A) citrate/NaOH at pH 6.0; (B) phosphate at pH 7.0; (C) ammonium bicarbonate at pH 8.4, and (D) borate/NaOH at pH 9.7. ISF BGEs (IS 20 mM) were composed of (A) His/Tris at pH 6.0; (B) His/Tris at pH 7.0; (C) Tris/CHES at pH 8.4, and (D) Tris/CHES at pH 9.7. Other CE conditions: uncoated fused silica capillary with i.d. of 50 μ m, effective length (l_{eff}) of 50.2 cm, and total length (L_{tot}) of 60.2 cm; high voltage of 30 kV with normal polarity; LIF detection with excitation wavelength of 488 nm.

heating generation (see section 3.2). The electrical field in the BGE zone is therefore much decreased to ensure the slowed-down migration, and thus the stacking of the target analytes at the sample/BGE boundary. With this strategy, the stacking is always maintained, whether the sample matrix has a low conductivity (e.g., water or diluted BGE) or a high ionic density (e.g., PBS). An exemplary comparison for A β 1–42 separation is obtained using ammonium bicarbonate BGE and an inorganic-free one composed of Tris/CHES (pH 8.4) (see inserts of Fig. 1). At least three-time improvement of peak height (H) (from 20 801 to 68 586 RFU) and a tenfold enhancement of theoretical plate number (N) (from 4731 to 48 095) were observed for the Tris/CHES BGE. Similar observation was also made for the peaks of fluorophore. At the same IS of 20 mM, these ISF BGEs generated electric currents of 9–10 μ A, which are much lower than those from conventional ones. The unwanted Joule heating effect would therefore be minimized in this case, even when the concentrations of BGE components go up to several hundreds of mM to ensure the equivalent IS. Such high concentrations are nevertheless not possible with conventional BGEs nor with UV detection.

3.2 Protein separation and EOF tuning with ISF BGEs

High resolution separations of proteins at high pH are often hardly realizable with uncoated fused silica capillaries due to possible adsorption of proteins to the capillary inner wall, as well as elevated EOF. This situation is reflected in Fig. 2A where trypsin inhibitor tagged with Alexa (TI-Alexa) was analyzed with CE-LIF using an ammonium bicarbonate buffer. Its peak is spreading over 10 min, and remarkably irreproducible (RSD for migration time = 15.7%) due to its adsorption to the silica capillary. The peak broadening can also come from the multi-tagged species (from three to six tags, according to the supplier) as trypsin inhibitor possesses different primary amines and lysine groups available for stable dye–protein conjugation with succinimidyl ester moiety of Alexa-488 [17]. The peak shape was much improved when replacing this conventional BGE with an ISF one composed of Tris/CHES (constant IS of 20 mM) although still exhibiting some asymmetry arising from the heterogeneity of the TI-Alexa (Fig. 2B). In addition, peak height was improved by more than three times. Reproducible peaks were also achieved with RSD for mi-

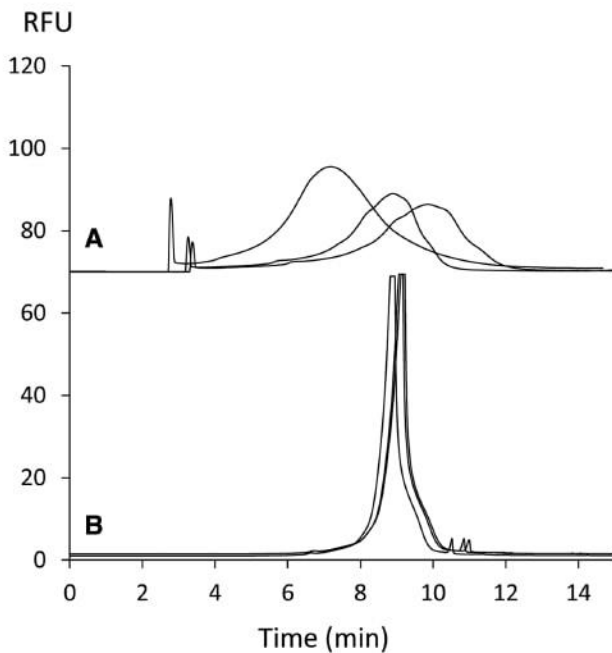


Figure 2. Electropherograms for CE-LIF (triplicates) of TI-Alexa (6.25 μM) prepared in 50 mM PBS (pH 7.4), using BGE (IS 20 mM, pH 8.4) composed of (A) ammonium bicarbonate and (B) Tris/CHES. Other CE conditions as in Fig. 1.

gration time decreased to 1%. These results clearly suggest less pronounced protein adsorption due to the high BGE concentrations. Moreover, the zwitterions in the ISF BGE could also associate with the protein and the capillary internal surface, thus preventing or minimizing electrostatic interactions and thereby protein adsorption [18]. This however was not the case with conventional BGEs whose concentrations cannot be much increased without generating Joule heating.

At a fixed pH, the magnitude of EOF generated inside an uncoated silica capillary can be tuned by variation of BGEs concentrations [19]. This EOF manipulation can be applied for both types of BGEs. By increasing the ionic strength of Tris/CHES BGE (pH 8.4) from 20 to 50 mM, the EOF magnitude was decreased twice (from 5.15×10^{-4} to 2.62×10^{-4} $\text{cm}^2/\text{V/s}$), provoking a retardation of TI-Alexa peak (Fig. 3). This increase in migration time led also to a net improvement of peak resolution in the case of Tris/CHES BGE, where different tagged forms of TI-Alexa could be partially resolved (Fig. 3A). Conveniently, protein adsorption could be further reduced by this IS increase. Using this ISF BGE, the peaks of TI-Alexa could be well identified whether the protein was prepared in PBS or BGE matrix, with slightly more broad peaks observed for the former due to a high conductivity of the PBS matrix (data not shown). In contrast, the reduction of EOF observed with the ammonium bicarbonate electrolyte did not lead to significant resolution improvement (Fig. 3B). The current increase from 17 to 52 μA is accompanied by a more pronounced Joule heating effect in

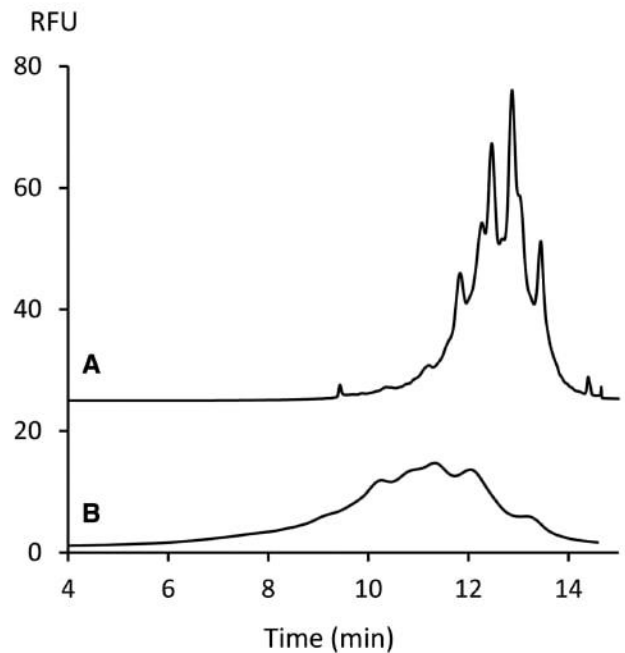


Figure 3. Electropherogram for CE-LIF of TI-Alexa (6.25 μM) prepared in 50 mM PBS (pH 7.4), using BGE (IS 50 mM, pH 8.4) composed of (A) Tris/CHES and (B) ammonium bicarbonate. Other CE conditions as in Fig. 1.

this case. This situation was reflected in Fig. 4 where we verified the presence of Joule heating with BGEs of different ionic strengths, using the method described elsewhere [20]. A linear correlation between applied voltages and induced currents was always achieved with Tris/CHES BGE regardless of the IS tested, proving an absence of Joule heating. This was however not the case with ammonium bicarbonate electrolyte at IS of 50 mM where the current increased non-linearly at voltages over 25 kV. The highest concentrations of ISF BGEs, which in turns leads to the maximum reduction of EOF, were indeed not limited by the acceptable current (as in the case of conventional BGE, see Fig. 4), but rather by the solubility of each organic component.

3.3 CE-LIF separation of protein labelled with different fluorophores

For the preliminary application, the ISF BGE composed of Tris/CHES (pH 8.4, IS 50 mM) was employed to investigate the separation performance in CE-LIF of a model protein (ovalbumin) labelled with different fluorophores in an uncoated fused silica capillary. Previously, CE-UV was used to study the heterogeneous population of ovalbumin's glycoforms [21]. Recently, capillary gel electrophoresis coupled with LIF was used for analysis of fluorescently tagged ovalbumin onto a single peak [22]. Herein, for the first time, effort has been made to separate fluorescently tagged

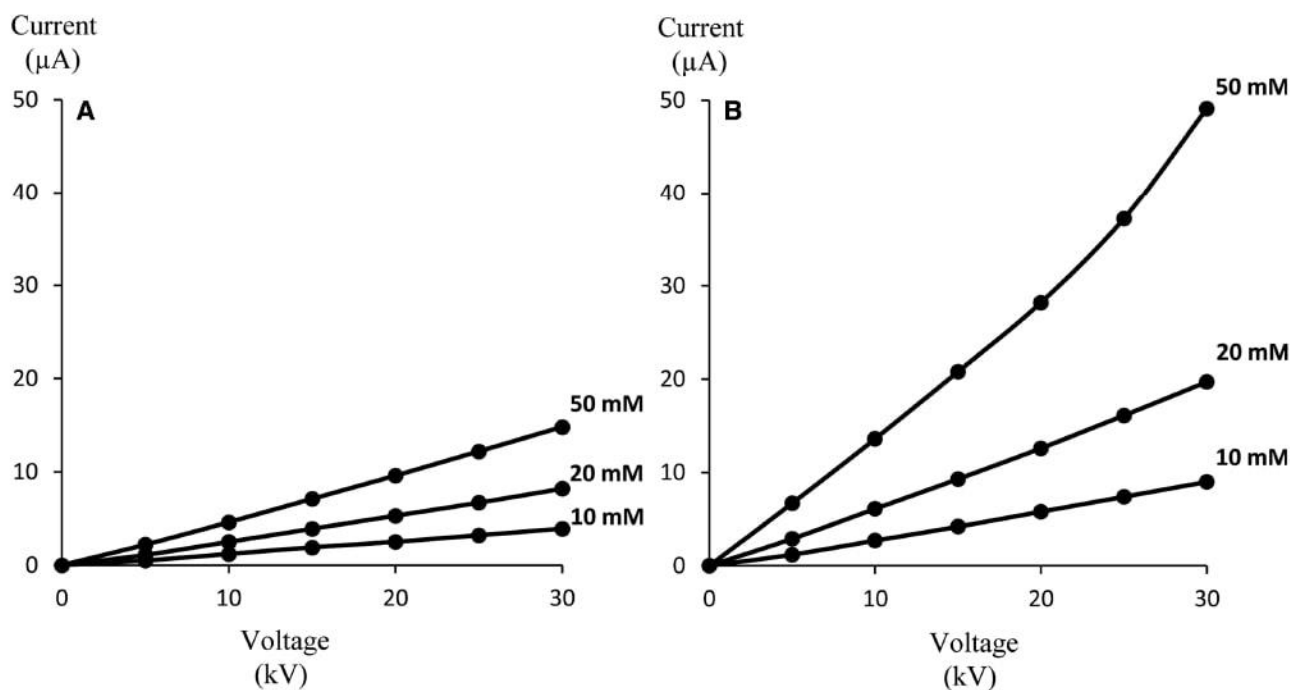


Figure 4. Comparison of the voltage versus current profiles for ISF BGE (A) and conventional BGE (B) at different ionic strengths (10, 20, and 50 mM). The ISF BGE was composed of Tris/CHES (pH 8.4). Conventional BGE was composed of ammonium bicarbonate (pH 8.4). The currents were measured on applying variable voltages over a 60.2 cm long uncoated fused silica capillary with i.d. of 50 μm.

ovalbumin having six cysteine groups available for covalent dye-protein conjugation with the maleimide group of the dyes. Normally, the choice of a fluorophore used to label target proteins/peptides is based on its extinction coefficient, emission efficiency, and excitation/emission wavelengths as well as the functional group present on the protein for covalent attachment. In this study, we paid more attention to the contribution of its charge-to-mass state to CE separation of the labelled ovalbumin. This aspect was approached by analyzing ovalbumin labelled either with CF-488, FP-488, Alexa-488, or Fluorescein-488 under the same CE-LIF conditions (Fig. 5). EOF was measured before and after this series of analyses, i.e. 24 runs performed on ovalbumin labelled with these four fluorophores. The electro-osmotic mobility did not deviate more than 2.4%, proving a low protein adsorption and an acceptable repeatability between runs in all cases. From the electropherograms, it can be deduced that the electrophoretic mobility of the negatively charged fluorophores decreases from Fluorescein-488, to Alexa-488, FP-488 and finally to CF-488. Accordingly, ovalbumin labelled with respective fluorophores is expected to have lower electrophoretic mobilities. Ovalbumin labelled with Fluorescein-488 and Alexa-488, dragged by the EOF towards the detector, thus had larger migration time. The peaks of ovalbumin labelled with Fluorescein-488 or Alexa-488 were better separated from the respective fluorophore. The peaks of labelled ovalbumin were found to spread over 2 min, coming from both multiple tagged species as well as the heterogeneity of its glycoform population. Note that un-

labelled ovalbumin glycoforms were distributed over more than 10 min using CE-UV with conventional BGEs and a dynamic coating to reduce EOF as well as minimize protein adsorption [21] whereas the peak distribution was much stacked in our case with an ISF-BGE in the absence of capillary coating (Fig. 5B). In the case of FP-488 and CF-488, labelled ovalbumin was merged into the fluorophore signal precluding its detection (Fig. 5C and D).

4 Concluding remarks

Highly concentrated ISF BGEs were successfully applied for CE separation and LIF detection of fluorescently labelled proteins and peptide. Such BGEs, which could not be used at high concentrations with UV detection, offer much improved peak resolution, signal intensity, and tuneable EOF. They also bring the possibility to minimize protein adsorption in CE-LIF and to use uncoated fused silica capillaries. These ISF BGEs with very low current generation can be used with high electrical field to improve separation performance and could be employed for CE in enclosed microchip channels without a risk of heat-induced bubble formation. Thanks to their excellent stacking effect, these ISF BGEs may find well their prospective applications in online electrokinetic preconcentrations of fluorescently labelled species prior to CE-LIF.

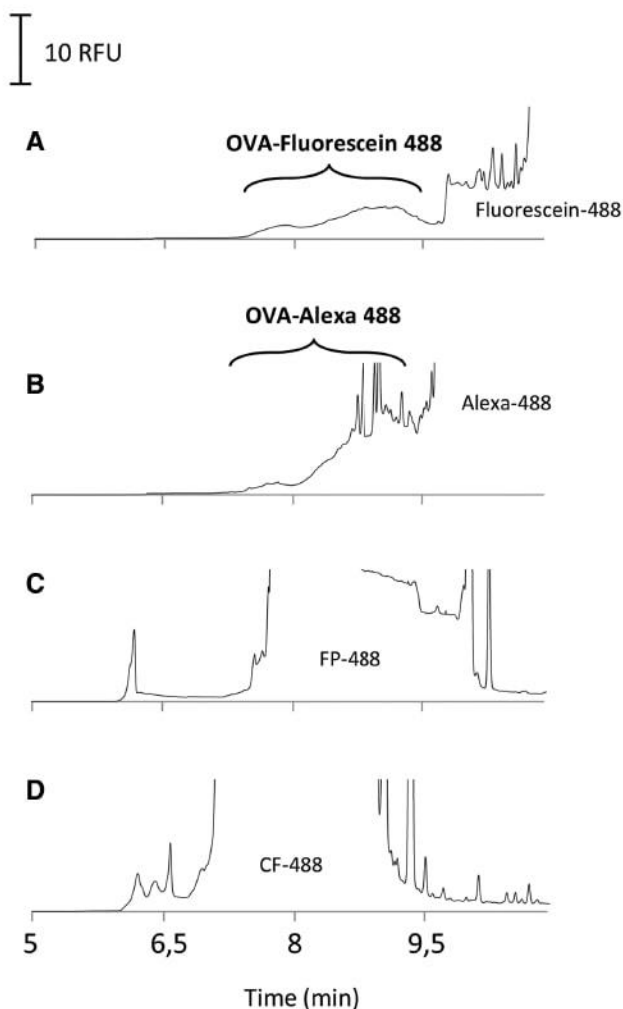


Figure 5. Electropherogram for CE-LIF of ovalbumin (50 μ M) derivatized with (A) Fluorescein-X5-Maleimide; (B) Alexa-488 maleimide; (C) Fluoprobe-488 maleimide, and (D) CF-488 maleimide. A molar fluorophore/protein ratio of 2 was used for the labeling. OVA denotes for Ovalbumin. BGE was composed of Tris/CHES (IS 50 mM, pH 8.4). Other CE conditions as in Fig. 1.

This work has been financially supported by the Institut Universitaire de France (for M. Taverna, senior member) and the French Investissements d'Avenir program (DIGIDIAG project) under the grant agreement ANR-10-NANO-02. The doctoral scholarship for Marco Morani was supported by the doctoral school 2MIB (Sciences Chimiques: Molécules, Matériaux, Instrumentation et Biosystèmes) – University Paris Saclay.

The authors have declared no conflict of interest.

5 References

- [1] Couderc, F., Ong-Meang, V., Poinot, V., *Electrophoresis* 2017, **38**, 135-149.
- [2] Kaneta, T., *Chem. Rec.* 2018, **18**, 1-1.
- [3] Galievsky, V. A., Stasheuski, A. S., Krylov, S. N., *Anal. Chim. Acta* 2016, **935**, 58-81.
- [4] Wuethrich, A., Quirino, J. P., *Electrophoresis* 2017, **39**, 82-96.
- [5] de Kort, B. J., de Jong, G. J., Somsen, G. W., *Anal. Chim. Acta* 2013, **766**, 13-33.
- [6] Varenne, A., Descroix, S., *Anal. Chim. Acta* 2008, **628**, 9-23.
- [7] Koval, D., Busnel, J.-M., Hlavacek, J., Jiracek, J., Kasicka, V., Peltre, G., *Electrophoresis* 2008, **29**, 3759-3767.
- [8] Busnel, J.-M., Le Saux, T., Descroix, S., Girault, H. H., Hennion, M.-C., Terabe, S., Peltre, G., *J. Chromatogr. A* 2008, **1182**, 226-232.
- [9] Righetti, P. G., Gelfi, C., Bossi, A., Olivieri, E., Castelletti, L., Verzola, B., Stoyanov, A. V., *Electrophoresis* 2000, **21**, 4046-4053.
- [10] Doble, P., Macka, M., Haddad, P. R., *Trends Anal. Chem.* 2000, **19**, 10-17.
- [11] Hjerten, S., Valtcheva, L., Elenbring, K., Liao, J.-L., *Electrophoresis* 1995, **16**, 584-594.
- [12] Doble, P., Macka, M., Haddad, P. R., *Electrophoresis* 1998, **19**, 2257-2261.
- [13] Kuban, P., Hauser, P. C., *Trends Anal. Chem.* 2018, **102**, 311-321.
- [14] Mai, T. D., Hauser, P. C., *Chem. Rec.* 2012, **12**, 106-113.
- [15] de Lassichere, C. C., Mai, T. D., Otto, M., Taverna, M., *Anal. Chem.* 2018, **90**, 2555-2563.
- [16] Hellqvist, A., Hedeland, Y., Pettersson, C., *Electrophoresis* 2013, **34**, 3252-3259.
- [17] Tollner, T. L., Yudin, A. I., Cherr, G. N., Overstreet, J. W., *Zygote* 2000, **8**, 127-137.
- [18] Bushey, M. M., Jorgenson, J. W., *J. Chromatogr. A* 1989, **480**, 301-310.
- [19] Corradini, D., Spreccacenero, L., *Chromatographia* 2003, **58**, 587-596.
- [20] Xuan, X., Li, D., *J. Chromatogr. A* 2005, **1064**, 227-237.
- [21] Che, F. Y., Song, J. F., Shao, X. X., Wang, K. Y., Xia, Q. C., *J. Chromatogr. A* 1999, **849**, 599-608.
- [22] Pan, J. Z., Fang, P., Fang, X. X., Hu, T. T., Fang, J., Fang, Q., *Sci. Rep.* 2018, **8**.

IV.4. CE-LIF method development to study the electrokinetic distribution of EVs

CE appears as an intriguing and little explored option for high performance profiling EVs and possibly distinguishing EV subtypes based on their electrophoretic behavior. When I started my thesis CE was not yet explored for intact EVs analysis at all. Furthermore, the volume of sample solution generated by the droplet platform intended to isolate the EVs at the forefront, which will be detailed in the next chapter, is compatible and combinable with this microscale electrophoresis technique. The main challenges encountered with CZE analysis of EVs is to avoid during the electrophoretic process their lysis, their adsorption to the capillary wall and formation of cluster or aggregates. Furthermore, when dealing with EVs extracted from CSF or plasma fluids, a high detection sensitivity is desirable, since their concentrations might be very low. For this reason, LIF was selected as the detection mode for EVs. The solutions that we developed to solve these difficulties, as well as the accomplishments gained using CZE for isolated EVs, will be discussed in detail in this part.

First, the above-presented ISF BGEs , which we demonstrated to improve the performance of CE-LIF for proteins and peptides in terms of improved peak resolution, sharper and higher peaks, and low electric conductivity [268], were further exploited to develop a CZE method prior to LIF detection of EVs. These BGEs were expected to satisfy several requirements for CE analysis of EVs, such as avoiding lysis during the electrophoretic process, avoiding adsorption of EVs to the silica capillary wall, and avoiding the formation of numerous spikes due to unwanted EV clusters or aggregates.

Prior to CE-LIF, EVs must be labeled with a fluorophore. In this context, it is important that the fluorescent dye used, label exclusively EVs, has a low background signal in its free form, lead to a high signal-to-noise ratio, and can preserve EVs' innate biological activity as well as their physical properties and integrity. EVs may be tagged with a variety of fluorescent dyes in different ways: by labeling proteins on the membrane surface, by intercalating dyes into the EVs lipid structure, or by labeling the EVs lumen [269]. Among these, we exploited the fluorescent luminal labelling using a membrane permeable dye that become fluorescent and EV-impermeable in its hydrolyzed forms following cleavage by internal EVs enzymes. Our objective was to develop a EVs labeling strategy while maintaining the EVs' natural physical characteristics by preventing size and charge modification after EVs fluorescent tagging, which otherwise would result in unwanted changes in their original electrophoretic mobilities.

The EVs to a certain extend can be considered (bio)nanoparticles. Therefore, before going into the details of the method's development for electrophoretic separation of EVs shown in the published

article 3 ([Morani et al., *Analytica Chimica Acta*, 2020](#) [270]), the relation between the electrophoretic migration behavior of nanoparticles (NPs) and their physical and chemical characteristics is discussed here, based on the background already established for CE of NPs.

Nanoparticles are generally defined as particles having one or more dimensions in the nanoscale (around 1 - 100 nm). CE is a relevant method for analyzing and characterizing NPs (e.g. noble-metal, metal oxide and polymeric NPs) [271]. It allows separation of particles according to their size and zeta (ζ) potential. When a rigidly charged sphere is immersed in an electrolyte solution, an ion cloud forms around it, perfectly compensating for its charge. The potential ζ is defined by the potential difference between the charged surface of the NP and the solvent molecules far from the particle. This can be determined from the measurement of electrophoretic mobility μ_{ep} [272, 273] depending on the value of κR_h , with R_h being the hydrodynamic radius of NP and κ the inverse of Debye's length (equation 6):

$$\kappa = \sqrt{\frac{e^2 N_A I}{\epsilon_r \epsilon_0 k_B T}} \quad (6)$$

where e is the elementary electric charge, N_A the Avogadro's number, I the ionic strength of the medium, ϵ_r the relative electric permittivity of the electrolyte, ϵ_0 the electric permittivity of vacuum, k_B the Boltzmann constant, T the absolute temperature. κ represents the thickness of the electronic double layer that forms on contact between the charged surface of the NP and the ions present in the electrolyte.

In the case where $\kappa R_h \ll 1$, in example when the size of the particle is small compared to the thickness of the double layer, the Hückel equation is valid:

$$\mu_{ep} = \frac{2\epsilon_r \epsilon_0 \zeta}{3\eta} \quad (7)$$

In the case where $\kappa R_h \gg 1$, i.e., when the electronic double layer is negligible compared to the size of the NP, the Smoluchowski equation is reached:

$$\mu_{ep} = \frac{\epsilon_r \epsilon_0 \zeta}{\eta} \quad (8)$$

Between the two, analytical approximations have been developed to obtain the potential ζ [274, 275].

However, the dependence of NP μ_{ep} on size, charge, or even charge-to-size ratio cannot be generalized. Before establishing a clear association between electrophoretic mobilities of NPs and one of their

specific properties, numerous criteria must be evaluated and determined. D'Orlyé et al. demonstrated some dependence of μ_{ep} to maghemite ($\gamma\text{-Fe}_2\text{O}_3$) NPs size in a particular range of 6-10 nm, assuming a uniform zeta potential, at a given electrolyte ionic strength [276]. Charge-based characterization of cationic bifunctional maghemite/silica core/shell NPs by CZE via their μ_{ep} was possible if NPs of homogeneous sizes could be obtained [277]. Liu et al. demonstrated that the geometry of NPs may affect their electrophoretic mobilities when they used CE to separate a mixture of silver nanorods and nanoparticles [278]. Vanifatova et al. observed that coexistence of different iron oxide NPs populations influenced their electrokinetic migration [279]. Other factors such as BGE ionic strength, pH and composition, applied electrical field, injected NPs quantity have been reported to influence electrophoretic mobilities [275]. Of course, the theory on CE of NPs cannot be applied directly to EVs, as the scenario is significantly more complex in the case of EVs. Their size distribution, in particular, is more heterogeneous, ranging from about 30 nm to a few micrometres. Additionally, EVs might differ significantly in terms of their membrane composition. As a consequence, the zeta potential of EVs, which is determined by their molecular surface composition (lipids, membrane proteins, etc...), may vary within a single EV population. Furthermore, EVs, like cells, may display shape, size and zeta potential variations in different buffer conditions [280, 281]. Considering all these challenges, we put our efforts to explore for the first time the power of CE-LIF for elucidation of electrokinetic distribution of EVs. The main achievements are described in the following article 3. To accomplish so, our commercial collaborator Excilone (Elancourt, France) supplied us with bovine milk-derived EVs with narrow size distribution, well-determined concentrations, and extensive characterizations by NTA, DLS, LC-MS / MS, and TEM. These EVs isolated by sucrose gradient ultracentrifugation were considered as EV standards for our CE-LIF method development. Excilone also provided us with samples of EVs from other sources, such as pony plasma / serum and human plasma that were isolated by SEC. In addition a collaboration with the Marja-Liisa Riekkola team (INAR Analytical Chemistry) from the University of Helsinki (Finland), enabled us to test our CE-LIF method on human plasma EVs isolated using their newly developed immunoaffinity chromatography technology [172].



Contents lists available at ScienceDirect

Analytica Chimica Acta

journal homepage: www.elsevier.com/locate/aca

Electrokinetic characterization of extracellular vesicles with capillary electrophoresis: A new tool for their identification and quantification

Marco Morani ^a, Thanh Duc Mai ^a, Zuzana Krupova ^b, Pierre Defrenaix ^b, Evgen Multia ^c, Marja-Liisa Riekkola ^c, Myriam Taverna ^{a, d, *}

^a Institut Galien Paris Sud, UMR 8612, Protein and Nanotechnology in Analytical Science (PNAS), CNRS, Univ. Paris-Sud, Univ. Paris-Saclay, 5 Rue Jean Baptiste Clément, 92290, Châtenay-Malabry, France

^b Excilone - 6, Rue Blaise Pascal - Parc Euclide, 78990, Elancourt, France

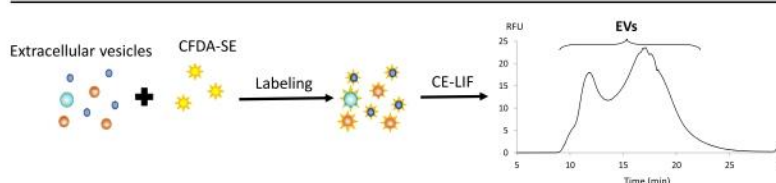
^c Department of Chemistry, P.O. Box 55, FI-00014, University of Helsinki, Finland

^d Institut Universitaire de France (IUF), France

HIGHLIGHTS

- A new CE-LIF tool for characterization and quantification of EVs was developed.
- The new BGE was applied for excellent performance of CE-LIF of EVs.
- Intra-membrane labelling was optimized without incurring EV morphology modification.
- Separation and detection of EVs from different animal and human origins were implemented.

GRAPHICAL ABSTRACT



ARTICLE INFO

Article history:

Received 14 June 2020

Accepted 29 June 2020

Available online 11 July 2020

Keywords:

Capillary electrophoresis

LIF detection

Membrane labeling

Extracellular vesicles

ABSTRACT

This work reports on the development of the first capillary electrophoresis methodology for the elucidation of extracellular vesicles' (EVs) electrokinetic distributions. The approach is based on capillary electrophoresis coupled with laser-induced fluorescence (LIF) detection for the identification and quantification of EVs after their isolation. Sensitive detection of these nanometric entities was possible thanks to an 'inorganic-species-free' background electrolyte. This electrolyte was made up of weakly charged molecules at very high concentrations to stabilize EVs, and an intra-membrane labelling approach was used to prevent EV morphology modification. The limit of detection for EVs achieved using the developed CE-LIF method reached 8×10^9 EV/mL, whereas the calibration curve was acquired from 1.22×10^{10} to 1.20×10^{11} EV/mL. The CE-LIF approach was applied to provide the electrokinetic distributions of various EVs of animal and human origins, and visualize different EV subpopulations from our recently developed high-yield EV isolation method.

© 2020 Elsevier B.V. All rights reserved.

Abbreviations: EVs, extracellular vesicles; CE, capillary electrophoresis; LIF, laser-induced fluorescence; DLS, dynamic light scattering; NTA, nanoparticle tracking analysis; PVA, polyvinyl alcohol; AsFFFF, Asymmetrical flow field-flow fractionation; MALS, multi angle light scattering; ISF BGE, inorganic-species-free background electrolyte; SEC, size exclusion chromatography.

* Corresponding author. Institut Galien Paris Sud, UMR 8612, Protein and Nanotechnology in Analytical Science (PNAS), CNRS, Univ. Paris-Sud, Univ. Paris-Saclay, 5 rue Jean Baptiste Clément, 92290, Châtenay-Malabry, France.

E-mail address: myriam.taverna@u-psud.fr (M. Taverna).

<https://doi.org/10.1016/j.aca.2020.06.073>

0003-2670/© 2020 Elsevier B.V. All rights reserved.

1. Introduction

Extracellular vesicles (EVs) are a common family of heterogeneous small vesicles secreted by all types of cells [1,2]. EVs contain distinct subsets of molecules characteristic of the mother cells from which they are secreted, conveying, in this way, many vital signals under normal or pathological conditions. This makes them useful

for biomarker discovery and much current research is focusing on them for their potential diagnostic and prognostic applications [3–5]. Despite overt evidence of the potential of EVs in clinical diagnostic practice, guidelines for analytical procedures have not yet been properly established. The isolation and enrichment of EVs from biofluids remains a challenging prerequisite before light can be shed on the target exosomal molecules (e.g. nucleic acids, proteins, growth factors, cytokines etc.) that are present in trace amounts. After this has been achieved, it is critical to verify the identity of EVs and monitor their purity and concentration.

Until now, most common physical characterization approaches have relied on microscopy-based methods, dynamic light scattering (DLS), nanoparticle tracking analysis (NTA) and tunable resistive pulse sensing vesicle flow cytometry (see Ref. [6,7]). To a lesser extent, immunoaffinity-based methods, notably enzyme-linked immunosorbent assays (ELISA) and amplified luminescent proximity homogeneous assay on beads (ExoScreen), have been employed to identify EVs' subpopulations from different cellular origins [8,9]. Each technique can provide only part of the information sets required for the confirmation and characterization of target EVs. EVs identification can also be done via analyses of exosomal lysates (e.g. immunoblotting or mass spectrometry for intra-exosomal proteins [6], or fluorocet kit to measure esterase activity released from lysed EVs [10]). Nevertheless, with such bulk measurements, the differentiation between small cells, debris and EVs may not be possible, and information on size and charge is not provided. To have access to reliable and fast identification and characterization of EVs, continued efforts have been directed toward the development of novel technologies. The most recent communications reported on exosome luminescent quantification [11] and electrical detection of polarized exosomes via capacitance-voltage measurements [12].

A satisfactory method should meet all the criteria for EV phenotyping, notably the ability to discriminate between different size sub-populations and to maintain EV integrity during analysis. High detection sensitivity in some cases is desirable, for example when working with EVs from cerebrospinal fluids, as their concentration after extraction may be very low. Till now, no single method has succeeded in meeting all of these criteria simultaneously or that can be used universally in a variety of infrastructures (i.e. depending on the equipment and expertise to hand). To provide sufficient physical and biological information on isolated EVs many complementary techniques have to be used. From this rationality, capillary electrophoresis (CE), which has shown its capability to provide nanoparticle analysis and characterization [13], emerges as an interesting and unexplored alternative to elucidate the electrokinetic distribution of nanoscaled EVs. The only electrokinetic approach, based on electrophoretic light scattering, was exploited by Ichiki's group for tracking exosomes and measuring their zeta potential, using a microchip format coupled with a laser dark-field microscope [14–16]. In addition, specific purpose-made instrumentation and manual operation are required for this new application.

Herein we report for the first time the use of CE coupled with laser-induced fluorescent (LIF) detection for the identification and quantification of EVs after their isolation. To this purpose, strategies for fluorescent labeling of EVs, EVs matrix substitution as well as background electrolyte optimization were developed. Then the developed CE-LIF method was employed to study the electrokinetic distribution of EVs isolates obtained from using various techniques, including the recently developed approach for high-yield EV isolation from human plasma [17]. After the submission of our manuscript on CE-LIF of EVs, another work on CE-UV of EVs was published [18]. Together with this pioneering work, we provide herein the first proof of concept on electrokinetic separation and

characterization of EVs.

2. Materials and methods

2.1. Chemicals and reagents

2-(Cyclohexylamino)ethanesulfonic acid (CHES), phosphate buffered saline (PBS 10x), sodium dodecyl sulfate (SDS, 98.5% (GC)), Tris(hydroxymethyl)aminomethane (Tris) and sodium acetate, anhydrous Na_2CO_3 , NaHCO_3 , and phosphate buffer saline tablets (PBS) were all obtained from Sigma Aldrich (St. Louis, MO, USA). Sodium hydroxide (1 M), hydrochloric (1 M) and acetic (99.9% purity) acids were obtained from VWR (Fontenay-sous-Bois, France). All buffers were prepared with deionized water. Vybrant™ CFDA SE Cell Tracer Kit (dye 5-(and-6)-Carboxyfluorescein diacetate succinimidyl ester, CFDA-SE) was purchased from Thermo Fisher Scientific (Waltham, MA, USA). 25% (v/v) ammonia was obtained from Riedel-de Haën (Seelze, Germany). CD9 Monoclonal Antibody (eBioSN4 (SN4 C3-3A2)), eBioscience™ was purchased from Thermo Fisher Scientific and purified mouse anti-human CD61 (clone VI-PL2) antibody was purchased from BD Biosciences (San Jose, CA, USA). CIM® CDI -0.34 mL disks and the disk housing were purchased from BIA Separations (Ajdovščina, Slovenia). Healthy human plasma for immunoaffinity isolations of EVs was obtained from Finnish Red Cross Blood Service (Helsinki, Finland). EVs samples of different purity degrees isolated from bovine milk, pony plasma, pony serum, and human plasma were provided by Excilone (Elancourt, France).

2.2. Apparatus and material

The CE-LIF studies were performed with a PA 800 Plus system (Sciex Separation, Brea, CA) equipped with a solid-state laser induced fluorescence detector ($\lambda_{\text{excitation}}$: 488 nm, $\lambda_{\text{emission}}$: 520 nm) purchased from Integrated Optics (Art. No. 40A-48A-52A-64A-14-DM-PT, distributed by Acal Bfi, Evry, France). Uncoated fused silica capillaries were purchased from CM Scientific (Silsden, UK). Polyvinyl Alcohol (PVA) neutral capillaries were obtained from Sciex. Data acquisition and instrument control were carried out using Karat 8.0 software (Sciex Separation, Brea, CA). Deionized water used in all experiments was purified using a Direct-Q3 UV purification system (Millipore, Milford, MA, USA). Conductivity and pH values of buffer solutions and samples were obtained with a SevenCompact pH meter (Mettler Toledo, Schwerzenbach, Switzerland). Preparation of background electrolyte (BGE) and buffer ionic strength (IS) calculations were based on simulations with the computer program PhoeBus (Analisis, Suarlée, Belgium).

Asymmetrical flow field-flow fractionation (AsFFFF) system used was from Postnova Analytics (AF2000 system, Landsberg, Germany). It was equipped with 350 μm spacer (Postnova AF2000 MF) and a 10 kDa mass cut-off regenerated cellulose membrane (Postnova AF2000 MT series) in a kite shaped channel (L_{tot} = 27.5 cm). The channel was followed by UV (SPD-20A Prominence, Shimadzu, Japan), multi-angle light scattering (MALS) (BI-MwA Molecular Weight Analyzer, USA), and DLS (Zetasizer Nano, Malvern Instruments, UK) detectors. The fractions were collected with CBM-20A modular system controller (Shimadzu, Japan) and FRC-10A fraction collector (Shimadzu, Japan). Fractions were further lyophilized for EVs enrichment using Heto PowerDry LL1500 freeze dryer (Thermo Scientific).

2.3. Methods

2.3.1. Isolation of bovine milk-derived EVs with sucrose gradient ultracentrifugation

Whole bovine milk samples were centrifuged at 3000×g for 30 min at 4 °C (Allegra X-15R, Beckman Coulter, France) to separate fat from skimmed milk. The whey was obtained after acid precipitation of milk (50 mL) with 5 mL of 10% acetic acid and incubation at 37 °C for 10 min. This was then continued by addition of 5 mL of 1 M sodium acetate, and incubation for 10 min at RT. This was followed by centrifugation at 1500×g, 4 °C for 15 min and filtration of supernatant using vacuum-driven filtration system Millipore Steritop, 0.22 µm. The whey supernatants were concentrated by centrifugation at 4000×g and 20 °C using Amicon 100 kDa centrifugal filter units (Merck Millipore). The obtained retentate was ultra-centrifuged for pelleting the EVs at 100 000×g for 1 h 10 at 4 °C (Beckman Coulter, Optima XPN-80, 50TI rotor). The pellets were solubilized in 500 µL of PBS then added to 11 mL of pre-prepared sucrose gradient 5–40% and ultra-centrifuged at 200 000×g for 18 h at 4 °C (Beckman Coulter, Optima XPN-80, SW41 rotor). Selected fractions corresponding to EVs' flotation densities (1 mL) were collected, diluted in 6 mL of PBS 1x and finally centrifuged at 100 000×g for 1 h 10 at 4 °C (Beckman Coulter, Optima XPN-80, 50TI rotor). The pellets were resuspended in 50 µL of PBS 1x and stored at –80 °C, until further analyses. Bovine milk-derived EVs with narrow size distribution, well-determined concentrations and characterized with dynamic light scattering (DLS), nanoparticle tracking analysis (NTA), transmission electron microscopy (TEM) as well as proteomic profiling were used as EV standards for CE-LIF methodology development.

Isolation of pony plasma/serum and human plasma derived EVs with size exclusion chromatography (SEC).

Preparation of plasma: Peripheral blood was collected into EDTA-coated vacutainer tubes. After ten-time inversion, samples were processed within the 60 min of collection. Consecutive centrifugation steps at 2500×g, 4 °C for 15 min and then at 15 000×g for 10 min were performed followed by filtration of the supernatant through 0.22 µm filters. **Preparation of serum:** Whole blood was collected into anticoagulant-free tubes and allowed to clot at room temperature for 45 min. The clot was removed by centrifuging at 3200×g, 4 °C for 15 min, followed by centrifugation at 15 000×g, 4 °C for 10 min and filtration of the supernatant through 0.22 µm filters.

500 µL of pre-treated plasma/serum was loaded onto a qEVO-iginal SEC column (Izon Science, New Zealand) previously washed and equilibrated with PBS. Fraction collection (0.5 mL per fraction) was carried out immediately using PBS as elution buffer. The selected elution fractions were pooled and were subsequently concentrated using 100 kDa Amicon centrifugal filter units (Merck Millipore). Post-treatment processing with several washing steps with PBS was applied to obtain highly pure EV fractions.

Isolation of human plasma derived EVs with monolithic disks via immunoaffinity chromatography.

EVs were isolated from human plasma using a recently developed monolithic affinity chromatography approach [17]. Briefly, diluted human plasma samples (250 µL of plasma diluted to 5 mL in PBS) were percolated through monolithic disk columns immobilized with either anti-human CD61 or anti-human CD9 antibodies. The enriched EVs were eluted with 2 mL of either ammonium hydroxide (NH₄OH, pH 11.3) or carbonate-bicarbonate (pH 11.3) solution after washing the unbound plasma with 3 mL of PBS. The ammonium hydroxide solution was prepared by diluting 2.26 mL of 25% ammonia to a final volume of 100 mL with Milli-Q water. The carbonate-bicarbonate solution was prepared by mixing 90 mL of 0.1 M Na₂CO₃ stock solution (1.06 g of anhydrous Na₂CO₃ dissolved

in 100 mL of Milli-Q water) with 10 mL of 0.1 M NaHCO₃ stock solution (0.84 g of NaHCO₃ in 100 mL of Milli-Q water) and adjusting the pH to 11.3 with 200 µL of 5 M NaOH. The pH of the isolates (final volume 0.5 mL) was adjusted by addition of 50 µL of 1 M HCl prior to characterization with Lowry method [19], NTA, Western blotting, and TEM [20]. The results of these characterizations can be found in our previous study [17].

Asymmetrical flow field-flow fractionation (AsFIFFF) coupled with UV, multi-angle light scattering (MALS) and flow DLS detectors were used to characterize and fractionate subpopulations of the eluents. EV isolation and characterization were performed using the protocol recently published [17] with some modifications. Briefly, 500 µL was injected with a flow of 0.1 mL/min over 5 min during the focus mode at the cross-flow rate of 3 mL/min. Detector flow rate was 0.5 mL/min and PBS was used as a running buffer. After the focusing step and 1 min of transition time, a 2 min linear decrease in cross-flow to 0.5 mL/min was implemented, followed by a linear decrease over 1 min to 0 mL/min. The run was continued for 15 min with only the detector flow (0.5 mL/min), followed by a rinse step (0.5 mL/min) for 2 min, making a total run time of 26 min. EV fractions (300 µL each) provided by AsFIFFF were frozen and subsequently lyophilized over 3 h at temperature of –110 °C. Before starting the labelling protocol, the fractions were rehydrated with 30 µL PBS for EVs enrichment.

2.3.2. Dynamic light scattering (DLS) of extracellular vesicles

Size distribution and zeta potential of EVs were measured using a Zetasizer Nano (Malvern Instruments, Malvern, UK). All measurements, using PBS as the dispersant, were undertaken in triplicates at 25 °C with scattering angle of 90° and refractive index of 1.332. Data processing and analysis were performed in the automatic mode with at least 13 measurements per run using Zetasizer software version 7.11.

2.3.3. Nanoparticle tracking analysis (NTA) of extracellular vesicles

Size distribution and particle concentration were determined with either Nanoparticle Tracking Analysis (NTA) systems: Zeta-view (Particle Metrix, Germany) or Nanosight (Malvern Instruments, UK). All experiments were carried out with pre-diluted samples in PBS according to input sample concentrations, leading to particle concentration within the 107–109 particles per mL range for optimal analysis.

The Zetaview system (Particle Metrix) was equipped with a 488 nm laser. Each experiment was performed in duplicate on 11 different positions within the sample cell with following specifications and analysis parameters: sensitivity 60, shutter 100, Max Area 100, Min Area 5, Min Brightness 25. The results were validated while obtaining at least 1000 valid tracks for each run. For data capture and analysis, the Nanoparticle Tracking Analysis Software (NTA) vs 8.05.04 was used.

Particle concentration and size distribution were also determined with a Nanosight NS300 instrument (Malvern, version NTA 3.2 Dev Build 3.2.16) equipped with a 405 nm laser, sCMOS camera type and the NTA software v3.1. The video acquisition was performed using a camera level of 14. Per sample, 3 videos of 90 s with a frame rate of 30 frames/s were captured at 25 °C and subsequently analyzed with a threshold set up at 5. The results were validated with at least 2000 valid tracks for each triplicate.

2.3.4. Fluorescent labelling of EVs

The fluorescently labelled EVs were prepared using the 5-(and-6)-Carboxyfluorescein diacetate succinimidyl ester (CFDA-SE). The CFDA-SE stock solution (10 mM) was prepared in DMSO following the manufacturer's instructions. Prior to staining, the working solution was diluted to 200 µM in PBS. 20 µL of EVs was mixed with

20 μL of 200 μM CFDA-SE solution (resulting in a final CFDA-SE concentration of 100 μM), and incubated for 2 h in the dark at 37 $^{\circ}\text{C}$ with gentle shaking.

2.3.5. Matrix substitution of EVs

Labelled EVs were obtained from two different matrix exchange approaches, using either centrifugal filtration on Nanosep Omega Membranes 3K (PALL Life Sciences, Port Washington, NY, USA) or EVs filtration with commercial Exosome Spin Columns (MW 3000) obtained from Thermo Fisher Scientific (Waltham, MA USA). The first approach (centrifugal filtration) was carried out by addition of the desired buffer to be substituted on the top of the labelled EVs, then centrifugal spinning of the column for approximately 4 min at 5000 $\times g$. This process was repeated four times. In the last step, a buffer volume equivalent to that of labelled EVs was used to maintain the same concentration before and after filtration. The second approach was carried out according to the manufacturer's instructions.

2.3.6. CE-LIF of fluorescently labelled EVs and EOF measurement

The fused silica capillary (I.D. of 50 μm , O.D. of 375 μm , effective length (L_{eff}) of 50.2 cm and total length (L_{tot}) of 60.2 cm) was pre-conditioned (using a pressure of 172 kPa at the capillary inlet) with the following sequence: water for 10 min, 1 M NaOH for 10 min, 1 M HCl for 10 min and then water for 10 min. The rinsing between two analyses was carried out with 50 mM SDS for 5 min, 1 M NaOH for 5 min, deionized water for 5 min, and finally the running BGE for 5 min using a pressure of 207 kPa. A plug of sample was hydrodynamically injected from the inlet end by applying a pressure of 3.4 kPa for 2 min. The separation was carried out under 25 kV (normal polarity) at 25 $^{\circ}\text{C}$ and the samples were maintained at 5 $^{\circ}\text{C}$ with the sample storage module of the PA 800 Plus equipment. The optimized BGE was composed of Tris/CHES (IS 90 mM, pH 8.4). This BGE was prepared as follows. First two stock solutions of 1.5 M Tris and 1.2 M CHES were prepared by dissolving 1.817 g of Tris base in 10 mL of water and 10.447 g of CHES in 42 mL of water. Then, 8 mL of 1.5 M Tris was mixed with 41.09 mL of 1.2 M CHES. Deionized water was then added to a total volume of 50 mL pH of the BGE after preparation was confirmed with a pH meter.

The calibration curve was acquired using bovine milk derived EV standards. The EVs isolates were diluted with 1X PBS to prepare different initial EVs concentrations from 1.65×10^{10} to 1.65×10^{11} EV/mL before the labeling and matrix removal on spin columns. 20 μL of EVs was mixed with 20 μL of CFDA-SE 200 μM solution (resulting in a final CFDA-SE concentration of 100 μM CFDA-SE), and incubated for 2 h at 37 $^{\circ}\text{C}$. Then 40 μL of labelled EVs was loaded into EV Spin Columns and recovered in Tris/CHES 90 mM. Calculations for final concentrations were based on initial concentration measured by NTA before the labeling and taking into account a recovery of 75% from the matrix substitution step. EOF mobility was measured with CE-LIF using 4-(4-Methoxybenzylamino)-7-nitro-2,1,3-benzoxadiazole (MBD, used as an EOF marker) which is a neutral and fluorescent compound [21]. The EOF marker was dissolved in a DMSO:CH₃OH (1:1 v/v) solution to a concentration of 20 mM, and then further diluted to 2 mM in BGE before use.

3. Results and discussion

3.1. Fluorescent labeling of EVs

Our preliminary attempts to determine EVs with CE-UV showed insufficient sensitivity in detecting low-abundant milk EVs purified by ultracentrifugation and suspended in PBS. To improve the detection sensitivity and specificity, an effort was made to

specifically tag EVs with a fluorescent dye for CE-LIF analysis. Among the different available strategies for the fluorescent labelling of EVs [22–25], the intra-membrane labelling approach using CFDA-SE, initially applied for flow cytometry of EVs derived from dendritic cell lines, was reported to result in no changes in size or charge of EVs [25]. This approach also avoided previous issues encountered with lipophilic dyes that form dye aggregates or micelles with similar signals to those of EVs, thereby inducing misleading data [26]. This intracellular covalent protein tagging method was therefore adapted to CE-LIF with further optimisations to label EVs. Different parameters, including incubation temperature, duration, dye concentration as well as agitation mode and speed, were optimized to achieve the highest difference between LIF signals of milk EVs samples and those from blanks (see Fig. S1 in the Electronic Supplementary Information ESI). We observed that EVs staining reached the saturation at dye concentrations higher than 200 μM (Fig. S1 A). By varying the EVs dye incubation time from 30 min to 12 h, it was found that much longer incubation times (at least 2 h) were required for EVs labelling than those normally used for cell labelling with CFDA-SE (5–15 min) [27]. This is presumably due to differences in size and esterase expression. Too long incubation time on the other hand resulted in lower signal-to-noise ratio in a time-dependent manner (Fig. S1 B), possibly due to EVs lysis or breaking of the covalent linkage in fluorescent dye over long time. Optimal conditions for EVs labelling with CFDA-SE were set at 37 $^{\circ}\text{C}$, 2 h of incubation, and shaking at 300 rpm. Quality control of CFDA-SE labelled EVs using DLS and NTA (see Fig. S2) revealed no significant change in size distributions (153 nm vs 147 nm), surface charges (–14.8 mV vs –15.4 mV), nor concentrations of EVs (determined with NTA) before and after labelling.

3.2. CE-LIF of fluorescently labelled EVs

CE-LIF method development was first conducted with bovine milk-derived EVs isolated with sucrose gradient ultracentrifugation and suspended in phosphate-buffered saline (PBS) buffer. Keeping the EVs in PBS during CE separation represents the best-case scenario to maintain both physiological pH and isotonic conditions. This allowed us to focus on BGE optimization by reducing the risk of EVs loss or lysis induced from sample treatment steps. Several issues were however encountered during our preliminary tests using conventional BGEs for CE-LIF (*i.e.* phosphate, borate, and Tricine/NaOH buffers). High conductivity of the PBS matrix of the samples was detrimental to CE stacking and separation, and adsorption of EVs to capillary wall led to undetectable and irreproducible signals. An effort was then made to exploit 'inorganic-species-free' (ISF) BGEs containing concentrated weakly charged molecules, which have recently been found to improve the performance of CE-LIF for proteins and peptides [28]. While both constituents of the ISF BGE used in this work are well known, the novelty lies in the use of unprecedentedly high concentrations (several hundred mM) of these large weakly charged molecules. Such high concentrations, while not favorable for conventional UV detection due to elevated background signal, were found advantageous for CE-LIF of EVs. This BGE at very high concentrations reduced spikes provoked by EVs aggregation/collision during electrophoresis, which was observed with other conventional BGEs. Interestingly, this observation was also reported in the recently released work on CE-UV of EVs, in which large ions (*i.e.* bis-tris propane ions) were employed to maintain the EV signal stability [18]. The ISF BGEs, which are tolerant to the presence of PBS in the sample matrix, were found to minimize protein adsorption to capillary wall and induce excellent stacking of slowly migrating proteins. They were expected to provide similar positive features when applied to EVs. The separations

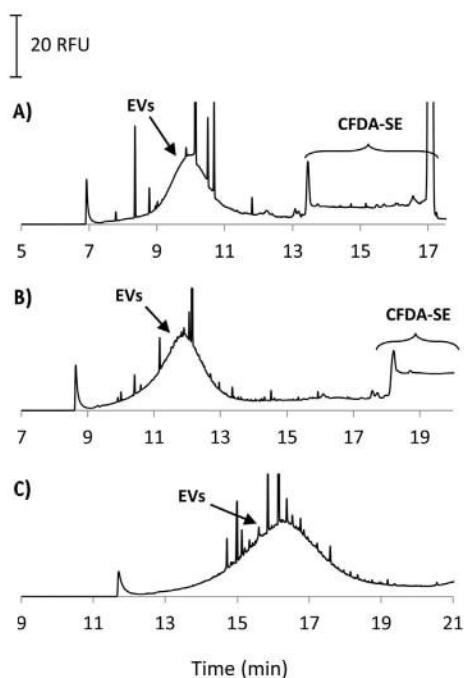


Fig. 1. CE-LIF of EVs (in PBS) derivatized with CFDA-SE, using ISF BGE Tris/CHES (pH 8.4) at different ionic strengths: A) 50 mM; B) 90 mM and C) 150 mM. Other CE conditions: uncoated fused silica capillary with I.D. of 50 μm , effective length (l_{eff}) of 50.2 cm and total length (L_{tot}) of 60.2 cm; Applied voltage: +25 kV; hydrodynamic injection at 3.4 kPa for 2 min. LIF detection with $\lambda_{\text{ex}} = 488 \text{ nm}$, $\lambda_{\text{em}}: 520 \text{ nm}$.

of labelled EVs from the abundant residual fluorophores in the PBS matrix are shown in Fig. 1. The ISF BGE was made up of Tris/CHES (pH 8.4) at different ionic strengths (50–150 mM). The use of extremely high BGE concentrations (630 mM Tris and 870 mM CHES, IS: 150 mM) was still possible without generating high current intensity (only 30 μA under 25 kV). Under the working conditions, the negatively charged EVs transported by an elevated EO mobility migrated faster than the residual CFDA-SE. The EO mobility was tuned from 26×10^{-9} to $12 \times 10^{-9} \text{ m}^2 \text{ V}^{-1} \text{ s}^{-1}$ by increasing IS from 50 to 150 mM. Under an IS of 90 mM (Fig. 1B), labelled EVs and CFSE fluorophore were much better separated than with IS of 50 mM (Fig. 1A), whereas the EV peak shape was not too broadened as was the case when observed with IS of 150 mM (Fig. 1C). Sufficient resolution between EVs and CFSE fluorophore was needed to avoid peak overlapping due to a time-dependent increase in CFSE fluorophore peak. Indeed, CFSE-protein conjugates can exit EVs or become degraded over time [29]. Peaks of EVs were broad and many spikes appeared in the profile. To understand the origin of these events, the analysis was performed with a commercial PVA neutral coating, using the same BGE. As can be seen in Fig. 2, EVs peaks were still broad, this phenomenon being even more pronounced with the PVA coating that decreased the apparent EVs velocity. These results disproved the hypothesis that the broad peaks observed came from EVs adsorption to the silica capillary wall. The large peaks of EVs were most likely the result of a large size distribution of EVs (153 nm \pm 60 nm, obtained from three measurements of the same sample). It can also be observed from Figs. 1 and 2 that the longer the migration time of EVs is, the more the spikes on EVs' peaks can be visualized. The EV standards (bovine milk-derived EVs) used in this study had a high purity, thus excluding the possibility of impurity-induced spikes. Indeed, our results with LC-MS/MS (see Fig. S3 in ESI) showed that the major milk protein contaminants (e.g. α -s1 casein, α -s2 casein, β -casein and κ -casein) as well as some whey milk proteins such as α -

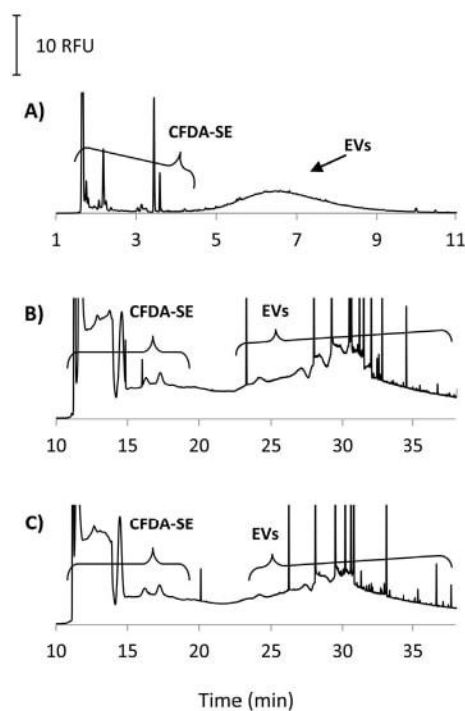


Fig. 2. CE-LIF of EVs (in PBS) derivatized with CFDA-SE in PVA coated capillary A) I.D. of 50 μm , effective length (l_{eff}) of 10 cm and total length (L_{tot}) of 60.2 cm using ISF BGE composed of Tris/CHES (IS 50 mM, pH 8.4); B) and C) I.D. of 50 μm , effective length (l_{eff}) of 50.2 cm and total length (L_{tot}) of 60.2 cm using ISF BGE composed of Tris/CHES IS 50 mM and 90 mM (pH 8.4) respectively. Other CE conditions: -25 kV; $\lambda_{\text{ex}} = 488 \text{ nm}$, $\lambda_{\text{em}}: 520 \text{ nm}$.

Lactalbumin, serum albumin, etc.) were not detected in the EVs standards. Furthermore, the TEM pictures for bovine-milk derived EVs with negative staining by uranyl acetate proved again the high purity of EVs with the absence of the contaminant protein traces in the TEM images (Fig. S4 in ESI). The appearance of spikes during the CE of nanometric entities was already discussed in other studies on nanoparticles and was frequently related to the formation of aggregates [30,31]. The particle aggregates can lead to some unwanted detector response (i.e. spike signals) due to the light scattering when passing through the detector [32,33]. This common problem observed with nanoparticles was also observed during the CE of liposomes [34]. Interestingly, another recent work on CE-UV of EVs also revealed the presence of spikes during electrophoresis [18]. Since EVs suspended in PBS were injected to the CE-LIF, the presence of PBS in the sample plugs (accounting for 10% of the total capillary volume) are likely to produce local Joule heating under a high electrical field due to its high conductivity. The slower the migration of EVs in PBS under high voltages is, the longer EVs suffer from this local heating inside the capillary, which in turn provokes more spike-reflected aggregation. Due to the selectivity offered by LIF detection, only the peaks of EVs and those of fluorophore appeared in the electropherogram (see Fig. 1), allowing us to tolerate larger injection volumes. Our experimental data obtained with injection volumes from 2% to 20% of the total capillary volume (see Fig. S5 in ESI) revealed that an improvement of peak height was observed with an increase in injection volume, regardless of the tested sample matrix (i.e. PBS or 90 mM Tris/Ches). At large injection volumes of 15 and 20%, the augmentation of peak intensity led to peak distortion where the signal did not drop to the normal baseline after the EVs peak. Furthermore, the distance between the EVs peak and the fluorophore-induced plateau became much closer at injection volumes of 15–20%,

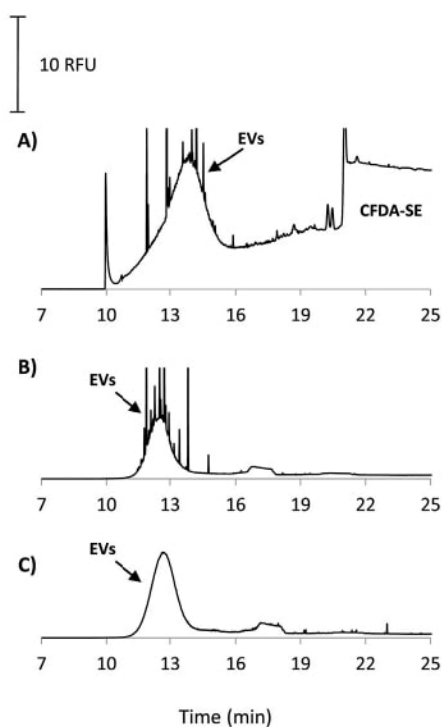


Fig. 3. CE-LIF of fluorescently labelled EVs (A) without filtration (in PBS); (B) after matrix removal with Nanosep unit using a Omega 3K membrane and reconstitution in Tris/CHES (IS 90 mM, pH 8.4); and (C) with Exosome Spin Columns (MW 3000) and reconstitution in Tris/CHES 90 mM at pH 8.4. BGE: Tris/CHES (IS 90 mM, pH 8.4). Other CE conditions as described in Fig. 1.

inducing more risk of peak overlapping upon inevitable increase in fluorescent signal over time (see section below). An injection volume of 10% was found to be optimal, offering high signal intensity compared to that for the case of 2–3% as in conventional hydrodynamic injection for CE, while maintaining sufficiently high separation resolution between EVs' and fluorophore's signals. Note also that, with the pioneering work on electrophoretic separation of EVs, we encountered more constraints than with the CE of nanoparticles (at least to our experience), notably more strict conditions for EVs stability, poorer signal intensity, and the high ionic-strength matrix required for biological entities which hinders efficient stacking. A compromise CE condition was therefore established taking into consideration all these constraints.

3.3. Matrix removal strategy

To avoid the aforementioned undesirable phenomenon during CE-LIF of EVs, two matrix cleanup approaches were tested, i) centrifugal filtration using Nanosep with Omega Membrane 3K, which was inspired from our previous work on matrix removal after fluorescent peptide labeling [35] and ii) EVs filtration with commercial Exosome Spin Columns (MW 3000) (see Fig. 3). In both cases, the EVs were recovered in the BGE. Both approaches offered efficient removal of redundant CFDA-SE, reflected by the absence of the peaks of fluorescent dyes. With the centrifugal filtration (Fig. 3B) multiple spikes were still detected. The aggregation of EVs was still induced in this case, presumably due to the centrifugal force at 5000 rpm required to eliminate the PBS ions through the 3K filter. However, such spikes were not observed when the sample was filtered with the Spin Column (Fig. 3C). Furthermore, unsatisfactory EVs recovery (less than 60%) was obtained with the centrifugal filtration approach, compared to that achieved with the

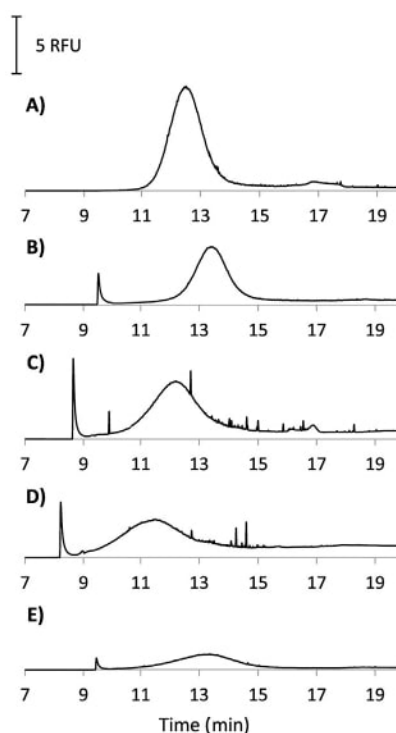


Fig. 4. CE-LIF of fluorescently labelled EVs after matrix substitution with Exosome Spin Column (MW 3000) by Tris/CHES (pH 8.4) at different ionic strengths: A) 90 mM; B) 50 mM; C) 20 mM; D) 5 mM and E) DI water. Other CE conditions as described in Fig. 3.

Spin Column-based alternative (75% recovery, with deviation less than 5% for a repeatability test on 4 EV samples), presumably due to EVs sticking to the NanoSep filter membranes [36]. A similar observation on low EVs recovery and reproducibility after filtration was also made in a recent work on CE-UV separation of EVs [18].

In a related context, another challenge encountered was to minimize or eliminate the lysis of EVs during analysis. Several studies have shown that EVs are stable under isotonic and hypotonic solutions [37,38]. At the same time, if the IS (or conductivity) of the EVs sample matrix is higher than that of the BGE, this would lead to unfavorable de-stacking of EVs during CE-LIF with degraded peak shape and detection sensitivity. To find a compromise, matrix substitution after the Spin Column-based filtration was implemented with water and Tris/CHES having IS from 5 to 90 mM. The respective electropherograms using the optimized BGE are shown in Fig. 4. The best signal of EVs was achieved for the sample matrix composed of Tris/CHES IS 90 mM. The signal-to-noise ratios for EVs peaks dropped from 524 to 89 with IS decreasing from 90 mM to 0 mM (DI water). Compared to other more diluted sample matrices, the 90 mM Tris/CHES did not produce any stacking effect since the matrix shares the same composition and concentration as the BGE employed. On the other hand, the rate of EVs lysis may be slowed down thanks to the IS being closer to isotonic conditions, resulting in a higher signal for EVs even without stacking effect. Sample matrices composed of Tris/CHES at higher IS (up to 240 mM) were also tested, but unsatisfactory data were obtained (data not shown) due to the unfavorable de-stacking with broader peaks when the IS of the sample matrix was higher than that of the BGE. The salient performance data obtained from these optimized conditions are shown in Table 1. The best detection limit for EVs achieved using the developed CE-LIF method reached approximately 8×10^9 EV/mL whereas the calibration curve was acquired up to 1.20×10^{11} EV/mL. The correlation between EVs concentrations and

peak areas ($R^2 = 0.968$) was not optimal. It was nevertheless deemed satisfactory, taking into consideration that it comprises all the operational errors accumulated from the different steps, including EVs labeling, buffer substitution, electrokinetic separation and LIF detection. In the recent work on CE-UV of EVs [18], the linear correlation achieved was also far from optimal ($R^2 = 0.81$), confirming the challenges currently encountered with electrokinetic separation of EVs. Note that the working EVs volume of 40 μL during the buffer substitution was at the lower limit of the recommended range (20–100 μL) for Exosome Spin columns, which in turn may lead to some dilution errors. Larger working volumes were not available due to limited EVs concentrations and limited initial sample volumes. Better performance would nevertheless be expected when working with more concentrated EVs samples. To minimize fluorescent signal deviation due to sample degradation over time after buffer substitution (evidenced by reappearance of fluorophore signals in the electropherogram of Fig. S6), a calibration curve was made with four samples of different concentrations prepared in parallel and analyzed promptly within the same day. Excellent intermediate precision was achieved for migration times ($RSD < 0.6\%$) whereas a satisfactory one was obtained for peak areas ($RSD < 5\%$).

3.4. Electrokinetic distribution of EVs from different animal and human origins

3.4.1. EVs purified with SEC or ultracentrifugation

Batches of EVs isolated from different animal and human origins using the established method (i.e. SEC and ultracentrifugation) were analyzed with our optimized CE-LIF method to demonstrate its potential in distinguishing EVs subpopulations based upon their electrophoretic mobilities (see Fig. 5). The EOF was measured before and after each EVs sample analysis and was shown to be remarkably stable (RSD less than 0.5% over the whole analysis series). The difference in migration times observed between different EVs populations hence came purely from variation in their electrophoretic mobilities. The size distributions of the EVs isolates measured with NTA were also included in Fig. 5 for cross comparison with results obtained with CE-LIF. To interpret further the obtained results, our initial efforts to related migration behavior of EVs to their physicochemical characteristics (notably size, charge, charge/size ratio and shape) were made based on previous studies on CE of nanoparticles (NPs). Both EVs and NPs were thought to share similar size and charge characteristics. After this deep investigation we came to the conclusion that the dependency of NPs' electrophoretic mobilities on their size, charge, charge-to-size ratio and shape cannot be determined by a general rule, but was rather possible only for very specific situations and under some specific conditions [39–42]. Indeed, many parameters should be well considered and defined before a clear correlation between the electrophoretic mobilities of NPs and one of their particular characteristics can be established. Parameters such as BGE ionic strength, pH and composition, applied electrical field, injected amount of NPs etc. were found to have impacts on NPs' electrophoretic mobilities ([43] and other references listed therein). This makes it very difficult to rule out the dependency of NPs

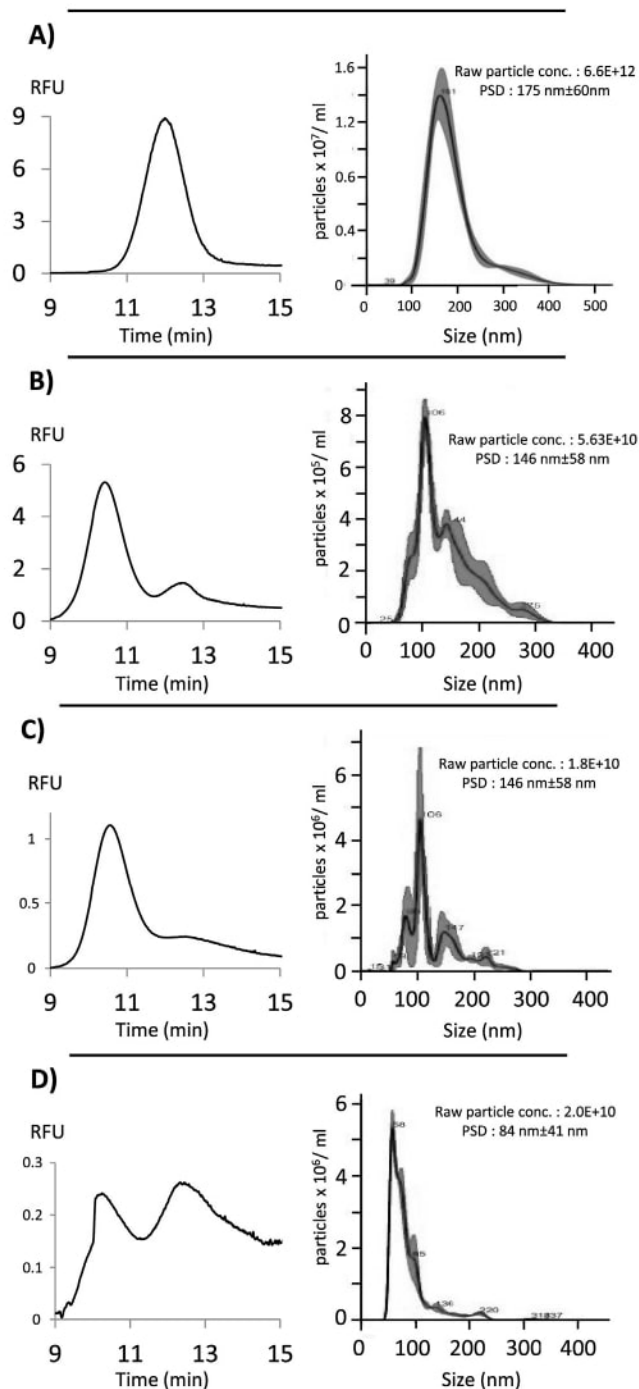


Fig. 5. CE-LIF electropherograms vs. NTA profiles for fluorescently labeled EVs (after matrix removal with Exosome Spin Columns (MW 3000) and reconstitution in Tris/CHES 90 mM at pH 8.4). The EVs were purified from A) bovine milk; B) pony plasma; C) pony serum and D) human plasma. BGE: Tris/CHES (IS 90 mM, pH 8.4). Other CE conditions as described in Fig. 1.

Table 1
Calibration range, coefficient of determination (R^2) for linearity, limit of detection (LOD) and repeatability ($n = 3$) for the CE-LIF determination of fluorescently labelled EVs.

| Calibration range (EVs/mL) ^a | R^2 | LOD (EVs/mL) ^b | RSD (%) migration times | RSD (%) peak areas |
|---|-------|---------------------------|-------------------------|--------------------|
| $1.22 \times 10^{10} - 12 \times 10^{10}$ | 0.968 | 7.86×10^9 | 0.6 | 4.3 |

^a 4 concentrations.

^b Based on peak heights corresponding to $S/N = 3$.

electrophoretic mobilities on a single parameter. In the case of EVs, the situation is even more complicated, since their size distributions are broader and different sub-populations can co-exist (as reflected by NTA data). With bovine milk-derived EVs (Fig. 5A) one main peak was detected with CE-LIF and NTA, evidencing a low degree of polydispersity. A large size distribution of $175 \text{ nm} \pm 60 \text{ nm}$ was observed in this case according to NTA measurements. This observation is contrary to the case of CE of nanoparticles reported by Jones *et al.*, in which sharp peaks reflected different particle populations, but each having a narrow particle size distribution [44]. A low degree of polydispersity however was not the case with pony plasma-derived EVs (Fig. 5B) or serum-derived EVs (Fig. 5C) where two subpopulations were clearly identified with CE-LIF, and several size-based peaks were observed with NTA. An interesting observation was made on human plasma-derived EVs (Fig. 5D), where NTA data demonstrated a relatively homogeneous size distribution whereas two equivalent subpopulations were revealed with CE-LIF, implying some pronounced population heterogeneity from the human EVs source. While a conclusion on the reason behind the different profiles obtained with CE-LIF and NTA cannot be made at this stage of proof-of-concept for electrokinetic characterization of EVs, we assumed that this was due to different origins of EVs. EVs from different origins probably have different proteins/biomolecules on their surface and also different shapes that may influence their electrophoretic mobilities. Note also that EVs can exhibit shape variations in different BGE conditions, similar to the behavior of cells. Lysis of EVs can also occur, requiring a careful and restricted selection of BGE composition and ionic strength. The application of a high electrical field, as suggested by Jones *et al.* and d'Orlyé *et al.* for better NPs separations [40,44], could not be utilized for EVs because it would provoke lysis. As a result, when applying these to the CE-LIF separations of EVs from different origins (Fig. 5), it was difficult to draw any conclusion. A deeper characterization study would therefore be needed to elucidate the EVs electrophoretic migration behavior, using EVs with a lower degree of polydispersity and narrower size distribution. Such pure EVs nevertheless are not yet available with existing methods for EV purification.

3.4.2. EVs isolated with monolithic disks via immunoaffinity chromatography

Our CE-LIF approach was used to verify the presence of sub-population of EVs isolated with our recent method based on functionalized monolithic disks. The reported isolation protocol using anti-human CD61 antibody [17] was herein extended using monolithic disk immobilized with monoclonal anti-human CD9 antibody. While monolithic disks immobilized with anti-CD61 antibody allow collection of platelet-derived EVs with sizes of 30–130 nm [17], those immobilized with anti-CD9 antibody were expected to capture more specifically a potential EV subtype historically claimed as “exosomes”, since CD9 is a tetraspanin that is thought to be enriched specifically in exosomes [45]. Note that according to the MISEV guidelines from ISEV, it is still not possible to propose a specific and universal marker of one or the other type of EVs. Distinct elutions from these two monolithic disks, using either ammonium hydroxide or sodium bicarbonate-carbonate as eluents are shown in Fig. 6. For comparison purpose, some NTA data for such elutions were provided in Fig. S7 in the ESI. From the electropherograms, three EV subpopulations from each of these elutions were detected with CE-LIF. Three fractions were also detected with asymmetrical flow field-flow fractionation (AsFIFFF) in our previous work [17], proving the concordance of the results obtained with CE-LIF. Based on the CE-LIF signal intensity, the highest concentration was found for the fraction with the longest migration time (17 min). When monolithic disks immobilized with

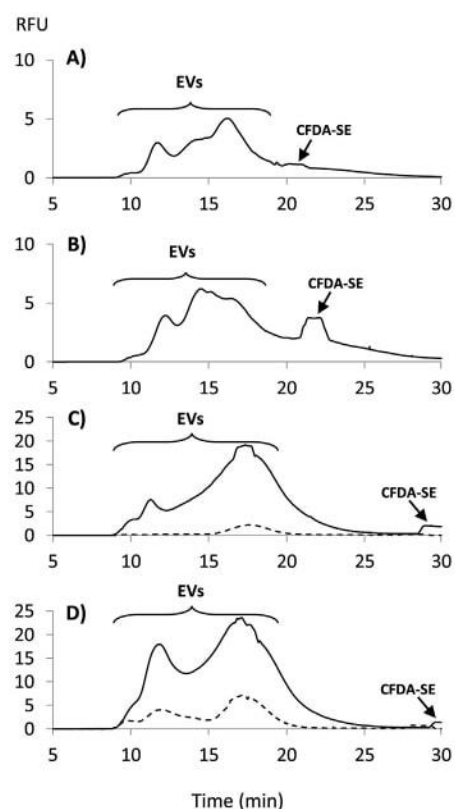


Fig. 6. CE-LIF of fluorescently labelled EVs isolated with affinity monolithic disks (continuous lines) after matrix substitution into Tris/CHES 90 mM (pH 8.4) with Exosome Spin Columns (MW 3000). The dashed lines represent the EV distributions in fractions further purified with AsFIFFF after the elution step. EVs elution from monolithic disks under alkaline conditions (pH 11.3) was performed with: (A) (B) ammonium hydroxide; (C) (D) sodium bicarbonate-carbonate. Monolithic disks were immobilized with: (A)(C) anti-human CD61; (B)(D) anti-human CD9. Other CE conditions as described in Fig. 1.

anti-CD9 antibody were employed, the signal of the second peak zone (10–12 min) became more intense (Fig. 6D). As already discussed above, no conclusion on the precise size and charge of EV subpopulations visualized with CE-LIF could be made due to the lack of reference data for the fractions collected after the elution step. In an effort to give a deeper insight into EVs after the monolithic affinity step, AsFIFFF was employed to further fractionate these eluents. Our CE-LIF approach was used to verify the quality of these EV fractions collected with AsFIFFF. Due to considerably lower EV concentrations in the AsFIFFF fractions compared to the whole monolithic disk isolates, lyophilization was used to enrich EVs prior to CE-LIF. This process was shown not to change the properties of EVs, or at least their physical characteristics [46]. The electropherograms for the AsFIFFF fractions expected to contain small EVs were shown in dashed lines in Fig. 6C and D. As can be seen, the presence of EVs in the AsFIFFF fractions (Fig. 6) was confirmed by the superposition of their profiles on those of the bulk collects. Based on our results, the CE-LIF shows a real potential in distinguishing different EV subpopulations from highly specific EV isolates, which provides crucial information for future studies in the EV field. The developed CE-LIF method visualized the EVs distribution in AsFIFFF fractions and demonstrated that further optimization of the AsFIFFF method would be needed to obtain purer fractions of the EV subpopulations. Interestingly, higher LIF intensities were always observed on carbonate-bicarbonate elutions (Fig. 6 C, D) compared to those of ammonium hydroxide ones (Figs. A, B), regardless of the antibody used. This led us to a deeper

study on CFDA-SE labelling in different media (see Fig. S6 in the ESI), which confirmed the less efficient labelling under an ammonium hydroxide medium due to unwanted conversion of CFDA-SE into side products in the presence of ammonium/amine groups.

4. Conclusion remarks

We successfully developed a fast and reliable CE-LIF method for the determination of labelled EVs, providing the first evidence that CE can be applied to distinguish EVs subpopulations from EV isolates, based on their electrophoretic mobilities. This new tool for the elucidation of electrokinetic distribution of EV populations adds valuable information to commonly-used size-based physical techniques such as NTA and transmission electron microscopy. The applicability of the CE-LIF approach was successfully demonstrated for tracing of EVs from different origins, as well as for quality control of EVs after isolation with different methods including monolithic disks and subpopulation fractionation with AsFIFFF. Inclusion of a forefront isolation step from highly complex biofluids into an integrated microfluidic platform is now envisaged for the electrokinetic characterization of EV subpopulations with tiny sample volumes and low EV concentrations. Translation of batch-wise EV sample treatment protocol into an integrated microfluidic platform is also desirable to reduce operation time and avoid cross contamination and EV loss. Prospective work to establish a solid theoretical background for the electrokinetic profiling of EVs will also be implemented when EVs with a better degree of polydispersity and narrower size (and charge) distribution could be obtained through improvement of EV purification technologies.

Declaration of competing interest

The authors declare that they have no known competing financial interests or personal relationships that could have appeared to influence the work reported in this paper.

Acknowledgement

This work has been financially supported by the Institut Universitaire de France (for M. Taverna, senior member). The doctoral scholarship for Marco Morani was supported by the doctoral school 2MIB (Sciences Chimiques: Molécules, Matériaux, Instrumentation et Biosystèmes) – University Paris Saclay. We thank Ms. Oihana Inda-Arsa for preliminary explorations in CE-UV and CE-LIF. Dr. Hervé Hillaireau and Magali Noiray from Institute Galien Paris Sud – University Paris Saclay are acknowledged for their help and support in NTA measurements. We thank Mr. Edward Mitchell for English grammar corrections. Financial support (E.M. and M.-L.R.) was also provided by the Research Council for Natural Sciences and Engineering, Academy of Finland (grant No 1311369).

Appendix A. Supplementary data

Supplementary data to this article can be found online at <https://doi.org/10.1016/j.aca.2020.06.073>.

References

- [1] G. van Niel, G. D'Angelo, G. Raposo, Shedding light on the cell biology of extracellular vesicles, *Nat. Rev. Mol. Cell Biol.* 19 (2018) 213–228.
- [2] G. Raposo, W. Stoorvogel, Extracellular vesicles: exosomes, microvesicles, and friends, *J. Cell Biol.* 200 (2013) 373–383.
- [3] H.C. Bu, D.G. He, X.X. He, K.M. Wang, Exosomes: isolation, analysis, and applications in cancer detection and therapy, *ChemBiochem* 20 (2019) 451–461.
- [4] M.T. Guo, A. Rotem, J.A. Heyman, D.A. Weitz, Droplet microfluidics for high-throughput biological assays, *Lab Chip* 12 (2012) 2146–2155.
- [5] J. Howitt, A.F. Hill, Exosomes in the pathology of neurodegenerative diseases,

- J. Biol. Chem.* 291 (2016) 26589–26597.
- [6] H.L. Shao, H. Im, C.M. Castro, X. Breakefield, R. Weissleder, H.H. Lee, New technologies for analysis of extracellular vesicles, *Chem. Rev.* 118 (2018) 1917–1950.
- [7] E.H. Koritzinsky, J.M. Street, R.A. Star, P.S.T. Yuen, Quantification of exosomes, *J. Cell. Physiol.* 232 (2017) 1587–1590.
- [8] R. Szataneck, M. Baj-Krzyworzeka, J. Zimoch, M. Lekka, M. Siedlar, J. Baran, The methods of choice for extracellular vesicles (EVs) characterization, *Int. J. Mol. Sci.* 18 (2017).
- [9] U. Erdbrugger, J. Lannigan, Analytical challenges of extracellular vesicle detection: a comparison of different techniques, *Cytometry Part A* 89A (2016) 123–134.
- [10] S. Biosciences, **FluoroCet exosome quantitation kit**. https://www.systembio.com/wp-content/uploads/MANUAL_FCET96A-1-1.pdf, 2017.
- [11] T. Hikita, M. Miyata, R. Watanabe, C. Oneyama, Sensitive and rapid quantification of exosomes by fusing luciferase to exosome marker proteins, *Sci. Rep.* 8 (2018).
- [12] M. Al Ahmad, Electrical detection, identification, and quantification of exosomes, *IEEE Access* 6 (2018) 22817–22826.
- [13] L. Trapiella-Alfonso, G. Ramirez-Garcia, F. d'Orlye, A. Varenne, Electromigration separation methodologies for the characterization of nanoparticles and the evaluation of their behaviour in biological systems, *Trac. Trends Anal. Chem.* 84 (2016) 121–130.
- [14] T. Akagi, K. Kato, M. Kobayashi, N. Kosaka, T. Ochiya, T. Ichiki, On-Chip immunoelectrophoresis of extracellular vesicles released from human breast cancer cells, *PLoS One* 10 (2015).
- [15] K. Kato, M. Kobayashi, N. Hanamura, T. Akagi, N. Kosaka, T. Ochiya, T. Ichiki, Electrokinetic evaluation of individual exosomes by on-chip microcapillary electrophoresis with laser dark-field microscopy, *Jpn. J. Appl. Phys.* 52 (2013).
- [16] T. Akagi, K. Kato, N. Hanamura, M. Kobayashi, T. Ichiki, Evaluation of desialylation effect on zeta potential of extracellular vesicles secreted from human prostate cancer cells by on-chip microcapillary electrophoresis, *Jpn. J. Appl. Phys.* 53 (2014).
- [17] E. Multia, C.J.Y. Tear, M. Palviainen, P. Siljander, M.-L. Riekkola, Fast isolation of highly specific population of platelet-derived extracellular vesicles from blood plasma by affinity monolithic column, immobilized with anti-human CD61 antibody, *Anal. Chim. Acta* 1091 (2019) 160–168.
- [18] M. Piotrowska, K. Ciura, M. Zalewska, M. Dawid, B. Correia, P. Sawicka, B. Lewczuk, J. Kasprzyk, L. Sola, W. Piekoszewski, B. Wielgomas, K. Waleron, S. Dziomba, Capillary zone electrophoresis of bacterial extracellular vesicles: a proof of concept, *J. Chromatogr. A* (2020) 461047.
- [19] O.H. Lowry, N.J. Rosebrough, A.L. Farr, R.J. Randall, Protein measurement with the folin phenol reagent, *J. Biol. Chem.* 193 (1951) 265–275.
- [20] M. Puhka, M.E. Nordberg, S. Valkonen, A. Rannikko, O. Kallioniemi, P. Siljander, T.M. af Hallstrom, KeepEX, A simple dilution protocol for improving extracellular vesicle yields from urine, *Eur. J. Pharm. Sci.* 98 (2017) 30–39.
- [21] A. Hellqvist, Y. Hedeland, C. Pettersson, Evaluation of electroosmotic markers in aqueous and nonaqueous capillary electrophoresis, *Electrophoresis* 34 (2013) 3252–3259.
- [22] A. Hoshino, B. Costa-Silva, T.L. Shen, G. Rodrigues, A. Hashimoto, M.T. Mark, H. Molina, S. Kohsaka, A. Di Giannatale, S. Ceder, S. Singh, C. Williams, N. Soplop, K. Uryu, L. Pharmed, T. King, L. Bojmar, A.E. Davies, Y. Ararso, T. Zhang, H. Zhang, J. Hernandez, J.M. Weiss, V.D. Dumont-Cole, K. Kramer, L.H. Wexler, A. Narendran, G.K. Schwartz, J.H. Healey, P. Sandstrom, K.J. Labori, E.H. Kure, P.M. Grandgenett, M.A. Hollingsworth, M. de Sousa, S. Kaur, M. Jain, K. Mallaya, S.K. Batra, W.R. Jarnagin, M.S. Brady, O. Fodstad, V. Muller, K. Pantel, A.J. Minn, M.J. Bissell, B.A. Garcia, Y. Kang, V.K. Rajasekhar, C.M. Ghajar, I. Matei, H. Peinado, J. Bromberg, D. Lyden, Tumour exosome integrins determine organotropic metastasis, *Nature* 527 (2015) 329–+.
- [23] H.D. Roberts-Dalton, A. Cocks, J.M. Falcon-Perez, E.J. Sayers, J.P. Webber, P. Watson, A. Clayton, A.T. Jones, Fluorescence labelling of extracellular vesicles using a novel thiol-based strategy for quantitative analysis of cellular delivery and intracellular traffic, *Nanoscale* 9 (2017) 13693–13706.
- [24] J. Lannigan, U. Erdbrugger, Imaging flow cytometry for the characterization of extracellular vesicles, *Methods* 112 (2017) 55–67.
- [25] A. Morales-Kastresana, B. Telford, T.A. Musich, K. McKinnon, C. Clayborne, Z. Braig, A. Rosner, T. Demberg, D.C. Watson, T.S. Karpova, G.J. Freeman, R.H. DeKruyff, G.N. Pavlakis, M. Terabe, M. Robert-Guroff, J.A. Berzofsky, J.C. Jones, Labeling extracellular vesicles for nanoscale flow cytometry, *Sci. Rep.* 7 (2017).
- [26] M. Dehghani, S.M. Gulvin, J. Flax, T.R. Gaboriski, Exosome Labeling by Lipophilic Dye PKH26 Results in Significant Increase in Vesicle Size, *bioRxiv*, 2019, p. 532028.
- [27] X.Q. Wang, X.M. Duan, L.H. Liu, Y.Q. Fang, Y. Tan, Carboxyfluorescein diacetate succinimidyl ester fluorescent dye for cell labeling, *Acta Biochim. Biophys. Sin.* 37 (2005) 379–385.
- [28] M. Morani, M. Taverna, T.D. Mai, A fresh look into background electrolyte selection for capillary electrophoresis-laser induced fluorescence of peptides and proteins, *Electrophoresis* 40 (2019) 2618–2624.
- [29] H.T. Banks, A. Choi, T. Huffman, J. Nardini, L. Poag, W.C. Thompson, Quantifying CFSE label decay in flow cytometry data, *Appl. Math. Lett.* 26 (2013) 571–577.
- [30] C. Quang, S.L. Petersen, G.R. Ducatte, N.E. Ballou, Characterization and separation of inorganic fine particles by capillary electrophoresis with an indifferent electrolyte system, *J. Chromatogr. A* 732 (1996) 377–384.

- [31] S.L. Petersen, N.E. Ballou, Separation of micrometer-size oxide particles by capillary zone electrophoresis, *J. Chromatogr. A* 834 (1999) 445–452.
- [32] S. Dziomba, K. Ciura, B. Correia, B. Wielgomas, Stabilization and isotachopheresis of unmodified gold nanoparticles in capillary electrophoresis, *Anal. Chim. Acta* 1047 (2019) 248–256.
- [33] S. Dziomba, K. Ciura, P. Kocalkowska, A. Prah, B. Wielgomas, Gold nanoparticles dispersion stability under dynamic coating conditions in capillary zone electrophoresis, *J. Chromatogr. A* 1550 (2018) 63–67.
- [34] M.A. Roberts, L. LocascioBrown, W.A. MacCrehan, R.A. Durst, Liposome behavior in capillary electrophoresis, *Anal. Chem.* 68 (1996) 3434–3440.
- [35] C.C. de Lassichere, T.D. Mai, M. Otto, M. Taverna, Online preconcentration in capillaries by multiple large-volume sample stacking: an alternative to immunoassays for quantification of amyloid beta peptides biomarkers in cerebrospinal fluid, *Anal. Chem.* 90 (2018) 2555–2563.
- [36] K.E. Petersen, F. Shiri, T. White, G.T. Bardi, H. Sant, B.K. Gale, J.L. Hood, Exosome isolation: cyclical electrical field flow fractionation in low-ionic-strength fluids, *Anal. Chem.* 90 (2018) 12783–12790.
- [37] E. Willms, H.J. Johansson, I. Mager, Y. Lee, K.E.M. Blomberg, M. Sadik, A. Alaarg, C.I.E. Smith, J. Lehtio, S.E.L. Andaloussi, M.J.A. Wood, P. Vader, Cells release subpopulations of exosomes with distinct molecular and biological properties, *Sci. Rep.* 6 (2016) 12.
- [38] V.S. Chernyshev, R. Rachamadugu, Y.H. Tseng, D.M. Belnap, Y.L. Jia, K.J. Branch, A.E. Butterfield, L.F. Pease, P.S. Bernard, M. Skliar, Size and shape characterization of hydrated and desiccated exosomes, *Anal. Bioanal. Chem.* 407 (2015) 3285–3301.
- [39] F. d'Orlye, A. Varenne, P. Gareil, Size-based characterization of nanometric cationic maghemite particles using capillary zone electrophoresis, *Electrophoresis* 29 (2008) 3768–3778.
- [40] F. d'Orlye, A. Varenne, T. Georgelin, J.M. Siaugue, B. Teste, S. Descroix, P. Gareil, Charge-based characterization of nanometric cationic bifunctional maghemite/silica core/shell particles by capillary zone electrophoresis, *Electrophoresis* 30 (2009) 2572–2582.
- [41] F.K. Liu, F.H. Ko, P.W. Huang, C.H. Wu, T.C. Chu, Studying the size/shape separation and optical properties of silver nanoparticles by capillary electrophoresis, *J. Chromatogr. A* 1062 (2005) 139–145.
- [42] N.G. Vanifatova, B.Y. Spivakov, J. Mattusch, U. Franck, R. Wennrich, Investigation of iron oxide nanoparticles by capillary zone electrophoresis, *Talanta* 66 (2005) 605–610.
- [43] U. Pyell, Characterization of nanoparticles by capillary electromigration separation techniques, *Electrophoresis* 31 (2010) 814–831.
- [44] H.K. Jones, N.E. Ballou, Separations of chemically different particles by capillary electrophoresis, *Anal. Chem.* 62 (1990) 2484–2490.
- [45] J. Kowal, G. Arras, M. Colombo, M. Jouve, J.P. Morath, B. Primdal-Bengtson, F. Dingli, D. Loew, M. Tkach, C. Théry, Proteomic comparison defines novel markers to characterize heterogeneous populations of extracellular vesicle subtypes, *Proc. Natl. Acad. Sci. Unit. States Am.* 113 (2016) E968.
- [46] A.E. Russell, A. Sneider, K.W. Witwer, P. Bergese, S.N. Bhattacharyya, A. Cocks, E. Cocucci, U. Erdbrügger, J.M. Falcon-Perez, D.W. Freeman, T.M. Gallagher, S. Hu, Y. Huang, S.M. Jay, S.-i. Kano, G. Lavieu, A. Leszczynska, A.M. Llorente, Q. Lu, V. Mahairaki, D.C. Muth, N. Noren Hooten, M. Ostrowski, I. Prada, S. Sahoo, T.H. Schøyen, L. Sheng, D. Tesch, G. Van Niel, R.E. Vandenbroucke, F.J. Verweij, A.V. Villar, M. Wauben, A.M. Wehman, H. Yin, D.R.F. Carter, P. Vader, Biological membranes in EV biogenesis, stability, uptake, and cargo transfer: an ISEV position paper arising from the ISEV membranes and EVs workshop, *J. Extracell. Vesicles* 8 (2019) 1684862.

Electronic Supporting Information

Electrokinetic characterization of extracellular vesicles with capillary electrophoresis: a new tool for their identification and quantification

Marco Morani¹, Thanh Duc Mai¹, Zuzana Krupova², Pierre Defrenaix², Evgen Multia³, Marja-Liisa Riekkola³ and Myriam Taverna^{1,4*}

¹ *Institut Galien Paris Sud, UMR 8612, Protein and Nanotechnology in Analytical Science (PNAS), CNRS, Univ. Paris-Sud, Univ. Paris-Saclay, 5 rue Jean Baptiste Clément, 92290 Châtenay-Malabry, France*

² *Excilone - 6, Rue Blaise Pascal - Parc Euclide - 78990 Elancourt - France*

³ *Department of Chemistry, P.O. Box 55, FI-00014 University of Helsinki, Finland.*

⁴ *Institut Universitaire de France (IUF)*

Correspondence: E-mail: myriam.taverna@u-psud.fr; Fax: +33-1-46-83-54-62

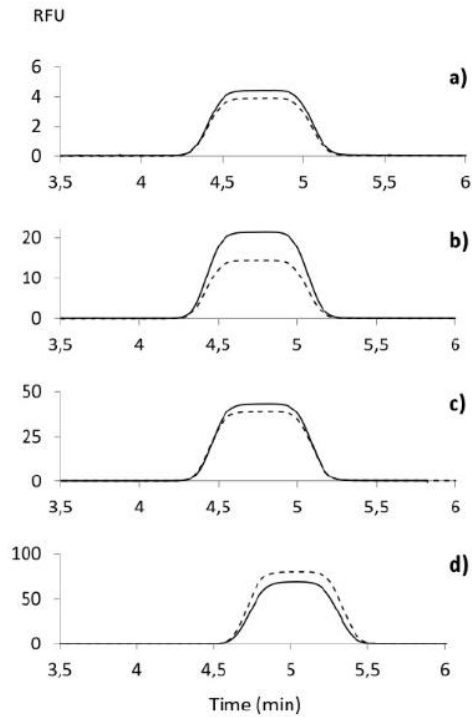


Fig. S1 A

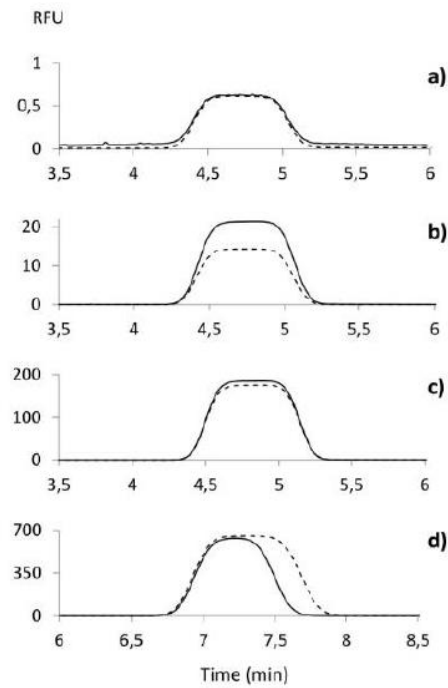


Fig. S1 B

Figure S1. Comparison of LIF signals of fluorescently labeled EVs (continuous line) vs. blanks (dashed line) for staining optimization with CFDA-SE (A) dye concentration : a) 40 μM ; b) 100 μM ; c) 200 μM ; d) 400 μM ; and (B) incubation time: a) 30 min; b) 2 h; c) 5h; d) 12h. CE conditions: uncoated fused silica capillary with I.D. of 50 μm , effective length (L_{eff}) of 50.2 cm and total length (L_{tot}) of 60.2 cm; applied pressure of 10.3 kPa; LIF detection with $\lambda_{\text{ex}} = 488 \text{ nm}$, $\lambda_{\text{em}}: 520 \text{ nm}$. Samples were hydrodynamically injected from the inlet end by applying a pressure of 3.4 kPa for 2 min.

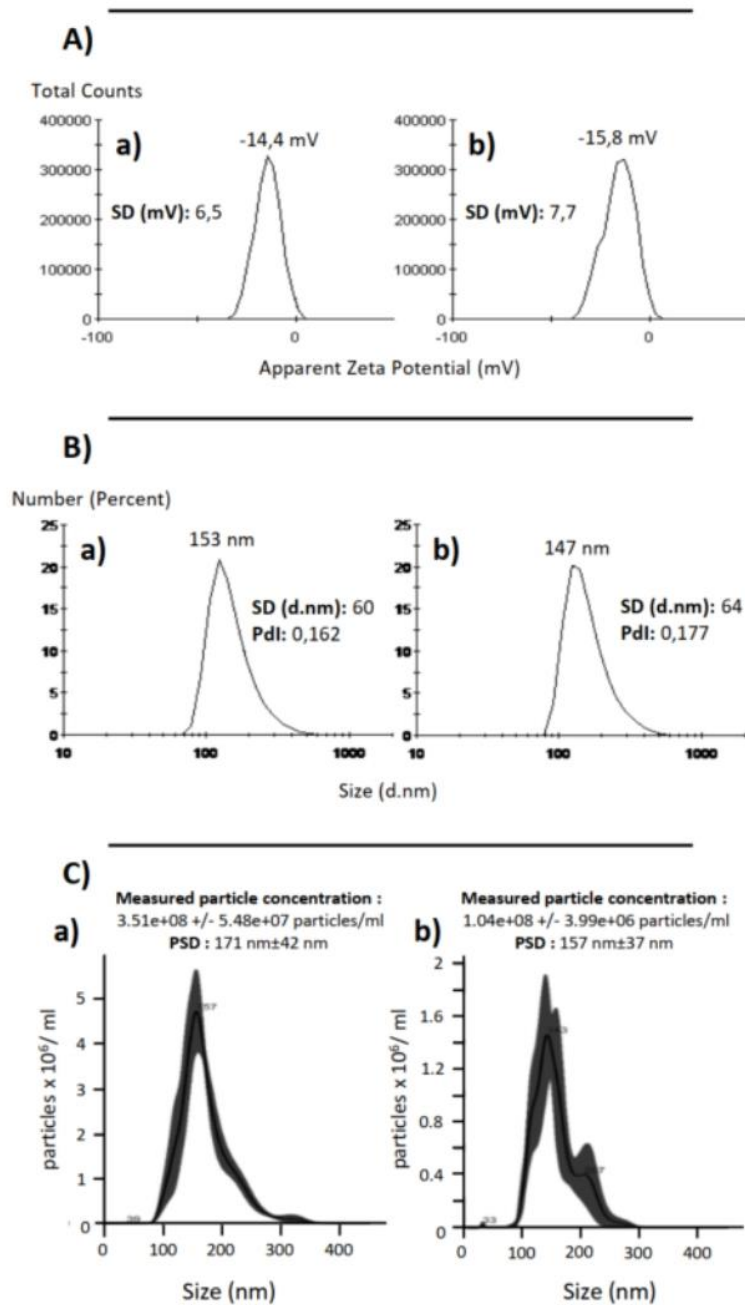


Figure S2. A) Zeta potential; B) particle size distribution with DLS (Dynamic Light Scattering) and C) particle concentration and size distribution with NTA (Nanoparticle Tracking Analysis) of bovine milk-derived EVs, (a) before and (b) after fluorescent labelling with CFDA-SE. For DLS measurements, representative data from three consecutive runs are shown. NTA histograms represent the mean of three replicate measurements of the same sample and standard deviation in grey.

| Protein name | Gene | Uniprot ID |
|--|-------------|--------------------------|
| Xanthine dehydrogenase/oxidase | XDH | F1MUT3 (F1MUT3_BOVIN) |
| Xanthine dehydrogenase/oxidase | XDH | P80457 (XDH_BOVIN) |
| Aldehyde oxidase 4 | AOX4 | E1BL62 (E1BL62_BOVIN) |
| Aldehyde oxidase | AOX1 | P48034 (ADO_BOVIN) |
| Butyrophilin subfamily 1 member A1 | BTN1A1 | P18892 (BT1A1_BOVIN) |
| Uncharacterized protein | SLK | G3X696 (G3X696_BOVIN) |
| BOVIN Butyrophilin (Fragment) | BTN | Q9TSF1 (Q9TSF1_BOVIN) |
| Fatty acid synthase | FASN | F1N647 (F1N647_BOVIN) |
| Fatty acid synthase | FASN | Q71SP7 (FAS_BOVIN) |
| Lactadherin | MFGE8 | F1MXX6 (F1MXX6_BOVIN) |
| Lactadherin | MFGE8 | G3MYW7 (G3MYW7_BOVIN) |
| Lactotransferrin | LTF | P24627 (TRFL_BOVIN) |
| Lactoferrin | | B3VTM3 (B3VTM3_BOVIN) |
| Lactoferrin (Fragment) | | Q95M57 (Q95M57_BOVIN) |
| Polymeric immunoglobulin receptor | PIGR | P81265 (PIGR_BOVIN) |
| Uncharacterized protein | PIGR | F1MR22 (F1MR22_BOVIN) |
| Platelet glycoprotein 4 | CD36 | P26201 (CD36_BOVIN) |
| Sodium-dependent phosphate transport protein 2B | SLC34A2 | F1N6D4 (F1N6D4_BOVIN) |
| Mucin-16 | MUC16 | F2FB38 (F2FB38_BOVIN) |
| Perilipin-2 | PLIN2 | Q9TUM6 (PLIN2_BOVIN) |
| ATP-binding cassette sub-family G member 2 | ABCG2 | Q4GZT4 (ABCG2_BOVIN) |
| Complement C3 | C3 | Q2UVX4 (CO3_BOVIN) |
| Ezrin | EZR | P31976 (EZRI_BOVIN) |
| Moesin | MSN | Q2HJ49 (MOES_BOVIN) |
| Radixin | RDX | Q32LP2 (RADI_BOVIN) |
| Uncharacterized protein | GP2 | F1N726 (F1N726_BOVIN) |
| Ectonucleotide pyrophosphatase/phosphodiesterase family member 3 | ENPP3 | P15396 (ENPP3_BOVIN) |
| Isocitrate dehydrogenase [NADP] cytoplasmic | IDH1 | Q9XSG3 (IDHC_BOVIN) |
| Isocitrate dehydrogenase [NADP] (Fragment) | IDH1 | Q0QEQ4 (Q0QEQ4_BOVIN) |

| | | |
|--|--------------|-----------------------|
| RAB1A, member RAS oncogene family | RAB1A | A1L528 (A1L528_BOVIN) |
| Ras-related protein Rab-18 | RAB18 | Q0IIG8 (RAB18_BOVIN) |
| Ras-related protein Rab-8A | RAB8A | A4FV54 (RAB8A_BOVIN) |
| Ras-related protein Rab-1B | RAB1B | Q2HJH2 (RAB1B_BOVIN) |
| RAB10 protein | RAB10 | A6QLS9 (A6QLS9_BOVIN) |
| Uncharacterized protein | RAB35 | F1MSJ9 (F1MSJ9_BOVIN) |
| Uncharacterized protein | RAB3D | E1BNX1 (E1BNX1_BOVIN) |
| RAB14 protein | RAB14 | Q3ZBG1 (Q3ZBG1_BOVIN) |
| Ras-related protein Rab-13 | RAB13 | Q58DS5 (RAB13_BOVIN) |
| Major allergen beta-lactoglobulin | | B5B0D4 (B5B0D4_BOVIN) |
| Beta-lactoglobulin | LGB | P02754 (LACB_BOVIN) |
| Beta-lactoglobulin variant D | LGB | O77777 (O77777_BOVIN) |
| Uncharacterized protein | GGT1 | G3N2D8 (G3N2D8_BOVIN) |
| Heat shock cognate 71 kDa protein | HSPA8 | P19120 (HSP7C_BOVIN) |
| Heat shock 70 kDa protein 1B | HSPA1B | Q27965 (HS71B_BOVIN) |
| Heat shock 70 kDa protein 1-like | HSPA1L | P0CB32 (HS71L_BOVIN) |
| Uncharacterized protein | HSPA6 | F1MWU9 (F1MWU9_BOVIN) |
| Uncharacterized protein | IPLL1 | F1MLW7 (F1MLW7_BOVIN) |
| Immunoglobulin light chain, lambda gene cluster | IGL@ | Q1RMN8 (Q1RMN8_BOVIN) |
| IGL@ protein | IGL@ | Q3T101 (Q3T101_BOVIN) |
| Uncharacterized protein | LOC100847119 | F1MLW8 (F1MLW8_BOVIN) |
| Annexin A5 | ANXA5 | P81287 (ANXA5_BOVIN) |
| Annexin A4 | ANXA4 | P13214 (ANXA4_BOVIN) |
| 5'-nucleotidase | NT5E | Q05927 (5NTD_BOVIN) |
| Actin, cytoplasmic 2 | ACTG1 | P63258 (ACTG_BOVIN) |
| Actin, cytoplasmic 1 | ACTB | P60712 (ACTB_BOVIN) |
| Actin, gamma-enteric smooth muscle | ACTG2 | Q5E9B5 (ACTH_BOVIN) |
| Fatty acid-binding protein, heart | FABP3 | P10790 (FABPH_BOVIN) |
| Rab GDP dissociation inhibitor beta | GDI2 | P50397 (GDIB_BOVIN) |
| Rab GDP dissociation inhibitor alpha | GDI1 | P21856 (GDIA_BOVIN) |
| Folate receptor alpha | FOLR1 | E1BJL8 (E1BJL8_BOVIN) |
| Folate receptor alpha | FOLR1 | P02702 (FOLR1_BOVIN) |
| Glycosylation-dependent cell adhesion molecule 1 | GLYCAM1 | P80195 (GLCM1_BOVIN) |

| | | |
|--|----------|-----------------------|
| Guanine nucleotide-binding protein G(I)/G(S)/G(T) subunit beta-1 | GNB1 | P62871 (GBB1_BOVIN) |
| Guanine nucleotide-binding protein G(I)/G(S)/G(T) subunit beta-2 | GNB2 | P11017 (GBB2_BOVIN) |
| CD9 antigen | CD9 | P30932 (CD9_BOVIN) |
| Elongation factor 2 | EEF2 | Q3SYU2 (EF2_BOVIN) |
| Ras-related protein Rab-11B | RAB11B | Q3MHP2 (RB11B_BOVIN) |
| Ras-related protein Rab-25 | RAB25 | Q58DW6 (RAB25_BOVIN) |
| Heat shock protein HSP 90-beta | HSP90AB1 | Q76LV1 (HS90B_BOVIN) |
| Heat shock protein HSP 90-alpha | HSP90AA1 | Q76LV2 (HS90A_BOVIN) |
| Ras-related C3 botulinum toxin substrate 1 | RAC1 | P62998 (RAC1_BOVIN) |
| Cell division control protein 42 homolog | CDC42 | Q2KJ93 (CDC42_BOVIN) |
| Ras homolog gene family, member G (Rho G) | RHOG | Q1RMI2 (Q1RMI2_BOVIN) |
| Cytoplasmic aconitate hydratase | ACO1 | Q0VCU1 (ACOC_BOVIN) |
| Mucin-1 | MUC1 | Q8WML4 (MUC1_BOVIN) |
| Elongation factor 1-alpha 1 | EEF1A1 | P68103 (EF1A1_BOVIN) |
| Monocyte differentiation antigen CD14 | CD14 | Q95122 (CD14_BOVIN) |
| Mannose 6 phosphate receptor binding protein 1 | M6PRBP1 | Q3SX32 (Q3SX32_BOVIN) |
| Uncharacterized protein (Fragment) | ATP13A4 | F1N272 (F1N272_BOVIN) |
| Membrane cofactor protein | CD46 | F1N4W5 (F1N4W5_BOVIN) |
| Uncharacterized protein | VAT1 | F1MUP9 (F1MUP9_BOVIN) |
| Alkaline phosphatase, tissue-nonspecific isozyme | ALPL | P09487 (PPBT_BOVIN) |
| Annexin A2 | ANXA2 | P04272 (ANXA2_BOVIN) |
| Uncharacterized protein | STXBP2 | F1MHC2 (F1MHC2_BOVIN) |
| 14-3-3 protein zeta/delta | YWHAZ | P63103 (1433Z_BOVIN) |
| 14-3-3 protein epsilon | YWHAE | P62261 (1433E_BOVIN) |
| 14-3-3 protein gamma | YWHAG | P68252 (1433G_BOVIN) |
| 14-3-3 protein beta/alpha | YWHAB | P68250 (1433B_BOVIN) |
| 14-3-3 protein theta | YWHAQ | Q3SZI4 (1433T_BOVIN) |
| 14-3-3 protein eta | YWHAH | P68509 (1433F_BOVIN) |
| Mucin-15 | MUC15 | Q8MI01 (MUC15_BOVIN) |
| Pyridoxal kinase | PDXK | Q0II59 (PDXK_BOVIN) |
| CD81 antigen | CD81 | Q3ZCD0 (CD81_BOVIN) |

| | | |
|---|----------|-----------------------|
| Tryptophan--tRNA ligase, cytoplasmic | WARS | P17248 (SYWC_BOVIN) |
| Pyruvate kinase | PKM2 | A5D984 (A5D984_BOVIN) |
| Transforming protein RhoA | RHOA | P61585 (RHOA_BOVIN) |
| Rho-related GTP-binding protein RhoC | RHOC | Q1RMJ6 (RHOC_BOVIN) |
| TKT protein | TKT | A5PJ79 (A5PJ79_BOVIN) |
| Peptidyl-prolyl cis-trans isomerase A | PPIA | P62935 (PPIA_BOVIN) |
| Guanine nucleotide-binding protein G(s) subunit alpha isoforms short | GNAS | P04896 (GNAS2_BOVIN) |
| Guanine nucleotide binding protein (G protein), alpha inhibiting activity polypeptide 3 | GNAI3 | Q3ZCA7 (Q3ZCA7_BOVIN) |
| Guanine nucleotide-binding protein G(i) subunit alpha-1 | GNAI1 | P63097 (GNAI1_BOVIN) |
| Guanine nucleotide-binding protein G(o) subunit alpha | GNAO1 | P08239 (GNAO_BOVIN) |
| GNAI2 protein | GNAI2 | A7MBH9 (A7MBH9_BOVIN) |
| Alpha-enolase | ENO1 | Q9XSJ4 (ENOA_BOVIN) |
| ENO2 protein | ENO2 | A6QR19 (A6QR19_BOVIN) |
| Unconventional myosin-Ic | MYO1C | Q27966 (MYO1C_BOVIN) |
| Rho GDP-dissociation inhibitor 1 | ARHGDI1 | P19803 (GDIR1_BOVIN) |
| UTP--glucose-1-phosphate uridylyltransferase | UGP2 | Q07130 (UGPA_BOVIN) |
| PP1201 protein | RECS1 | Q6QRN7 (Q6QRN7_BOVIN) |
| Fructose-bisphosphate aldolase | ALDOC | Q3ZBY4 (Q3ZBY4_BOVIN) |
| Fructose-bisphosphate aldolase | ALDOA | A6QLL8 (A6QLL8_BOVIN) |
| Uncharacterized protein | SLC7A4 | E1BCI3 (E1BCI3_BOVIN) |
| CD59 molecule, complement regulatory protein | CD59 | Q32PA1 (Q32PA1_BOVIN) |
| Glycerol-3-phosphate dehydrogenase [NAD(+)], cytoplasmic | GPD1 | Q5EA88 (GPDA_BOVIN) |
| GPD1L protein | GPD1L | A6QQR7 (A6QQR7_BOVIN) |
| Selenium-binding protein 1 | SELENBP1 | Q2KJ32 (SBP1_BOVIN) |
| ACSS2 protein | ACSS2 | A7YWF1 (A7YWF1_BOVIN) |
| Uncharacterized protein | SLC5A1 | F1MD24 (F1MD24_BOVIN) |
| L-lactate dehydrogenase B chain | LDHB | Q5E9B1 (LDHB_BOVIN) |
| Pituitary tumor-transforming 1 interacting protein | PTTG1IP | Q2KI48 (Q2KI48_BOVIN) |

| | | |
|---|---------|-----------------------|
| Polyubiquitin-B | UBB | P0CG53 (UBB_BOVIN) |
| Clathrin heavy chain 1 | CLTC | P49951 (CLH1_BOVIN) |
| NADH-cytochrome b5 reductase 3 | CYB5R3 | P07514 (NB5R3_BOVIN) |
| Glyceraldehyde-3-phosphate dehydrogenase | GAPDH | P10096 (G3P_BOVIN) |
| Toll-like receptor 2 | TLR2 | Q95LA9 (TLR2_BOVIN) |
| 6-phosphogluconate dehydrogenase, decarboxylating | PGD | Q3ZCI4 (Q3ZCI4_BOVIN) |
| Ras-related protein Rab-7a | RAB7A | F1MJQ1 (F1MJQ1_BOVIN) |
| STX3 protein | STX3 | A6QLH3 (A6QLH3_BOVIN) |
| Uncharacterized protein | TMC4 | E1BNW4 (E1BNW4_BOVIN) |
| Phosphoglycerate kinase 1 | PGK1 | Q3T0P6 (PGK1_BOVIN) |
| Tyrosine-protein phosphatase non-receptor type substrate 1 | SIRPA | G3X6M9 (G3X6M9_BOVIN) |
| Aldose 1-epimerase | GALM | Q5EA79 (GALM_BOVIN) |
| Phosphatidylethanolamine-binding protein 1 | PEBP1 | P13696 (PEBP1_BOVIN) |
| Solute carrier family 29 (Nucleoside transporters), member 1 (Fragment) | SLC29A1 | Q0V8K9 (Q0V8K9_BOVIN) |
| Annexin A7 | ANXA7 | P20072 (ANXA7_BOVIN) |
| Uncharacterized protein | DYNC1H1 | E1BDX8 (E1BDX8_BOVIN) |
| ADP-ribosylation factor 4 | ARF4 | Q3SZF2 (ARF4_BOVIN) |
| ADP-ribosylation factor 2 | ARF2 | P84081 (ARF2_BOVIN) |
| ADP-ribosylation factor 1 | ARF1 | P84080 (ARF1_BOVIN) |
| IST1 homolog | IST1 | F1MXJ5 (F1MXJ5_BOVIN) |
| Acyl-CoA synthetase long-chain family member 1 | ACSL1 | Q0VCZ8 (Q0VCZ8_BOVIN) |
| Ras-related protein Rap-1A | RAP1A | P62833 (RAP1A_BOVIN) |
| Phosphoserine aminotransferase | PSAT1 | A6QR28 (A6QR28_BOVIN) |
| Phosphoglycerate mutase 1 | PGAM1 | Q3SZ62 (PGAM1_BOVIN) |
| Basigin | BSG | Q3ZBX0 (Q3ZBX0_BOVIN) |
| Uncharacterized protein (Fragment) | BSPRY | F1MKU3 (F1MKU3_BOVIN) |
| Synaptobrevin homolog YKT6 | YKT6 | Q3T000 (YKT6_BOVIN) |
| Ethylmalonyl-CoA decarboxylase | ECHDC1 | Q2HJD5 (ECHD1_BOVIN) |
| Uncharacterized protein | GNAQ | E1BA29 (E1BA29_BOVIN) |
| Uncharacterized protein (Fragment) | GNAI3 | G5E6P3 (G5E6P3_BOVIN) |

| | | |
|---|---------|-----------------------|
| Guanine nucleotide-binding protein subunit alpha-11 | GNA11 | P38409 (GNA11_BOVIN) |
| Monocarboxylate transporter 1 | SLC16A1 | Q3MHW6 (MOT1_BOVIN) |
| Uncharacterized protein | SLC39A8 | E1BQ28 (E1BQ28_BOVIN) |
| Nucleoside diphosphate kinase B | NME2 | Q3T0Q4 (NDKB_BOVIN) |
| PCDHGA2 protein | PCDHGA2 | A5D7Q6 (A5D7Q6_BOVIN) |
| RAB2A, member RAS oncogene family | RAB2A | Q148J4 (Q148J4_BOVIN) |
| Uncharacterized protein | KRAS | E1BMX0 (E1BMX0_BOVIN) |
| SCAMP2 protein | SCAMP2 | A6QR35 (A6QR35_BOVIN) |
| CIDEA protein | CIDEA | A4FUX1 (A4FUX1_BOVIN) |
| Uncharacterized protein | TMC5 | F1MIU3 (F1MIU3_BOVIN) |
| Malate dehydrogenase, cytoplasmic | MDH1 | Q3T145 (MDHC_BOVIN) |
| CD82 protein | CD82 | A5D7E6 (A5D7E6_BOVIN) |
| Endoglin | ENG | Q1RMV1 (Q1RMV1_BOVIN) |
| Ras related v-ral simian leukemia viral oncogene homolog A (Fragment) | RALA | Q1JPH2 (Q1JPH2_BOVIN) |
| RALB protein | RALB | A5D977 (A5D977_BOVIN) |
| Uncharacterized protein (Fragment) | VPS4A | G3X8E2 (G3X8E2_BOVIN) |
| Vacuolar protein sorting-associated protein 4B | VPS4B | Q0VD48 (VPS4B_BOVIN) |
| Retinal dehydrogenase 1 | ALDH1A1 | P48644 (AL1A1_BOVIN) |
| G protein-coupled receptor, family C, group 5, member B | GPRC5B | Q1JPD9 (Q1JPD9_BOVIN) |
| Ras-related protein Rab-5C | RAB5C | Q58DS9 (RAB5C_BOVIN) |
| Ras-related protein Rab-5A | RAB5A | Q0IIG7 (RAB5A_BOVIN) |
| Uncharacterized protein (Fragment) | RAB5B | F1MNI4 (F1MNI4_BOVIN) |
| Glutathione S-transferase Mu 1 | GSTM1 | Q9N0V4 (GSTM1_BOVIN) |
| Glutathione S-transferase mu 3 (Brain) | GSTM3 | Q2KIV8 (Q2KIV8_BOVIN) |
| GSTM1 protein | GSTM1 | A4IFG0 (A4IFG0_BOVIN) |
| Chloride intracellular channel protein 4 | CLIC4 | Q9XSA7 (CLIC4_BOVIN) |
| Cytosol aminopeptidase | LAP3 | P00727 (AMPL_BOVIN) |
| Uncharacterized protein | MST4 | F1N5W5 (F1N5W5_BOVIN) |
| Purine nucleoside phosphorylase | PNP | P55859 (PNPH_BOVIN) |
| Tissue specific transplantation antigen P35B | TSTA3 | Q2KIT8 (Q2KIT8_BOVIN) |

| | | |
|---|---------|-----------------------|
| Alpha/beta hydrolase domain-containing protein 14B | ABHD14B | A7YY28 (ABHEB_BOVIN) |
| CD47 molecule | CD47 | Q08DW0 (Q08DW0_BOVIN) |
| Arachidonate 12-lipoxygenase, 12S-type | ALOX12 | P27479 (LOX12_BOVIN) |
| Uncharacterized protein (Fragment) | SLC15A2 | F1MPK7 (F1MPK7_BOVIN) |
| Staphylococcal nuclease domain-containing protein 1 | SND1 | Q863B3 (SND1_BOVIN) |
| Uncharacterized protein | NPEPPS | E1BP91 (E1BP91_BOVIN) |
| Cytosolic non-specific dipeptidase | CNDP2 | Q3ZC84 (CNDP2_BOVIN) |
| Uncharacterized protein | MPP5 | E1BIQ8 (E1BIQ8_BOVIN) |
| Uncharacterized protein | IQGAP1 | F1MC48 (F1MC48_BOVIN) |
| Uncharacterized protein | BROX | F1MU85 (F1MU85_BOVIN) |
| PDZ domain-containing protein GIPC2 | GIPC2 | Q1JQD4 (GIPC2_BOVIN) |
| G-protein coupled receptor family C group 5 member C | GPRC5C | Q2YDG0 (GPC5C_BOVIN) |
| Uncharacterized protein | EHD4 | E1BJV0 (E1BJV0_BOVIN) |
| Protein shisa-5 | SHISA5 | Q3T0A9 (SHSA5_BOVIN) |
| Peroxiredoxin-1 | PRDX1 | Q5E947 (PRDX1_BOVIN) |
| Glucose-6-phosphate isomerase | GPI | Q3ZBD7 (G6PI_BOVIN) |
| Ribonuclease/angiogenin inhibitor 1 | RNH1 | Q3SZN8 (Q3SZN8_BOVIN) |
| Cofilin-1 | CFL1 | Q5E9F7 (COF1_BOVIN) |
| Inorganic pyrophosphatase | PPA1 | P37980 (IPYR_BOVIN) |
| Glycerol-3-phosphate acyltransferase 4 | AGPAT6 | A3FPG8 (GPAT4_BOVIN) |
| Sterol-4-alpha-carboxylate 3-dehydrogenase, decarboxylating | NSDHL | Q3ZBE9 (NSDHL_BOVIN) |
| Uncharacterized protein | SLC3A2 | F1N2B5 (F1N2B5_BOVIN) |
| Alcohol dehydrogenase [NADP(+)] | AKR1A1 | Q3ZCJ2 (AK1A1_BOVIN) |
| FGR protein | FGR | A5PKG9 (A5PKG9_BOVIN) |
| Syntenin | SDCBP | A5D9B6 (A5D9B6_BOVIN) |
| Tubulin alpha-1B | | P81947 (TBA1B_BOVIN) |
| Syndecan-2 | SDC2 | Q58DD4 (SDC2_BOVIN) |
| Synaptosomal-associated protein | SNAP23 | Q2T9M8 (Q2T9M8_BOVIN) |
| Triosephosphate isomerase | TPI1 | Q5E956 (TPIS_BOVIN) |

| | | |
|---|----------|-----------------------|
| EXOC4 protein | EXOC4 | A6QLD1 (A6QLD1_BOVIN) |
| Uncharacterized protein | ADAM9 | F1MZJ5 (F1MZJ5_BOVIN) |
| Ubiquitin-like modifier-activating enzyme 1 | UBA1 | A3KMOV5 (UBA1_BOVIN) |
| Charged multivesicular body protein 1b | CHMP1B | Q5E994 (CHM1B_BOVIN) |
| Na(+)/H(+) exchange regulatory cofactor NHE-RF1 | SLC9A3R1 | Q3SZK8 (NHRF1_BOVIN) |
| Phospholipid scramblase 2 | PLSCR2 | Q3ZBG9 (PLS2_BOVIN) |
| Golgi phosphoprotein 3 (Coat-protein) | GOLPH3 | Q1RMW9 (Q1RMW9_BOVIN) |
| Tyrosine-protein kinase Lyn | Lyn | D4QGC1 (D4QGC1_BOVIN) |
| Protein lin-7 homolog C | LIN7C | Q0P5F3 (LIN7C_BOVIN) |
| TSG101 protein | TSG101 | A3KN51 (A3KN51_BOVIN) |
| Beta-centractin | ACTR1B | F2Z4F0 (F2Z4F0_BOVIN) |
| EXOC1 protein | EXOC1 | A6QQU0 (A6QQU0_BOVIN) |
| Serine--tRNA ligase, cytoplasmic | SARS | Q9GMB8 (SYSC_BOVIN) |
| Excitatory amino acid transporter 3 | SLC1A1 | Q95135 (EAA3_BOVIN) |
| Calcium-binding protein 39 | CAB39 | Q29RI6 (CAB39_BOVIN) |
| Protein DJ-1 | PARK7 | Q5E946 (PARK7_BOVIN) |
| Chromatin modifying protein 2A | CHMP2A | Q3T0U5 (Q3T0U5_BOVIN) |
| Leucine-rich repeat-containing protein 8C | LRRC8C | A5PK13 (LRC8C_BOVIN) |
| GTP-binding protein Rheb | RHEB | Q56JV3 (RHEB_BOVIN) |
| Serine/threonine-protein phosphatase 2A 65 kDa regulatory subunit A alpha isoform | PPP2R1A | Q32PI5 (2AAA_BOVIN) |
| CD63 antigen | CD63 | Q9XSK2 (CD63_BOVIN) |

Figure S3. Whole proteome profiling of the bovine milk-derived EVs with LC-MS/MS.

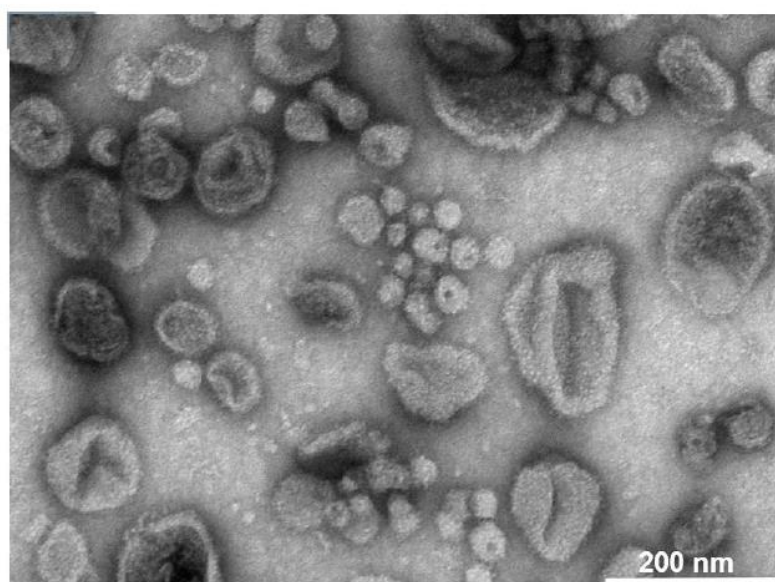
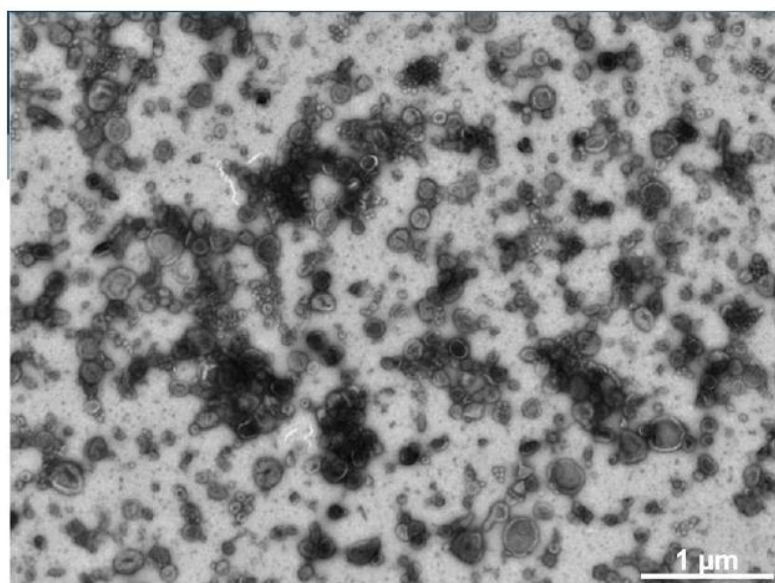
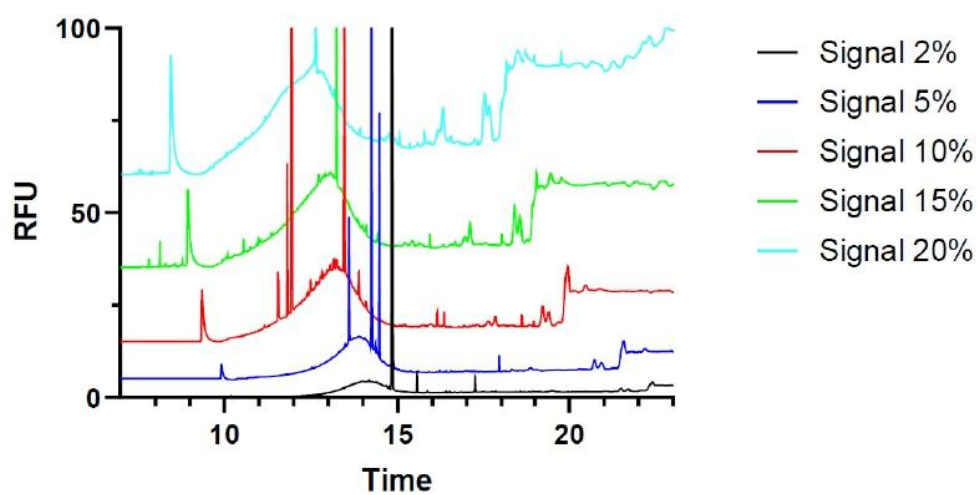
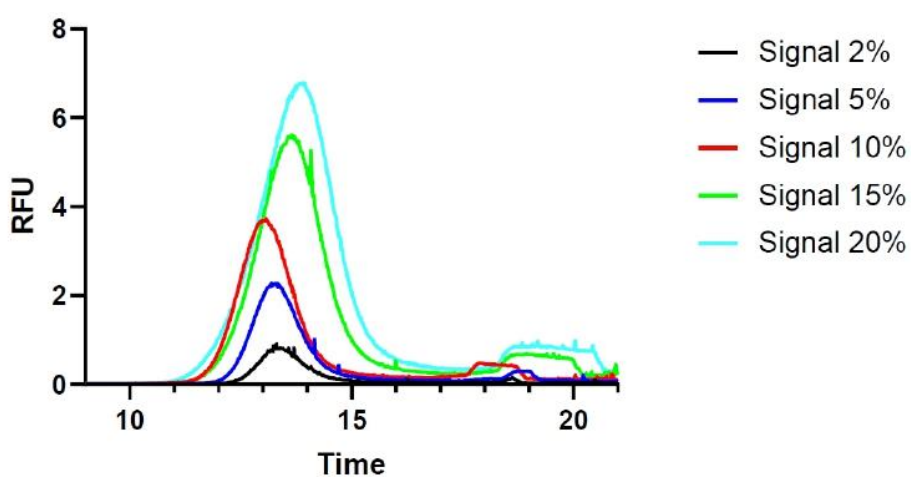


Figure S4. Transmission Electron Microscopy with negative staining by uranyl acetate of bovine milk derived EVs.



A)



B)

Figure S5. Electropherograms for injection of different EVs sample volumes (from 2 % to 20 % of the total capillary volume). A) EVs samples right after fluorescent labeling (labelled EVs in PBS matrix); B) EVs samples after buffer substitution (labelled EVs in Tris/Ches 90 mM matrix). CE conditions as in Fig. 1.

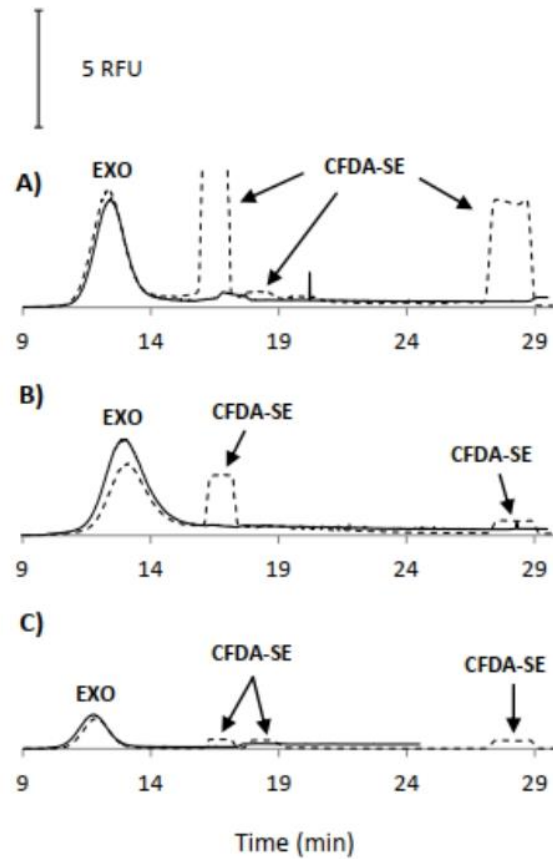


Figure S6. Electropherograms for CE-LIF of fluorescently labeled bovine milk-derived EVs after matrix substitution with Exosome Spin Column (MW 3000). EV recovery in 90 mM Tris / CHES at pH 8.4. Labelling was performed in A) PBS (pH 7.4); B) sodium bicarbonate-carbonate (pH 9); C) ammonium hydroxide (pH 7). Continuous line electropherograms were recorded immediately after matrix removal, whereas in dotted line, one day after. Other CE conditions as described in Fig. 1. The adjustment to more neutral pH reduced the hydrolysis of EVs due to alkaline pH and helped preserve samples for the longest possible time.

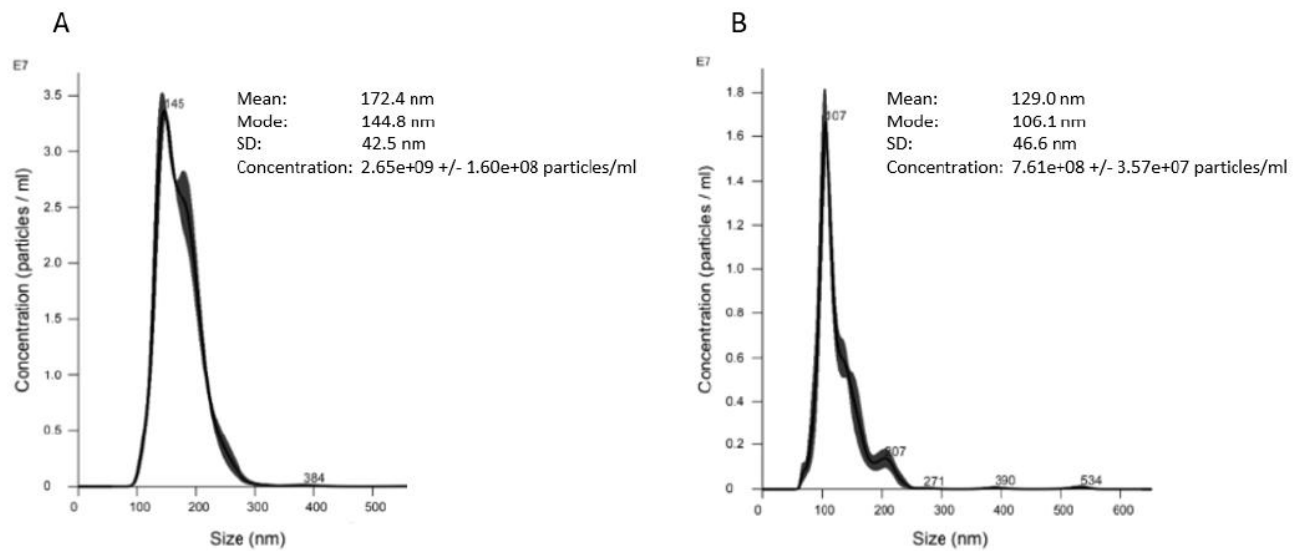


Figure S7. NTA profiles for EVs isolated with affinity monolithic disks. EV elution from monolithic disks under alkaline condition (pH 11.3) was performed with ammonium hydroxide. Monolithic disks were immobilized with (A) anti-human CD61 and (B) anti-human CD9. Dilution factor was 1:100 for the CD61+ EVs and 1:1000 for the CD9+ EVs. NTA histograms represent the mean of three replicate measurements of the same sample and SD in grey.

IV.5. Development of in-line electrokinetic preconcentration prior to CE-LIF separation of EVs

In comparison to the CE-UV methods recently developed for the electrophoretic profile of EVs [252, 255], our proposed CE-LIF approach provided superior detection limits. However, improved detection limits are still needed when dealing with low concentrated EVs samples. This section therefore focuses on our efforts to develop in-capillary, online, and automated electrokinetic preconcentration of EVs. In-line electrokinetic preconcentration of analytes is based on variations in the analyte migration velocity across discontinuous solution/electrolyte interfaces that are created inside the capillary. As a result, the analytes dissolved in a sample matrix distinct from the BGE are accumulated (stacked) at the boundary of the two solutions, resulting in electrokinetic preconcentration of target analytes. Numerous in-line preconcentration approaches have been developed to date, notably large volume sample stacking (LVSS), isotachopheresis (ITP), Field amplified sample stacking (FASS), field-amplified sample injection (FASI) and dynamic pH-junction [282, 283]. However, special attention should be given to EVs when considering the appropriate preconcentration strategies due to their possible instability. We have indeed to preserve their integrity and avoid any agglomeration/aggregation or lysis of EVs during the preconcentration process under high electric fields. Furthermore, for some of these methodologies to be applied to EVs, a deeper understanding is necessary. For example, ITP concentrates the sample between a leading electrolyte (LE) and the terminating electrolyte (TE), which have higher and lower mobility, respectively. However, predicting the precise electrophoretic mobility of migrating EVs at the stacking zone is challenging. Dynamic pH-junction, which operates when an analyte's ionisation state changes when it is moved to a different pH zone in the capillary, necessitates a thorough investigation of the surface charge of EVs as pH varies. Furthermore, a sudden rise or decrease in pH might affect the stability of the EV membrane. While electrokinetic preconcentration of NPs have been reported [284], this approach has never been applied to EVs which are more challenging and fragile entities than NPs. As field-amplified stacking and LVSS approaches were already successfully applied for NPs [284], we first explored electrokinetic preconcentration of EVs using these two strategies. Field-amplified stacking methods (FASS, FASI) rely on the utilization of samples prepared in a matrix (e.g, water or diluted BGE) having lower ionic strengths (thus lower conductivity) than that of the BGE. Due to the inverse relationship between the electric field (E) and conductivity (σ) ($\sigma = \frac{J}{E}$ where J is the magnitude of the current density), and considering Eq. 3 from the introduction of this chapter ($v = \mu \times E$), analytes move quicker inside the sample zone where the electric field is

greater and are slowed down when they approach the sample/BGE interface. A decrease in buffer conductivity may be accomplished by lowering the ionic strength ($IS = 1/2 \sum_i c_i z_i^2$ where z_i is the valence of ion i and c_i is the concentration). Our preliminary tests with FASS of EVs did not lead to significant signal improvement (article 3, paragraph 3.3 in the publication). Indeed, we demonstrated the need of maintaining physiological and isotonic conditions during electrokinetic preconcentration (FASS) and separation in order to minimize EV lysis and aggregation/collision. Such conditions are nevertheless not favourable EVs stacking preconcentration.

We then diverted our effort to develop an in-line preconcentration technique based on larger sample volume injection (LVSS). In general, in CZE, the injected sample volume should not exceed 1 to 3 % of the capillary volume in order to obtain a good separation efficiency. During the method development for CE-LIF of EVs, we indeed employed large sample volume injection (10% of total capillary volume) to boost the sensitivity of EVs detection (paper 3, paragraph 3.2). We then explored further this direction with single and multiple cycles of LVSS and provide here our pioneering results in the LVSS preconcentration of EVs.

IV.5.1. Large volume sample stacking (LVSS) with polarity switching of EVs

First, we chose to test the LVSS approach, which allows for the injection of very large sample volumes, up to 100 % of the capillary volume when the electrophoretic mobility of the analytes is opposed to the EOF [283], which is the case in the CZE-LIF method that we developed (Figure 29). The capillary is filled with a large volume of sample having a low conductivity and then voltage is applied so that the elevated EOF in the sample zone is directed towards the injection side of the capillary, which will drive the sample matrix out of the capillary. At the same time, the difference in conductivity between the sample matrix and the BGE will induce an enrichment of analytes at the boundary of the two media, as in FASS. During this step, the current increases as the sample matrix is gradually replaced by the BGE and the analytes are pushed towards the entrance of the capillary. When almost all the sample matrix is removed from the capillary, i.e. when the current intensity is between 90% and 95% of the maximum intensity obtained for a capillary filled with 100 % BGE, the voltage is reversed and the classical separation method is then applied.

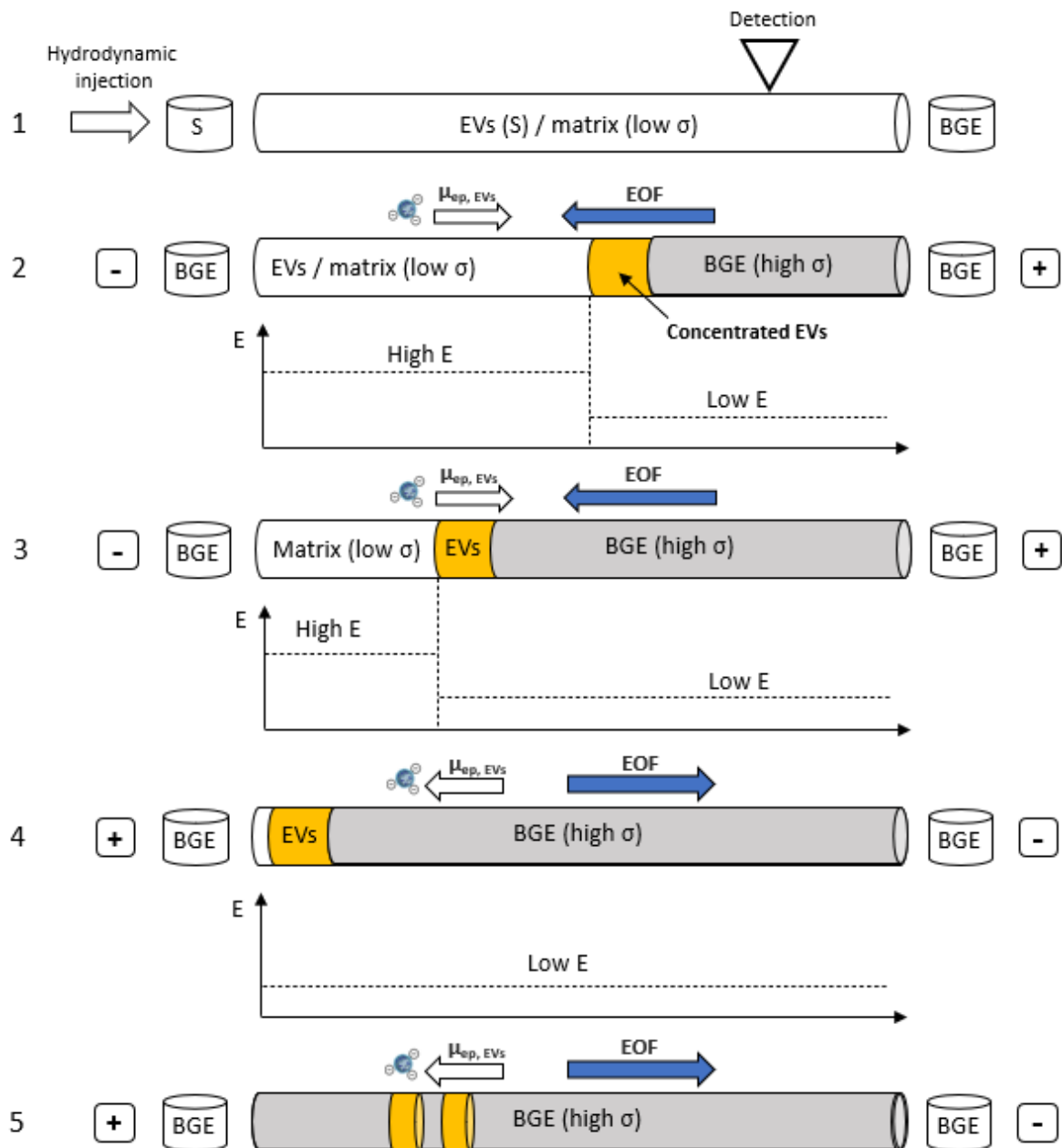


Figure 29: Principle of preconcentration by LVSS in a silica capillary (in the presence of EOF) for EVs. 1. Hydrodynamic injection of a very large sample volume (100%) with low conductivity. 2. Application of a voltage (25 kV) and creation of a discontinuous electric field in the capillary with accumulation of EVs at the sample/BGE boundary. The generated EOF begins to eliminate the matrix 3. Elimination of almost all of the matrix 4. Reversal of polarity. 5. Conventional separation by CZE.

In this study, the LVSS procedure was applied to a sample of bovine milk-derived EVs previously purified by Excilone and considered here as a standard. Details for EVs analysis can be seen in our previous article 3 (paragraphs 2.3.4, 2.3.5, 2.3.6). Briefly, fluorescently labelled EVs were prepared using the 5-(and-6)-Carboxyfluorescein diacetate succinimidyl ester (CFDA-SE). Commercial Exosome

Spin Columns (MW 3000) (Thermo Fisher Scientific) were used here both for removal of residual CFDA-SE and for matrix substitution in different low conductivity solutions. Labelled EVs were analyzed in a fused silica capillary having ID of 50 μm , effective length (L_{eff}) of 50.2 cm and total length (L_{tot}) of 60.2 cm. Our first test was realized with fluorescently labelled EVs substituted in Tris/CHES (IS 5 mM, pH 8.4) with low conductivity, and ISF-BGE composed of Tris/CHES (IS 140 mM, pH 8.4) with a 28 times higher conductivity. As shown in Figure 30 we observed insufficient EV stacking, as well as appearance of multiple spikes that were attributed to EVs aggregation/collision during electrophoresis.

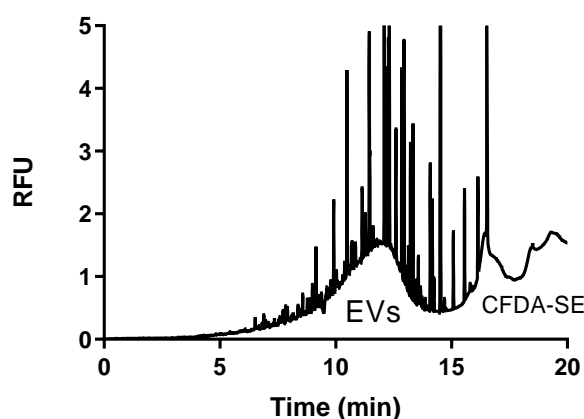


Figure 30: LVSS-CE-LIF of fluorescently labelled EVs after matrix substitution in Tris/CHES 5 mM, using ISF BGE Tris/CHES (IS 140 mM, pH 8.4) for both preconcentration and CZE steps. Other CE conditions: uncoated fused silica capillary with I.D. of 50 μm , effective length (L_{eff}) of 50.2 cm and total length (L_{tot}) of 60.2 cm; Applied voltage: 25 kV; LIF detection λ_{ex} 488 nm, λ_{em} 520 nm.

As a reminder, the EOF is considerably influenced by the counter ions in the buffer electrolyte, since the ionic strength of the counter ions affects the zeta potential (see Eq. 1, subchapter IV.2.1. of this chapter). As a result, when working with low IS sample matrix, the local generated EOF is high, and this is required to achieve preconcentration. But at the same time lysis of EVs may occurred due to the too low ionic strengths (lower than isotonic conditions). This may be the origin of unwanted spikes induced by EVs lysis, and thus poor EVs signal in Fig. 30. Then, sample matrices composed of Tris/CHES at higher IS (up to 50 mM) were also examined, but unsatisfactory data were obtained (data not shown). On the other hand, the BGE employed (Tris/CHES, IS 140 mM, pH 8.4), which may be advantageous in producing high IS without generating high current as previously showed in our paper 2 (see subchapter IV.3. of this chapter) cannot be used to generate a high enough EOF required to implement successfully LVSS. Indeed, the high concentrations of the large weakly charged molecules constituting the BGE led to significant reduction of EOF. As a consequence, Fig. 30 shows that the EVs' peaks are still wide and

that the longer the EVs are exposed to high voltages, the more the spikes on the EVs' peaks may be seen, reflected by more spikes observed on the second half of EVs peak. In an effort to address these challenges, we tested two strategies: i) the addition of sugars to the sample matrix (i.e., diluted BGE to maintain a low ionic strength required to generate a high EOF magnitude) with the goal of stabilizing the EVs without incurring high conductivity of the sample zone; and ii) the use of the optimized ISF BGE Tris / CHES (IS 90 mM, pH 8.4) for both preconcentration and CZE steps which was demonstrated in our paper 3 to achieve a higher EOF while maintaining a sufficient resolution between the EVs and the CFSE fluorophore. A combination of sucrose and dextrose was recently demonstrated to maintain the osmolarity and physiological condition in a microdevice to capture EVs across a porous dialysis membrane under application of electric field [285]. From this rationality, such composition was tested for our LVSS study. Thus, with the use of commercial Exosome Spin Columns, the EVs were resuspended in Tris / CHES 5 mM with the addition of i) sucrose (30 mM) in combination with dextrose (145 mM); ii) mannose (from 100 to 200 mM) and iii) trehalose (from 25 to 200 mM). As can be seen in Fig. 31A for preliminary test in this direction using the combination of sucrose and dextrose EVs peak was still broad, but in turn provokes much less spike-reflected aggregation. Fig. 31B shows the results obtained using a mannose concentration of 100 and 200 mM. Also here, less spike-reflected aggregation was observed but EV peak was still broad. A concentration of 200 mM was found to slow down the rate of EVs lysis probably thanks to the sugar concentrations being closer to isotonic conditions, resulting in a higher signal for EVs comparing to that obtained with 100 mM of mannose. We then extended our study with the addition of trehalose (consisting of two molecules of glucose) since it has been shown to minimize EV aggregation and maintain EV integrity throughout freezing and thawing [286]. As clearly seen in Fig. 31C, the EVs signal increased significantly with much less spikes when the trehalose concentration was increased from 25 to 200 mM. The best signal for EVs was obtained using a sample matrix comprised of Tris/CHES IS 5 mM and trehalose 200 mM and the BGE composed of Tris/CHES (IS 90 mM, pH 8.4). Peak intensity was increased in comparison to our previously published CZE-LIF approach that did not include a preconcentration phase (see the dashed electropherogram in Fig. 31C). In terms of peak heights, trehalose enhanced the EVs signal by nearly 7-fold, and the enhancement was only 2-fold using sucrose/dextrose or mannose. Thus, trehalose proved to be the best likely owing to its better ability to maintain sufficient repulsion by shielding attractive interactions between vesicles [286]. Note also that when using the optimised sample matrix containing trehalose, the EVs peak obtained was still much broader than that obtained with CE-LIF of EVs without the preconcentration. This may be due to residual trehalose that may increase buffer viscosity, impairing the high EOF mobility required to assure baseline separation of enriched EVs.

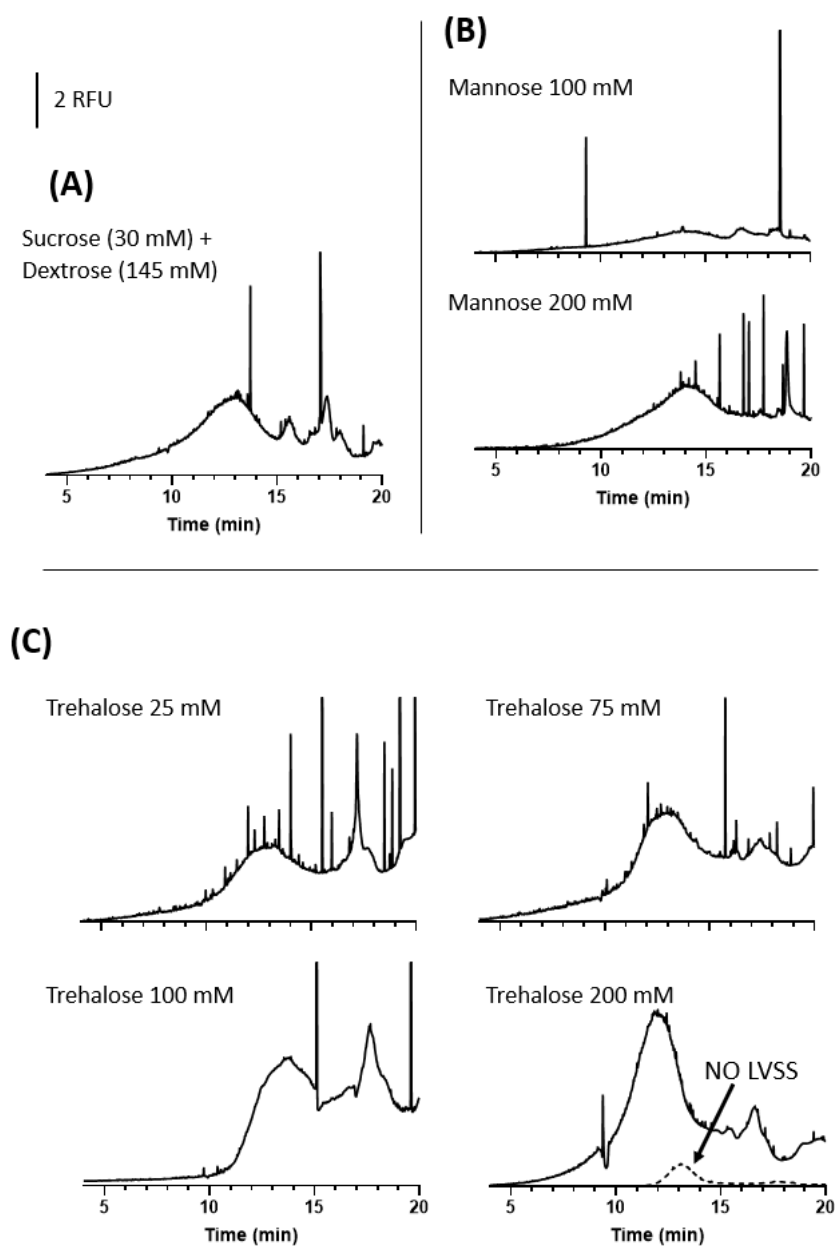


Figure 31: LVSS-CE-LIF of fluorescently labelled EVs after matrix substitution in Tris/CHES 5 mM in combination with (A) sucrose (30 mM) + dextrose (145 mM); (B) mannose at 100 mM and 200 mM; (C) trehalose at 25 mM, 75 mM, 100 mM and 200 mM, using ISF BGE Tris/CHES (IS 90 mM, pH 8.4) for both preconcentration and CZE steps. The dashed lines represent CE-LIF of fluorescently labelled EVs (see conditions in paper 3). Other CE conditions as described in Fig. 26.

IV.2. Online Preconcentration in Capillaries by Multiple LVSS of EVs

Following a single LVSS, the approach was extended to multiple cycles of electrokinetic preconcentration as shown in figure 32, in order to further increase detection sensitivity, as inspired by a similar approach previously described by our group [287]. This protocol, which relies on repeated

cycles of injection of very large sample volumes for analyte stacking and matrix removal using an EOF directed to the inlet capillary, was investigated to enable in-capillary enrichment and separation of EVs from unlimited sample volumes. For multiple LVSS, we performed the same process for LVSS for the first injection (100 % of total capillary volume) and the applied voltage was kept the same (25 kV). In this case, when almost all the sample matrix is removed from the capillary, unlike classic LVSS, a second sample injection is carried out, followed by another step of matrix sample removal using an EOF toward the inlet capillary. These steps in theory may be repeated several times (cycles) for further preconcentration of freshly injected EVs during each cycle. As for classic LVSS, multiple LVSS procedure was applied to a sample of fluorescently bovine milk-derived EVs resuspended in Tris/CHES 5 mM and trehalose 200 mM. ISF BGE Tris/CHES (IS 90 mM, pH 8.4) was used for all preconcentration cycles and CZE steps. Labelled EVs were analyzed in a fused silica capillary having ID of 50 μm , effective length (L_{eff}) of 50.2 cm and total length (L_{tot}) of 60.2 cm.

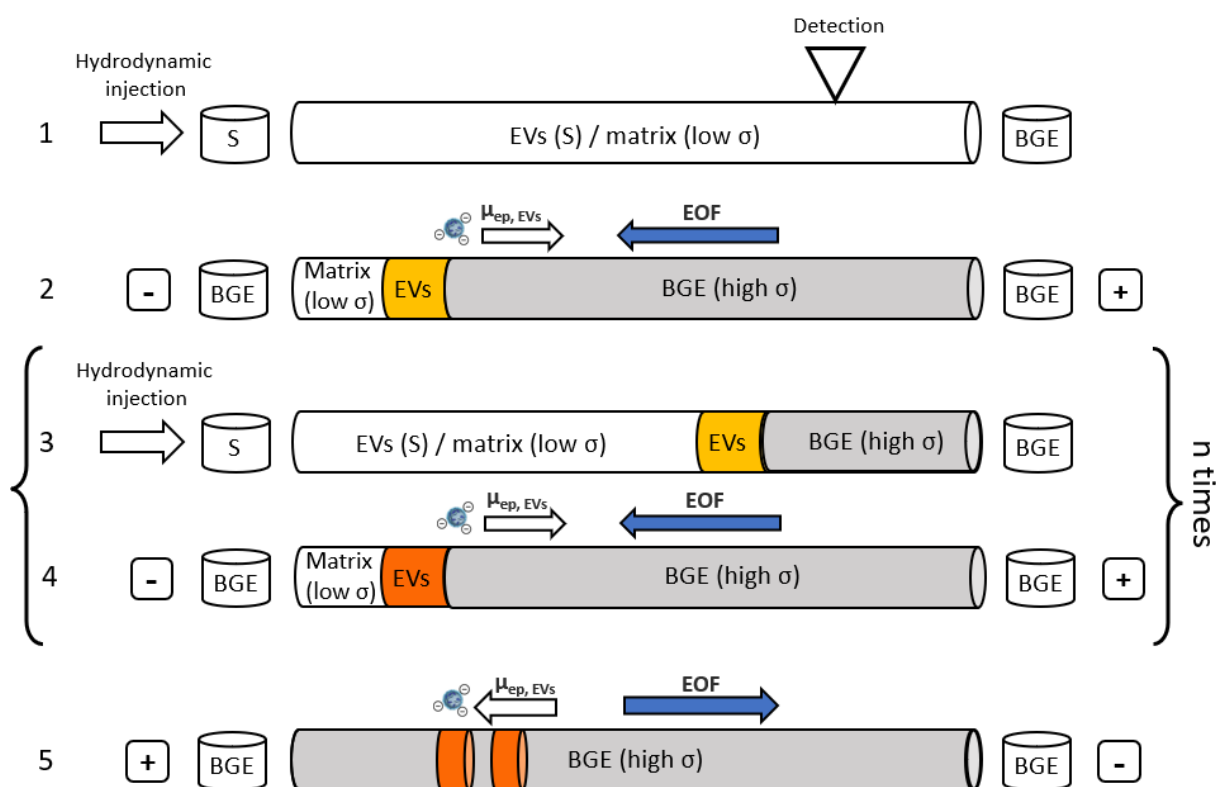


Figure 32: Schematic principle of a multiple LVSS for EVs. (1) Sample injection equivalent to 100% of the capillary volume, (2) application of pre-concentration potential (reverse polarity), (3) Second hydrodynamic injection, (4) Second process of pre-concentration, (5) Separation and detection of EVs. Steps 3 and 4 may be repeated several times (cycles) for further pre-concentration of freshly injected EVs during each cycle. Other CE conditions: uncoated fused silica capillary with I.D. of 50 μm , effective length (L_{eff}) of 50.2 cm and total length (L_{tot}) of 60.2 cm; Applied voltage: 25 kV; LIF detection λ_{ex} 488 nm, λ_{em} 520 nm.

Results obtained after 3 cycles are shown in figure 33A. After filling 100% of the capillary and preconcentration in the first cycle, the second injection was carried out with the sample filled to 90% of the capillary. After the second round of preconcentration, a third injection with 50% of the capillary volume and preconcentration were performed before CZE separation. The observed signals, however, did not correspond to the expected total sample plug concentration.

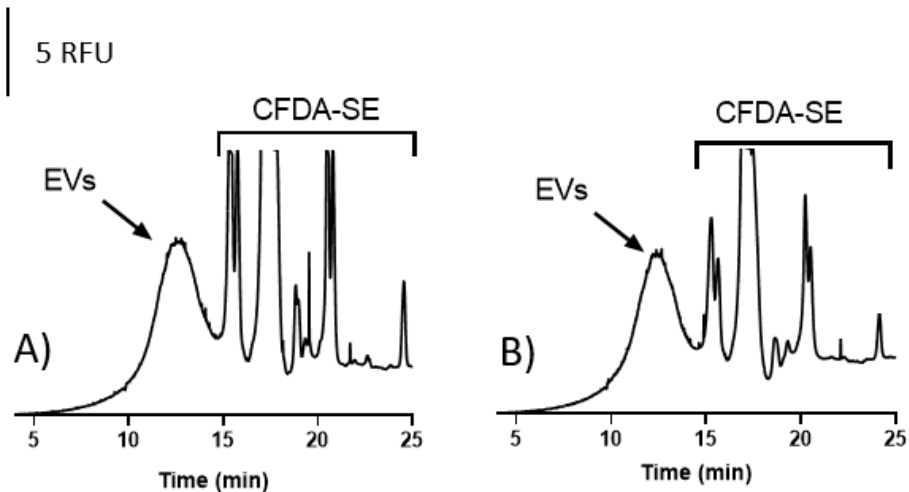


Figure 33: Multiple LVSS-CE-LIF of fluorescently labelled EVs after matrix substitution in Tris/CHES 5 mM and trehalose 200 mM. For the first injection, the capillary is totally filled with the sample. For the subsequent cycles, (A) 90% and 50% of sample are injected for second and third cycles respectively. (B) 50% of sample is injected for second cycle of preconcentration. ISF BGE Tris/CHES (IS 90 mM, pH 8.4) for both preconcentration and CE steps. CFDA-SE indicate the region of migration of the dye. Other CE conditions as described in Fig. 28.

The obtained results indicates that the detection sensitivity was comparable to that of a single LVSS. This may be attributed to sample loss caused by the repetition of cycles. Indeed, it is possible that during the preconcentration step, i.e. the reverse polarity is applied when the current intensity reaches 90-95 % of its maximum value obtained when the capillary is completely filled with buffer (namely 21 μ A), part of the EVs inside the capillary are not fully preconcentrated at the capillary inlet due to their lower μ_{ep} . Moreover, the profile obtained shows a loss of resolution between the peaks of the EVs and excess fluorophore (CFDA-SE). To better understand this observation, a second test was conducted using just two cycles. We performed a sample injection, filling 100% of the capillary and applied the process of LVSS. Then a second injection of the sample but this time of 50% of the capillary volume was applied and the same process of preconcentration was done before CZE separation. However, as can be seen in Fig. 33B, there was no difference between a 2 or a 3 cycle LVSS preconcentration in

term of signal intensity for the EVs peak. This confirmed our observation that a portion of the sample is stacked from the second cycle of preconcentration.

A loss of resolution was noted once again. When using the optimised sample matrix containing trehalose, the EVs peak obtained was still much broader than that obtained with CE-LIF of EVs without the preconcentration. This loss of resolution is most likely caused by the existence of a rather significant electroosmotic flow (EOF) ($2 \times 10^{-4} \text{ cm}^2 \cdot \text{V}^{-1} \cdot \text{s}^{-1}$), during electrophoresis, which requires manual switching of polarity to trigger the electrophoretic separation of enriched EVs. This resolution lost is expected to alleviate if EOF can be quasi-totally suppressed to allow EVs to electrokinetically migrate against the EOF, thus does not require polarity switching between the LVSS and CE separation steps. Furthermore, the presence of a significant amount of free fluorescent dye (CFDA-SE) was indicated in these studies by the reappearance of fluorophore signals in the electropherograms as a consequence of sample degradation over time. Indeed, this behaviour was already documented in our Paper 3. As a result, for the moment unsatisfactory results were obtained with our preliminary tests on EVs electrokinetic preconcentration with LVSS.

IV.3. Concluding remarks

Among current CE methods for EV electrophoretic profiles, our CE-LIF approach has the best limit of detection to date (around 10^{10} EVs/mL). Efforts were made to improve the sensitivity of EVs detection via development of a forefront in-line electrokinetic preconcentration step. However, all the electrokinetic methods for in-capillary preconcentration that we developed have not yet overcome the hurdles encountered when working with EVs. Indeed, as previously noted, finding a compromise between high performance EVs stacking (via an EVs sample matrix with a conductivity significantly lower than that of the BGE), and avoidance of EVs lysis under such extreme conditions (low or high conductivities) remains a difficult requirement. We have to keep in mind that if low conductivities can destroy the EVs, high conductivity media can induce joule heating during electrophoresis that leads to damage of EVs as well. From this rationality, capillary isoelectric focusing (cIEF, for separation of target analytes into bands along a pH gradient in a capillary induced by an electric field in the presence of ampholytes) is expected to be a more compatible separation and preconcentration approach for EVs. Exploration of cIEF for EVs enrichment and separation is envisioned in the next phase of the project. Furthermore, other principles might be investigated, notably ITP that concentrates the sample between a leading electrolyte (LE) and the terminating electrolyte (TE), which have higher and lower

mobility, respectively. However, predicting the precise electrophoretic mobility of migrating EVs at the stacking zone might be challenging.

IV.6. Size-based characterization of EVs by Taylor Dispersion Analysis (TDA)

It is generally established that EVs are highly heterogeneous in size, but it is difficult to distinguish between true heterogeneity and that caused by impurities, aggregated or debris of EVs, and this is strongly related to their isolation mode, which is addressed in the second chapter of the thesis, but also to the characterization methods. Most EVs have a diameter of 100 nm or more, but exosomes are considered to have a smaller size between 30 and 100 nm. Nevertheless, the top size limit of EVs is still unknown [288]. As previously indicated in Chapter II.2. of this thesis, employing DLS and NTA to determine the distribution of EVs is a common method. While these methods are simple to apply, the results may be deceptive, since NTA and DLS are very sensitive to the presence of aggregates. Furthermore NTA can hardly detect particles of sizes smaller than 50 nm. Other methods like electron microscopy, flow cytometry, and atomic force microscopy should be used to verify the data obtained by these systems.

TDA is an absolute and simple separative technique based on dispersion for calculating the diffusion coefficient (or hydrodynamic radius) from the peak dispersion observed in an open tube under Poiseuille laminar flow conditions [289]. The diffusion coefficients of a broad range of structures, including viruses and NPs, have been determined using TDA [276, 290-293]. However, determining the mean collective diffusion coefficients (and mean hydrodynamic radii) of EVs has never been explored previously. Based on this logic, this technique, which can be implemented on a CE apparatus, is particularly compatible with our aim to build a micro platform for the separation and analysis of EVs. Indeed, following the isolation of the EVs via the droplet system module, that will be described in the following chapter, this technique could represent a characterization module to be coupled either directly to the isolation module (Droplet-TDA) or on-line to the CZE method (Droplet-CZE-TDA). We have indeed seen that the CZE method is currently limited for the size elucidation of the separated subpopulations. The TDA-CZE hyphenation would allow the determination of the diffusion coefficient (or hydrodynamic radius) of each EV zone previously separated by CZE. Furthermore, the amount of sample solution required with TDA is substantially small (2 μL for TDA versus 1 mL for DLS/NTA), which represents an advantage for sample volumes of EVs generated by the droplet platform (only some μL range).

In this section the principle of TDA will be given, followed by preliminary experiments to explore, for the first time, TDA combined with UV and LIF detection to estimate the size of standard EVs. A

comparison of data obtained for different EVs sources to NTA results is also performed and discussed. TDA experiments were carried out in collaboration with Hervé Cottet and Joseph Chamieh (Institut des Biomolécules Max Mousseron, Montpellier).

IV.6.1. Principle of Taylor Dispersion Analysis (TDA)

The source for the theoretical portion of this part regarding the TDA is Lucie Labied's doctoral thesis, publicly defended on 17/12/2021 (<http://www.theses.fr/s218954>). Recently, Moser and Baker also provided an intriguing instructional tutorial review of TDA, aimed to help analytical chemists and separation scientists better understand and use this sizing approach [294].

Taylor dispersion is a phenomenon initially reported by Sir Geoffrey Taylor in 1953 [289, 295, 296]. It refers to the dispersion that occurs when a molecule is exposed to laminar flow in a tube with little diffusion along the tube. Its principle is shown schematically in figure 34. The velocity profile of laminar flow in a circular section tube is parabolic (represented by blue arrows). The fluid's speed is the strongest in the middle of the tube and almost null towards the walls. When a sample is injected by pressure, the species in the middle of the tube move faster than the species at the walls, resulting in the formation of a concentration gradient.

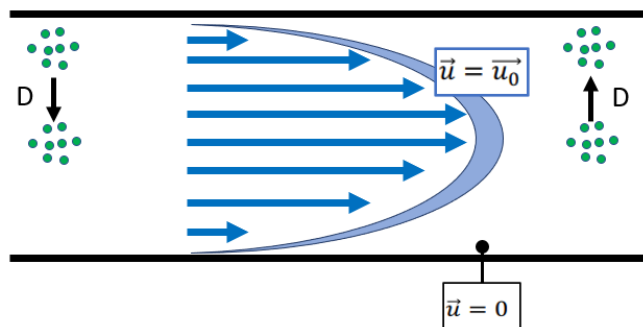


Figure 34 : Principle of Taylor dispersion analysis in cylindrical microchannel with parabolic flow profile. The distribution D moves at velocity u between the center of the capillary and the walls. u_0 is the mean fluid velocity defined as the fluid velocity averaged over the cross section of the capillary.

Taylor dispersion analysis is valid if the axial diffusion can be neglected [296]. The Péclet number (Pe), which describes the relative rates of mass transfer along the axis of the capillary due to convection and diffusion [291, 297], must be chosen such that [298]:

$$Pe = \frac{uR_c}{D} \geq 40 \quad (9)$$

where u is the linear velocity of the fluid, R_c is the capillary radius, D is the molecular diffusion coefficient. The dimensionless diffusion time τ , defined as the ratio of the mean solute residence time to the time necessary for a solute to diffuse over a distance equal to the capillary's radius [291, 297], must be chosen in such a way that [298]:

$$\tau = \frac{D t_0}{R_c^2} \geq 1.25 \quad (10)$$

where t_0 is the residence time of the peak in the capillary.

Only radial diffusion occurs under these circumstances and relative error on the determination of D is lower than 3% [298]. The species in the capillary's core disperse towards the walls, where their speed decreases. Similarly, species near the walls disperse and accelerate towards the centre. These diffusion phenomena cause the speed of the species in solution to be distributed around the mean speed. The signal detected at the output of the capillary (typically at the detection window of one capillary when using a CE instrument) as a function of time can then be assimilated to a Gaussian peak and is called taylorgram. A schematic representation is given in figure 35. Small molecules diffuse rapidly, resulting in a small deviation around the average speed, and therefore t_0 . The detected peak is then thin. In contrast, the diffusion of a bigger analyte, such as a protein or NP, is slower, thus the observed peak is wide.

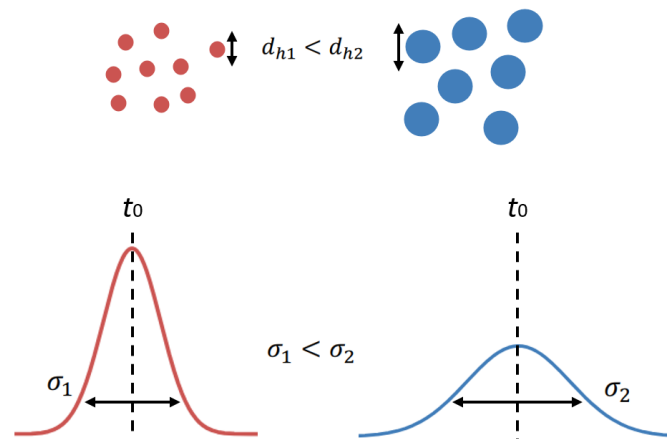


Figure 35: Schematic form of a taylorgram according to the size of the species detected. d_h indicates hydrodynamic diameter, σ the temporal variance of the peak and t_0 the average residence time peak.

The peak of a taylorgram for a solution containing a molecule with a diffusion coefficient D can be modelled by a Gaussian:

$$S(t) = y_0 + \frac{A}{\sigma\sqrt{2\pi}} \exp\left(-\frac{1}{2} \frac{(t - t_0)^2}{\sigma^2}\right) \quad (11)$$

where S is the signal as a function of the analysis time t , y_0 the baseline, A the area of the peak, which depends on the detection and the concentration, σ the temporal variance of the peak, t_0 the average residence time peak.

The molecular diffusion coefficient D may thus be represented as a function of the Gaussian parameters t_0 using the following equation:

$$D = \frac{R_c^2 t_0}{24\sigma^2} \quad (12)$$

IV.6.2. From diffusion to size determination: experimental considerations

TDA was originally proposed as a method for determining the diffusion coefficients of small molecules, however the Stokes-Einstein equation allows for a direct relationship between D and the size of a given spherical analyte present in a diluted sample:

$$D = \frac{k_B T}{6\pi\eta R_h} \quad (13)$$

where k_B is Boltzmann constant, T the temperature, η the fluid's viscosity, R_h the hydrodynamic radius.

The hydrodynamic radius is defined as the radius of a theoretical sphere with the same diffusion coefficient as the object under consideration (molecule, NP, protein, etc.).

In the 50's and 60's, analytical tools did not meet the criteria of validity to study analytes or objects bigger than molecules. However, thanks to improvements in capillary tube fabrication and in instrumentation, the validity conditions of equations (9) and (10) could be met for macromolecules, particles or assemblies with smaller diffusion coefficients, and thus bigger objects. Nowadays, TDA may be set up simply on a commercial CE device equipped with UV-vis detection by applying pressure to the capillary's inlet instead of applying an electric field.

The experimental limits of TDA have been explored and deepened by the work of Chamieh et al. [299]. For a given hydrodynamic radius R_h , the authors summarized the conditions of equations (9 and 10) in a unique inequality that relies solely on the applied pressure and capillary dimensions:

$$\frac{17k_B T L_c}{R_h R_c^3} \geq \Delta P \geq \frac{0.34k_B T L_d L_c}{R_h R_c^4} \quad (14)$$

where L_c is the total length of the capillary and L_d the capillary length to the detector, ΔP the mobilization pressure, R_c is the capillary radius and R_h the hydrodynamic radius.

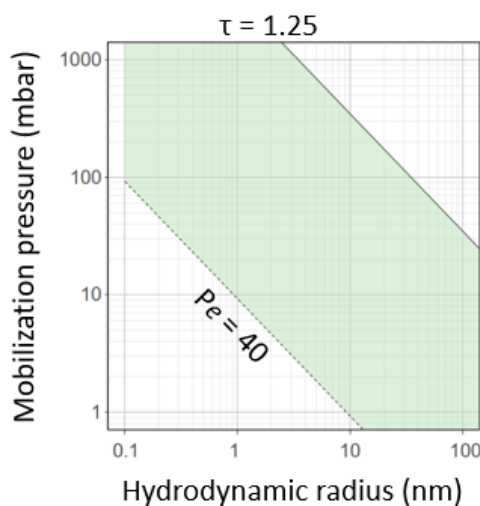


Figure 36: Representation of the experimental parameters adapted to a capillary with an internal diameter of 75 μm and a length of 70 cm. The area coloured in green represents the theoretically measurable hydrodynamic radii for a given mobilization pressure. From Labied's thesis (<http://www.theses.fr/s218954>).

This inequality makes it possible to draw graphs of $\log \Delta P = f(\log R_h)$ for a given type of capillary. Figure 36 shows an example of a capillary with an internal diameter of 75 μm and a length of 70 cm, where the green zone indicates zone where the Taylor regime occurs meaning that the conditions of the equations (9) and (10) are respected. This working zone may be changed by adjusting the capillary's geometric parameters: a larger object can be measured with a thinner or longer capillary. However, there is a limit for oversized objects. If the chosen capillary diameter is too small for the species considered ($R_h / R_c \geq 0.0051$), the Taylor dispersion takes place in a hydrodynamic chromatography regime. Large species are excluded by the capillary walls under these circumstances, and the sample "sees" a smaller capillary, which distorts the size predicted from equations (12) and (13). For a capillary with an internal diameter of 75 μm , it is possible to measure sizes up to a diameter of the order of 382 nm with less than 3% error due to the hydrodynamic chromatography regime [299].

TDA was used by Belongia and Baygents to determine the diffusion coefficients of large species like tobacco mosaic virus (TMV), a rodlike virus with a length of 300 nm and a diameter of 18 nm, as well as hydrophilic and hydrophobic polystyrene latex and hydrophobic polymethyl methacrylate particles

ranging in size from 0.19 μm to 0.83 μm [290]. The authors demonstrated, using a wax-coated (50 μm diameter) and a polyethylene glycol-coated (50 μm diameter) capillary, all the care that must be taken to suppress interactions between the particle and the capillary walls if the dispersion results are to be interpreted using traditional TDA theory. Using didodecyldimethylammonium bromide (DDAB) coated capillaries, d'Orlyè et al. determined the mean collective diffusion coefficients of maghemite ($\gamma\text{-Fe}_2\text{O}_3$) NPs in the range of 6–10 nm diameter [291]. Compared to DLS data, TDA particle mean solid radii were lower owing to more particle contribution of the largest particles in light scattering. Furthermore, several research groups have achieved successful on-line CE-TDA integration for nanoparticle characterisation [300-303]. Oukacine et al., for example, used CE-TDA to determine the R_h of a bimodal mixture of nanolatexes (56 and 70 nm in size) [302]. Before TDA could be done, a baseline separation of the two nanolatexes using CE was necessary. In this investigation, a UV detector and capillary with three detection windows in a looping design were employed. The reported values of D agreed well with the values obtained by TDA of the two nanolatexes separately, confirming CE-TDA as a feasible technique for the analysis of mixtures of nanoparticles of comparable size. Furthermore, Labied et al. [304] recently established a unique coupling, TDA-inductively coupled plasma-mass spectrometry (ICP-MS), that enabled the direct determination of the size and stability of ultra-small Gadolinium NPs (sizes less than 5 nm) in complex biological fluids (i.e., blood serum, urine, cerebrospinal fluid)

In view of the literature reporting successful TDA analysis of virus, organic or hybrid or inorganic particles, TDA appears as a promising alternative for the size characterization of EVs. Indeed, TDA is an absolute approach (no calibration required) for determining the molecular diffusion coefficient, D , and the hydrodynamic radius, R_h , with no size bias because the contribution of small and large solutes is proportional to their mass abundance in the mixture.

Herein, TDA was tested for the first time for the size characterization of our high-quality EVs isolated from bovine milk with narrow size distribution, which were given by our commercial partner Excilone (France). As a reminder, NTA, DLS, LC-MS / MS, and TEM data are available in the supplementary information of our CZE-LIF paper in section IV.4. of this chapter. TDA-UV and TDA-LIF using CE were both investigated for this purpose for native EVs and EVs fluorescently labelled using the method reported in our paper in section IV.4. of this chapter.

IV.6.3. CE procedure

TDA-UV experiments were carried out with a P/ACE MDQ (Beckman Coulter, Brea, CA, USA) equipped with a UV detection at 200 nm. TDA-LIF studies were performed with a PA 800 Plus system (Sciex Separation, Brea, CA) equipped with a solid-state laser induced fluorescence detector (λ_{ex} : 488 nm,

λ_{em} : 520 nm). The fused silica capillary (I.D. of 50 μm , O.D. of 375 μm , effective length (L_{eff}) of 50.2 cm and total length (L_{tot}) of 60.2 cm) was preconditioned (using a pressure of 25 psi at the capillary inlet) with the following sequence: water, 1 M NaOH, 1 M HCl and then water, for 10 min each. Between the measurements, the capillaries were flushed for 5 min each with 50 mM SDS, 1 M NaOH, deionized water, and finally the running buffer using a pressure of 30 psi. EVs were introduced by pressure injection (0.4 psi) for 9 s (0.96% Vol to detector). Experiments were performed using a mobilization pressure of 0.4 psi. TDA-UV and TDA-LIF were performed with bovine milk-derived EVs isolated with sucrose gradient ultracentrifugation and human plasma EVs with monolithic disks via immunoaffinity chromatography. The techniques for EV separation and fluorescent labelling, as well as the matrix replacement approach for recovering EVs in PBS 1X and removing excess residual fluorophores, can be found in our paper, which is described in section IV.4. of this chapter.

Taylorgrams were recorded using karat 32 software and then were exported to Microsoft Excel for subsequent data processing. The deconvolution of the taylorgrams with a finite number of Gaussian functions and the data fitting were conducted using the Least Significant Difference method using the “GRG nonlinear” in Microsoft Excel.

IV.6.4. Results

IV.6.4.1. TDA-UV and TDA-LIF of bovine milk derived EVs

To evaluate the performance of TDA under physiological conditions (i.e., neutral pH with high salt concentrations), the TDA-UV approach was initially tried on high pure EVs extracted from bovine milk using sucrose gradient ultracentrifugation and suspended in PBS 1X buffer. Unmodified silica capillary were used with 1X PBS as the mobilization buffer. Figure 37 shows the taylorgram obtained for bovine milk-derived EVs diluted to a concentration of 2×10^{12} EV/mL in PBS 1X.

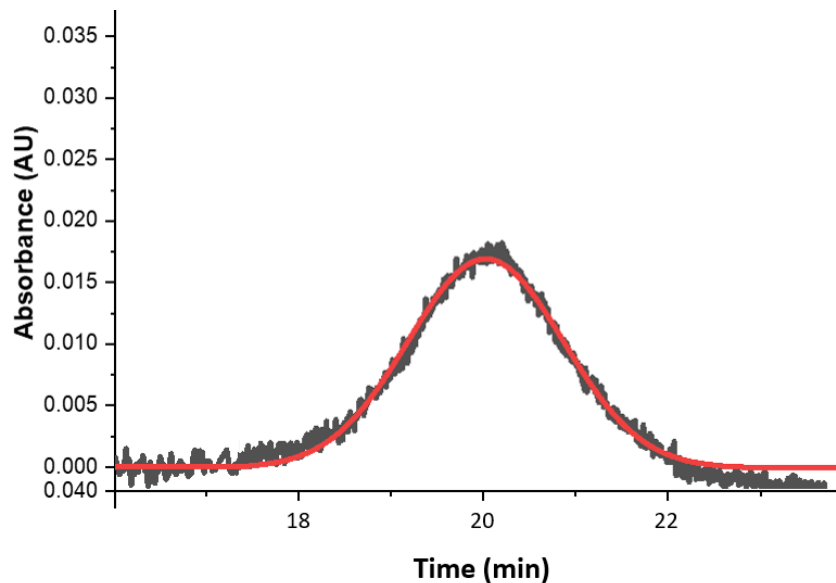


Figure 37: TDA-UV: Representative taylorgram (black line) and corresponding fit (red line) for bovine milk-derived EVs. Experimental conditions: uncoated fused silica capillary (50 μm i.d., length 60 cm); buffer PBS 1X, pH 7.4; injection 0.4 psi 9 s; applied pressure 0.4 psi; the wavelength used was 200 nm.

Taylorgram was fitted and deconvoluted by the team of H. Cottet. The possibility of analyte-capillary adsorption, which might lead to peak asymmetry in the resultant taylorgram, should be considered. Interestingly, here no adsorption onto the capillary wall was detected, as evidenced by the symmetric signal. Diffusion coefficients were provided by inserting σ and t_R values into eq 12, and hydrodynamic radii were calculated using the Stokes equation (eq13). The Taylor dispersion analysis showed a R_h of 96.5 nm. The agreement between our experimental results and NTA values was satisfactory (see table 3).

In addition to UV, TDA was coupled to LIF to detect fluorescently labelled bovine milk-derived EVs using the CFDA-SE dye already reported for the CZE-LIF method presented in section IV.4. of this chapter. According to NTA data, the intra-membrane labeling approach, resulted in no significant changes in the size distribution of EVs. Indeed, NTA data showed only a very slight size shift towards smaller particles when EVs were labelled (D_h : 171 nm \pm 42 nm before vs D_h : 157 nm \pm 37 nm after the labelling; see Fig. S2 from paper 3) that was rather attributed to partial EVs lysis or leakage of the covalently bound fluorescent dye over long time, as previously evidenced with the CE-LIF method (see Fig. S6 from paper 3). TDA-LIF, on the other hand, was able to distinguish two distinct R_h populations. The taylorgram for fluorescently labelled bovine milk-derived EVs diluted to a concentration of 1.05×10^{12} EV/mL in PBS 1X is shown in Figure 38.

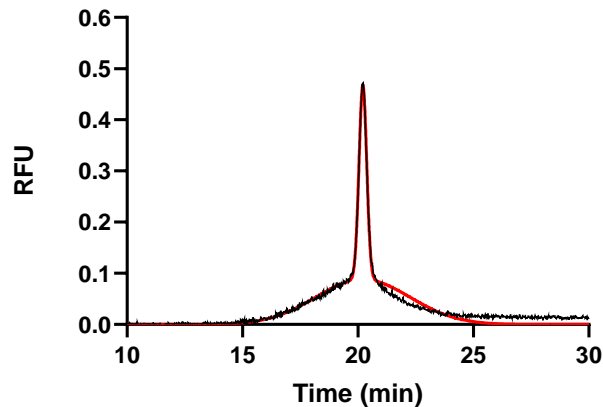


Figure 38: TDA-LIF: Representative Taylorgram (black line) and corresponding fit (red line) for bovine milk-derived EVs. Experimental conditions: uncoated fused silica capillary (50 μm i.d., length 60 cm); buffer PBS 1X, pH 7.4; injection 0.4 psi 9 s; applied pressure 0.4 psi; λ_{ex} 488 nm, λ_{em} 520 nm.

By performing a fit of the experimental trace with a sum of two Gaussian functions, two radii could be simultaneously determined. A first population was sized at 111 nm R_h ($\sim 75\%$ of the signal), which corresponds to the EVs, while a second smaller population was sized at 0.74 nm R_h ($\sim 25\%$ of the signal), which most likely corresponds to the released or excess of CSDA-SE. Based on these results, the TDA has a substantial better potential for discriminating EVs from smaller subpopulations that would not be identified by conventional techniques such as DLS and NTA due to their detection limits. Interestingly, TDA results also showed a size shift toward bigger particles with fluorescently labeled EVs (R_h : 96 nm before vs R_h : 111 nm after labeling). While a conclusion on the reason behind such shift observed with TDA cannot be made at this stage of proof-of-concept, we hypothesized that this was due to labeling occurring on the outer membrane of EVs. However, RSD of the TDA measurements by performing a reproducibility study from a given sample would help determining if those differences are significant or not.

IV.6.4.2. TDA-UV and TDA-LIF of human plasma derived EVs

Preliminary studies on uncoated silica capillaries were also performed on more complex biological samples. For this, we used human plasma EVs isolated via immunoaffinity chromatography using monolithic disk immobilized with monoclonal anti-human CD9 [172] and human plasma EVs found in an ELISA kit provided by HansaBioMed and extracted from human plasma by SEC and concentrated by tangential flow filtration. Experiments were conducted under the same settings as mentioned above. According to preliminary NTA data, the final concentration before TDA-LIF analysis for EVs separated

via immunoaffinity chromatography and by HansaBioMed should be roughly 1.9×10^{11} EV/mL and 9×10^{11} EV/mL. The resulting taylorgrams are given in figure 39.

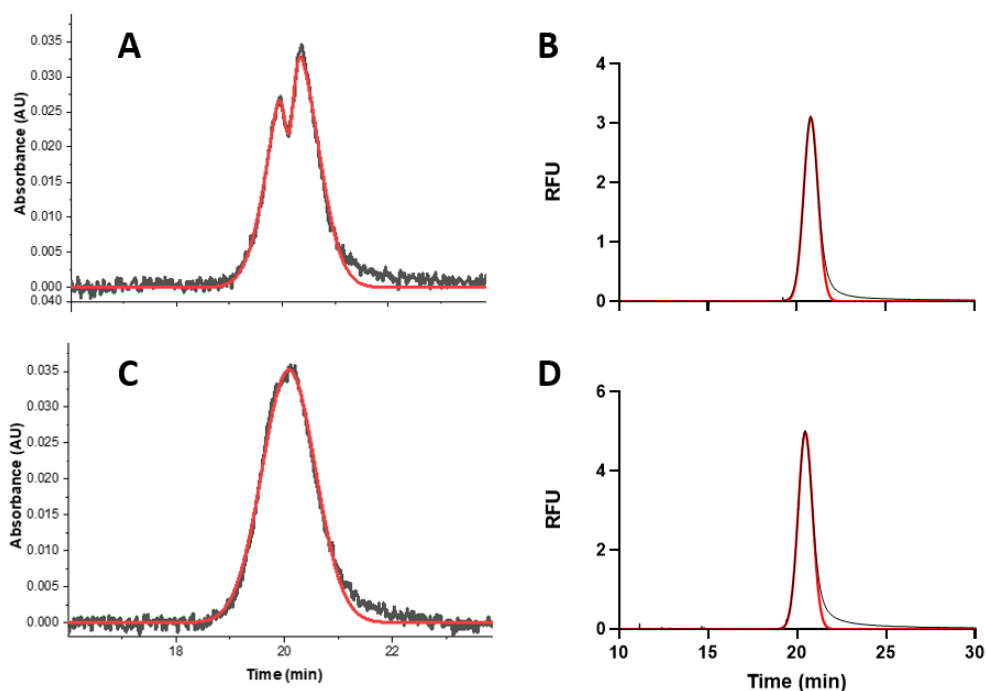


Figure 39: TDA-UV (on the left) and TDA-LIF (on the right): Representative Taylorgram (black line) and corresponding fit (red line) for (A)(B) human plasma EVs isolated with affinity monolithic disks; (C)(D) standard human plasma EVs from HansaBioMed. Experimental conditions: uncoated fused silica capillary (50 μm i.d., length 60 cm); buffer PBS 1X, pH 7.4; injection 0.4 psi 9 s; applied pressure 0.4 psi; UV: 200 nm; LIF: λ_{ex} 488 nm, λ_{em} 520 nm.

The peaks obtained with both EVs samples were much sharper than the peak obtained with bovine milk-derived EVs. The hydrodynamic radii resulting from Gaussian corrections were 5.4 nm (UV) and 4.2 nm (LIF) for the isolated EVs with monolithic disks, and 6.6 nm (UV) and 4.3 nm (LIF) for the conventional EVs. These values are not in agreement with NTA data, where the radius measurement was at least 13 times greater than that of the TDA (see table 3). In an attempt to explain this phenomenon, some aspects have been considered. Given that the silica capillary surface contains negatively charged silanol functions and that the surface of EVs at pH 7.4 may contain some positive charges due to the presence of various amine functions on EVs membrane proteins or, to a lesser extent, amines on the head groups of the membrane lipid phosphatidylethanolamine, we first suspected a possible EV adsorption with the wall of the capillary. However, if this occurs, the resultant Taylorgram will be broader and the diameter obtained by TDA would give larger sizes. Another reason might be because samples from plasma include contaminants associated with the mode of isolation used, which interact with the capillary wall and the EVs too, adding an additional dispersion

phenomenon to Taylor's one. Moreover, these little entities detected by TDA, but invisible to NTA due to its detection limit at 40-50 nm, would represent the majority of the species in these samples. Further techniques to confirm this are then envisaged (e.g., cryo-TEM). Finally, further TDA investigations on EVs isolates with better purity from different origins and provided by our commercial collaborator Excilone, are envisaged.

Table 3: Mean hydrodynamic radius of bovine milk-derived and human plasma EVs measured by TDA-UV/LIF by NTA.

| | TDA – UV (R_h in nm) | TDA – LIF (R_h in nm) | NTA (mean $R_h \pm SD$ in nm) |
|---------------------------------|-------------------------|---------------------------|-------------------------------|
| Bovine milk derived EVs | 96.5 | 111 (~ 75%) 21 (~ 25%) | 87 ± 26 |
| EVs - affinity monolithic disks | 5.14 | 4.2 | 64 ± 21 |
| EVs - HansaBioMed | 4.2 | 4.3 | 67 ± 22 |

IV.6.5. Concluding remarks

TDA performed with a capillary electrophoresis equipment proved to be a quick, straightforward, and reliable approach for measuring EV diffusion coefficients, providing access to particle Stokes radii through the Stokes–Einstein equation. We effectively demonstrated a unique approach and viable alternative to DLS, NTA, and cryo-transmission electron microscopy that are commonly used for EVs size characterization, providing the first evidence that TDA can be applied to this kind of bio-nanoparticles for precise size evaluation. Furthermore, TDA-LIF seemed to be capable of detecting minor variations in hydrodynamic radius that might be caused by fluorescent labelling at the outer membrane of EVs. However, knowing the RSD of the TDA measurements via a reproducibility study on a specific sample might aid in assessing whether or not such variations are significant. While TDA was found to characterize the size of highly pure EVs (i.e., bovine milk derived EVs) with satisfactory results, this was not the case for other source of EVs. Since a logical explanation cannot be given at this time, this could be due to the high presence of small impurities in EV samples, such as plasma proteins and lipoprotein particles, which may overlap with the Taylor diffusion.

Finally, including a first step of capillary zone electrophoresis (CZE) to differentiate EV subpopulations based on their electrophoretic mobilities, followed by a second step of TDA-LIF/UV measurements to determine the diffusion coefficients of each EV subpopulation could be a perspective of this work (CZE-TDA-LIF/UV) in order to provide a platform with dual characterization potential. Furthermore, it may

constitute an attractive option for EV quality control by allowing the detection of contaminants caused by different isolation techniques.

Chapter V: New micro-sized method for the isolation of EVs

V.1. Introduction

In the Chapter IV, I explored and developed several CE-based approaches, serving as the downstream microscale separation module of the analytical droplet platform for EVs. These methods allow now to characterize EVs profile, serving for EVs identification and representativeness for further diagnostic and theranostic applications. In the second part of my thesis, I focused on the development of the first module of this platform in order to isolate and purify EVs from complex matrices (typically biological fluids) and concentrate them to a sufficient extend for downstream EVs analysis and / or characterization. Several isolation strategies using various mechanisms have already been discussed in chapter II.1.. Briefly, the four most popular isolation procedures are ultracentrifugation (UC), size-based separation (such as size exclusion chromatography or ultrafiltration), immunoaffinity, and precipitation-based methods. However, none of existing approaches can satisfy all criteria of high purity, high isolation yield and high throughput (via automation).

The use of microfluidic techniques has gained more and more attention, as it brings new functionalities, not available with macroscopic techniques, and offers the ability to minimize sample amount, cost, reagent consumption, speed up operations, and execute several tests in small devices at the same time. Microfluidic approaches hold the potential to meet all aforementioned requirements for EVs purification. Several examples of microfluidic-based devices for such purpose were covered in Chapter III. Among all branches of microfluidics, we paid particular attention to droplet-based microfluidic platforms. Droplet-based microfluidics may be defined as the science and technology of creating, manipulating, reacting, analyzing, and screening micro to femtoliter microreactors that are employed as discrete functional units [305, 306]. Such microreactors (typically in aqueous phases) are confined and separated by immiscible phases (typically with fluorinated oil for different bio-applications). This technology can be divided into two main categories: "Stationary Droplet Microfluidics", in which the solutions are typically manipulated by pipetting, without the use of external pressure or flow control systems, and "Dynamic Droplet Microfluidics," in which electrical potentials or pressure-driven flows can be used to actuate the droplets [306]. For the work in this thesis, we focused on pressure-driven flows, often known as "Droplet Microfluidics" [307] or also renamed "Continuous Droplet Microfluidics" [306]. Droplet microfluidics systems generally mix two (or more) immiscible fluids in microfluidic channels, resulting in controlled emulsions of one phase

within the other. This ensures consistent compartmentalization of sample and reagents while decreasing, in comparison to standard lab-scale techniques, both the amount of liquid required for analysis and minimizing the risks of contamination with the surrounding environment.

Recently, droplet-based microfluidic devices that used micro or nanometric magnetic beads (MB) as solid support to transfer target analytes (e.g. nucleic acids, proteins, cells and viruses) between different droplets, serving for extraction and purification and detection of target analytes have been reported [306]. Indeed, MB have the advantages of:

- i) being able to be functionalized on their surface with a wide range of surface chemistries, allowing various strategies for the covalent linking of ligands
- ii) having a high surface to volume ratio due to their micro/nanometric sizes, which guarantees an improved performance of target analyte capture
- iii) having the possibility to be controlled with an automatic and high-throughput manner by an external magnetic field from a distance.

Given the versatility and widespread use of functionalized MB for EV isolation and detection in both conventional macroscopic protocols, their integration in droplet-based microfluidic systems for EV isolation holds considerable promise, in our opinion. When I started the work on EVs isolation, droplet microfluidics was reported twice for immunoassay-based EV detection [308, 309]. However, in both cases it was not for extracting EVs but rather to quantify them or to determine surface EV protein composition and has never been explored for high performance and high throughput isolation of EVs.

Droplet microfluidics fits well with our aim to develop a platform (Droplet-CE), in which micro/nanometric droplets are utilized as carriers of target analytes (EVs) to hyphenate droplet-based sample preparation and handling with electrophoretic separation (i.e., capillary electrophoresis) [310]. Our group recently presented an in-house droplet-based sample handling system in which micro/nanometric droplets serve as a bridge for MB-based immunoassays for the sequential identification of amyloid-beta (A β) peptide biomarkers for Alzheimer's disease molecular diagnosis [311]. Based on these first achievements, in this work we developed and evaluated different bead-based strategies for isolating and recovering intact EVs, and then to adapt the most performing one to the microfluidic droplet platform that we developed.

EVs may be isolated using immunoaffinity bead-based kits, which employ specific antibodies for EV surface proteins (transmembrane proteins such as CD81, CD63, CD9, annexin, and Alix are among the most often used). However, after separation, such commercial kits do not provide any elution protocol to recover intact EVs. In this regard, we first investigated conditions compatible with the elution of EVs

from commercial immunoaffinity MB. Some common conditions reported to break antibody/antigen affinity were tested to elute EVs after their immunocapture. However, classical protocols usually require extreme pH to break the antibody-antigen bond which could damage the recovered EVs. We therefore investigated alternative and antibody-free strategies reported in a few recent studies to capture and eventually elute EVs using MB. Once in tube optimized and validated, we then translated this in-tube protocol to the microfluidic droplet platform. At the same time, attention had to be paid on possible beads clustering and poor recirculation during in-droplet incubation with regular droplet back and forth movements. As a consequence, we studied multiple approaches to address these challenges.

The first part of this chapter presents some principle of microfluidic droplets and MB manipulation. The second one will present our efforts for the development of an intact EVs capture and release using immunocapture bead-based approaches, while the third one focus on antibody-free approaches and achievements obtained with our microfluidic droplet platform for EVs isolation from complex matrices.

V.2. Principle of microfluidic droplets and their combination with MB

V.2.1. General statements on Droplet Microfluidics

Droplet microfluidics is a very effective technique for creating and controlling very small quantities of fluid (μl to fl). Droplet microfluidics is based on the use of two immiscible fluid, most often oil and aqueous solutions. These droplet emulsions are often generated by specific channel geometries, such as T-junctions and flow-focusing, or by pipetting robots (as employed in the present work), and are conveyed in a pressure-driven flow [312].

Droplet microfluidics was selected in this work to enable the development of our platform for the separation, preconcentration, and characterization of EVs (Droplet-CE). Unlike conventional continuous flow microfluidic systems, which are limited by the number of steps and operations that can be made in series because it implies necessarily a device size increases (almost linearly with the number of operation needed for a sample treatment/preconcentration/enrichment for instance), droplet-based systems may execute a high number of steps without increasing the device size nor its complexity. Moreover, droplet-based microfluidics allows for independent control of each droplet, resulting in individual micro-reactors that may be transported, mixed together, split, and analyzed separately. Droplets that act as bridges and carriers of EVs from the sample, where they are diluted and confined with other species, until their injection into CE systems, as isolated and enriched EVs sample, may overcome the limitations of working dimension mismatch and low module integration.

V.2.2. Magnetic beads as cargos: principle and theory

When MB are used in combination to a droplet train, they need to be extracted from one droplet and then transferred into the subsequent droplet (see Fig. 40).

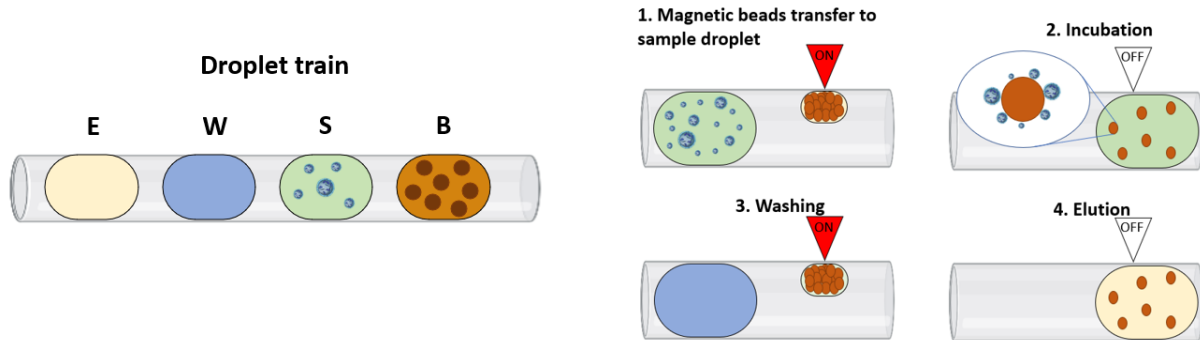


Figure 40: On the left, schematic drawing of droplet train containing solution of B: magnetic beads; S: sample; W: washing and E: elution. On the right, schematic drawing showing the magnetic tweezers technology.

The extraction of MB contained in a droplet is primarily influenced by two forces: the magnetic force (F_{mag}) acting on the beads through an external magnetic field and the interfacial force (F_{int}) associated with the droplet interface [306]. The force acting on the beads can be approximated by

$$F_{mag} \approx (Q / \rho) \cdot M \cdot \nabla B \quad (15)$$

where Q is the quantity of particles, ρ is their density, M is the magnetization of a particle and ∇B is the gradient local magnetic field [313].

On the other side, the presence of an interface between two immiscible fluids is involved for multiphase microfluidics. This interface is defined by a capillary interfacial force, which for a spherical meniscus may be expressed as $F_{int} \propto \gamma L$, where γ is the interfacial tension between the immiscible fluids and L is a representative length of the system, such as the radius of curvature of the meniscus [306].

As a result, a magnetic force greater than the interface's interfacial force ($F_{mag} > F_{int}$) is needed to extract the MB from a given droplet. Implementation of a multistep procedure such as the one required to capture one specific analyte, wash nonspecific capture and elute the captured analyte, requires successive extraction of beads from droplets and redispersion of them in a different droplet. A first strategy for MB extraction from the droplet is based on the hydrodynamic splitting of droplets containing magnetic particles, with one of the two resultant droplets possessing a high concentration of magnetic particles due to its proximity to the magnet present in the microfluidic chip (see Fig. 41A) [314]. Despite the fact that this method provides for high throughput handling, it has a poor

purification yields owing to inadequate supernatant removal. Other techniques based on the same hydrodynamic separation concept but with different geometries have been developed to improve the beads capture rate [306]. However, the redispersion of the extracted magnetic cluster into the next droplet to perform subsequent typical biological operations, such as rinse steps or immunoassays, can be difficult to integrate, since additional microchannel circuitry is required. Another method, which was utilized in the system I used in the thesis is the direct magnetic extraction of the MB. The separation is no longer caused by the splitting of the initial droplet at the junction of two channels, but by the balance of the viscous drag force that pushes the drop forward in the channel, the capillary forces that tend to keep the drop entire, and the magnetic force which retains magnetic particles as a cluster. This strategy allows a very high purification yield rate compared to other techniques because the second droplet created by the extraction contains the aggregate of MB and only a small amount of initial solution. Furthermore, using the magnetic tweezers system employed in our laboratory, we can sequentially capture and release the beads in droplets for multistep operation. Indeed, the magnetic field is generated by current flowing through a coil, generating a local magnetic field, and is concentrated close to the capillary through which the droplets travel due to the presence of a paramagnetic tip. When a droplet containing MB approaches, the current is activated, the magnetic field is triggered on, and the beads join together to form a compact aggregate (or cluster) that is removed from the parent droplet (Fig. 41B). Because this cluster is confined in an aqueous sub-droplet, it is never in contact with the oil or the tube walls. However, if high flow rates or droplet viscosity are used, partial extraction or trapping failure of magnetic particles may occur.

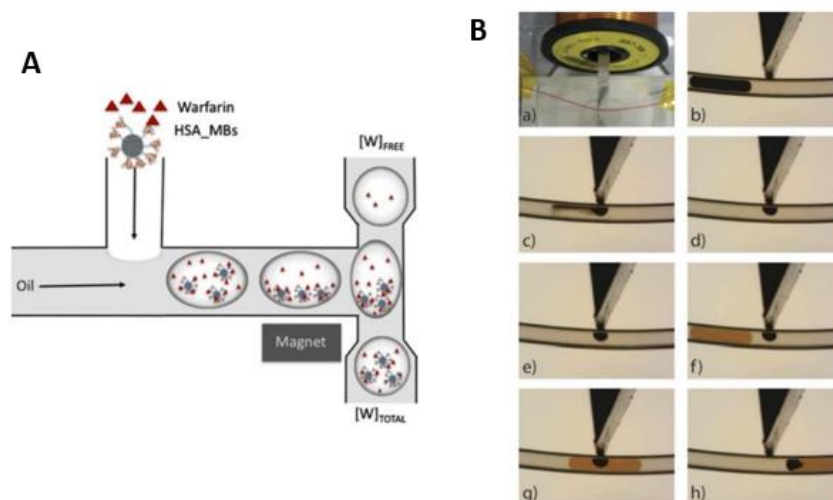


Figure 41: (A) Schematics of the device proposed by Lombardi and Dittrich. Emulsified in oil is an aqueous solution comprising magnetic beads coated with human serum albumin (HAS_MBs) that bind warfarin. The droplets are symmetrically divided at a T-junction, but the addition of an external magnet causes the magnetic beads to be concentrated in half of the initial volume. Reprinted from [314] with permission. Copyright (2011) Analytical and bioanalytical chemistry. (B) Sequence of images showing the magnetic tweezers technology. a) Photos of the paramagnetic tip placed in the coil and close to the capillary, b) to h) sequence of extraction and redispersion of magnetic beads in droplets by turning on and off the magnetic field while droplets are passing in front of it. MB act as carriers to transport analytes from one droplet to another. Reprinted from [315].

The microfluidic droplet technology employed in this study has been already exploited in our lab prior to my arrival, for a droplet-based enzyme-linked immunosorbent assay (ELISA) sequential detection of amyloid-beta ($A\beta$) a peptide biomarkers for molecular diagnosis of Alzheimer's disease [311]. Briefly, this platform included a syringe pump and a motorized pipettor arm for droplet formation, as well as a 384-well plate (for sample and reagent storage) mounted on an x-y-z adjustable holder. Four pairs of magnetic tweezers were put around the tubing and triggered by a magnetic coil to catch and release antibody-grafted MB, which were then re-suspended in different droplets containing various reagents for the ELISA process (see Fig. 42). In comparison to traditional ELISA, this droplet-based alternative provided automation, a decrease in working volume (200 nL / analysis for the droplet protocol vs 50–100 μ L for conventional ELISA), and a considerable reduction in operating time (8 analyses per hour for droplet protocol vs 2 h per analysis required for conventional ELISA).

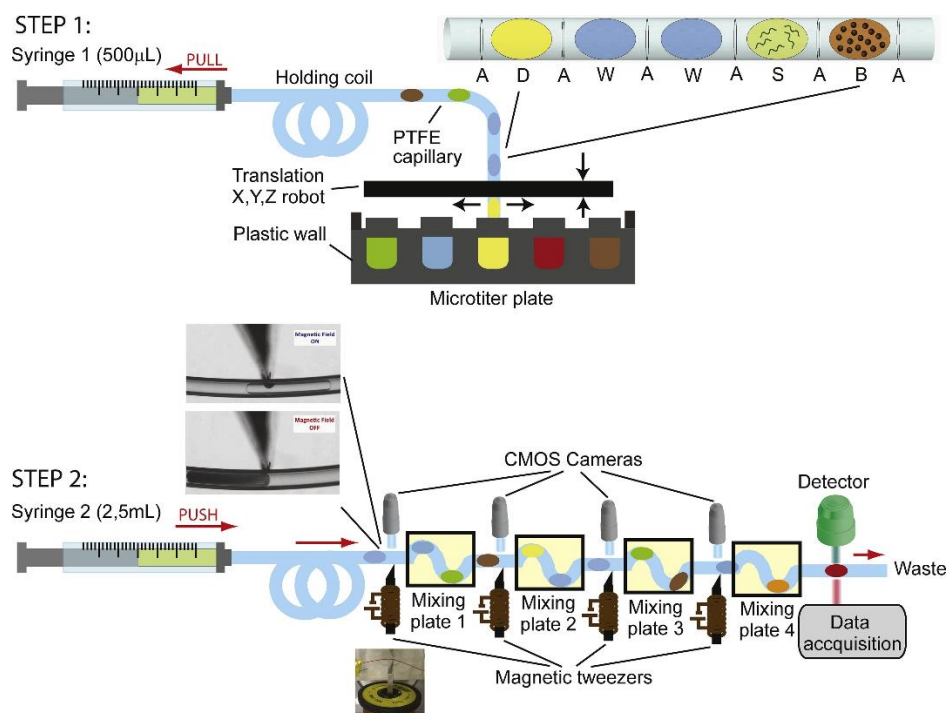


Figure 42: Schematic drawing of the microfluidic droplet configuration. D is for detection droplet; W stands for washing droplet; S stands for sample droplet; B stands for magnetic bead droplet; and A stands for air bubble. Oil separates the droplets. Reprinted from [311].

V.3. Capture and Elution of EVs from commercial immuno-based beads

V.3.1. Introduction of preliminary in-tube experiments

Immunoaffinity-based methods are one possibility to purify or isolate EVs. They generally use beads that are functionalized (with antibodies or aptamers) in a way to capture any protein or membrane components expressed on EVs. To this regard, they are more suitable for purifying specific subpopulations of EVs based on their surface markers but much less for universal EV extraction. Among the technologies used to isolate EVs using antibodies, MB are the most common and are simple to handle by using an external magnetic field. Before developing the microfluidic droplet extraction, we first did some in-tube preliminary experiments in order to select the best MB and affinity strategy to be used. We investigated antibody-based approach and also antibody-free ones.

Accordingly, in our preliminary experiments, a combination of beads coated with a varied portfolio of EVs-specific antibodies, such as anti-CD9, anti-CD63, and anti-CD81, was planned in order to collect the highest amount of EVs in the most precise manner possible. For preliminary results, we selected to work exclusively on commercially available Exosome-Human CD9 Isolation Reagent kit purchased from Thermo Fisher Scientific (Waltham, MA, USA). This kit was tested for EVs capture and subsequent

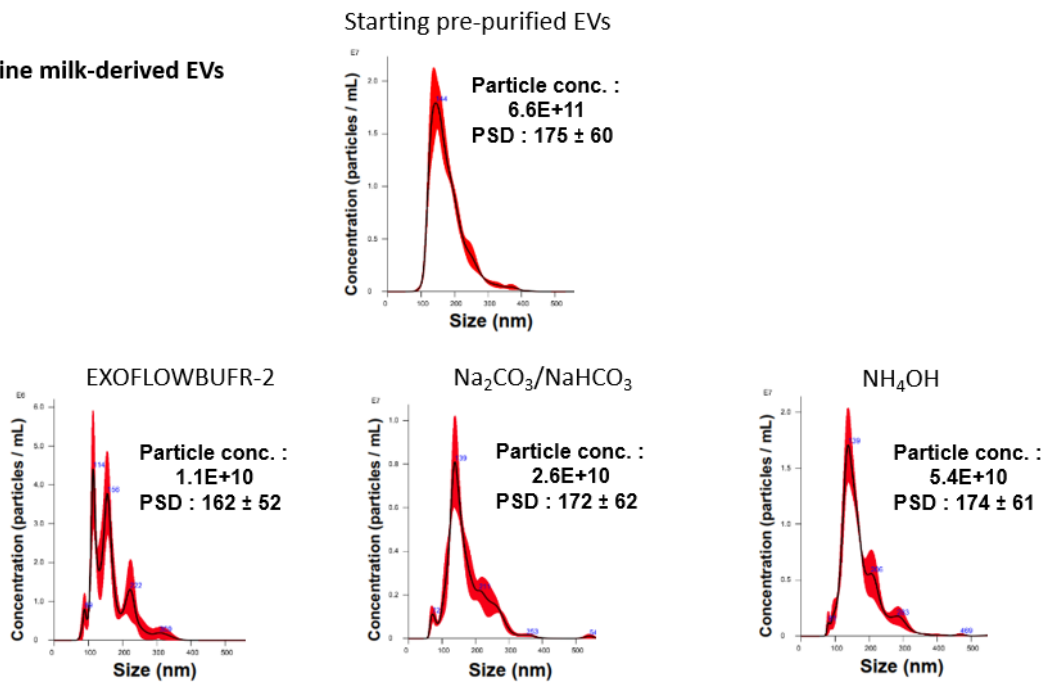
elution, using standard EVs (bovine milk-derived EVs), provided by our commercial collaborator Excilone (Elancourt, France), and human plasma EVs isolated with monolithic disks via immunoaffinity chromatography from a collaboration with the Marja-Liisa Riekkola team (INAR Analytical Chemistry) from the University of Helsinki (Finland). The way these two EVs preparation were obtained are fully detailed in paper 3 ([Morani et al., *Analytica Chimica Acta*, 2020](#)) in chapter IV.4.. Inspired by the method reported by Multia et al. for elution of EVs from a monolithic disk immobilized with anti-human CD9 antibody [172], I tested the same high alkaline conditions to elute EVs from MB (see Materials and methods part of paper 3 in chapter IV.4. for details). These were compared to a commercial elution solution (EXOFLOWBUFR-2), purchased separately from Ozyme (France), intended to allow elution from MB grafted with either anti-CD9, CD63, or CD81.

V.3.2. Preliminary in-tube experiments to select MB capture and elution conditions

Following the manufacturer's instructions (Invitrogen), 10 μL Dynabeads-CD9 from (2.7 μm dia.) were incubated in 100 μL of bovine milk-derived or human plasma EVs samples overnight at 4°C with gentle shaking to promote attachment of EVs. Next, a magnetic separator was used to remove the supernatant and collect the captured EVs. After washing 3 consecutive times with 300 μL of PBS, the enriched EVs were eluted in 100 μL of either ammonium hydroxide (NH_4OH , pH 11.3) or carbonate-bicarbonate ($\text{Na}_2\text{CO}_3/\text{NaHCO}_3$, pH 11.3) solution and neutralized immediately with the addition of 10 μL 1 M HCl [172]. EXOFLOWBUFR-2 was also tested for intact EVs elution. NTA was used to assess the supernatant containing the collected EVs from both pre-purified bovine milk-derived and human plasma-derived EVs (see Fig. 43). The video acquisition was performed using a camera level of 14. Per sample, 3 videos of 90 seconds with a frame rate of 30 frames/sec were captured at 25°C and subsequently analyzed with a threshold set up at 5. Tests were conducted using pre-diluted samples in PBS resulting in particle concentrations between 10^6 and 10^9 particles per ml for best analysis.

(A)

Bovine milk-derived EVs



(B)

Human plasma-derived EVs

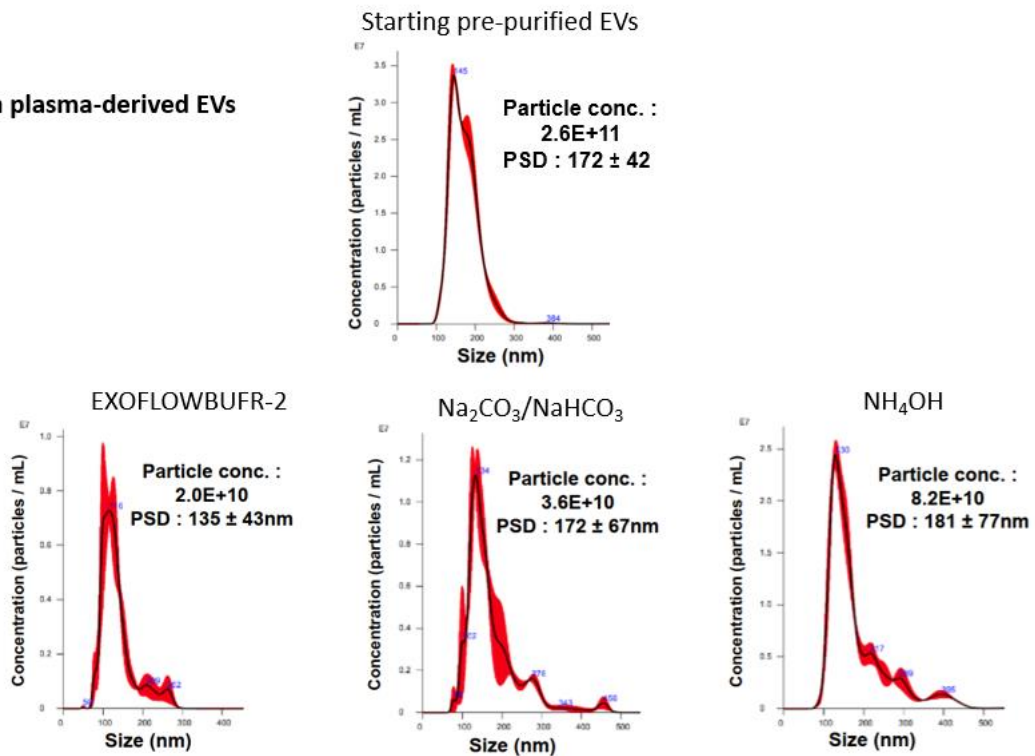


Figure 43: NTA profiles for (A) bovine milk-derived EVs and (B) human plasma-derived EVs. (a) Starting pre-purified EVs sample profiles. EV elution from Dynabeads-CD9 with EXOFLWBUR-2 solution, and under alkaline condition (pH 11.3) with Na₂CO₃/NaHCO₃ or NH₄OH. PSD: particle size distribution. NTA histograms represent the mean of three replicate measurement of the same sample and SD in red.

According to the NTA analysis (Fig. 43), regardless of the type of elution used, the quantity of EVs captured by this Exosome-Human CD9 Isolation commercial kit compared to the total population of EVs in the initial sample was higher with human plasma-derived EVs (from 9 to 36 %) than with bovine milk-derived EVs (from 2 to 8 %). This is most likely due to the kit's increased specificity for EVs of human origins. The maximum EV recovery, on the other hand, was obtained when elution from MB was done using ammonium hydroxide (8.16×10^{10} particles / mL). EVs concentration was four times higher with this ammonium solution than the commercial solution proposed by Ozyme and more than two times higher than the sodium carbonate-bicarbonate solution. Furthermore, when the EVs were eluted with the EXOFLWBFR-2 commercial solution, the size (135nm) differed from the two other alkaline solutions (170 and 180 nm for $\text{Na}_2\text{CO}_3/\text{NaHCO}_3$ and NH_4OH respectively). These latter alkaline solutions provide a mean size distribution closer to the one of EVs starting diameter of 172 nm. To better understand the origin of these results, NTA was utilized to analyse a blank containing just the solutions used for the different elutions. Surprisingly, the EXOFLWBFR-2 solution included particles with a size distribution of 125 ± 57 nm and a concentration of 1.64×10^{10} particles / mL, while the two alkaline solutions contained no particles. Since the composition of this solution is confidential, it was impossible to determine their nature. However, given their high concentration, they might explain why the EVs eluted with this kind of solution shifted toward lower size values. In an effort to improve the performance of EVs capture and thus isolation yield with ammonium hydroxide elution, higher beads concentrations were also tested (20 and 40 μL of MB in 100 μL final volume). However, they did not result in significantly higher EV isolation yields (see Fig. 44).

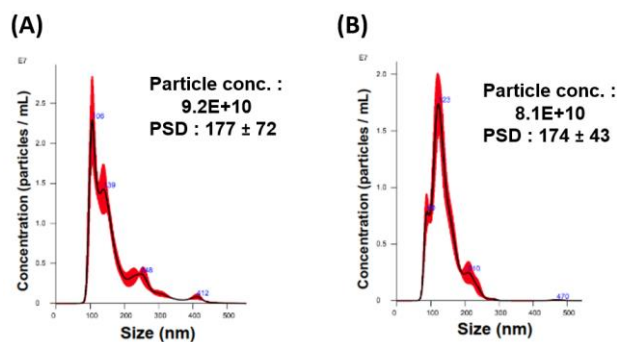


Figure 44: NTA profiles for human plasma-derived EVs isolated with Dynabeads-CD9 from pre-purified samples. Incubation with (A) 20 μL and (B) 40 μL of magnetic beads in 100 μL final volume. Elution under alkaline condition (pH 11.3) was performed with ammonium hydroxide. NTA histograms represent the mean of three replicate measurement of the same sample and SD are indicated by the red lines.

While the specificity isolation methods, this strategy may also be restrictive since it is likely to extract just one sub-population of EVs. There is currently a lack of sufficient knowledge on which EVs markers are present on distinct EV subpopulations, or which markers are constantly present on all EVs surface (even though their proportion may vary for different sub-population) as well as the subcellular and cellular origins of these EVs. Based on NTA analysis, the CD9+ population profile of pre-purified EVs samples seems to be identical to that of the original sample when the CD9 protein used for their capture. The ammonium hydroxide solution (pH 11.3) provided the highest recovery yield for this isolation method. A combination of coated beads with a varied range of EVs-specific antibodies such as anti-CD9, anti-CD63, and anti-CD81 might be interesting. Although this experiment could only be performed with anti-CD9 coated beads due to time constraints for the thesis, it gives early information on possible elution of EVs from MB functionalized with specific antibodies under alkaline conditions. However, further research is required to determine the influence of these elution conditions on EVs integrity. Indeed, the extreme pH levels required to break the antibody-antigen bond may cause considerable damage to EVs which could be the reason of unsatisfied results obtained. These might impair the biological activity of the recovered EVs and cause a misleading conclusions in the subsequent function analysis.

V.4. Alternative MB-based strategies to extract EVs

When using the antibody-antigen strategy, we encountered two major problems: i) the harsh elution conditions that can damage EVs and ii) the lack of universal EVs markers to ensure entire capture of all EVs. As a result, we have reoriented our strategy and explored other and current methodologies that employ MB for non-specific capture and release of EVs.

We therefore compared some alternative approaches reported in the literature to capture EVs: via phosphatidylserine (PS) displayed on the EVs surface [177], via lipid-based nanoprobe [316], via anionic exchange [317] and via selective adsorption [318]. We choose among them, those that could be easily adapted to droplet operations and to our microfluidic system. The first is the only commercially available alternative (ExoCAS-2), based on the electrostatic interaction [317]. The second method which relies on EVs precipitation on MB in the presence of PEG as it was considered the most cost-effective and did not require any functionalization on the surface of the MB [318]. This study constituted the basis for a manuscript, which was submitted to *Talanta* (manuscript under peer-review) and is discussed in the second section of this subchapter.

V.4.1. Recent alternative MB-based methods to extract intact EVs: a brief revision of the literature

Aside from immunoaffinity MB that target specific protein markers, lipid-related proteins and phospholipids may be regarded "universal" markers and might potentially be used to develop MB-based EV isolations. Additionally, EVs have specific biophysical/chemical characteristics that may be exploited to capture them with adapted MB. For instance EVs have a net-negative surface charge owing to the composition of their surface molecules, which include glycans, phospho and sulpho groups (see chapter I.) that can be used for extracting them with an ion exchange mechanism. These kind of characteristics have been exploited to develop recent antibody-free MB-based isolations of EVs, which are summarized in Fig. 45.

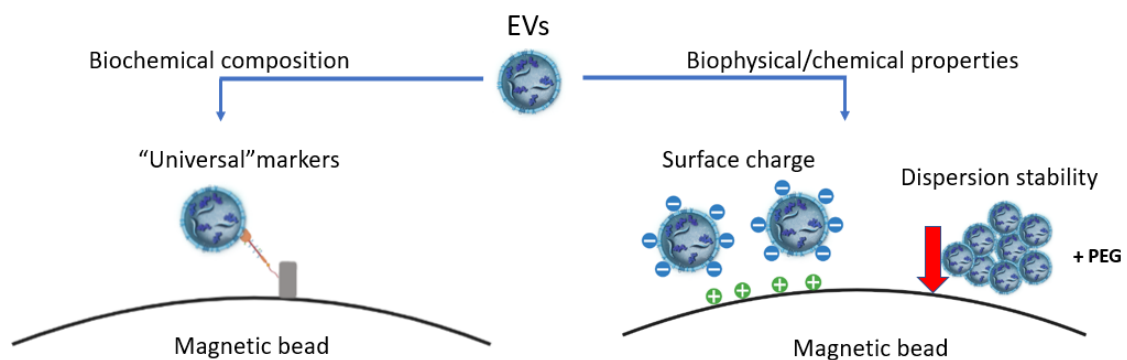


Figure 45: Principle of the two categories of antibody-free MB-based EV capture and elution. It may be done using “universal” markers. Isolation may also be accomplished using biophysical or chemical properties, such as surface charge or EV dispersion stability linked to their solubility.

Regarding the universal markers approaches: In addition to specific surface proteins, phospholipids, which form the basis of EV membranes, might be considered as "universal" markers for EV isolation. This kind of approach was developed by Nakai et al. who employed T cell immunoglobulin and mucin domain protein 4 (Tim 4), a transmembrane protein expressed on macrophages and phosphatidylserine receptor that is Ca^{2+} -dependent in its ligand binding [177]. For EV capture in the presence of Ca^{2+} , the authors employed the extracellular domain of murine Tim4 fused to the Fc segment of human IgG and immobilized Tim4-Fc protein on MB. By adding a buffer containing a Ca^{2+} chelating agent (EDTA), the collected EVs were easily released from the beads. NTA revealed lower mean size for EVs isolated using Tim4-affinity technique compared to ultracentrifugation or polymer precipitation, due to increased population of aggregated or fused EVs. The determination of the Total protein content revealed a two-fold higher yield with polymer precipitation compared to the Tim4-affinity approach. Tim4-affinity isolated EVs, on the other hand, were mostly devoid of protein

contaminations and enriched in EVs proteins. However, this approach was only validated with cultured cell supernatants and not with more complicated biological fluids like as human plasma, where the widely varying amount of phosphatidylserine may impair EV purity. Furthermore, there is no logical explanation for the removal of contaminants by this sort of capture.

Rather than focusing exclusively on one type of phospholipid, Wan et al. developed a lipid nanoprobe composed of DSPE (1,2-distearoyl-sn-glycero-3-phosphoethanolamine)-PEG-desthiobiotin, which contains two hydrophobic fatty acid tails, for the rapid isolation of EVs from cell culture supernatant and plasma [316]. Non-covalent interactions between the two hydrophobic fatty acid tails of DSPE and the lipid membranes of EVs allow DSPE to be introduced into EV membranes. Following labelling with the lipid nanoprobe, EVs were collected by Neutravidin-coated magnetic particles within 15 min and released by DSPE-PEG-desthiobiotin displacement with biotin. There were no discernible variations in the contents of EVs (DNA, RNA, and proteins) recovered by ultracentrifugation against those obtained by the lipid nanoprobe. This method eliminated the need for recurrent ultracentrifugation purification stages since the one-step separation procedure removes 68 % of proteins. However, this technique might affect the physicochemical properties of separated EVs since released EVs will bear the lipid nanoprobe employed to capture them on their surface.

Regarding the approaches using biophysical or chemical properties: Kim and Shin developed a MB-based ion exchange commercial kit (ExoCAS-2) for the isolation of EVs from blood plasma within 40 min [317]. The EVs were separated by electrostatic interactions between negatively charged EVs and positively charged poly-L-lysine-coated cationic beads. The EVs bonded to the surface of the coated beads and are then flushed using an elution solution with varying ionic strengths to break the electrostatic interactions. When compared to ExoQuick (exosome commercial precipitation kit), NTA indicated that the EVs concentration for ExoQuick (2.25×10^{11} EVs/mL) was approximately two-fold that of ExoCAS-2. However, the ExoCAS-2 approach produced less protein contamination than ExoQuick (20 times lower), but it was still roughly 2.3-fold greater than ultracentrifugation. Among these methods, the ExoCAS-2 approach showed the greatest purity ratio (particle concentration to protein concentration). Western blot analysis also exhibited the strongest bands for the reference EV protein markers (ALIX, TSG101, CD9, and CD81) when ExoCAS-2 was used.

As described in Section II.1.4. of Chapter II, PEG is extensively used as a precipitating agent to extract EVs. A MB-mediated selective adsorption technology (MagExo) has recently enhanced the PEG-based isolation approach [318]. Fang et al. discovered that EVs could preferentially precipitate on MB with 5% of PEG added to the EVs solutions, whereas most proteins remained in the supernatant. The

significant hydrophilic impact of PEG might explain this phenomenon. Indeed, PEG locks up a lot of water molecules in a solution. As a result, the EV dispersion stability changes, forcing them to aggregate and precipitate on the surface of silica MB. The best EV yield and lowest protein residues under optimal conditions were 79 and 12 %, respectively. When EVs extracted from plasma using MagExo were compared to gold standard techniques and other commercial kits, they had the greatest particle yield (103, 3.04, and 2.01 times higher than those of differential ultracentrifugation (DG-UC), SEC, and ExoQuick Ultra, respectively). The second greatest purity (19.2×10^{10} particles/mg protein) was reached by repeating the full technique twice (two-step MagExo), while the yield was 1.60, 2.43, and 82.4 times higher than ExoQuick Ultra, SEC, and DG-UC, respectively.

Among the various strategies outlined above, we investigated two newly disclosed batchwise EV-enrichment processes that employ MB and successfully elute intact EVs and have the highest potential for eventual downscaling to microfluidic droplet format, from our viewpoint. The first, known as ExoCAS-2, uses an ionic exchange mechanism to rapidly capture negatively charged EVs through electrostatic contact, employing MB covered with a polycationic polymer called poly-L-lysine (PLL) [317]. This one was chosen because it is the only one that is currently on the market (sold by Microgentas Inc., Republic of Korea). The second is a MB-mediated selective adsorption strategy known as MagExo, which takes advantage of the presence of a water-excluding polymer, polyethylene glycol (PEG), to lock up a significant number of water molecules, forcing EVs to aggregate and precipitate on the surface of MB [318]. We used EV standards derived from bovine milk with a narrow size range (provided by Excilone), allowing allows for more precise EV recovery evaluation. The amount of isolated EVs with the selected MB-based methods were analyzed using NTA and our novel CE-LIF characterization tool. The refined batchwise approach was then turned and adapted into a microfluidic droplet procedure to give high automation and integration, lower sample/reagent quantities, and better isolation efficiency. This was then utilized to separate EVs from more complicated matrices. The details of this work are described in the following manuscript that has been submitted to Talanta for publication (Morani, Talanta, 2022).

V.4.2. Development of a microfluidic droplet platform with an antibody-free magnetic-bead-based strategy for high through-put and efficient EVs isolation (submitted to Talanta)

PAPER 4

Development of a microfluidic droplet platform with an antibody-free magnetic-bead-based strategy for high through-put and efficient EVs isolation

Marco Morani¹, Myriam Taverna^{1,2}, Zuzana Krupova³, Lucile Alexandre¹, Pierre Defreinaix³, and Thanh Duc Mai^{1*}

¹ Université Paris-Saclay, CNRS, Institut Galien Paris-Saclay, 92296, Châtenay-Malabry, France.

² Institut Universitaire de France (IUF)

³ Excilone - 6, Rue Blaise Pascal - Parc Euclide - 78990 Elancourt - France

Correspondence: E-mail: thanh-duc.mai@u-psud.fr

Keywords: extracellular vesicles; isolation; magnetic beads; polymer precipitation; microfluidic droplets

Abstract

In this study, we present a novel microfluidic droplet-based strategy for high performance isolation of extracellular vesicles (EVs). For EVs capture and release, a magnetic bead-based approach without having recourse to any antibody was optimized in batch and then adapted to the microfluidic droplet system. This antibody-free capture approach relies on the presence of a water-excluding polymer, polyethylene glycol (PEG), to precipitate EVs on the surface of negatively charged magnetic beads. We significantly improved the reproducibility of EV recovery and avoided positive false bias by including a washing step and optimizing the protocol. Well-characterized EV standards derived from pre-purified bovine milk were used for EVs isolation performance evaluation. An EVs recovery of up to 25% estimated with nanoparticle tracking analysis (NTA) was achieved for this batchwise PEG-based approach. The confirmation of isolated EVs identity was also made with our recently developed capillary electrophoresis (CE) method coupled with laser-induced fluorescent (LIF). In parallel, a purpose-made droplet platform working with magnetic tweezers was developed for translation of this PEG-based method into a droplet microfluidic protocol to further improve the performance in terms of EVs capture efficiency and high throughput. The droplet-based protocol offers a significant improvement of recovery rate (up to 50 %) while reducing sample and reagent volumes (by more than 10 folds) and operation time (by 3 folds) compared to the batch-wise mode.

Introduction

Extracellular vesicles (EVs) are phospholipid bilayer-delimited particles produced by most cell types and present in many body fluids [1, 2]. EVs contain and carry diverse biomolecules that are specific to the mother cells from which they are secreted, allowing them to transmit a variety of essential signals under both normal and pathological conditions. Hence, the potential of EVs as prognostic or diagnostic biomarkers has attracted significant attention in recent years [3-5]. Furthermore, due to their high specific targeting ability, EVs have gained much interest as engineered drug delivery systems for clinical and pharmaceutical applications [6, 7]. However, there are still technological hurdles to purify, analyze and characterize such nanometric bio-entities. Many methods for isolating EVs have been developed so far, including ultracentrifugation (UC), gradient ultracentrifugation, ultrafiltration (UF), polymer co-precipitation, size-exclusion liquid chromatography (SEC), immuno-extraction [8]. Among these, ultracentrifugation is widely considered as the gold standard in all EV applications. However, this technique presents many drawbacks, such as time-consuming procedures, contamination of EV populations by protein aggregates and other particles, damage to the EVs membrane structure and possible considerable loss of EVs (EVs yield may drop to 2%) [9, 10]. Thus, there is still an urgent need for emerging EVs isolation approaches that can provide EV purity and integrity in a reproducible and high-throughput manner. Many modern isolation methods have been developed in this direction, such as flow field-flow fractionation, ion-exchange, electrokinetic approaches as well as the combination of multiple techniques, like UC with UF or SEC [11-13]. In parallel, microfluidic technologies have made significant progresses for such purpose, exploiting both physical and biochemical properties of EVs at micro/nanoscale level for their capture and/or detection [14-19]. The majority of microfluidic approaches rely on immunoaffinity to selectively capture EVs. Immunoaffinity bead-based kits allow highly selective isolation of EVs through antibodies specific for target EVs surface

proteins [20-23]. However, following isolation, those commercial kits, which are rather used for subsequent EVs downstream lysis and analysis, do not provide any efficient elution possibility to recover intact EVs. Moreover, the main disadvantage of those strategies is the absence of universal EVs markers to ensure total capture of all EVs. Few recent works on capture and eventual elution of EVs on magnetic beads have been reported, using either electrostatic interaction [24], polymer mediated adsorption of EVs on magnetic beads [25], a DNA aptamer-based system [26] or DNA linker spacers [27]. No EVs recovery efficiency was reported in these works that used cell culture media and/or plasma samples as starting materials from which accurate EVs quantification is not trivial. At the actual stage, these works had to be realized batchwise with multiple in-tube steps without automation.

The goal of this study was to investigate bead-based strategies for isolating and recovering intact EVs without the use of immunoaffinity recognition and to adapt them to droplet microfluidics. For such purposes, well-characterized high-quality EVs isolated from bovine milk were used as EVs standards rather than non-quantified EVs from cell culture and plasma samples. Then, we transferred the more performing batchwise approach into an automated and high-throughput protocol relying on a microfluidic droplet train. Different operations in microfluidic droplets were developed and optimized to overcome the challenges of beads clustering and poor recirculation in droplets in the presence of viscous polymers, allowing to realise EVs capture on beads, washing and elution with a droplet sequence. So far, droplet microfluidics has been communicated only twice for immunoassay-based detection of EVs [28, 29] and has never been exploited for high performance and high throughput isolation of EVs.

Materials and methods

Chemicals and reagents

2-(Cyclohexylamino)ethanesulfonic acid (CHES), phosphate buffered saline (PBS 10x), sodium dodecyl sulfate (SDS, 98.5% (GC)), Tris(hydroxymethyl)aminomethane (Tris), Polyethylene glycol (PEG 8000), Albumin from human serum, IgG from human serum and Transferrin human were all obtained from Sigma Aldrich (St. Louis, MO, USA). Sodium hydroxide (1 M) and hydrochloric acid (1 M) were obtained from VWR (Fontenay-sous-Bois, France). All solutions were prepared with deionized water purified with a Direct- Q3 UV purification system (Millipore, Milford, MA, USA). Vybrant™ CFDA SE Cell Tracer Kit (dye 5-(and-6)-Carboxyfluorescein diacetate succinimidyl ester, CFDA-SE) was purchased from Thermo Fisher Scientific (Waltham, MA, USA). Fluorinert oil FC-40 (ZF-0002-1308-0) was purchased from 3 M (USA). The surfactant 1H, 1H, 2H, 2H – perfluoro-1-decanol was obtained from Sigma Aldrich. ExoCAS-2 kit containing poly-L-lysine-coated magnetic beads, washing and elution buffer solutions was purchased from Microgentas (Seongbuk-gu, Republic of Korea). Carboxylate functionalized magnetic beads (Dynabeads MyOne, 10 mg/mL, diameter of 1 µm) and silica-based magnetic beads (Dynabeads MyOne SILANE, 40 mg/ml, diameter of 1 µm) were obtained from Thermo Fisher Scientific. EVs samples isolated from bovine milk were provided by Excilone (Elancourt, France).

Apparatus and Material

For macroscale protocols, all magnetic-bead-based assays in batch were carried out in protein LoBind 1.5 mL tubes purchased from Eppendorf (Hamburg, Germany). For retaining magnetic beads, a neodymium magnet purchased from Ademtech (Adem Mag MSV, Bessac, France) was used. Shaking of magnetic bead suspensions during the incubation and washing steps was realized with a mixer (Eppendorf ThermoMixer C).

For droplet microfluidic operations, a microfluidic droplet platform was constructed and was inspired from our previous configuration [30]. It comprises a syringe pump (from Nemesys, Cetoni GmbH) equipped with 1 mL glass syringes (purchased from SGE) and a motorized pipettor arm (Rotaxys, Cetoni GmbH), used for droplets generation. A 96-well plate (Thermo Scientific) was used for sample storage and reagent solutions. The plate was mounted on a custom-made holder that can be moved in the X, Y, and Z directions. PTFE tubing with ID of 0.3 mm and OD of 0.6 mm (Z609692-1PAK, Sigma Aldrich) was used to conduct the droplet trains. Fluorinated oil FC-40 mixed with the surfactant (1H, 1H, 2H, 2H – perfluoro-1-decanol, 2% w/w) was used to separate aqueous droplets inside PTFE tubing. In the protocol, a magnetic tweezer, prepared in-house was used. It is composed of a paramagnetic tip activated by a magnetic coil. Macro Objective (MLH-10X) mounted on a low-cost CMOS Cameras (acA1300-60 gm, Basler) and white LED back light illumination (Schott Lighting and Imaging) were employed for droplet observation.

The CE-LIF analyses were performed with a PA 800 Plus system (Sciex Separation, Brea, CA) equipped with a solid-state laserinducedfluorescence detector (excitation wavelength of 488 nm, emission wavelength of 520 nm) purchased from Integrated Optics (Art. No. 40A-48A-52A-64A-14-DM-PT, distributed by Acal BFi, Evry, France). Uncoatedfused silica capillaries were purchased from CM Scientific (Silsden,UK). Data acquisition and instrument control were carried out using Karat 8.0 software (Sciex Separation, Brea, CA).

Methods

Isolation of bovine milk-derived EVs with sucrose gradient ultracentrifugation

Skimmed bovine milk samples were obtained by centrifugation of 50 ml whole milk at 3,000 g for 30 min at 4°C (Allegra X-15R, Beckman Coulter, France). The whey was obtained after acid

precipitation with 10% (v/v) acetic acid, incubation at 37 °C for 10 minutes and 10% (v/v) 1M sodium acetate for 10 minutes at RT followed by centrifugation at 1500g, 4°C for 15 min and filtration using vacuum-driven filtration system Millipore Steritop, 0.22 µm. The whey supernatants were concentrated using Amicon 100kDa centrifugal filter units (Merck Millipore) at 4,000 g and 20°C up to final volume of 6 mL. The obtained retentate was ultra-centrifuged for pelleting the EVs at 100 000 g for 1h10 at 4°C (Beckman Coulter, Optima XPN-80, 50TI rotor). The pellets were solubilized in 500 µL of PBS then added to 11 ml of pre-prepared sucrose gradient 5-40% and ultra-centrifuged at 200 000 g for 18h at 4°C (Beckman Coulter, Optima XPN-80, SW41 rotor). Fractions of 1 mL were collected and the selected ones containing targeted exosome population were diluted in 6 ml of PBS 1X and finally centrifuged at 100 000 g for 1h10 at 4°C (Beckman Coulter, Optima XPN-80, 50TI rotor). The pellets were resuspended in 50 µL of PBS 1X and stored at -80°C, until further analyses.

Isolation of pony plasma and serum derived EVs with size exclusion chromatography (SEC)

Preparation of plasma: Peripheral blood was collected into EDTA-coated vacutainer tubes. After ten-time inversion, samples were processed within the 60 minutes of collection. Consecutive centrifugation steps at 2,500 g, 4°C for 15 minutes and then at 15 000 g for 10 minutes were performed followed by filtration of the supernatant through 0.22µm filters. Preparation of serum: Whole blood was collected into anticoagulant-free tubes and allowed to clot at room temperature for 45 minutes. The clot was removed by centrifuging at 3 200 g, 4°C for 15 minutes, followed by centrifugation at 15 000 g, 4°C for 10 minutes and filtration of the supernatant through 0.22µm filters. 500 µl of pre-treated plasma/serum was loaded onto a qEVoriginal SEC column (Izon Science, New Zealand) previously washed and equilibrated with PBS. Fraction collection (0.5 mL per fraction) was carried out immediately using PBS 1X as elution buffer. The selected elution fractions were pooled and were subsequently

concentrated using 100 kDa Amicon centrifugal filter units (Merck Millipore). Post-treatment processing with several washing steps with PBS was applied to obtain highly pure EV fractions highly enriched with exosomes.

EV isolation using commercial kits

ExoCAS-2 magnetic bead-based ion exchange kit was used for the study of EV yield performance. The experimental procedure is described in a paper recently published [24]. Briefly, PLL-coated beads were mixed with our standard EVs (bovine milk derived EVs), followed by incubation of the mixture for 30 min at 4° C in a rocking platform mixer. After incubation, the EVs-bound beads were carefully washed with 2 mL of ExoCAS-2 washing solution and then re-suspended in ExoCAS-2 elution solution by shaking for 5 min at 1000 rpm. Finally, a magnet was employed to retain magnetic beads and the supernatant containing yielded EVs was collected.

PEG-based EVs precipitation on magnetic beads in batch mode

For PEG-based EVs precipitation on magnetic beads in batch, a volume of 200 µL of PEG (25 % m/v), 150 µL of carboxylate functionalized magnetic beads (10 mg/mL) and 250 µL of deionized water was incubated with 400 µL of standard EVs or biological fluid (simulated human serum and pony plasma and serum, 5 times diluted with deionized water) on a mixer at 25 ° C for 1 h at 700 rpm. Beads were then carefully washed twice with PEG 5%/ NaCl 0.2 M. After removal of washing solution, the magnetic beads in tubes were re-dispersed in 400 µL of PBS 1X solution and then incubated on shaking for 5 min at 25 °C for EV elution. A magnet was used to remove the magnetic beads, and EVs were recovered in the supernatant.

PEG-based EVs precipitation on magnetic beads using the microfluidic droplet platform

A robotic arm and a 500 μ L syringe were utilized to pipette the droplets from separate reservoirs into a PTFE tube in a fully automated manner. To complete one PEG-based EVs precipitation protocol, a train of 5 droplets (each containing 6 μ L) confined and separated by oil was required. It includes: i) one droplet of carboxylate functionalized magnetic beads (1.5 mg/mL), ii) one droplet of EV sample in PEG 5%, iii-iv) two droplets of washing solution (PEG 5%/NaCl 0.2 M) and v) one droplet of elution solution (PBS 1X). Beads were trapped out of one droplet and released into another by electronic triggering of the magnetic tweezer. The incubation was carried out with regular droplet back and forth movements at RT for 25 min. After incubation, two washing droplets are flushed over EVs-bound beads. The EVs-bound beads were then dispersed into the elution droplet with regular droplet back and forth movements at RT for 5 min. The elution droplet containing released EVs was then collected in a tube for downstream analysis.

Nanoparticle Tracking Analysis (NTA) of EVs

Particle concentration and size distribution were determined with a Nanosight NS300 instrument (Malvern, version NTA 3.2 Dev Build 3.2.16) equipped with a 405 nm laser, sCMOS camera type and the NTA software v3.1. The video acquisition was performed using a camera level of 14. Per sample, 3 videos of 90 seconds with a frame rate of 30 frames/sec were captured at 25°C and subsequently analyzed with a threshold set up at 5. The results were validated with at least 2,000 valid tracks for each triplicate. All experiments were carried out with pre-diluted samples in PBS according to input sample concentrations, leading to particle concentration within the 10^6 - 10^9 particles per ml range for optimal analysis.

The Zetaview system (Particle Metrix, Germany) was equipped with a 488 nm laser. Measurement concentrations were obtained by pre-diluting the samples to the ideal 50–200 particles/frame. Each experiment was performed in duplicate on 11 different positions within the sample cell with following specifications and analysis parameters: cell temperature 25°C, sensitivity 70, shutter 100, Max Area 1000, Min Area 10, Min Brightness 25. The results were validated while obtaining at least 1 000 valid tracks for each run. For data capture and analysis, the Nanoparticle Tracking Analysis Software (ZNTA) vs 8.05.04 was used.

CE-LIF of fluorescent labelled EVs

Details on the CE-LIF method for EVs analysis can be seen in our recent work [31]. Briefly, fluorescently labelled EVs were prepared using the 5-(and-6)-Carboxyfluorescein diacetate succinimidyl ester (CFDA-SE). After removal of residual CFDA-SE via filtration with commercial Exosome Spin Columns (MW 3000, Thermo Fisher Scientific Waltham, MA USA), labelled EVs were analysed with CE-LIF using a fused silica capillary having I.D. of 50 μm , effective length (L_{eff}) of 50.2 cm and total length (L_{tot}) of 60.2 cm. The capillary was pre-conditioned with water for 10 min, 1 M NaOH for 10 min, 1 M HCl for 10 min and then water for 10 min. The rinsing between two analyses was carried out with 50 mM SDS for 5 min, 1 M NaOH for 5 min, deionized water for 5 min, and finally the running BGE composed of Tris / CHES (IS 90 mM, pH 8.4) for 5 min using a pressure of 30 psi. EVs samples were injected hydrodynamically from the inlet end by applying a pressure of 0.5 psi for 2 min. The separation was carried out under 25 kV (normal polarity) at 25 °C and the samples were kept at 5 °C with the sample storage module of the PA 800 Plus equipment.

Results and Discussion

Batchwise EVs isolation development

With the aim to establish a high-performance and high-throughput microfluidic droplet system for EVs isolation, we evaluated two recently communicated batchwise EV-enrichment strategies that are alternative approaches to the immunoaffinity-based ones. They hold high potential for subsequent translation into a microfluidic format in terms of minimal forefront preparations, non-laborious operations, as well as ease of manipulation and step transition thanks to the use of magnetic beads as cargos. The first one is a magnetic bead-mediated selective adsorption strategy (MagExo), exploiting the presence of a water-excluding polymer, polyethylene glycol (PEG), to lock up a significant number of water molecules, forcing thereby the EVs to aggregate and precipitate on the surface of magnetic beads [25]. The second strategy called ExoCAS-2 relies on an ionic exchange mechanism, using magnetic beads coated with a polycationic polymer, poly-L-lysine (PLL), to quickly trap negatively charged EVs via electrostatic interaction [24]. For performance comparison, EVs standards derived from bovine milk having narrow size distribution, with well-defined concentrations and exhaustive characterizations by NTA, DLS, LC-MS/MS and TEM, were used as starting sample. TEM images revealed the absence of contaminating protein residues in these EVs standards (Fig. S1A in the supporting information ESI), and major protein contaminants (e.g. α -s1 casein, β -casein, α -Lactalbumin and serum albumin) were not found according to the LC-MS/MS analysis (Fig. S1B). The use of EV standards of high purity allowed to evaluate the EVs recovery more accurately. In our case, quantification of EVs isolation yields obtained with MagExo and ExoCAS-2 methods was possible by comparing the EVs concentrations before and after isolation processes (see Fig. 1). Unsatisfactory EVs recovery (less than 10%) was obtained with commercial PLL-coated beads, compared to that achieved when using PEG and silica magnetic beads (34 %). NTA data also showed a size shift towards smaller particles when

EVs were eluted from PLL beads. This could be a consequence of PLL release from the beads during the elution process. This was confirmed by the CE-LIF analysis (discussion below). This led to a critical PLL concentration in the eluent that is high enough to cause EVs lysis. Indeed, several studies have shown that PLL can penetrate through vesicles via interaction with the lipid membrane [32-34], provoking vesicle lysis from a certain threshold concentration of PLL [35]. In parallel to NTA measurements for EVs recovery evaluation, we used our recently developed CE-LIF approach [31] to validate the identity of EVs collected with MagExo and ExoCAS-2 methods (see Fig.2). The peak profile of EVs collected with PEG-based protocol corresponds well to the fingerprint of bovine milk-derived EVs, confirming the presence of intact EVs in the eluent (Fig. 2A). On the contrary, with the ion exchange method, multiple tagged species were detected. To understand the origin of these peaks, solutions containing different PLL concentrations without the presence of EVs were analyzed. As can be seen in Fig. 2B, many peaks were still detected, whose intensities were related to the PLL concentrations. These results confirmed the hypotheses that the peaks observed come from PLL leakage from the magnetic beads, which could not be visualized with conventional NTA. The released PLL which can be labelled by the residual CFDA-SE dye through its amino groups lead to unwanted products in the eluent. The ExoCAS-2 method was therefore not further considered and the PEG-based method (MagExo) was chosen for further optimisation.

Besides the preservation of intact EVs after purification, protocol reproducibility is another important point to consider to guarantee consistency of isolated EVs population and quality. Indeed, by reproducing the MagExo procedure described in reference [25], we observed significant batch-to-batch variation in vesicle concentration (RSD 30 %). The lack of EVs washing between the capture and elution steps in the original protocol led to misleading data. To minimize this cross contamination and to recover intact EVs for further characterization, we

developed a washing protocol after the EVs capture step. By adding two consecutive washing steps with PEG 5% w/v to remove residual unbound EVs while maintaining captured EVs on magnetic beads, we significantly improved the repeatability (RSD) to 8 %. This came with some penalty, as the EV isolation yield fell to 17%. To further improve the performance of EVs capture and thus isolation yield, we carried out different optimizations on magnetic bead concentrations (0.5 – 1.5 mg/mL), bead chemical surface (with carboxylic or silane groups), incubation temperature for EVs capture (4 – 25 °C) as well as PEG concentrations (5-15 % w/v) (see Fig. S2 in the ESI). The highest EVs recovery rate (after 2 washing steps) of 25 % was achieved with the optimized conditions using PEG concentration of 5% and carboxylic magnetic beads' concentration of 1.5 mg/mL with 1 h incubation at 25 °C. Higher PEG or beads' concentrations were also tested but did not lead to better EVs isolation yields. Conveniently, the working temperature of 25°C is well adapted for subsequent translation of batchwise protocol into a microfluidic format where cooling function is not readily available.

Droplet microfluidics for EVs isolation: proof of concept

The optimised batchwise PEG-based method was subsequently converted into a microfluidic droplet protocol in order to provide a high level of automation and integration, significant reduction in sample/reagent amounts, and a higher performance in terms of isolation efficiency. The instrumental setup of the purpose-made microfluidic platform, composed of a syringe pump, a motorized pipettor arm for droplet production, a 96-well plate for sample and reagent storage and a magnetic tweezer for manipulation of magnetic beads, is shown in Fig. 3. With this system, we used a train of 6 μ L droplets containing in a defined sequence (i) the magnetic bead suspension, (ii) EVs sample, (iii) washing and (iv) elution solutions to replace different tube-based steps. When working with the droplet-wise multi-step protocol, one hurdle encountered is the difficulty to efficiently transfer the target species (EVs in this case) from one

droplet to another without any risk of cross contamination. This was expected to be overcome with our setup through the use of magnetic beads as the controllable carrier of target analytes between droplets. A purpose-made magnetic tweezer, composed of a paramagnetic tip activated by an electrical coil [30, 36], was employed to manipulate magnetic beads between droplets via application of an external electrical field. Table 1 provides an overview of the operation sequence. A train of droplets containing different solutions and sample in a defined order was delivered through the magnetic tweezer where the beads were extracted from the first droplet and transported into the sample one containing EVs. The incubation was subsequently performed by pushing the droplet train back and forth inside the tubing. The magnetic beads that retain EVs on their surface were then trapped by the magnetic tweezer and the supernatant droplet was washed away, followed by flushing of the trapped magnetic beads with two washing droplets. The washed beads were finally released into an elution droplet that was finally collected in an oil-containing tube for further analyses.

Several problems were however encountered that led to failure of such droplet protocol in our first experiments, notably beads clustering and poor recirculation in droplets in the presence of PEG. Indeed, the beads often stayed at the rear of moving droplet, forming undesired bead clusters when the droplet moved inside the tubing over an extended distance. This was ascribed to come from the presence of PEG which significantly increased droplet viscosity [37], which in turn impaired the effective recirculation of the beads (see Fig. S3 in the ESI). To enhance recirculation of the beads within a droplet, we put our efforts on optimizing the droplet movement pattern and travel volume (i.e., the oil volume required to push and pull the droplet) during the back-and-forth movement. Chaotic trajectories are known to enhance mixing efficiency [38, 39]. Consequently, different droplet movement patterns were also tested, including the straight, the U-shaped patterns (i.e., the tubing was shaped over a metallic

guideline) and the spiral-formed one (i.e., the tubing was coiled around a cylindrical support) (see Fig. S4 in ESI). With the straight pattern, bead aggregation was always observed in the presence of PEG, regardless of the travel volume (Fig. S3A). For other movement patterns, bead clustering was alleviated but still visible when working with a large travel volume of 10 μL (Fig. S3 B and C). This undesired phenomenon was finally avoided when employing the spiral or U-shaped patterns with a short travel volume of 6 μL (equivalent to a droplet volume). By keeping these optimized setups and conditions, we further investigated the in-droplet incubation duration (from 5 to 45 min) during the EVs capture step (Fig. S5 in the ESI). The best EVs recovery of 27 % was found for 25 min incubation when using the spiral-formed pattern. Longer incubation time did not result in any improvement of EVs recovery. Under the same optimized conditions, the U-shaped pattern offered the best EVs recovery rate of 39%. Note that the droplet system offers higher EVs isolation yields than that obtained with the batchwise setup, regardless of the droplet movement pattern used. To obtain more precise information on the quality of the isolated EVs, the samples were analyzed with Particle Metrix' ZetaView [40]. As revealed by Zetaview data (Fig. 4B), 80% of the recovered EVs fell within the range of the initial size distribution, while the remaining 20% were represented by larger aggregates. These aggregates are presumably formed due to the PEG capacity to wrap and condense hundreds of EVs, making them hard to resuspend in the absence of PEG during the elution step.

Microfluidic droplet-based isolation of EVs from biofluids

The developed microfluidic droplet instrument and protocol were then used to isolate EVs from more complex matrices. First, we used PBS mixed with three main extracellular matrix proteins, including albumin, IgG and transferrin to imitate human extracellular fluids [41]. This simulated human serum was then spiked with standard EVs (i.e., bovine milk derived EVs at

1.02×10^{11} particles/mL) and passed through the microfluidic droplet system to evaluate the EVs isolation performance. As indicated in Fig. 5, the concentration of collected EVs was 3.69×10^{10} particles/mL, giving an EVs recovery rate of 36% with spiked simulated human serum, which was not far from that obtained with pure standard EVs (39%). We then applied the droplet protocol to pony plasma and serum (Fig. S6 in ESI). When dealing with such complex biofluid matrices, the droplet approach gave an overall NTA-measured particle concentration eight-time higher than that obtained with the in-tube method. To confirm the identity of EVs isolated from plasma and serum samples, the elution droplets were also analysed with CE-LIF to reveal different EVs subpopulations (Fig. 6). Based on the peak intensities in each electropherogram, the highest concentration was found for the fraction with the shortest migration time (9-12 min) whereas the signal of the second peak zone (12-15 min) was less intense and this is more remarked for the serum samples. This kind of EVs fingerprints was found similar to those obtained in our previous work with EVs from pony plasma and serum isolated by SEC [31]. Interestingly, the third peak zone (15-20 min) appeared in the electropherograms obtained with both in-batch mode and the droplet system, suggesting that a distinct subpopulation emerges when using the PEG-based isolation methods. Indeed, different isolation methods may lead to the shift or differences in size distributions of the collected EVs, as already evidenced for SEC and UC isolation methods [42, 43]. In our case, the PEG-based method is expected to capture non-selectively all EVs subpopulations, leading to more EVs fractions being visualized with CE-LIF as seen in Fig. 6. NTA measurements for both pony serum and plasma revealed a shift towards smaller size distributions when using the droplet approach (Fig. S6 in ESI). This may correspond to an increased concentration of the small-sized subpopulations, which may correlate to the more pronounced appearance of the third peak zone (15-20 min) in the CE-LIF electropherograms. Nevertheless, no further speculation was made to interpret the presence of these three subpopulations observed by CE as no clear

relationship between size and charge properties of EVs and their electrophoretic mobilities can be stated at this stage.

Conclusion remarks

We successfully developed a new approach (instrumentation and methodology) for EVs isolation from both pre-purified standards and biofluid samples, for the first time in microfluidic droplet format. Using a train of micrometric droplets containing respectively magnetic beads, sample, washing and elution solutions, we allowed significant sample and reagent volume reduction (by 5 times), minimization of manual operations, diminution of operation time (by twice) and improvement of EVs recovery rate by almost 2 folds. Thanks to automatization and miniaturization that we achieved with droplet microfluidics higher throughput can now be expected. Integration of this microfluidic EVs isolation module as a forefront of downstream EVs analysis and characterization is now envisaged.

Acknowledgement

This work has been financially supported by the Institut Universitaire de France (for M. Taverna, senior member) and the Agence Nationale de la Recherche (ANR, France) with the grant no. ANR-18-CE29-0005-01. The European fellowship for Lucile Alexandre was supported by the project H2020-MSCA-IF-2019 (IMPED 896313). The doctoral scholarship for Marco Morani was supported by the doctoral school 2MIB (Sciences Chimiques: Molécules, Matériaux, Instrumentation et Biosystèmes) – University Paris Saclay.

The authors have declared no conflict of interest.

References:

- [1] G. van Niel, G. D'Angelo, G. Raposo, Shedding light on the cell biology of extracellular vesicles, *Nat. Rev. Mol. Cell Biol* 19(4) (2018) 213-228. <https://doi.org/10.1038/nrm.2017.125>.
- [2] L.M. Doyle, M.Z. Wang, Overview of Extracellular Vesicles, Their Origin, Composition, Purpose, and Methods for Exosome Isolation and Analysis, *Cells* 8(7) (2019) 24. <https://doi.org/10.3390/cells8070727>.
- [3] C. Thery, Diagnosis by extracellular vesicles, *Nature* 523(7559) (2015) 161-162.
- [4] J. Howitt, A.F. Hill, Exosomes in the Pathology of Neurodegenerative Diseases, *J. Biol. Chem.* 291(52) (2016) 26589-26597. <https://doi.org/10.1074/jbc.R116.757955>.
- [5] W. Guo, Y.B. Gao, N. Li, F. Shao, C.N. Wang, P. Wang, Z.L. Yang, R.D. Li, J. He, Exosomes: New players in cancer, *Oncology Reports* 38(2) (2017) 665-675. <https://doi.org/10.3892/or.2017.5714>.
- [6] P. Vader, E.A. Mol, G. Pasterkamp, R.M. Schiffelers, Extracellular vesicles for drug delivery, *Advanced drug delivery reviews* 106 (2016) 148-156.
- [7] H.C. Bu, D.G. He, X.X. He, K.M. Wang, Exosomes: Isolation, Analysis, and Applications in Cancer Detection and Therapy, *Chembiochem* 20(4) (2019) 451-461. <https://doi.org/10.1002/cbic.201800470>.
- [8] Z. Zhao, H. Wijerathne, A.K. Godwin, S.A. Soper, Isolation and analysis methods of extracellular vesicles (EVs), *Extracellular Vesicles and Circulating Nucleic Acids* 2(1) (2021) 80-103.
- [9] C. Gardiner, D. Di Vizio, S. Sahoo, C. Thery, K.W. Witwer, M. Wauben, A.F. Hill, Techniques used for the isolation and characterization of extracellular vesicles: results of a worldwide survey, *J. Extracell. Vesicles* 5 (2016). <https://doi.org/10.3402/jev.v5.32945>.
- [10] M.Y. Konoshenko, E.A. Lekhnov, A.V. Vlassov, P.P. Laktionov, Isolation of Extracellular Vesicles: General Methodologies and Latest Trends, *Biomed Res. Int.* (2018) 27. <https://doi.org/10.1155/2018/8545347>.
- [11] H. Yan, Y. Li, S. Cheng, Y. Zeng, Advances in Analytical Technologies for Extracellular Vesicles, *Analytical chemistry* 93(11) (2021) 4739-4774.
- [12] T. Liangsupree, E. Multia, M.-L. Riekkola, Modern isolation and separation techniques for extracellular vesicles, *J. Chromatogr. A* 1636 (2021) 461773. <https://doi.org/https://doi.org/10.1016/j.chroma.2020.461773>.
- [13] M. Morani, T.D. Mai, Z. Krupova, G. van Niel, P. Defrenaix, M. Taverna, Recent electrokinetic strategies for isolation, enrichment and separation of extracellular vesicles, *TrAC Trends in Analytical Chemistry* (2021) 116179.
- [14] S. Hassanpour Tamrin, A. Sanati Nezhad, A. Sen, Label-Free Isolation of Exosomes Using Microfluidic Technologies, *ACS Nano* (2021).
- [15] Y. Meng, M. Asghari, M.K. Aslan, A. Yilmaz, B. Mateescu, S. Stavrakis, A.J. deMello, Microfluidics for extracellular vesicle separation and mimetic synthesis: Recent advances and future perspectives, *Chemical Engineering Journal* 404 (2021) 126110.
- [16] D. Yang, W. Zhang, H. Zhang, F. Zhang, L. Chen, L. Ma, L.M. Larcher, S. Chen, N. Liu, Q. Zhao, P.H.L. Tran, C. Chen, R.N. Veedu, T. Wang, Progress, opportunity, and perspective on exosome isolation - efforts for efficient exosome-based theranostics, *Theranostics* 10(8) (2020) 3684-3707. <https://doi.org/10.7150/thno.41580>.
- [17] W.T. Su, H.J. Li, W.W. Chen, J.H. Qin, Microfluidic strategies for label-free exosomes isolation and analysis, *Trac-Trends Anal. Chem.* 118 (2019) 686-698. <https://doi.org/10.1016/j.trac.2019.06.037>.

- [18] Y. Jia, Z.H. Ni, H. Sun, C. Wang, Microfluidic Approaches Toward the Isolation and Detection of Exosome Nanovesicles, *Ieee Access* 7 (2019) 45080-45098. <https://doi.org/10.1109/access.2019.2907123>.
- [19] S.J. Lin, Z.X. Yu, D. Chen, Z.G. Wang, J.M. Miao, Q.C. Li, D.Y. Zhang, J. Song, D.X. Cui, Progress in Microfluidics-Based Exosome Separation and Detection Technologies for Diagnostic Applications, *Small* 16(9) (2020). <https://doi.org/10.1002/sml.201903916>.
- [20] H. Shao, J. Chung, K. Lee, L. Balaj, C. Min, B.S. Carter, F.H. Hochberg, X.O. Breakefield, H. Lee, R. Weissleder, Chip-based analysis of exosomal mRNA mediating drug resistance in glioblastoma, *Nature communications* 6(1) (2015) 1-9.
- [21] M. Garcia-Contreras, S.H. Shah, A. Tamayo, P.D. Robbins, R.B. Golberg, A.J. Mendez, C. Ricordi, Plasma-derived exosome characterization reveals a distinct microRNA signature in long duration Type 1 diabetes, *Scientific Reports* 7 (2017) 10. <https://doi.org/10.1038/s41598-017-05787-y>.
- [22] M.N. Madison, J.L. Welch, C.M. Okeoma, Isolation of Exosomes from Semen for in vitro Uptake and HIV-1 Infection Assays, *Bio-protocol* 7(7) (2017) 21. <https://doi.org/10.21769/BioProtoc.2216>.
- [23] C. Campos-Silva, H. Suárez, R. Jara-Acevedo, E. Linares-Espinós, L. Martinez-Piñeiro, M. Yáñez-Mó, M. Valés-Gómez, High sensitivity detection of extracellular vesicles immune-captured from urine by conventional flow cytometry, *Scientific reports* 9(1) (2019) 1-12.
- [24] H. Kim, S. Shin, ExoCAS-2: Rapid and Pure Isolation of Exosomes by Anionic Exchange Using Magnetic Beads, *Biomedicines* 9(1) (2021) 12. <https://doi.org/10.3390/biomedicines9010028>.
- [25] X. Fang, C. Chen, B. Liu, Z. Ma, F. Hu, H. Li, H. Gu, H. Xu, A magnetic bead-mediated selective adsorption strategy for extracellular vesicle separation and purification, *Acta biomaterialia* (2021).
- [26] K. Zhang, Y. Yue, S. Wu, W. Liu, J. Shi, Z. Zhang, Rapid capture and nondestructive release of extracellular vesicles using aptamer-based magnetic isolation, *ACS sensors* 4(5) (2019) 1245-1251.
- [27] D. Brambilla, L. Sola, A.M. Ferretti, E. Chiodi, N. Zarovni, D. Fortunato, M. Criscuoli, V. Dolo, I. Giusti, V. Murdica, EV Separation: Release of Intact Extracellular Vesicles Immunocaptured on Magnetic Particles, *Analytical chemistry* 93(13) (2021) 5476-5483.
- [28] C. Liu, X. Xu, B. Li, B. Situ, W. Pan, Y. Hu, T. An, S. Yao, L. Zheng, Single-exosome-counting immunoassays for cancer diagnostics, *Nano letters* 18(7) (2018) 4226-4232.
- [29] J. Ko, Y. Wang, K. Sheng, D.A. Weitz, R. Weissleder, Sequencing-Based Protein Analysis of Single Extracellular Vesicles, *ACS Nano* 15(3) (2021) 5631-5638. <https://doi.org/10.1021/acsnano.1c00782>.
- [30] T.D. Mai, D. Ferraro, N. Aboud, R. Renault, M. Serra, N.T. Tran, J.-L. Viovy, C. Smadja, S. Descroix, M. Taverna, Single-step immunoassays and microfluidic droplet operation: Towards a versatile approach for detection of amyloid-beta peptide-based biomarkers of Alzheimer's disease, *Sens. Actuators B* 255 (2018) 2126-2135.
- [31] M. Morani, T.D. Mai, Z. Krupova, P. Defrenaix, E. Multia, M.-L. Riekkola, M. Taverna, Electrokinetic characterization of extracellular vesicles with capillary electrophoresis: a new tool for their identification and quantification, *Anal. Chim. Acta* (2020).
- [32] D. Volodkin, V. Ball, P. Schaaf, J.C. Voegel, H. Mohwald, Complexation of phosphocholine liposomes with polylysine. Stabilization by surface coverage versus aggregation, *Biochim. Biophys. Acta-Biomembr.* 1768(2) (2007) 280-290. <https://doi.org/10.1016/j.bbamem.2006.09.015>.

- [33] D. Volodkin, H. Mohwald, J.C. Voegel, V. Ball, Coating of negatively charged liposomes by polylysine: Drug release study, *Journal of Controlled Release* 117(1) (2007) 111-120. <https://doi.org/10.1016/j.jconrel.2006.10.021>.
- [34] Y. Takechi, H. Tanaka, H. Kitayama, H. Yoshii, M. Tanaka, H. Saito, Comparative study on the interaction of cell-penetrating polycationic polymers with lipid membranes, *Chem. Phys. Lipids* 165(1) (2012) 51-58. <https://doi.org/10.1016/j.chemphyslip.2011.11.002>.
- [35] A. Gorman, K.R. Hossain, F. Cornelius, R.J. Clarke, Penetration of phospholipid membranes by poly-L-lysine depends on cholesterol and phospholipid composition, *Biochim. Biophys. Acta-Biomembr.* 1862(2) (2020) 10. <https://doi.org/10.1016/j.bbamem.2019.183128>.
- [36] A. Ali-Cherif, S. Begolo, S. Descroix, J.-L. Viovy, L. Malaquin, Programmable Magnetic Tweezers and Droplet Microfluidic Device for High-Throughput Nanoliter Multi-Step Assays, *Angew. Chem. Int. Ed.* 51(43) (2012) 10765-10769. <https://doi.org/https://doi.org/10.1002/anie.201203862>.
- [37] U. Gündüz, Viscosity prediction of polyethylene glycol–dextran–water solutions used in aqueous two-phase systems, *Journal of Chromatography B: Biomedical Sciences and Applications* 743(1-2) (2000) 181-185.
- [38] M.A. Stremmer, F.R. Haselton, H. Aref, Designing for chaos: applications of chaotic advection at the microscale, *Philos. Trans. R. Soc. A-Math. Phys. Eng. Sci.* 362(1818) (2004) 1019-1036. <https://doi.org/10.1098/rsta.2003.1360>.
- [39] D. Bedding, C. Hidrovo, Asme, Investigation Of Mixing in Colliding Droplets Generated in Flow-Focusing Configurations Using Laser Induced Fluorescence, *Amer Soc Mechanical Engineers*, New York, 2016.
- [40] D. Bachurski, M. Schuldner, P.H. Nguyen, A. Malz, K.S. Reiners, P.C. Grenzi, F. Babatz, A.C. Schauss, H.P. Hansen, M. Hallek, E.P. von Strandmann, Extracellular vesicle measurements with nanoparticle tracking analysis - An accuracy and repeatability comparison between NanoSight NS300 and ZetaView, *J. Extracell. Vesicles* 8(1) (2019). <https://doi.org/10.1080/20013078.2019.1596016>.
- [41] J.A. Jaros, P.C. Guest, S. Bahn, D. Martins-de-Souza, Affinity depletion of plasma and serum for mass spectrometry-based proteome analysis, *Proteomics for Biomarker Discovery*, Springer 2013, pp. 1-11.
- [42] K. Takov, D.M. Yellon, S.M. Davidson, Comparison of small extracellular vesicles isolated from plasma by ultracentrifugation or size-exclusion chromatography: yield, purity and functional potential, *Journal of extracellular vesicles* 8(1) (2019) 1560809.
- [43] K. Brennan, K. Martin, S. FitzGerald, J. O'Sullivan, Y. Wu, A. Blanco, C. Richardson, M. Mc Gee, A comparison of methods for the isolation and separation of extracellular vesicles from protein and lipid particles in human serum, *Sci. Rep.* 10(1) (2020) 1-13.

Table 1: Operation sequence of the microfluidic droplet protocol using droplets of 6 μL each

| Operation | Droplet composition | Flowrate ($\mu\text{L/s}$) | Incubation time (min) | Back-and-forth droplet travel distance (+/- μL) |
|-------------------|---|--|----------------------------------|--|
| Sample incubation | EVs sample + PEG 5% (w/v) + magnetic beads (1.5 mg/mL | 4 | 25 | 6 |
| Washing 1 | PEG 5% / NaCl 0.2 M | 0.5 | Flush | - |
| Washing 2 | PEG 5% / NaCl 0.2 M | 0.5 | Flush | - |
| Sample elution | PBS 1X | 4 | 5 | 6 |

Figure:

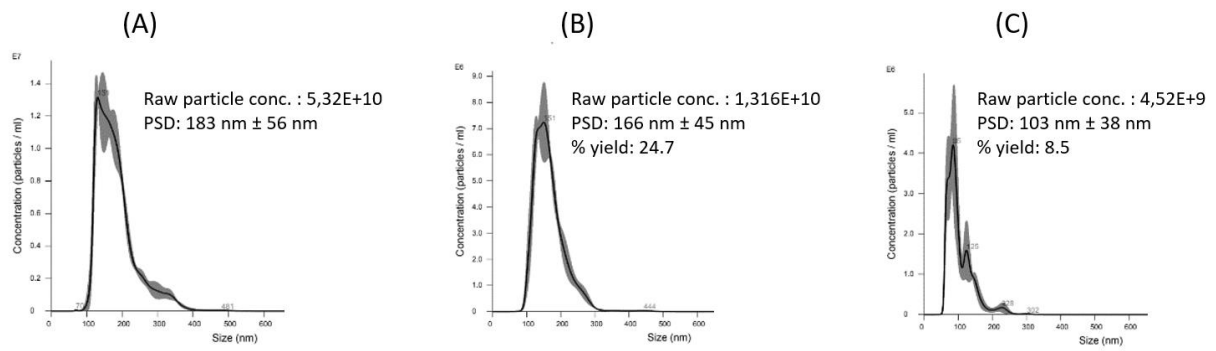


Fig. 1. NTA measurements of EVs isolated from bovine milk before purification (A) and after purification with (B) MagExo or (C) ExoCAS-2 method.

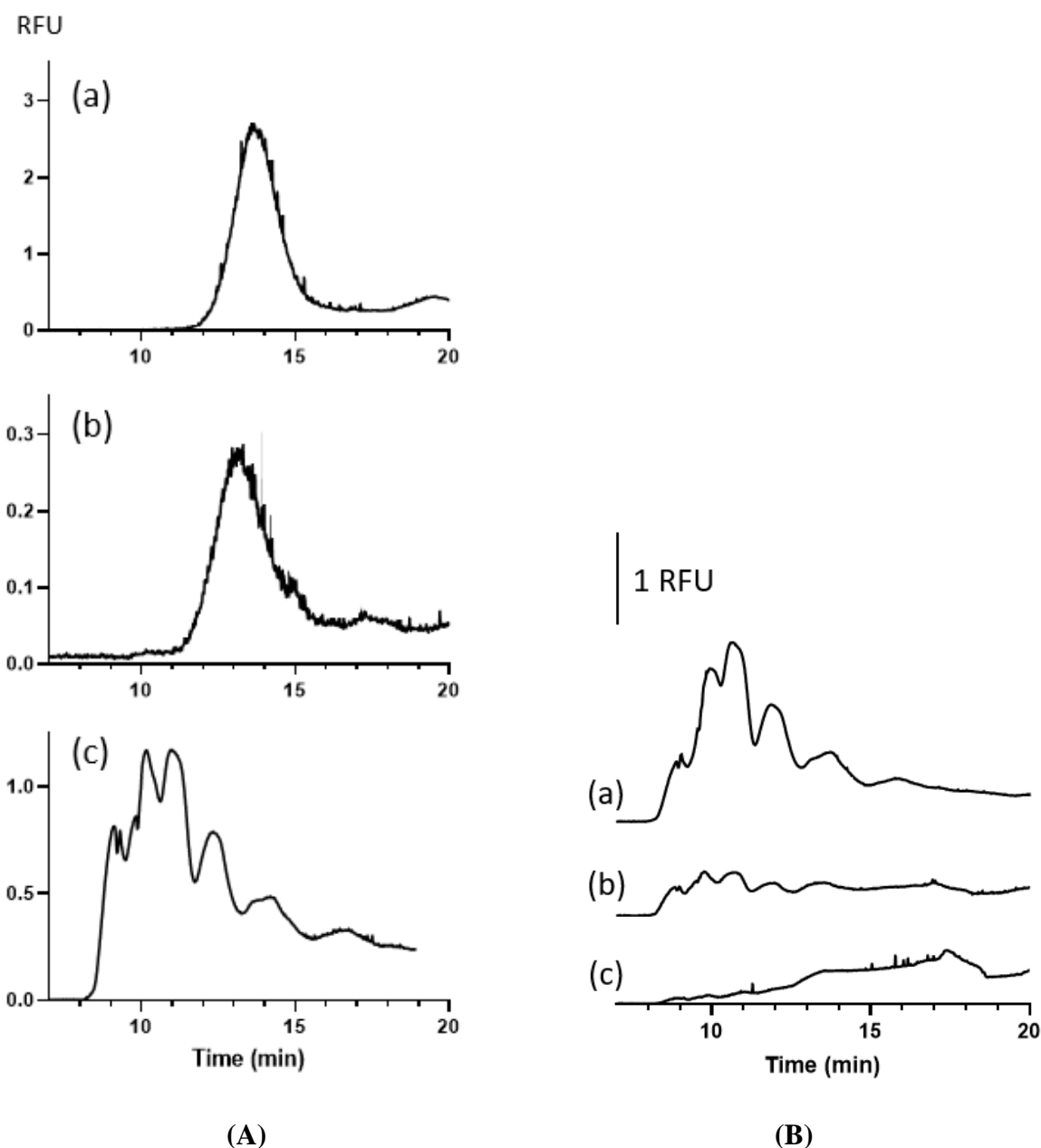


Fig. 2. (A) CE-LIF measurements of EVs before purification (a), and after purification with (b) MagExo or (c) ExoCAS-2 method. (B) CE-LIF profiles of solutions of PLL at different concentrations, corresponding to PLL-coated beads suspension volumes of (a) 1 mL; (b) 0.5 mL; (c) 0.1 mL. CE-LIF conditions: fused silica capillary having I.D. of 50 μm , effective length (L_{eff}) of 50.2 cm and total length (L_{tot}) of 60.2 cm; BGE composed of Tris / CHES (IS 90 mM, pH 8.4); applied voltage: 25 kV (normal polarity).

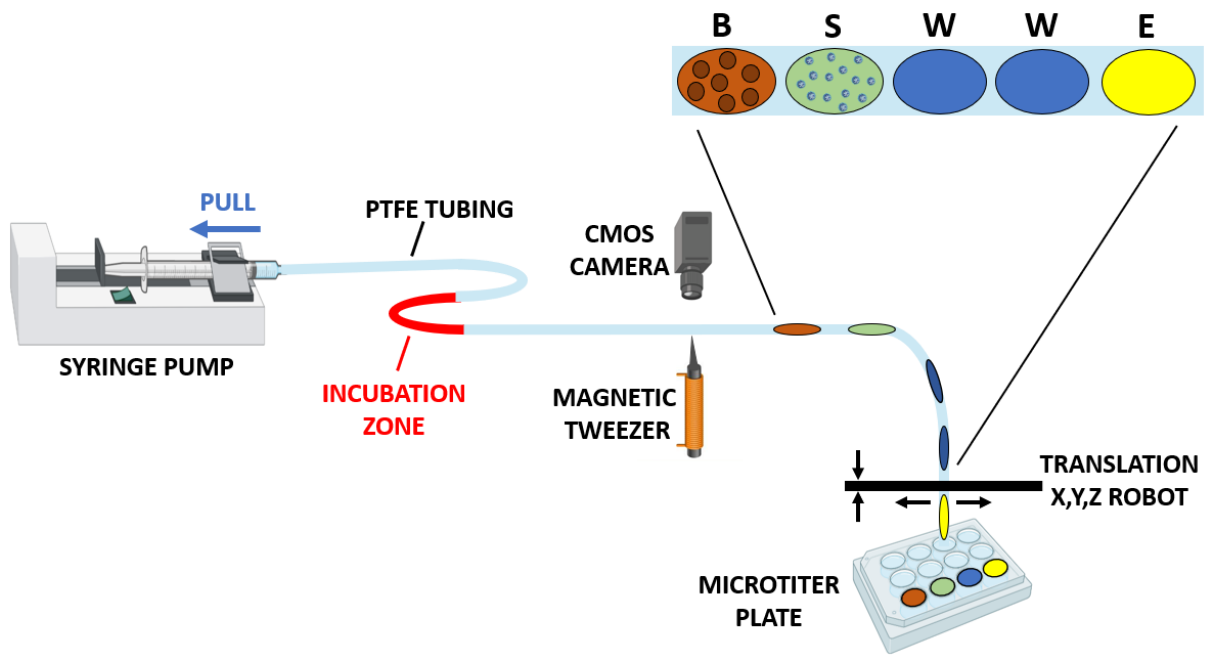
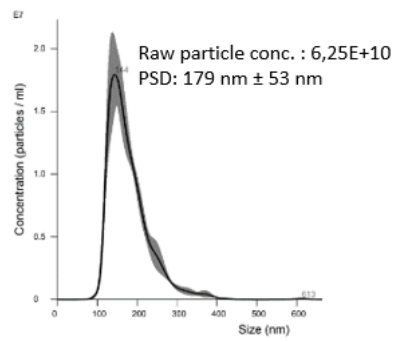
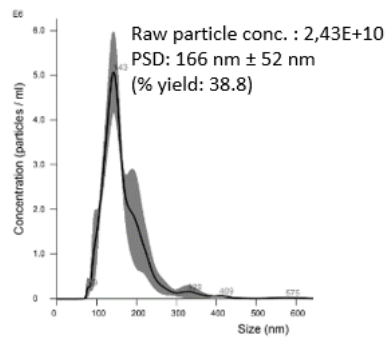


Fig. 3. Schematic drawing of microfluidic droplet system. B: droplet containing magnetic beads; S: sample droplet; W: washing droplet; E: droplet containing the elution solution. Droplets are separated by oil.

(a)

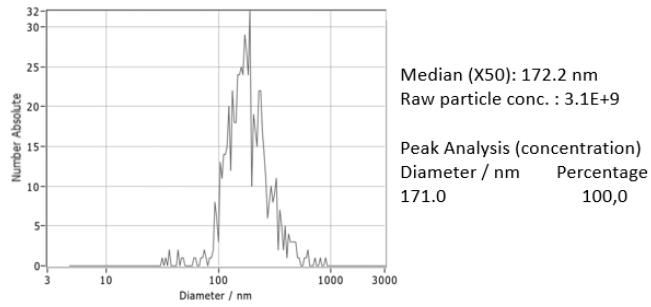


(b)

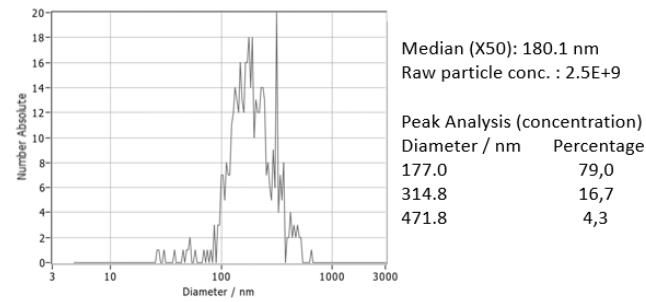


(A)

(a)



(b)



(B)

Fig. 4. Comparison between (A) Nanosight NS300 (Malvern) vs (B) Zetaview NTA (Particle Metrix) for EVs standard before (a) and after (b) purification with the microfluidic droplet platform using the U-shaped pattern.

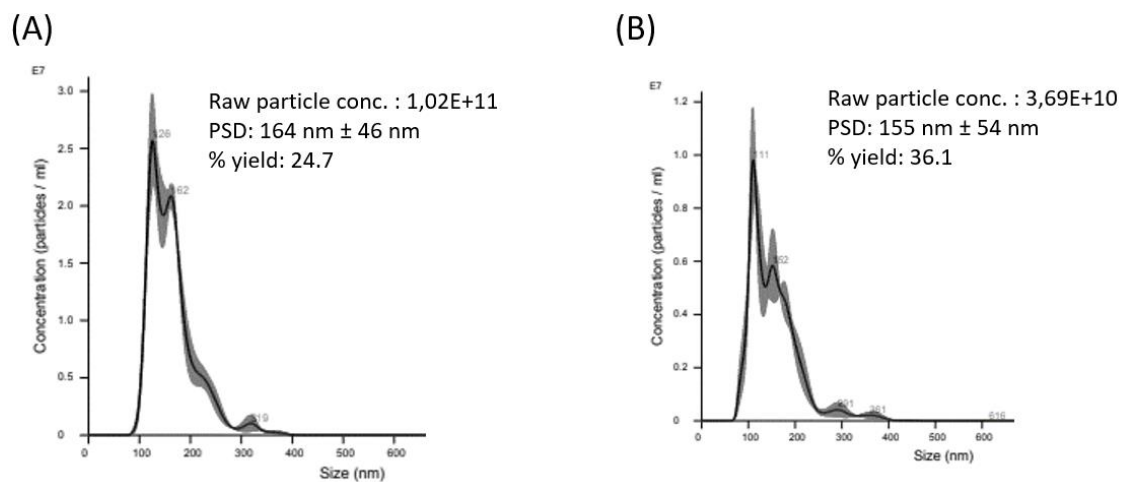


Fig. 5. NTA measurements of EVs-spiked artificial serum before (A) and after (B) EVs isolation using the microfluidic droplet platform. The sample was 5-time diluted with PBS prior to microfluidic droplet operations. NTA histograms represent the mean of three replicate measurements of the same sample, with the standard deviation (SD) in grey.

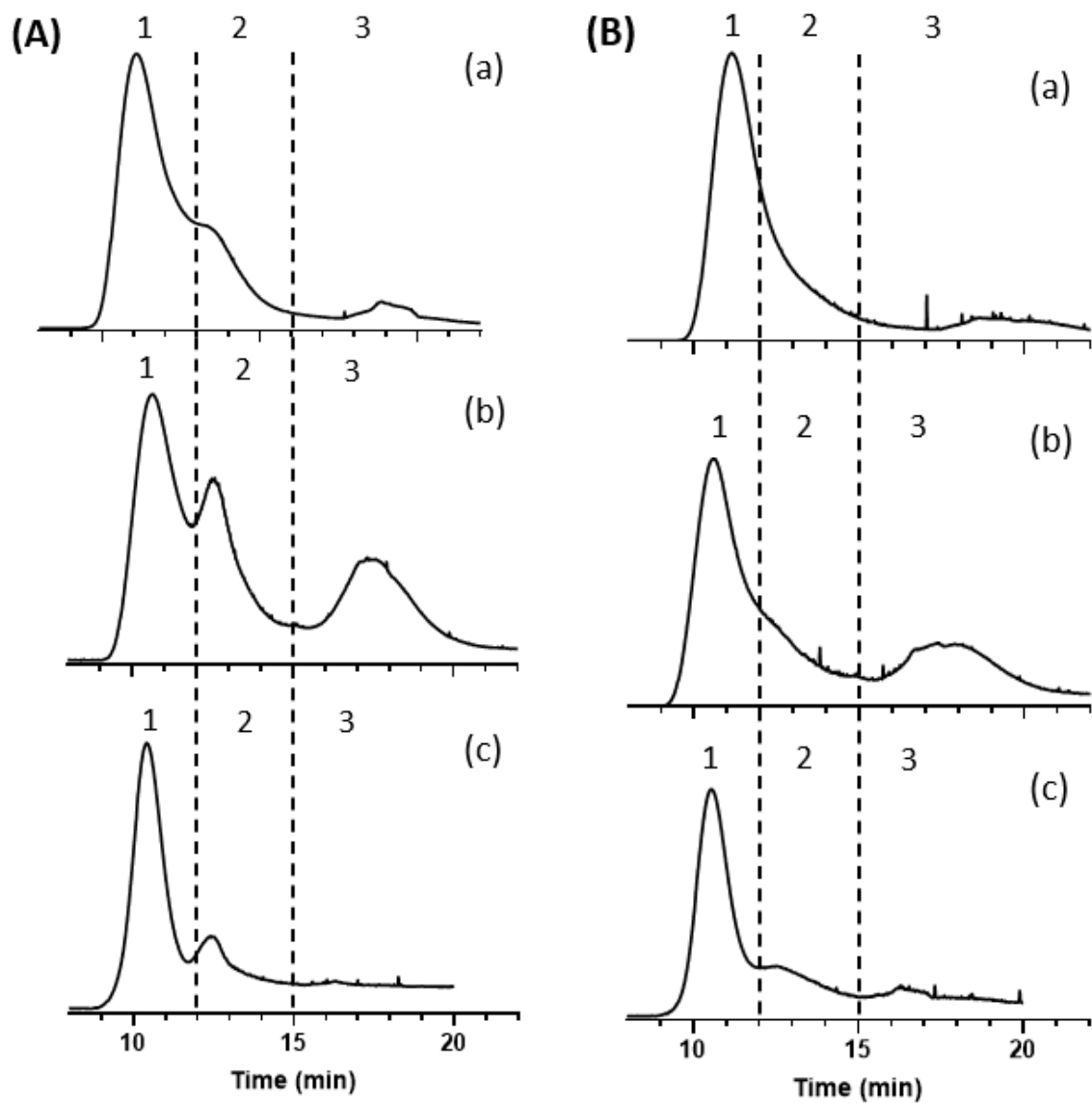


Fig. 6. CE-LIF for EVs from pony plasma (I) and serum (II), isolated with PEG-based EVs precipitation method in batch mode (A); with the microfluidic droplet system using the U-shaped pattern (B) and isolated with SEC (C). CE conditions as in Fig. 2.

Electronic Supporting Information

Development of a microfluidic droplet platform with an antibody-free magnetic-bead-based strategy for high through-put and efficient EVs isolation

Marco Morani¹, Myriam Taverna^{1,3}, Zuzana Krupova², Lucile Alexandre¹, Pierre Defreinaix², and Thanh Duc Mai^{1*}

¹ *Institut Galien Paris Saclay, UMR 8612, CNRS, Univ. Paris-Saclay, Protein and Nanotechnology in Analytical Science (PNAS) Châtenay-Malabry, France*

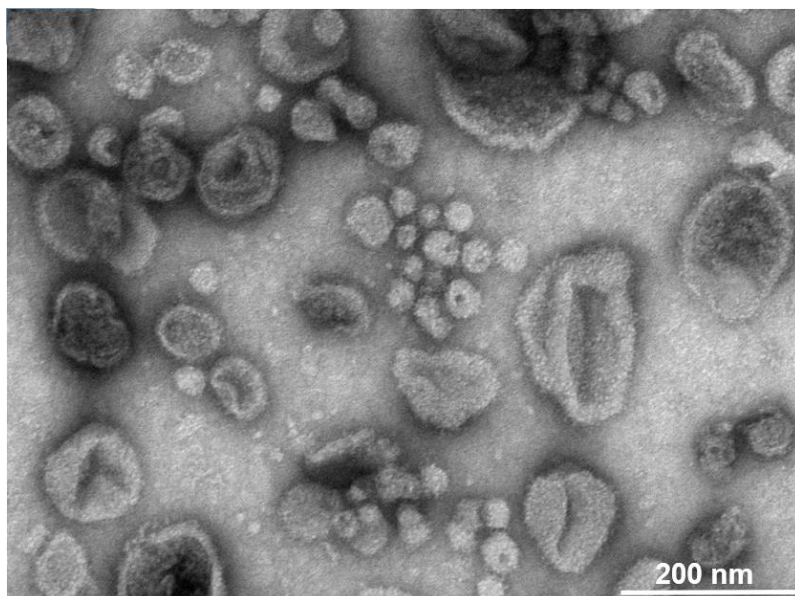
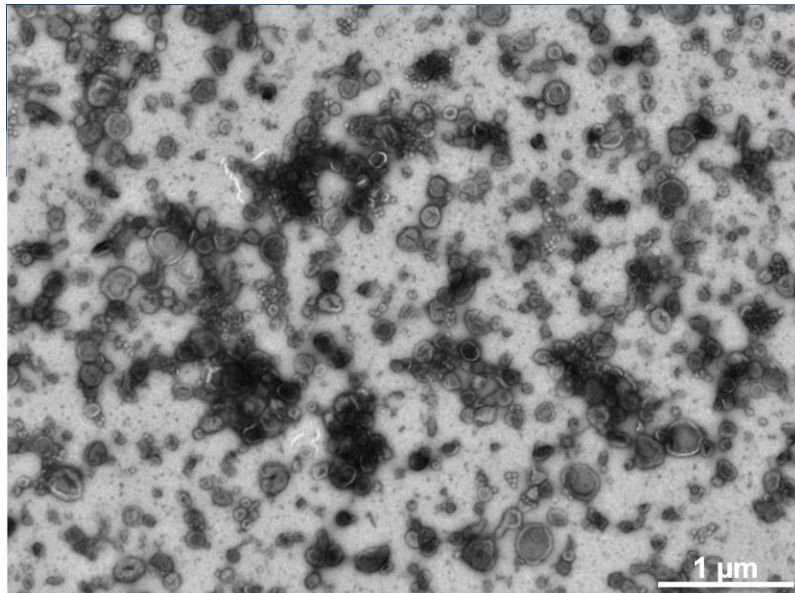
² *Excilone - 6, Rue Blaise Pascal - Parc Euclide - 78990 Elancourt - France*

³ *Institut Universitaire de France (IUF)*

Correspondence: E-mail: thanh-duc.mai@u-psud.fr

Figure S1. (A) Transmission Electron Microscopy with negative staining by uranyl acetate of bovine milk-derived EVs. (B) Whole proteome profiling of the bovine milk-derived EVs with LC-MS/MS.

A)



B)

| Protein name | Gene | Uniprot ID |
|--|-------------|--------------------------|
| Xanthine dehydrogenase/oxidase | XDH | F1MUT3 (F1MUT3_BOVIN) |
| Xanthine dehydrogenase/oxidase | XDH | P80457 (XDH_BOVIN) |
| Aldehyde oxidase 4 | AOX4 | E1BL62 (E1BL62_BOVIN) |
| Aldehyde oxidase | AOX1 | P48034 (ADO_BOVIN) |
| Butyrophilin subfamily 1 member A1 | BTN1A1 | P18892 (BT1A1_BOVIN) |
| Uncharacterized protein | SLK | G3X696 (G3X696_BOVIN) |
| BOVIN Butyrophilin (Fragment) | BTN | Q9TSF1 (Q9TSF1_BOVIN) |
| Fatty acid synthase | FASN | F1N647 (F1N647_BOVIN) |
| Fatty acid synthase | FASN | Q71SP7 (FAS_BOVIN) |
| Lactadherin | MFGE8 | F1MXX6 (F1MXX6_BOVIN) |
| Lactadherin | MFGE8 | G3MYW7 (G3MYW7_BOVIN) |
| Lactotransferrin | LTF | P24627 (TRFL_BOVIN) |
| Lactoferrin | | B3VTM3 (B3VTM3_BOVIN) |
| Lactoferrin (Fragment) | | Q95M57 (Q95M57_BOVIN) |
| Polymeric immunoglobulin receptor | PIGR | P81265 (PIGR_BOVIN) |
| Uncharacterized protein | PIGR | F1MR22 (F1MR22_BOVIN) |
| Platelet glycoprotein 4 | CD36 | P26201 (CD36_BOVIN) |
| Sodium-dependent phosphate transport protein 2B | SLC34A2 | F1N6D4 (F1N6D4_BOVIN) |
| Mucin-16 | MUC16 | F2FB38 (F2FB38_BOVIN) |
| Perilipin-2 | PLIN2 | Q9TUM6 (PLIN2_BOVIN) |
| ATP-binding cassette sub-family G member 2 | ABCG2 | Q4GZT4 (ABCG2_BOVIN) |
| Complement C3 | C3 | Q2UVX4 (CO3_BOVIN) |
| Ezrin | EZR | P31976 (EZRI_BOVIN) |
| Moesin | MSN | Q2HJ49 (MOES_BOVIN) |
| Radixin | RDX | Q32LP2 (RADI_BOVIN) |
| Uncharacterized protein | GP2 | F1N726 (F1N726_BOVIN) |
| Ectonucleotide pyrophosphatase/phosphodiesterase family member 3 | ENPP3 | P15396 (ENPP3_BOVIN) |
| Isocitrate dehydrogenase [NADP] cytoplasmic | IDH1 | Q9XSG3 (IDHC_BOVIN) |
| Isocitrate dehydrogenase [NADP] (Fragment) | IDH1 | Q0QEQ4 (Q0QEQ4_BOVIN) |

| | | |
|--|--------------|-----------------------|
| RAB1A, member RAS oncogene family | RAB1A | A1L528 (A1L528_BOVIN) |
| Ras-related protein Rab-18 | RAB18 | Q0IIG8 (RAB18_BOVIN) |
| Ras-related protein Rab-8A | RAB8A | A4FV54 (RAB8A_BOVIN) |
| Ras-related protein Rab-1B | RAB1B | Q2HJH2 (RAB1B_BOVIN) |
| RAB10 protein | RAB10 | A6QLS9 (A6QLS9_BOVIN) |
| Uncharacterized protein | RAB35 | F1MSJ9 (F1MSJ9_BOVIN) |
| Uncharacterized protein | RAB3D | E1BNX1 (E1BNX1_BOVIN) |
| RAB14 protein | RAB14 | Q3ZBG1 (Q3ZBG1_BOVIN) |
| Ras-related protein Rab-13 | RAB13 | Q58DS5 (RAB13_BOVIN) |
| Major allergen beta-lactoglobulin | | B5B0D4 (B5B0D4_BOVIN) |
| Beta-lactoglobulin | LGB | P02754 (LACB_BOVIN) |
| Beta-lactoglobulin variant D | LGB | O77777 (O77777_BOVIN) |
| Uncharacterized protein | GGT1 | G3N2D8 (G3N2D8_BOVIN) |
| Heat shock cognate 71 kDa protein | HSPA8 | P19120 (HSP7C_BOVIN) |
| Heat shock 70 kDa protein 1B | HSPA1B | Q27965 (HS71B_BOVIN) |
| Heat shock 70 kDa protein 1-like | HSPA1L | P0CB32 (HS71L_BOVIN) |
| Uncharacterized protein | HSPA6 | F1MWU9 (F1MWU9_BOVIN) |
| Uncharacterized protein | IGLL1 | F1MLW7 (F1MLW7_BOVIN) |
| Immunoglobulin light chain, lambda gene cluster | IGL@ | Q1RMN8 (Q1RMN8_BOVIN) |
| IGL@ protein | IGL@ | Q3T101 (Q3T101_BOVIN) |
| Uncharacterized protein | LOC100847119 | F1MLW8 (F1MLW8_BOVIN) |
| Annexin A5 | ANXA5 | P81287 (ANXA5_BOVIN) |
| Annexin A4 | ANXA4 | P13214 (ANXA4_BOVIN) |
| 5'-nucleotidase | NT5E | Q05927 (5NTD_BOVIN) |
| Actin, cytoplasmic 2 | ACTG1 | P63258 (ACTG_BOVIN) |
| Actin, cytoplasmic 1 | ACTB | P60712 (ACTB_BOVIN) |
| Actin, gamma-enteric smooth muscle | ACTG2 | Q5E9B5 (ACTH_BOVIN) |
| Fatty acid-binding protein, heart | FABP3 | P10790 (FABPH_BOVIN) |
| Rab GDP dissociation inhibitor beta | GDI2 | P50397 (GDIB_BOVIN) |
| Rab GDP dissociation inhibitor alpha | GDI1 | P21856 (GDIA_BOVIN) |
| Folate receptor alpha | FOLR1 | E1BJL8 (E1BJL8_BOVIN) |
| Folate receptor alpha | FOLR1 | P02702 (FOLR1_BOVIN) |
| Glycosylation-dependent cell adhesion molecule 1 | GLYCAM1 | P80195 (GLCM1_BOVIN) |

| | | |
|--|----------|-----------------------|
| Guanine nucleotide-binding protein G(I)/G(S)/G(T) subunit beta-1 | GNB1 | P62871 (GBB1_BOVIN) |
| Guanine nucleotide-binding protein G(I)/G(S)/G(T) subunit beta-2 | GNB2 | P11017 (GBB2_BOVIN) |
| CD9 antigen | CD9 | P30932 (CD9_BOVIN) |
| Elongation factor 2 | EEF2 | Q3SYU2 (EF2_BOVIN) |
| Ras-related protein Rab-11B | RAB11B | Q3MHP2 (RB11B_BOVIN) |
| Ras-related protein Rab-25 | RAB25 | Q58DW6 (RAB25_BOVIN) |
| Heat shock protein HSP 90-beta | HSP90AB1 | Q76LV1 (HS90B_BOVIN) |
| Heat shock protein HSP 90-alpha | HSP90AA1 | Q76LV2 (HS90A_BOVIN) |
| Ras-related C3 botulinum toxin substrate 1 | RAC1 | P62998 (RAC1_BOVIN) |
| Cell division control protein 42 homolog | CDC42 | Q2KJ93 (CDC42_BOVIN) |
| Ras homolog gene family, member G (Rho G) | RHOG | Q1RMI2 (Q1RMI2_BOVIN) |
| Cytoplasmic aconitate hydratase | ACO1 | Q0VCU1 (ACOC_BOVIN) |
| Mucin-1 | MUC1 | Q8WML4 (MUC1_BOVIN) |
| Elongation factor 1-alpha 1 | EEF1A1 | P68103 (EF1A1_BOVIN) |
| Monocyte differentiation antigen CD14 | CD14 | Q95122 (CD14_BOVIN) |
| Mannose 6 phosphate receptor binding protein 1 | M6PRBP1 | Q3SX32 (Q3SX32_BOVIN) |
| Uncharacterized protein (Fragment) | ATP13A4 | F1N272 (F1N272_BOVIN) |
| Membrane cofactor protein | CD46 | F1N4W5 (F1N4W5_BOVIN) |
| Uncharacterized protein | VAT1 | F1MUP9 (F1MUP9_BOVIN) |
| Alkaline phosphatase, tissue-nonspecific isozyme | ALPL | P09487 (PPBT_BOVIN) |
| Annexin A2 | ANXA2 | P04272 (ANXA2_BOVIN) |
| Uncharacterized protein | STXBP2 | F1MHC2 (F1MHC2_BOVIN) |
| 14-3-3 protein zeta/delta | YWHAZ | P63103 (1433Z_BOVIN) |
| 14-3-3 protein epsilon | YWHAE | P62261 (1433E_BOVIN) |
| 14-3-3 protein gamma | YWHAG | P68252 (1433G_BOVIN) |
| 14-3-3 protein beta/alpha | YWHAB | P68250 (1433B_BOVIN) |
| 14-3-3 protein theta | YWHAQ | Q3SZI4 (1433T_BOVIN) |
| 14-3-3 protein eta | YWHAH | P68509 (1433F_BOVIN) |
| Mucin-15 | MUC15 | Q8MI01 (MUC15_BOVIN) |
| Pyridoxal kinase | PDXK | Q0II59 (PDXK_BOVIN) |
| CD81 antigen | CD81 | Q3ZCD0 (CD81_BOVIN) |
| Tryptophan--tRNA ligase, cytoplasmic | WARS | P17248 (SYWC_BOVIN) |

| | | |
|---|----------|-----------------------|
| Pyruvate kinase | PKM2 | A5D984 (A5D984_BOVIN) |
| Transforming protein RhoA | RHOA | P61585 (RHOA_BOVIN) |
| Rho-related GTP-binding protein RhoC | RHOC | Q1RMJ6 (RHOC_BOVIN) |
| TKT protein | TKT | A5PJ79 (A5PJ79_BOVIN) |
| Peptidyl-prolyl cis-trans isomerase A | PPIA | P62935 (PPIA_BOVIN) |
| Guanine nucleotide-binding protein G(s) subunit alpha isoforms short | GNAS | P04896 (GNAS2_BOVIN) |
| Guanine nucleotide binding protein (G protein), alpha inhibiting activity polypeptide 3 | GNAI3 | Q3ZCA7 (Q3ZCA7_BOVIN) |
| Guanine nucleotide-binding protein G(i) subunit alpha-1 | GNAI1 | P63097 (GNAI1_BOVIN) |
| Guanine nucleotide-binding protein G(o) subunit alpha | GNAO1 | P08239 (GNAO_BOVIN) |
| GNAI2 protein | GNAI2 | A7MBH9 (A7MBH9_BOVIN) |
| Alpha-enolase | ENO1 | Q9XSJ4 (ENOA_BOVIN) |
| ENO2 protein | ENO2 | A6QR19 (A6QR19_BOVIN) |
| Unconventional myosin-Ic | MYO1C | Q27966 (MYO1C_BOVIN) |
| Rho GDP-dissociation inhibitor 1 | ARHGDI1 | P19803 (GDIR1_BOVIN) |
| UTP--glucose-1-phosphate uridylyltransferase | UGP2 | Q07130 (UGPA_BOVIN) |
| PP1201 protein | RECS1 | Q6QRN7 (Q6QRN7_BOVIN) |
| Fructose-bisphosphate aldolase | ALDOC | Q3ZBY4 (Q3ZBY4_BOVIN) |
| Fructose-bisphosphate aldolase | ALDOA | A6QLL8 (A6QLL8_BOVIN) |
| Uncharacterized protein | SLC7A4 | E1BCI3 (E1BCI3_BOVIN) |
| CD59 molecule, complement regulatory protein | CD59 | Q32PA1 (Q32PA1_BOVIN) |
| Glycerol-3-phosphate dehydrogenase [NAD(+)], cytoplasmic | GPD1 | Q5EA88 (GPDA_BOVIN) |
| GPD1L protein | GPD1L | A6QQR7 (A6QQR7_BOVIN) |
| Selenium-binding protein 1 | SELENBP1 | Q2KJ32 (SBP1_BOVIN) |
| ACSS2 protein | ACSS2 | A7YWF1 (A7YWF1_BOVIN) |
| Uncharacterized protein | SLC5A1 | F1MD24 (F1MD24_BOVIN) |
| L-lactate dehydrogenase B chain | LDHB | Q5E9B1 (LDHB_BOVIN) |
| Pituitary tumor-transforming 1 interacting protein | PTTG1IP | Q2KI48 (Q2KI48_BOVIN) |
| Polyubiquitin-B | UBB | P0CG53 (UBB_BOVIN) |
| Clathrin heavy chain 1 | CLTC | P49951 (CLH1_BOVIN) |
| NADH-cytochrome b5 reductase 3 | CYB5R3 | P07514 (NB5R3_BOVIN) |

| | | |
|---|---------|-----------------------|
| Glyceraldehyde-3-phosphate dehydrogenase | GAPDH | P10096 (G3P_BOVIN) |
| Toll-like receptor 2 | TLR2 | Q95LA9 (TLR2_BOVIN) |
| 6-phosphogluconate dehydrogenase, decarboxylating | PGD | Q3ZCI4 (Q3ZCI4_BOVIN) |
| Ras-related protein Rab-7a | RAB7A | F1MJQ1 (F1MJQ1_BOVIN) |
| STX3 protein | STX3 | A6QLH3 (A6QLH3_BOVIN) |
| Uncharacterized protein | TMC4 | E1BNW4 (E1BNW4_BOVIN) |
| Phosphoglycerate kinase 1 | PGK1 | Q3T0P6 (PGK1_BOVIN) |
| Tyrosine-protein phosphatase non-receptor type substrate 1 | SIRPA | G3X6M9 (G3X6M9_BOVIN) |
| Aldose 1-epimerase | GALM | Q5EA79 (GALM_BOVIN) |
| Phosphatidylethanolamine-binding protein 1 | PEBP1 | P13696 (PEBP1_BOVIN) |
| Solute carrier family 29 (Nucleoside transporters), member 1 (Fragment) | SLC29A1 | Q0V8K9 (Q0V8K9_BOVIN) |
| Annexin A7 | ANXA7 | P20072 (ANXA7_BOVIN) |
| Uncharacterized protein | DYNC1H1 | E1BDX8 (E1BDX8_BOVIN) |
| ADP-ribosylation factor 4 | ARF4 | Q3SZF2 (ARF4_BOVIN) |
| ADP-ribosylation factor 2 | ARF2 | P84081 (ARF2_BOVIN) |
| ADP-ribosylation factor 1 | ARF1 | P84080 (ARF1_BOVIN) |
| IST1 homolog | IST1 | F1MXJ5 (F1MXJ5_BOVIN) |
| Acyl-CoA synthetase long-chain family member 1 | ACSL1 | Q0VCZ8 (Q0VCZ8_BOVIN) |
| Ras-related protein Rap-1A | RAP1A | P62833 (RAP1A_BOVIN) |
| Phosphoserine aminotransferase | PSAT1 | A6QR28 (A6QR28_BOVIN) |
| Phosphoglycerate mutase 1 | PGAM1 | Q3SZ62 (PGAM1_BOVIN) |
| Basigin | BSG | Q3ZBX0 (Q3ZBX0_BOVIN) |
| Uncharacterized protein (Fragment) | BSPRY | F1MKU3 (F1MKU3_BOVIN) |
| Synaptobrevin homolog YKT6 | YKT6 | Q3T000 (YKT6_BOVIN) |
| Ethylmalonyl-CoA decarboxylase | ECHDC1 | Q2HJD5 (ECHD1_BOVIN) |
| Uncharacterized protein | GNAQ | E1BA29 (E1BA29_BOVIN) |
| Uncharacterized protein (Fragment) | GNA13 | G5E6P3 (G5E6P3_BOVIN) |
| Guanine nucleotide-binding protein subunit alpha-11 | GNA11 | P38409 (GNA11_BOVIN) |
| Monocarboxylate transporter 1 | SLC16A1 | Q3MHW6 (MOT1_BOVIN) |
| Uncharacterized protein | SLC39A8 | E1BQ28 (E1BQ28_BOVIN) |
| Nucleoside diphosphate kinase B | NME2 | Q3T0Q4 (NDKB_BOVIN) |

| | | |
|---|---------|-----------------------|
| PCDHGA2 protein | PCDHGA2 | A5D7Q6 (A5D7Q6_BOVIN) |
| RAB2A, member RAS oncogene family | RAB2A | Q148J4 (Q148J4_BOVIN) |
| Uncharacterized protein | KRAS | E1BMX0 (E1BMX0_BOVIN) |
| SCAMP2 protein | SCAMP2 | A6QR35 (A6QR35_BOVIN) |
| CIDEA protein | CIDEA | A4FUX1 (A4FUX1_BOVIN) |
| Uncharacterized protein | TMC5 | F1MIU3 (F1MIU3_BOVIN) |
| Malate dehydrogenase, cytoplasmic | MDH1 | Q3T145 (MDHC_BOVIN) |
| CD82 protein | CD82 | A5D7E6 (A5D7E6_BOVIN) |
| Endoglin | ENG | Q1RMV1 (Q1RMV1_BOVIN) |
| Ras related v-ral simian leukemia viral oncogene homolog A (Fragment) | RALA | Q1JPH2 (Q1JPH2_BOVIN) |
| RALB protein | RALB | A5D977 (A5D977_BOVIN) |
| Uncharacterized protein (Fragment) | VPS4A | G3X8E2 (G3X8E2_BOVIN) |
| Vacuolar protein sorting-associated protein 4B | VPS4B | Q0VD48 (VPS4B_BOVIN) |
| Retinal dehydrogenase 1 | ALDH1A1 | P48644 (AL1A1_BOVIN) |
| G protein-coupled receptor, family C, group 5, member B | GPRC5B | Q1JPD9 (Q1JPD9_BOVIN) |
| Ras-related protein Rab-5C | RAB5C | Q58DS9 (RAB5C_BOVIN) |
| Ras-related protein Rab-5A | RAB5A | Q0IIG7 (RAB5A_BOVIN) |
| Uncharacterized protein (Fragment) | RAB5B | F1MNI4 (F1MNI4_BOVIN) |
| Glutathione S-transferase Mu 1 | GSTM1 | Q9N0V4 (GSTM1_BOVIN) |
| Glutathione S-transferase mu 3 (Brain) | GSTM3 | Q2KIV8 (Q2KIV8_BOVIN) |
| GSTM1 protein | GSTM1 | A4IFG0 (A4IFG0_BOVIN) |
| Chloride intracellular channel protein 4 | CLIC4 | Q9XSA7 (CLIC4_BOVIN) |
| Cytosol aminopeptidase | LAP3 | P00727 (AMPL_BOVIN) |
| Uncharacterized protein | MST4 | F1N5W5 (F1N5W5_BOVIN) |
| Purine nucleoside phosphorylase | PNP | P55859 (PNPH_BOVIN) |
| Tissue specific transplantation antigen P35B | TSTA3 | Q2KIT8 (Q2KIT8_BOVIN) |
| Alpha/beta hydrolase domain-containing protein 14B | ABHD14B | A7YY28 (ABHEB_BOVIN) |
| CD47 molecule | CD47 | Q08DW0 (Q08DW0_BOVIN) |
| Arachidonate 12-lipoxygenase, 12S-type | ALOX12 | P27479 (LOX12_BOVIN) |
| Uncharacterized protein (Fragment) | SLC15A2 | F1MPK7 (F1MPK7_BOVIN) |
| Staphylococcal nuclease domain-containing protein 1 | SND1 | Q863B3 (SND1_BOVIN) |

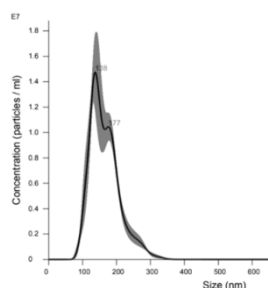
| | | |
|---|----------|-----------------------|
| Uncharacterized protein | NPEPPS | E1BP91 (E1BP91_BOVIN) |
| Cytosolic non-specific dipeptidase | CNDP2 | Q3ZC84 (CNDP2_BOVIN) |
| Uncharacterized protein | MPP5 | E1BIQ8 (E1BIQ8_BOVIN) |
| Uncharacterized protein | IQGAP1 | F1MC48 (F1MC48_BOVIN) |
| Uncharacterized protein | BROX | F1MU85 (F1MU85_BOVIN) |
| PDZ domain-containing protein GIPC2 | GIPC2 | Q1JQD4 (GIPC2_BOVIN) |
| G-protein coupled receptor family C group 5 member C | GPRC5C | Q2YDG0 (GPC5C_BOVIN) |
| Uncharacterized protein | EHD4 | E1BJV0 (E1BJV0_BOVIN) |
| Protein shisa-5 | SHISA5 | Q3T0A9 (SHSA5_BOVIN) |
| Peroxiredoxin-1 | PRDX1 | Q5E947 (PRDX1_BOVIN) |
| Glucose-6-phosphate isomerase | GPI | Q3ZBD7 (G6PI_BOVIN) |
| Ribonuclease/angiogenin inhibitor 1 | RNH1 | Q3SZN8 (Q3SZN8_BOVIN) |
| Cofilin-1 | CFL1 | Q5E9F7 (COF1_BOVIN) |
| Inorganic pyrophosphatase | PPA1 | P37980 (IPYR_BOVIN) |
| Glycerol-3-phosphate acyltransferase 4 | AGPAT6 | A3FPG8 (GPAT4_BOVIN) |
| Sterol-4-alpha-carboxylate 3-dehydrogenase, decarboxylating | NSDHL | Q3ZBE9 (NSDHL_BOVIN) |
| Uncharacterized protein | SLC3A2 | F1N2B5 (F1N2B5_BOVIN) |
| Alcohol dehydrogenase [NADP(+)] | AKR1A1 | Q3ZCJ2 (AK1A1_BOVIN) |
| FGR protein | FGR | A5PKG9 (A5PKG9_BOVIN) |
| Syntenin | SDCBP | A5D9B6 (A5D9B6_BOVIN) |
| Tubulin alpha-1B | | P81947 (TBA1B_BOVIN) |
| Syndecan-2 | SDC2 | Q58DD4 (SDC2_BOVIN) |
| Synaptosomal-associated protein | SNAP23 | Q2T9M8 (Q2T9M8_BOVIN) |
| Triosephosphate isomerase | TPI1 | Q5E956 (TPIS_BOVIN) |
| EXOC4 protein | EXOC4 | A6QLD1 (A6QLD1_BOVIN) |
| Uncharacterized protein | ADAM9 | F1MZJ5 (F1MZJ5_BOVIN) |
| Ubiquitin-like modifier-activating enzyme 1 | UBA1 | A3KMV5 (UBA1_BOVIN) |
| Charged multivesicular body protein 1b | CHMP1B | Q5E994 (CHM1B_BOVIN) |
| Na(+)/H(+) exchange regulatory cofactor NHE-RF1 | SLC9A3R1 | Q3SZK8 (NHRF1_BOVIN) |
| Phospholipid scramblase 2 | PLSCR2 | Q3ZBG9 (PLS2_BOVIN) |
| Golgi phosphoprotein 3 (Coat-protein) | GOLPH3 | Q1RMW9 (Q1RMW9_BOVIN) |
| Tyrosine-protein kinase Lyn | Lyn | D4QGC1 (D4QGC1_BOVIN) |

| | | |
|---|---------|-----------------------|
| Protein lin-7 homolog C | LIN7C | Q0P5F3 (LIN7C_BOVIN) |
| TSG101 protein | TSG101 | A3KN51 (A3KN51_BOVIN) |
| Beta-centractin | ACTR1B | F2Z4F0 (F2Z4F0_BOVIN) |
| EXOC1 protein | EXOC1 | A6QQU0 (A6QQU0_BOVIN) |
| Serine--tRNA ligase, cytoplasmic | SARS | Q9GMB8 (SYSC_BOVIN) |
| Excitatory amino acid transporter 3 | SLC1A1 | Q95135 (EAA3_BOVIN) |
| Calcium-binding protein 39 | CAB39 | Q29RI6 (CAB39_BOVIN) |
| Protein DJ-1 | PARK7 | Q5E946 (PARK7_BOVIN) |
| Chromatin modifying protein 2A | CHMP2A | Q3T0U5 (Q3T0U5_BOVIN) |
| Leucine-rich repeat-containing protein 8C | LRRC8C | A5PK13 (LRC8C_BOVIN) |
| GTP-binding protein Rheb | RHEB | Q56JV3 (RHEB_BOVIN) |
| Serine/threonine-protein phosphatase 2A 65 kDa regulatory subunit A alpha isoform | PPP2R1A | Q32PI5 (2AAA_BOVIN) |
| CD63 antigen | CD63 | Q9XSK2 (CD63_BOVIN) |

Figure S2. NTA profiles for optimization of PEG-based EVs precipitation method in tube. I: Representative NTA profile for bovine milk-derived EVs before PEG-based precipitation. Prior to each parameter adjustment, the concentration of EVs was assessed. II: (A) magnetic beads functionalization (silane vs carboxylic group), (B) Incubation temperature (4 vs 25 °C), (C) magnetic beads concentration (0.5 – 1 – 2 mg/mL), (D) PEG concentration (5 – 10 – 15 % w/v). NTA histograms represent the mean of three replicate measurements of the same sample and SD in grey.

I.

Bovine milk EVs before PEG-based precipitation

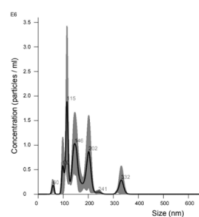


Stats: Merged Data
 Mean: 165.0 nm
 Mode: 137.2 nm
 SD: 44.3 nm
 Concentration: 1.31e+09 +/- 6.54e+07 particles/ml
 Dilution factor: 50
 Original concentration: 6.55E+10

II.

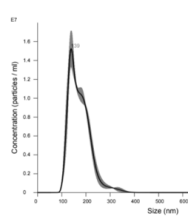
A) Magnetic beads functionalization:

Silane groups



Stats: Merged Data
 Mean: 161.9 nm
 Mode: 114.7 nm
 SD: 61.7 nm
 Concentration: 8.87e+07 +/- 1.29e+07 particles/ml
 (1-2 particles identified > no statistically significant result)

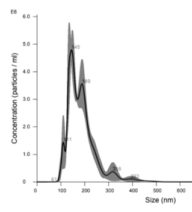
Carboxylic acid groups



Stats: Merged Data
 Mean: 173.4 nm
 Mode: 138.7 nm
 SD: 44.1 nm
 Concentration: 1.33e+09 +/- 2.36e+07 particles/ml
 Dilution factor: 20
 Original concentration: 2.66E+10 (% yield: 61%)

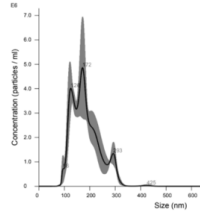
B) Incubation temperature:

4° C



Stats: Merged Data
 Mean: 185.1 nm
 Mode: 144.8 nm
 SD: 60.1 nm
 Concentration: $4.39 \times 10^8 \pm 1.92 \times 10^7$ particles/ml
 Dilution factor: 20
 Original concentration: 8.78×10^9 (% yield: **17,2%**)

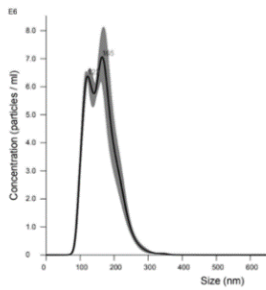
25° C



Stats: Merged Data
 Mean: 183.5 nm
 Mode: 171.5 nm
 SD: 54.8 nm
 Concentration: $5.11 \times 10^8 \pm 2.57 \times 10^7$ particles/ml
 Dilution factor: 20
 Original concentration: 1.022×10^{10} (% yield: **20%**)

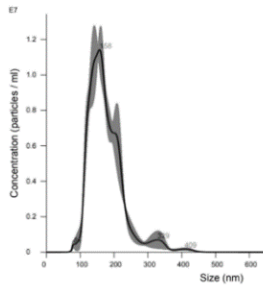
C) Magnetic beads concentration:

0.5 mg/mL



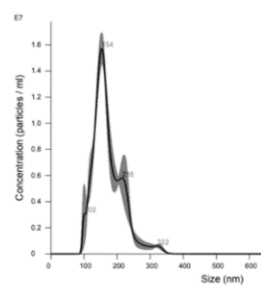
Stats: Merged Data
 Mean: 162.2 nm
 Mode: 164.6 nm
 SD: 43.1 nm
 Concentration: $7.45 \times 10^8 \pm 7.28 \times 10^7$ particles/ml
 Dilution factor: 20
 Original concentration: 1.49×10^{10} (% yield: **22,7**)

1.5 mg/mL



Stats: Merged Data
 Mean: 176.1 nm
 Mode: 157.1 nm
 SD: 53.2 nm
 Concentration: $1.12 \times 10^9 \pm 2.45 \times 10^7$ particles/ml
 Dilution factor: 20
 Original concentration: 2.24×10^{10} (% yield: **34,2%**)

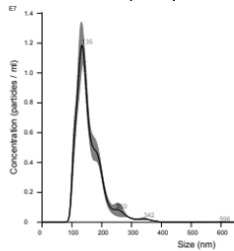
2 mg/mL



Stats: Merged Data
 Mean: 172.0 nm
 Mode: 153.6 nm
 SD: 44.9 nm
 Concentration: $1.21 \times 10^9 \pm 3.27 \times 10^7$ particles/ml
 Dilution factor: 20
 Original concentration: 2.42×10^{10} (% yield: **36,9%**)

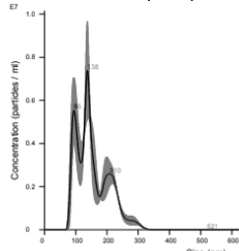
D) PEG concentration :

5 % (w/v)



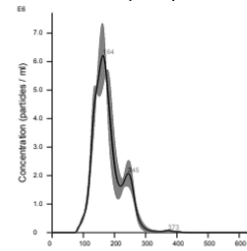
Stats: Merged Data
 Mean: 159.0 nm
 Mode: 134.0 nm
 SD: 50.7 nm
 Concentration: $8.31 \times 10^8 \pm 4.00 \times 10^7$ particles/ml
 Dilution factor: 20
 Original concentration: $1,66 \times 10^{10}$ (% yield: **22%**)

10 % (w/v)



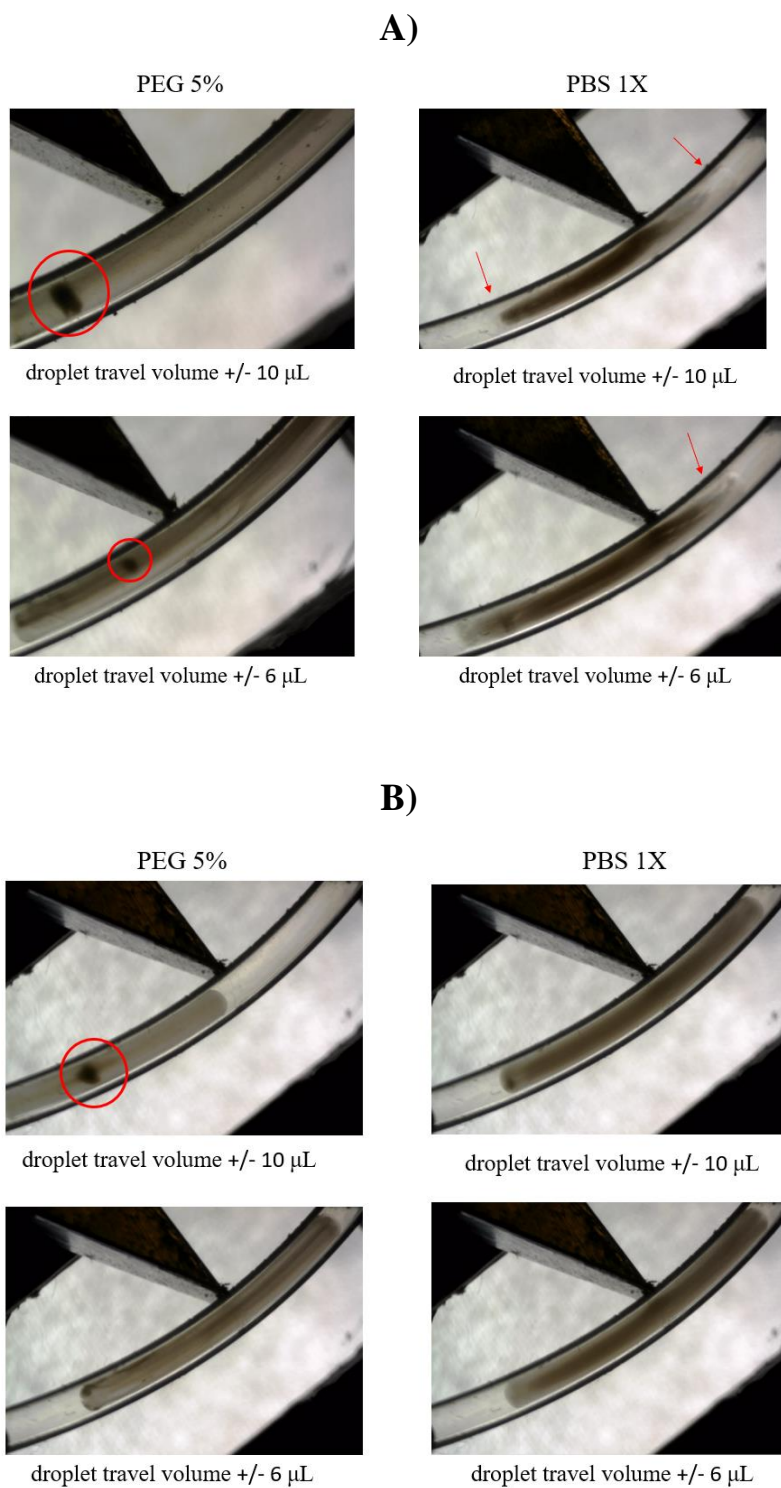
Stats: Merged Data
 Mean: 153.6 nm
 Mode: 137.0 nm
 SD: 51.9 nm
 Concentration: $5.71 \times 10^8 \pm 5.48 \times 10^7$ particles/ml
 Dilution factor: 20
 Original concentration: $1,14 \times 10^{10}$ (% yield: **20,1%**)

15 % (w/v)



Stats: Merged Data
 Mean: 178.6 nm
 Mode: 163.3 nm
 SD: 46.0 nm
 Concentration: $5.36 \times 10^8 \pm 2.66 \times 10^7$ particles/ml
 Dilution factor: 20
 Original concentration: $1,07 \times 10^{10}$ (% yield: **18,9%**)

Figure S3. Photos of beads behavior inside a droplet during incubation with back-and-forth motions in the matrix composed of either PEG 5% or PBS 1x over 5 min. A) incubation across tubing without optimization; B) incubation across spiral pattern; C) incubation across U-shaped pattern.



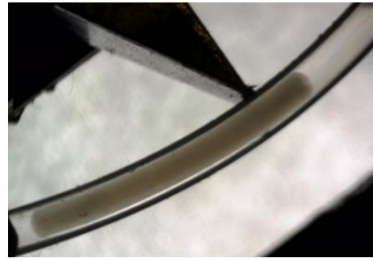
C)

PEG 5%

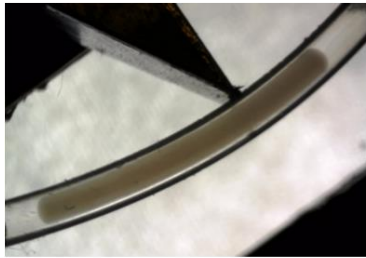


droplet travel volume +/- 10 μL

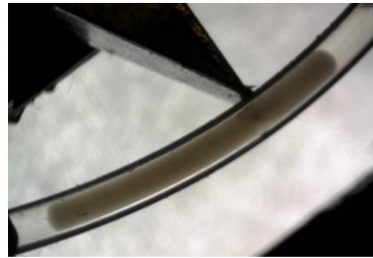
PBS 1X



droplet travel volume +/- 10 μL

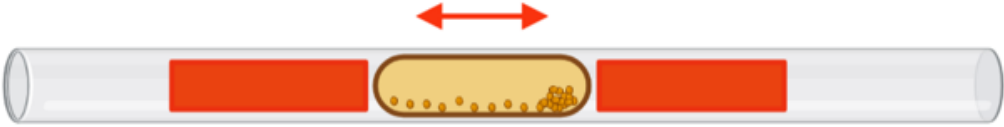


droplet travel volume +/- 6 μL

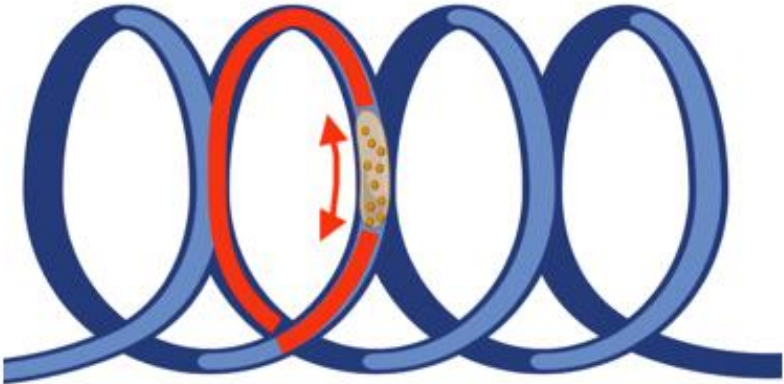


droplet travel volume +/- 6 μL

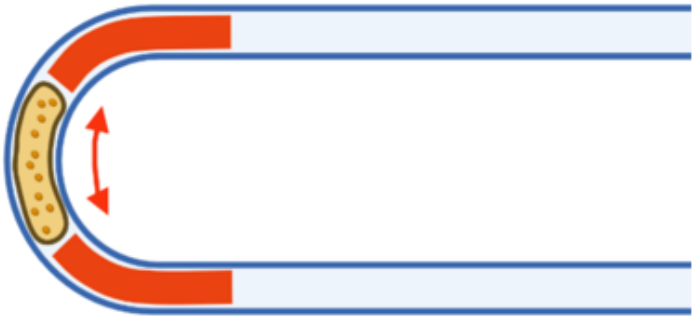
Figure S4. Schematic drawing of droplet movement pattern: (A) straight pattern, (B) spiral pattern and (C) U-shaped. Highlighted in red the back-and-forth droplet travel distance.



(A)



(B)



(C)

Figure S5. Relationship between in-droplet incubation time and yield of EVs, using the spiral-formed pattern and a travel volume of 6 μL . The percentage of EVs recovered was calculated using NTA analysis before and after incubation.

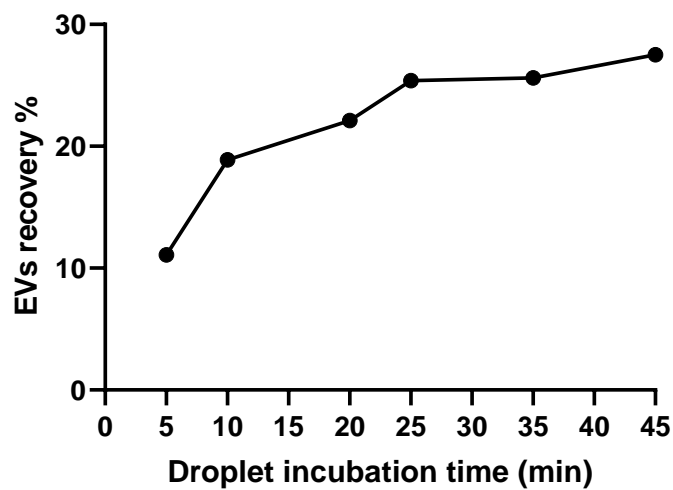
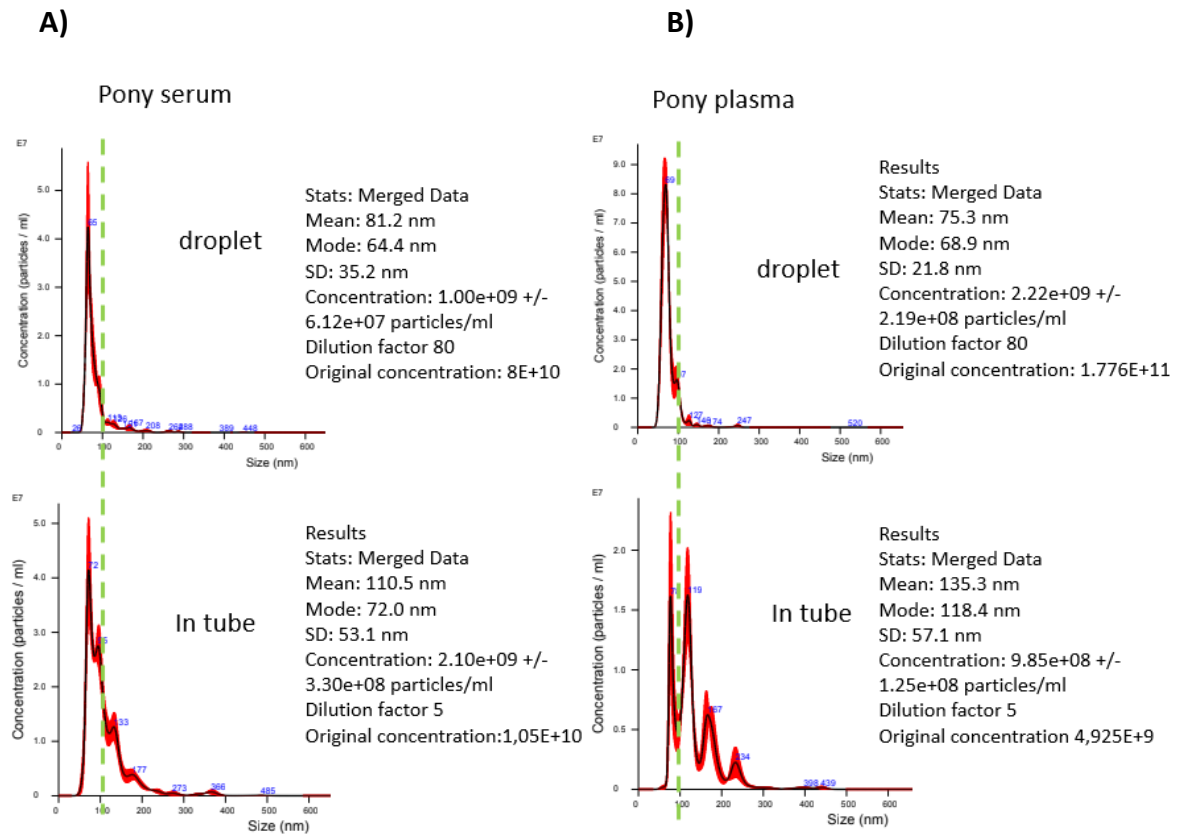


Figure S6. NTA measurements for EVs isolated from (A) pony serum and (B) pony plasma with the microfluidic droplet system using the U-shaped pattern and in-tube protocol.



Conclusion and perspectives

For some years, EVs have been identified as a possible source of biomarkers since their internal RNA, internal or membrane proteins derive directly from the emitting cells and reflect the latter's physiological or pathological condition. Thus, scientists are developing novel diagnostic methods based on the utilization of EVs either for identification of specific pathology-indicating vesicles or as a source of biomarker, notably in the area of cancer. However, only a few biomarkers have been validated till now for cancer diagnosis. The obstacles associated with standardizing this liquid biopsy approach for diagnosis are enormous. To be effective in the clinic, an EV-based biomarker must be extensively validated, and a high degree of repeatability throughout the process is needed. On the other hand, owing to their capacity to transmit bioactive components and cross biological barriers, EVs are also being investigated as possible therapeutic vectors or agents. For future clinical trials and for the transition to regulatory-approved clinical therapy, it is necessary to have not only higher purity, retained integrity and functionality but also standard operating procedures (SOPs) for reproducibility, quality control criteria. Because of this, ISEV has produced recommendations on a regular basis since its creation in 2011 in order to best define practices in the area of EVs and promote the development of new isolation and characterisation strategies. However, the field is still in its early stages.

The state of art on emerging microfluidic technologies has permitted to identify a number of problems that must be solved before EVs can become widely used. The development of a new platform based on a complete microfluidic system capable of extracting EVs from biological fluids, in high quality control standards, with a technique capable of simultaneously providing physical and biological information on isolated EVs, emerged as a major objective of my thesis but as a difficult challenge. The idea was to avoid the numerous complementary techniques that must be used nowadays and to propose an automated method of EV isolation and multi-characterization that can be reproducible and standardizable.

Several separation modes/mechanisms of Capillary Electrophoresis for EVs characterisation were thus evaluated in this thesis. A solid knowledge of this technique has allowed for a better understanding of the difficulties surrounding the development of novel systems for the separation and analysis of EVs. The CZE method we developed was able to evidence differences in electrophoretic mobilities from EVs isolated from different animal origins (e.g. bovine milk, pony serum and pony plasma derived EVs). Furthermore, when applied to human plasma-derived EVs isolated via immunoaffinity

chromatography using monolithic disk columns selecting either CD61 or CD9 surface marker of EVs, our method revealed three distinct peak zones with varying signal intensities depending on the targeted marker. However, at this stage no clear relationship between the size and/or charge characteristics of EVs and their electrophoretic mobilities can be defined. The translation of CE theory and experience on nanoparticles to such heterogeneous bioentities seems indeed not trivial. To understand the electrophoretic behaviour of EVs, a deeper characterisation study utilizing EVs with a lower degree of polydispersity and narrow size distribution or well defined zeta potential would be required. However, such pure EVs are not currently obtainable using current EV purifying technologies. Another alternative could be to collect the subfractions from CZE runs and analyze them. However, subfraction analysis from CZE would need a higher resolution in order to collect only a specific subfraction and several injection/collection cycles due to the low injected volumes used in CE (around 125 nL, for a 60-cm capillary and 50- μm id). The resolution will be maximum with values of EOF close to those of the electrophoretic mobilities (μep) of the EVs. We could therefore try to better tune the EOF to improve the resolution between subfractions and collect this way purer fractions by adding EOF modulators such as detergents or alkylamines.

When compared to CE-UV approaches developed by other groups throughout the course of my thesis, the LIF detection used in our work enabled us to achieve superior LODs (on the order of 10^{10} EVs/mL). However this is still not sufficient to address low abundant EVs samples, a good target would be to decrease this limit to about 10^8 EVs/mL. We have conducted some pioneering research on viable ways for in-capillary electrokinetic preconcentration for EVs in order to boost the sensitivity of our CE-LIF detection). All of the electrokinetic approaches tested for in-capillary preconcentration (FASS, LVSS and multiple cycle-LVSS), however, were found unsuitable for EVs. It has been indeed challenging to find a balance between an EVs sample matrix with a conductivity significantly lower than that of the BGE while limiting or eliminating EV lysis during analysis under these extreme conditions (low or high conductivities). Actually, we must bear in mind that, low conductivities may harm EVs whereas high conductivities can cause joule heating and damage EVs. Alternative electrokinetic preconcentration modes that might preconcentrate EVs that I have not yet attempted (for example, capillary isoelectric focusing (cIEF) or isotachopheresis (ITP)) could be an interesting possibility to consider in future.

Beside CZE developments, we showed that TDA-UV performed with a commercial CE device by using pressure to the capillary's inlet could successfully estimate the size of bovine milk EVs in accordance with those evaluated by NTA. Additionally, TDA-LIF seemed capable of detecting very subtle changes in hydrodynamic radius that might be produced by fluorescent labeling at the outer membrane of EVs and also to detect the presence of smaller entities (R_h 20 nm) most likely due to either the release of

fluorescent dye (CFDA-SE) from EVs over the time (phenomenon also observed in CE) or excess of CSDA-SE that contaminated the samples. Conversely these features were not detected by NTA.

While TDA proved out to be an excellent method for determining the size of extremely pure EVs (i.e., EVs obtained from bovine milk), this was not the case for human plasma-derived EVs. This is possibly due to a high concentration of small contaminants in those plasma EV samples, such as plasma proteins and lipoprotein particles, which may overlap with the Taylor diffusion phenomenon. To confirm this it would be worth investigating TDA on other EV isolates of higher purity for instance and also derived from different biological sources.

This TDA-based characterisation method is intended to be integrated to the isolation module in the future, either directly for direct EVs sizing (as an alternative to the CZE profiling) or on-line to CZE (CZE-TDA) to calculate the diffusion coefficients of each previously separated EV subpopulations.

With the objective of realizing a complete and integrated platform for EVs isolation and analysis, the development of a microfluidic droplet system combined to magnetic beads used as cargo between each step of the EV capture process was then investigated.

The use of PEG to precipitate EVs onto magnetic beads, as an alternative to antibodies, has the advantage of being less expensive and not requiring any special functionalization of the magnetic beads. After having optimized the extraction condition in tube, its further translation into a droplet microfluidic procedure was successful to enable EVs recovery from more complex biofluids such as diluted pony serum and plasma. When dealing with such complex biofluid matrices, the droplet technique resulted in an 8-fold increase in the total NTA-measured particle concentration compared to the in-tube method ($1.7E10^{11}$ particles/mL for pony plasma, for example). The PEG-based method is expected to capture non-selectively all EV subpopulations, but it is also possible that contaminants (e.g. aggregated proteins and lipoproteins) may co-isolate with them. Because no further interpretation of the profiles obtained by our CZE approach is possible, LC-MS or western blot should be investigated in the future to identify total proteins of these separated EVs.

The natural next step in this study will be to connect the function of the microfluidic droplet-based technique to the CE system, with the goal of developing a full microfluidic instrument. However, droplet-interfacing for CE is only in its infancy at the moment, and its coupling is only possible via yet-to-be-developed interfaces. This means that at the moment manual transfer between the droplet-based procedure and CE system of the final droplet containing eluted EVs is required before complete automation and high-throughput are attainable.


The many conceivable combinations of this integrated platform's capabilities may allow for a broad range of applications. For example, if magnetic beads were used for non-specific EV isolation, when coupled to CZE-TDA, a screen of the totality of the isolated EVs and potential additional information based on the origin of the sample as well as a quality control would be possible. On the other hand, if one wants to employ particular magnetic beads for capturing specific EVs surface proteins identified as biomarkers of one disease, when coupled to the CZE-TDA, it will provide fresh information on precisely extracted EVs. Again, once the EVs have been isolated using either non-specific or specific magnetic bead-based approaches, a lysis step of the EVs prior characterization is conceivable. If this approach is chosen, the CZE would enable, for example, a screening of a selected intravesicular protein, which may result in the identification of novel potential biomarkers that may serve in determining specific disease progression. It should be noted that CZE-LIF for internal proteins may be somewhat challenging owing to the derivatization phase, which may result in many tagged species. Therefore, it may be worthwhile to target just one protein or glycoprotein and attempt to profile it, for example. Thus, our platform's potential applications could be useful for the diagnosis or discovery of potential biomarkers for cancer, but as mentioned in the previous bibliographic section, the study of EV alterations, whether on their surfaces or in their content, represent a promising and potential source of biomarkers for a wide variety of diseases such as neurodegenerative diseases, arthritis or diabetes.

References

1. Eguchi, A., et al., *Extracellular vesicles, the liquid biopsy of the future*. Journal of hepatology, 2019. **70**(6): p. 1292.
2. Rani, S., et al., *Mesenchymal stem cell-derived extracellular vesicles: toward cell-free therapeutic applications*. Molecular Therapy, 2015. **23**(5): p. 812-823.
3. Thery, C., et al., *Minimal information for studies of extracellular vesicles 2018 (MISEV2018): a position statement of the International Society for Extracellular Vesicles and update of the MISEV2014 guidelines*. J. Extracell. Vesicles, 2018. **7**(1): p. 43.
4. Lin, S.J., et al., *Progress in Microfluidics-Based Exosome Separation and Detection Technologies for Diagnostic Applications*. Small, 2020. **16**(9).
5. Chargaff, E. and R. West, *THE BIOLOGICAL SIGNIFICANCE OF THE THROMBOPLASTIC PROTEIN OF BLOOD*. Journal of Biological Chemistry, 1946. **166**(1): p. 189-197.
6. Wolf, P., *The nature and significance of platelet products in human plasma*. British journal of haematology, 1967. **13**(3): p. 269-288.
7. Aaronson, S., et al., *Ultrastructure of intracellular and extracellular vesicles, membranes, and myelin figures produced by Ochromonas danica*. Journal of Ultrastructure Research, 1971. **35**(5-6): p. 418-&.
8. Trams, E.G., et al., *EXFOLIATION OF MEMBRANE ECTO-ENZYMES IN THE FORM OF MICRO-VESICLES*. Biochimica Et Biophysica Acta, 1981. **645**(1): p. 63-70.
9. Harding, C., J. Heuser, and P. Stahl, *RECEPTOR-MEDIATED ENDOCYTOSIS OF TRANSFERRIN AND RECYCLING OF THE TRANSFERRIN RECEPTOR IN RAT RETICULOCYTES*. Journal of Cell Biology, 1983. **97**(2): p. 329-339.
10. Pan, B.-T. and R.M. Johnstone, *Fate of the transferrin receptor during maturation of sheep reticulocytes in vitro: selective externalization of the receptor*. Cell, 1983. **33**(3): p. 967-978.
11. Johnstone, R.M., et al., *VESICLE FORMATION DURING RETICULOCYTE MATURATION - ASSOCIATION OF PLASMA-MEMBRANE ACTIVITIES WITH RELEASED VESICLES (EXOSOMES)*. Journal of Biological Chemistry, 1987. **262**(19): p. 9412-9420.
12. Raposo, G., et al., *B lymphocytes secrete antigen-presenting vesicles*. Journal of Experimental Medicine, 1996. **183**(3): p. 1161-1172.
13. Valadi, H., et al., *Exosome-mediated transfer of mRNAs and microRNAs is a novel mechanism of genetic exchange between cells*. Nature Cell Biology, 2007. **9**(6): p. 654-U72.
14. Di Vizio, D., et al., *Large Oncosomes in Human Prostate Cancer Tissues and in the Circulation of Mice with Metastatic Disease*. American Journal of Pathology, 2012. **181**(5): p. 1573-1584.
15. Meehan, B., J. Rak, and D. Di Vizio, *Oncosomes—large and small: what are they, where they came from?* Journal of extracellular vesicles, 2016. **5**(1): p. 33109.
16. Brody, I., G. Ronquist, and A. Gottfries, *ULTRASTRUCTURAL-LOCALIZATION OF THE PROSTASOME - AN ORGANELLE IN HUMAN SEMINAL PLASMA*. Upsala Journal of Medical Sciences, 1983. **88**(2): p. 63-80.
17. Ronquist, G. and I. Brody, *THE PROSTASOME - ITS SECRETION AND FUNCTION IN MAN*. Biochimica Et Biophysica Acta, 1985. **822**(2): p. 203-218.
18. Le Pecq, J.B., *Dexosomes as a therapeutic cancer vaccine: From bench to bedside*. Blood Cells Molecules and Diseases, 2005. **35**(2): p. 129-135.
19. Vlassov, A.V., et al., *Exosomes: Current knowledge of their composition, biological functions, and diagnostic and therapeutic potentials*. Biochimica Et Biophysica Acta-General Subjects, 2012. **1820**(7): p. 940-948.
20. Cocucci, E. and J. Meldolesi, *Ectosomes and exosomes: shedding the confusion between extracellular vesicles*. Trends in Cell Biology, 2015. **25**(6): p. 364-372.

21. Gyorgy, B., et al., *Membrane vesicles, current state-of-the-art: emerging role of extracellular vesicles*. Cellular and Molecular Life Sciences, 2011. **68**(16): p. 2667-2688.
22. Anderson, H.C., *Matrix vesicles and calcification*. Current rheumatology reports, 2003. **5**(3): p. 222-226.
23. Karlsson, M., et al., *"Tolerosomes" are produced by intestinal epithelial cells*. European Journal of Immunology, 2001. **31**(10): p. 2892-2900.
24. Christian, J.L., *Argosomes: intracellular transport vehicles for intercellular signals?* Science Signaling, 2002. **2002**(124): p. pe13-pe13.
25. Gould, S.J. and G. Raposo, *As we wait: coping with an imperfect nomenclature for extracellular vesicles*. Journal of extracellular vesicles, 2013. **2**(1): p. 20389.
26. Van der Pol, E., et al., *Recent developments in the nomenclature, presence, isolation, detection and clinical impact of extracellular vesicles*. Journal of thrombosis and haemostasis, 2016. **14**(1): p. 48-56.
27. Witwer, K.W. and C. Théry, *Extracellular vesicles or exosomes? On primacy, precision, and popularity influencing a choice of nomenclature*. 2019, Taylor & Francis.
28. They, C., et al., *Minimal information for studies of extracellular vesicles 2018 (MISEV2018): a position statement of the International Society for Extracellular Vesicles and update of the MISEV2014 guidelines*. Journal of Extracellular Vesicles, 2018. **7**(1): p. 43.
29. Raposo, G. and W. Stoorvogel, *Extracellular vesicles: Exosomes, microvesicles, and friends*. J. Cell Biol., 2013. **200**(4): p. 373-383.
30. Doyle, L.M. and M.Z. Wang, *Overview of Extracellular Vesicles, Their Origin, Composition, Purpose, and Methods for Exosome Isolation and Analysis*. Cells, 2019. **8**(7): p. 24.
31. Jadli, A.S., et al., *Inside(sight) of tiny communicator: exosome biogenesis, secretion, and uptake*. Molecular and Cellular Biochemistry, 2020. **467**(1-2): p. 77-94.
32. Hessvik, N.P. and A. Llorente, *Current knowledge on exosome biogenesis and release*. Cellular and Molecular Life Sciences, 2018. **75**(2): p. 193-208.
33. Mobius, W., et al., *Immunolectron microscopic localization of cholesterol using biotinylated and non-cytolytic perfringolysin O*. Journal of Histochemistry & Cytochemistry, 2002. **50**(1): p. 43-55.
34. Henne, W.M., N.J. Buchkovich, and S.D. Emr, *The ESCRT pathway*. Developmental cell, 2011. **21**(1): p. 77-91.
35. Hurley, J.H., *ESCRTs are everywhere*. The EMBO journal, 2015. **34**(19): p. 2398-2407.
36. Jabbari, N., et al., *Tumor-derived extracellular vesicles: insights into bystander effects of exosomes after irradiation*. Lasers in Medical Science, 2020. **35**(3): p. 531-545.
37. Trajkovic, K., et al., *Ceramide triggers budding of exosome vesicles into multivesicular Endosomes*. Science, 2008. **319**(5867): p. 1244-1247.
38. Booth, A.M., et al., *Exosomes and HIV Gag bud from endosome-like domains of the T cell plasma membrane*. Journal of Cell Biology, 2006. **172**(6): p. 923-935.
39. Piper, R.C. and D.J. Katzmann, *Biogenesis and function of multivesicular bodies*. Annual Review of Cell and Developmental Biology, 2007. **23**: p. 519-547.
40. Yanez-Mo, M., et al., *Biological properties of extracellular vesicles and their physiological functions*. J. Extracell. Vesicles, 2015. **4**: p. 60.
41. Turturici, G., et al., *Extracellular membrane vesicles as a mechanism of cell-to-cell communication: advantages and disadvantages*. American Journal of Physiology-Cell Physiology, 2014. **306**(7): p. C621-C633.
42. Skotland, T., K. Sandvig, and A. Llorente, *Lipids in exosomes: current knowledge and the way forward*. Progress in lipid research, 2017. **66**: p. 30-41.
43. Möbius, W., et al., *Recycling compartments and the internal vesicles of multivesicular bodies harbor most of the cholesterol found in the endocytic pathway*. Traffic, 2003. **4**(4): p. 222-231.

44. Lydic, T.A., et al., *Rapid and comprehensive 'shotgun' lipidome profiling of colorectal cancer cell derived exosomes*. *Methods*, 2015. **87**: p. 83-95.
45. Skotland, T., et al., *An emerging focus on lipids in extracellular vesicles*. *Advanced drug delivery reviews*, 2020. **159**: p. 308-321.
46. Laulagnier, K., et al., *Mast cell-and dendritic cell-derived exosomes display a specific lipid composition and an unusual membrane organization*. *Biochemical Journal*, 2004. **380**(1): p. 161-171.
47. Parolini, I., et al., *Microenvironmental pH is a key factor for exosome traffic in tumor cells*. *Journal of Biological Chemistry*, 2009. **284**(49): p. 34211-34222.
48. Wubbolts, R., et al., *Proteomic and biochemical analyses of human B cell-derived exosomes: potential implications for their function and multivesicular body formation*. *Journal of Biological Chemistry*, 2003. **278**(13): p. 10963-10972.
49. Brouwers, J.F., et al., *Distinct lipid compositions of two types of human prostasomes*. *Proteomics*, 2013. **13**(10-11): p. 1660-1666.
50. Alvarez-Erviti, L., et al., *Delivery of siRNA to the mouse brain by systemic injection of targeted exosomes*. *Nature biotechnology*, 2011. **29**(4): p. 341-345.
51. Ridder, K., et al., *Extracellular vesicle-mediated transfer of genetic information between the hematopoietic system and the brain in response to inflammation*. *PLoS biology*, 2014. **12**(6): p. e1001874.
52. Osteikoetxea, X., et al., *Differential detergent sensitivity of extracellular vesicle subpopulations*. *Organic & biomolecular chemistry*, 2015. **13**(38): p. 9775-9782.
53. Ristorcelli, E., et al., *Human tumor nanoparticles induce apoptosis of pancreatic cancer cells*. *The FASEB Journal*, 2008. **22**(9): p. 3358-3369.
54. Ristorcelli, E., et al., *Essential role of Notch signaling in apoptosis of human pancreatic tumoral cells mediated by exosomal nanoparticles*. *International journal of cancer*, 2009. **125**(5): p. 1016-1026.
55. Beloribi, S., et al., *Exosomal lipids impact notch signaling and induce death of human pancreatic tumoral SOJ-6 cells*. 2012.
56. Beloribi-Djefafli, S., C. Siret, and D. Lombardo, *Exosomal lipids induce human pancreatic tumoral MiaPaCa-2 cells resistance through the CXCR4-SDF-1 α signaling axis*. *Oncoscience*, 2015. **2**(1): p. 15.
57. Record, M., et al., *Extracellular vesicles: lipids as key components of their biogenesis and functions*. *Journal of Lipid Research*, 2018. **59**(8): p. 1316-1324.
58. Van Niel, G., et al., *Exosomes: a common pathway for a specialized function*. *Journal of biochemistry*, 2006. **140**(1): p. 13-21.
59. Kleijmeer, M.J., et al., *Selective enrichment of tetraspan proteins on the internal vesicles of multivesicular endosomes and on exosomes secreted by human B-lymphocytes*. *Journal of Biological Chemistry*, 1998. **273**(32): p. 20121-20127.
60. Andreu, Z. and M. Yáñez-Mó, *Tetraspanins in extracellular vesicle formation and function*. *Frontiers in immunology*, 2014. **5**: p. 442.
61. Théry, C., et al., *Molecular characterization of dendritic cell-derived exosomes: selective accumulation of the heat shock protein hsc73*. *The Journal of cell biology*, 1999. **147**(3): p. 599-610.
62. Véron, P., et al., *Accumulation of MFG-E8/lactadherin on exosomes from immature dendritic cells*. *Blood Cells, Molecules, and Diseases*, 2005. **35**(2): p. 81-88.
63. Liang, Y., et al., *Complex N-linked glycans serve as a determinant for exosome/microvesicle cargo recruitment*. *Journal of Biological Chemistry*, 2014. **289**(47): p. 32526-32537.
64. Menck, K., et al., *Tumor-derived microvesicles mediate human breast cancer invasion through differentially glycosylated EMMPRIN*. *Journal of molecular cell biology*, 2015. **7**(2): p. 143-153.

65. Williams, C., et al., *Glycosylation of extracellular vesicles: current knowledge, tools and clinical perspectives*. Journal of Extracellular Vesicles, 2018. **7**(1): p. 1442985.
66. Melo, S.A., et al., *Glypican-1 identifies cancer exosomes and detects early pancreatic cancer*. Nature, 2015. **523**(7559): p. 177-182.
67. Han, P., et al., *Platelet P-selectin initiates cross-presentation and dendritic cell differentiation in blood monocytes*. Science advances, 2020. **6**(11): p. eaaz1580.
68. Crenshaw, B.J., B. Sims, and Q.L. Matthews, *Biological function of exosomes as diagnostic markers and therapeutic delivery vehicles in carcinogenesis and infectious diseases*, in *Nanomedicines*. 2018, IntechOpen.
69. Ratajczak, J., et al., *Membrane-derived microvesicles: important and underappreciated mediators of cell-to-cell communication*. Leukemia, 2006. **20**(9): p. 1487-1495.
70. Mateescu, B., et al., *Obstacles and opportunities in the functional analysis of extracellular vesicle RNA—an ISEV position paper*. Journal of extracellular vesicles, 2017. **6**(1): p. 1286095.
71. Jeppesen, D.K., et al., *Reassessment of exosome composition*. Cell, 2019. **177**(2): p. 428-445. e18.
72. Balaj, L., et al., *Tumour microvesicles contain retrotransposon elements and amplified oncogene sequences*. Nature communications, 2011. **2**(1): p. 1-9.
73. Camussi, G., et al., *Exosomes/microvesicles as a mechanism of cell-to-cell communication*. Kidney international, 2010. **78**(9): p. 838-848.
74. Kosaka, N., et al., *Secretory Mechanisms and Intercellular Transfer of MicroRNAs in Living Cells** . Journal of Biological Chemistry, 2010. **285**(23): p. 17442-17452.
75. van Niel, G., G. D'Angelo, and G. Raposo, *Shedding light on the cell biology of extracellular vesicles*. Nat. Rev. Mol. Cell Biol 2018. **19**(4): p. 213-228.
76. Hur, Y.H., R.A. Cerione, and M.A. Antonyak, *Extracellular vesicles and their roles in stem cell biology*. Stem Cells, 2020. **38**(4): p. 469-476.
77. Verweij, F.J., et al., *Live tracking of inter-organ communication by endogenous exosomes in vivo*. Developmental cell, 2019. **48**(4): p. 573-589. e4.
78. Webber, J., V. Yeung, and A. Clayton. *Extracellular vesicles as modulators of the cancer microenvironment*. in *Seminars in cell & developmental biology*. 2015. Elsevier.
79. Shimoda, M. and R. Khokha, *Metalloproteinases in extracellular vesicles*. Biochimica et Biophysica Acta (BBA)-Molecular Cell Research, 2017. **1864**(11): p. 1989-2000.
80. Becker, A., et al., *Extracellular Vesicles in Cancer: Cell-to-Cell Mediators of Metastasis*. Cancer Cell, 2016. **30**(6): p. 836-848.
81. Safaei, R., et al., *Abnormal lysosomal trafficking and enhanced exosomal export of cisplatin in drug-resistant human ovarian carcinoma cells*. Molecular cancer therapeutics, 2005. **4**(10): p. 1595-1604.
82. Nehrbas, J., et al., *Extracellular vesicles and chemotherapy resistance in the AML microenvironment*. Frontiers in oncology, 2020. **10**: p. 90.
83. Wieckowski, E.U., et al., *Tumor-derived microvesicles promote regulatory T cell expansion and induce apoptosis in tumor-reactive activated CD8+ T lymphocytes*. The Journal of Immunology, 2009. **183**(6): p. 3720-3730.
84. Bellingham, S.A., et al., *Exosomes: vehicles for the transfer of toxic proteins associated with neurodegenerative diseases?* Frontiers in physiology, 2012. **3**: p. 124.
85. Polanco, J.C., et al., *Exosomes taken up by neurons hijack the endosomal pathway to spread to interconnected neurons*. Acta neuropathologica communications, 2018. **6**(1): p. 1-14.
86. Stuenkel, A., et al., *Induction of α -synuclein aggregate formation by CSF exosomes from patients with Parkinson's disease and dementia with Lewy bodies*. Brain, 2016. **139**(2): p. 481-494.
87. Pegtel, D.M., et al., *Functional delivery of viral miRNAs via exosomes*. Proceedings of the National Academy of Sciences, 2010. **107**(14): p. 6328-6333.

88. Schorey, J.S. and C.V. Harding, *Extracellular vesicles and infectious diseases: new complexity to an old story*. The Journal of clinical investigation, 2016. **126**(4): p. 1181-1189.
89. Group, F.-N.B.W., *BEST (Biomarkers, EndpointS, and other Tools) Resource [Internet]*. 2016.
90. Stremersch, S., S.C. De Smedt, and K. Raemdonck, *Therapeutic and diagnostic applications of extracellular vesicles*. Journal of Controlled Release, 2016. **244**: p. 167-183.
91. Taylor, D.D. and C. Gercel-Taylor, *MicroRNA signatures of tumor-derived exosomes as diagnostic biomarkers of ovarian cancer*. Gynecologic oncology, 2008. **110**(1): p. 13-21.
92. Rabinowits, G., et al., *Exosomal microRNA: a diagnostic marker for lung cancer*. Clinical lung cancer, 2009. **10**(1): p. 42-46.
93. Wang, W., et al., *Peripheral blood microvesicles are potential biomarkers for hepatocellular carcinoma*. Cancer Biomarkers, 2013. **13**(5): p. 351-357.
94. Rahbari, M., et al., *Exosomes: novel implications in diagnosis and treatment of gastrointestinal cancer*. Langenbeck's archives of surgery, 2016. **401**(8): p. 1097-1110.
95. <https://assets.thermofisher.com/TFS-Assets/LSG/manuals/mp12883.pdf>.
96. Lane, R., et al., *Extracellular vesicles as circulating cancer biomarkers: opportunities and challenges*. Clinical and translational medicine, 2018. **7**(1): p. 1-11.
97. Shender, V.O., et al., *Proteome–metabolome profiling of ovarian cancer ascites reveals novel components involved in intercellular communication*. Molecular & Cellular Proteomics, 2014. **13**(12): p. 3558-3571.
98. Im, H., et al., *Label-free detection and molecular profiling of exosomes with a nano-plasmonic sensor*. Nature biotechnology, 2014. **32**(5): p. 490-495.
99. Zhou, J., et al., *Urinary microRNA-30a-5p is a potential biomarker for ovarian serous adenocarcinoma*. Oncology reports, 2015. **33**(6): p. 2915-2923.
100. Szajnik, M., et al., *Exosomes in plasma of patients with ovarian carcinoma: potential biomarkers of tumor progression and response to therapy*. Gynecology & obstetrics (Sunnyvale, Calif.), 2013: p. 003.
101. Li, J., et al., *Claudin-containing exosomes in the peripheral circulation of women with ovarian cancer*. BMC cancer, 2009. **9**(1): p. 1-11.
102. Cappellesso, R., et al., *Programmed cell death 4 and micro RNA 21 inverse expression is maintained in cells and exosomes from ovarian serous carcinoma effusions*. Cancer cytopathology, 2014. **122**(9): p. 685-693.
103. Øverbye, A., et al., *Identification of prostate cancer biomarkers in urinary exosomes*. Oncotarget, 2015. **6**(30): p. 30357.
104. McKiernan, J., et al., *A novel urine exosome gene expression assay to predict high-grade prostate cancer at initial biopsy*. JAMA oncology, 2016. **2**(7): p. 882-889.
105. Bryant, R., et al., *Changes in circulating microRNA levels associated with prostate cancer*. British journal of cancer, 2012. **106**(4): p. 768-774.
106. Rodríguez, M., et al., *Identification of non-invasive miRNAs biomarkers for prostate cancer by deep sequencing analysis of urinary exosomes*. Molecular cancer, 2017. **16**(1): p. 1-6.
107. Huang, X., et al., *Exosomal miR-1290 and miR-375 as prognostic markers in castration-resistant prostate cancer*. European urology, 2015. **67**(1): p. 33-41.
108. Sun, Y., et al., *Comparative proteomic analysis of exosomes and microvesicles in human saliva for lung cancer*. Journal of proteome research, 2018. **17**(3): p. 1101-1107.
109. Fang, T., et al., *Tumor-derived exosomal miR-1247-3p induces cancer-associated fibroblast activation to foster lung metastasis of liver cancer*. Nature communications, 2018. **9**(1): p. 1-13.
110. Li, Y., et al., *Proteomic identification of exosomal LRG1: a potential urinary biomarker for detecting NSCLC*. Electrophoresis, 2011. **32**(15): p. 1976-1983.
111. Skog, J., et al., *Glioblastoma microvesicles transport RNA and proteins that promote tumour growth and provide diagnostic biomarkers*. Nature cell biology, 2008. **10**(12): p. 1470-1476.

112. Akers, J.C., et al., *MiR-21 in the extracellular vesicles (EVs) of cerebrospinal fluid (CSF): a platform for glioblastoma biomarker development*. PloS one, 2013. **8**(10): p. e78115.
113. Jia, L., et al., *Concordance between the assessment of A β 42, T-tau, and P-T181-tau in peripheral blood neuronal-derived exosomes and cerebrospinal fluid*. Alzheimer's & Dementia, 2019. **15**(8): p. 1071-1080.
114. Kapogiannis, D., et al., *Dysfunctionally phosphorylated type 1 insulin receptor substrate in neural-derived blood exosomes of preclinical Alzheimer's disease*. The FASEB Journal, 2015. **29**(2): p. 589-596.
115. Liu, C.-G., et al., *MicroRNA-193b is a regulator of amyloid precursor protein in the blood and cerebrospinal fluid derived exosomal microRNA-193b is a biomarker of Alzheimer's disease*. Molecular medicine reports, 2014. **10**(5): p. 2395-2400.
116. Shi, M., et al., *Plasma exosomal α -synuclein is likely CNS-derived and increased in Parkinson's disease*. Acta neuropathologica, 2014. **128**(5): p. 639-650.
117. Cao, Z., et al., *α -Synuclein in salivary extracellular vesicles as a potential biomarker of Parkinson's disease*. Neuroscience letters, 2019. **696**: p. 114-120.
118. Oeckl, P., et al., *Multicenter validation of CSF neurofilaments as diagnostic biomarkers for ALS*. Amyotrophic Lateral Sclerosis and Frontotemporal Degeneration, 2016. **17**(5-6): p. 404-413.
119. Selmaj, I., et al., *Global exosome transcriptome profiling reveals biomarkers for multiple sclerosis*. Annals of neurology, 2017. **81**(5): p. 703-717.
120. Wang, S., et al., *Proteomic analysis of urinary extracellular vesicles reveal biomarkers for neurologic disease*. EBioMedicine, 2019. **45**: p. 351-361.
121. Jansen, F., G. Nickenig, and N. Werner, *Extracellular vesicles in cardiovascular disease: potential applications in diagnosis, prognosis, and epidemiology*. Circulation research, 2017. **120**(10): p. 1649-1657.
122. Akbar, N., et al., *Extracellular vesicles in metabolic disease*. Diabetologia, 2019. **62**(12): p. 2179-2187.
123. Zhou, B., et al., *Application of exosomes as liquid biopsy in clinical diagnosis*. Signal transduction and targeted therapy, 2020. **5**(1): p. 1-14.
124. Biosciences, M.b.C., *Exosome cancer diagnostic reaches market*. Nature biotechnology, 2016. **34**(4): p. 359.
125. Maroto, R., et al., *Effects of storage temperature on airway exosome integrity for diagnostic and functional analyses*. Journal of extracellular vesicles, 2017. **6**(1): p. 1359478.
126. Vizoso, F.J., et al., *Mesenchymal stem cell secretome: toward cell-free therapeutic strategies in regenerative medicine*. International journal of molecular sciences, 2017. **18**(9): p. 1852.
127. Arslan, F., et al., *Mesenchymal stem cell-derived exosomes increase ATP levels, decrease oxidative stress and activate PI3K/Akt pathway to enhance myocardial viability and prevent adverse remodeling after myocardial ischemia/reperfusion injury*. Stem cell research, 2013. **10**(3): p. 301-312.
128. Lai, R.C., et al., *Exosome secreted by MSC reduces myocardial ischemia/reperfusion injury*. Stem cell research, 2010. **4**(3): p. 214-222.
129. Ibrahim, A.G.-E., K. Cheng, and E. Marbán, *Exosomes as critical agents of cardiac regeneration triggered by cell therapy*. Stem cell reports, 2014. **2**(5): p. 606-619.
130. Li, T., et al., *Exosomes derived from human umbilical cord mesenchymal stem cells alleviate liver fibrosis*. Stem cells and development, 2013. **22**(6): p. 845-854.
131. Xin, H., et al., *Exosome-mediated transfer of miR-133b from multipotent mesenchymal stromal cells to neural cells contributes to neurite outgrowth*. Stem cells, 2012. **30**(7): p. 1556-1564.
132. Badiavas, E.V. and V. Falanga, *Treatment of chronic wounds with bone marrow-derived cells*. Archives of dermatology, 2003. **139**(4): p. 510-516.
133. Gao, D. and L. Jiang, *Exosomes in cancer therapy: a novel experimental strategy*. American journal of cancer research, 2018. **8**(11): p. 2165.

134. Doeppner, T.R., et al., *Concise review: extracellular vesicles overcoming limitations of cell therapies in ischemic stroke*. Stem cells translational medicine, 2017. **6**(11): p. 2044-2052.
135. Tran, T.-H., et al., *Exosomes as nanocarriers for immunotherapy of cancer and inflammatory diseases*. Clinical immunology, 2015. **160**(1): p. 46-58.
136. Perocheau, D., et al., *Clinical applications for exosomes: are we there yet?* British Journal of Pharmacology, 2021. **178**(12): p. 2375-2392.
137. Devhare, P.B. and R.B. Ray, *A novel role of exosomes in the vaccination approach*. Annals of translational medicine, 2017. **5**(1).
138. Polak, K., et al., *Extracellular vesicle-based vaccine platform displaying native viral envelope proteins elicits a robust anti-SARS-CoV-2 response in mice*. BioRxiv, 2020.
139. Gardiner, C., et al., *Techniques used for the isolation and characterization of extracellular vesicles: results of a worldwide survey*. J. Extracell. Vesicles, 2016. **5**.
140. Li, P., et al., *Progress in exosome isolation techniques*. Theranostics, 2017. **7**(3): p. 789.
141. Momen-Heravi, F., et al., *Impact of biofluid viscosity on size and sedimentation efficiency of the isolated microvesicles*. Frontiers in physiology, 2012. **3**: p. 162.
142. Linares, R., et al., *High-speed centrifugation induces aggregation of extracellular vesicles*. Journal of extracellular vesicles, 2015. **4**(1): p. 29509.
143. Théry, C., et al., *Isolation and characterization of exosomes from cell culture supernatants and biological fluids*. Current protocols in cell biology, 2006. **30**(1): p. 3.22. 1-3.22. 29.
144. Van Deun, J., et al., *The impact of disparate isolation methods for extracellular vesicles on downstream RNA profiling*. Journal of extracellular vesicles, 2014. **3**(1): p. 24858.
145. Abramowicz, A., P. Widlak, and M. Pietrowska, *Proteomic analysis of exosomal cargo: the challenge of high purity vesicle isolation*. Molecular BioSystems, 2016. **12**(5): p. 1407-1419.
146. Yuana, Y., et al., *Co-isolation of extracellular vesicles and high-density lipoproteins using density gradient ultracentrifugation*. Journal of extracellular vesicles, 2014. **3**(1): p. 23262.
147. Witwer, K.W., et al., *Standardization of sample collection, isolation and analysis methods in extracellular vesicle research*. Journal of extracellular vesicles, 2013. **2**(1): p. 20360.
148. Alvarez, M.L., et al., *Comparison of protein, microRNA, and mRNA yields using different methods of urinary exosome isolation for the discovery of kidney disease biomarkers*. Kidney international, 2012. **82**(9): p. 1024-1032.
149. Raj, D.A., et al., *A multiplex quantitative proteomics strategy for protein biomarker studies in urinary exosomes*. Kidney international, 2012. **81**(12): p. 1263-1272.
150. Lobb, R.J., et al., *Optimized exosome isolation protocol for cell culture supernatant and human plasma*. Journal of extracellular vesicles, 2015. **4**(1): p. 27031.
151. Zeringer, E., et al., *Strategies for isolation of exosomes*. Cold Spring Harbor Protocols, 2015. **2015**(4): p. pdb. top074476.
152. Cheruvanky, A., et al., *Rapid isolation of urinary exosomal biomarkers using a nanomembrane ultrafiltration concentrator*. American Journal of Physiology-Renal Physiology, 2007. **292**(5): p. F1657-F1661.
153. Kornilov, R., et al., *Efficient ultrafiltration-based protocol to deplete extracellular vesicles from fetal bovine serum*. Journal of extracellular vesicles, 2018. **7**(1): p. 1422674.
154. Liangsupree, T., E. Multia, and M.-L. Riekkola, *Modern isolation and separation techniques for extracellular vesicles*. Journal of Chromatography A, 2020: p. 461773.
155. Vergauwen, G., et al., *Confounding factors of ultrafiltration and protein analysis in extracellular vesicle research*. Scientific reports, 2017. **7**(1): p. 1-12.
156. Busatto, S., et al., *Tangential flow filtration for highly efficient concentration of extracellular vesicles from large volumes of fluid*. Cells, 2018. **7**(12): p. 273.
157. Xu, R., et al., *Highly-purified exosomes and shed microvesicles isolated from the human colon cancer cell line LIM1863 by sequential centrifugal ultrafiltration are biochemically and functionally distinct*. Methods, 2015. **87**: p. 11-25.

158. Nordin, J.Z., et al., *Ultrafiltration with size-exclusion liquid chromatography for high yield isolation of extracellular vesicles preserving intact biophysical and functional properties*. *Nanomedicine: Nanotechnology, Biology and Medicine*, 2015. **11**(4): p. 879-883.
159. Guerreiro, E.M., et al., *Efficient extracellular vesicle isolation by combining cell media modifications, ultrafiltration, and size-exclusion chromatography*. *PLoS one*, 2018. **13**(9): p. e0204276.
160. Benedikter, B.J., et al., *Ultrafiltration combined with size exclusion chromatography efficiently isolates extracellular vesicles from cell culture media for compositional and functional studies*. *Scientific reports*, 2017. **7**(1): p. 1-13.
161. Bano, R., F. Ahmad, and M. Mohsin, *A perspective on the isolation and characterization of extracellular vesicles from different biofluids*. *RSC Advances*, 2021. **11**(32): p. 19598-19615.
162. Takov, K., D.M. Yellon, and S.M. Davidson, *Comparison of small extracellular vesicles isolated from plasma by ultracentrifugation or size-exclusion chromatography: yield, purity and functional potential*. *Journal of extracellular vesicles*, 2019. **8**(1): p. 1560809.
163. Arntz, O.J., et al., *An optimized method for plasma extracellular vesicles isolation to exclude the copresence of biological drugs and plasma proteins which impairs their biological characterization*. *PLoS one*, 2020. **15**(7): p. e0236508.
164. Garcia-Romero, N., et al., *Polyethylene glycol improves current methods for circulating extracellular vesicle-derived DNA isolation*. *Journal of translational medicine*, 2019. **17**(1): p. 1-11.
165. Rider, M.A., S.N. Hurwitz, and D.G. Meckes Jr, *ExtraPEG: a polyethylene glycol-based method for enrichment of extracellular vesicles*. *Scientific reports*, 2016. **6**: p. 23978.
166. Weng, Y., et al., *Effective isolation of exosomes with polyethylene glycol from cell culture supernatant for in-depth proteome profiling*. *Analyst*, 2016. **141**(15): p. 4640-4646.
167. Lv, C.-y., et al., *A PEG-based method for the isolation of urinary exosomes and its application in renal fibrosis diagnostics using cargo miR-29c and miR-21 analysis*. *International urology and nephrology*, 2018. **50**(5): p. 973-982.
168. Shin, H., et al., *High-yield isolation of extracellular vesicles using aqueous two-phase system*. *Scientific reports*, 2015. **5**(1): p. 1-11.
169. Kirbaş, O.K., et al., *Optimized isolation of extracellular vesicles from various organic sources using aqueous two-phase system*. *Scientific reports*, 2019. **9**(1): p. 1-11.
170. Tauro, B.J., et al., *Comparison of ultracentrifugation, density gradient separation, and immunoaffinity capture methods for isolating human colon cancer cell line LIM1863-derived exosomes*. *Methods*, 2012. **56**(2): p. 293-304.
171. Ueda, K., et al., *Antibody-coupled monolithic silica microtips for highthroughput molecular profiling of circulating exosomes*. *Scientific reports*, 2014. **4**(1): p. 1-9.
172. Multia, E., et al., *Fast isolation of highly specific population of platelet-derived extracellular vesicles from blood plasma by affinity monolithic column, immobilized with anti-human CD61 antibody*. *Anal. Chim. Acta*, 2019. **1091**: p. 160-168.
173. Multia, E., et al., *Automated on-line isolation and fractionation system for nanosized biomacromolecules from human plasma*. *Analytical chemistry*, 2020. **92**(19): p. 13058-13065.
174. Zhang, K., et al., *Rapid capture and nondestructive release of extracellular vesicles using aptamer-based magnetic isolation*. *ACS sensors*, 2019. **4**(5): p. 1245-1251.
175. Song, Z., et al., *Development of a CD63 Aptamer for Efficient Cancer Immunochemistry and Immunoaffinity-Based Exosome Isolation*. *Molecules*, 2020. **25**(23): p. 5585.
176. Brambilla, D., et al., *EV Separation: Release of Intact Extracellular Vesicles Immunocaptured on Magnetic Particles*. *Analytical chemistry*, 2021. **93**(13): p. 5476-5483.
177. Nakai, W., et al., *A novel affinity-based method for the isolation of highly purified extracellular vesicles*. *Scientific reports*, 2016. **6**(1): p. 1-11.

178. Cai, S., et al., *Immuno-modified superparamagnetic nanoparticles via host-guest interactions for high-purity capture and mild release of exosomes*. *Nanoscale*, 2018. **10**(29): p. 14280-14289.
179. Giebel, B. and C. Helmbrecht, *Methods to analyze EVs*. *Exosomes and microvesicles*, 2017: p. 1-20.
180. Zhang, H.Y., et al., *Identification of distinct nanoparticles and subsets of extracellular vesicles by asymmetric flow field-flow fractionation*. *Nat. Cell Biol.*, 2018. **20**(3): p. 332-+.
181. Zhang, H.Y. and D. Lyden, *Asymmetric-flow field-flow fractionation technology for exomere and small extracellular vesicle separation and characterization*. *Nature Protocols*, 2019. **14**(4): p. 1027-1053.
182. György, B., et al., *Detection and isolation of cell-derived microparticles are compromised by protein complexes resulting from shared biophysical parameters*. *Blood, The Journal of the American Society of Hematology*, 2011. **117**(4): p. e39-e48.
183. Szatanek, R., et al., *The Methods of Choice for Extracellular Vesicles (EVs) Characterization*. *Int. J. Mol. Sci.*, 2017. **18**(6).
184. Van Der Pol, E., et al., *Optical and non-optical methods for detection and characterization of microparticles and exosomes*. *Journal of Thrombosis and Haemostasis*, 2010. **8**(12): p. 2596-2607.
185. Soo, C.Y., et al., *Nanoparticle tracking analysis monitors microvesicle and exosome secretion from immune cells*. *Immunology*, 2012. **136**(2): p. 192-197.
186. Dragovic, R.A., et al., *Sizing and phenotyping of cellular vesicles using Nanoparticle Tracking Analysis*. *Nanomedicine: Nanotechnology, Biology and Medicine*, 2011. **7**(6): p. 780-788.
187. Serrano-Pertierra, E., et al., *Extracellular vesicles: Current analytical techniques for detection and quantification*. *Biomolecules*, 2020. **10**(6): p. 824.
188. Maas, S.L., et al., *Possibilities and limitations of current technologies for quantification of biological extracellular vesicles and synthetic mimics*. *Journal of Controlled Release*, 2015. **200**: p. 87-96.
189. Vogel, R., et al., *Quantitative sizing of nano/microparticles with a tunable elastomeric pore sensor*. *Analytical chemistry*, 2011. **83**(9): p. 3499-3506.
190. Anderson, W., et al., *Observations of tunable resistive pulse sensing for exosome analysis: improving system sensitivity and stability*. *Langmuir*, 2015. **31**(23): p. 6577-6587.
191. Garza-Licudine, E., et al. *Portable nanoparticle quantization using a resizable nanopore instrument-The IZON qNano™*. in *2010 Annual International Conference of the IEEE Engineering in Medicine and Biology*. 2010. IEEE.
192. Akers, J.C., et al., *Comparative analysis of technologies for quantifying extracellular vesicles (EVs) in clinical cerebrospinal fluids (CSF)*. *PLoS one*, 2016. **11**(2): p. e0149866.
193. Koliha, N., et al., *A novel multiplex bead-based platform highlights the diversity of extracellular vesicles*. *Journal of extracellular vesicles*, 2016. **5**(1): p. 29975.
194. Aass, H.C.D., et al., *Fluorescent particles in the antibody solution result in false TF-and CD14-positive microparticles in flow cytometric analysis*. *Cytometry Part A*, 2011. **79**(12): p. 990-999.
195. Stoner, S.A., et al., *High sensitivity flow cytometry of membrane vesicles*. *Cytometry Part A*, 2016. **89**(2): p. 196-206.
196. Van der Pol, E., et al., *Particle size distribution of exosomes and microvesicles determined by transmission electron microscopy, flow cytometry, nanoparticle tracking analysis, and resistive pulse sensing*. *Journal of Thrombosis and Haemostasis*, 2014. **12**(7): p. 1182-1192.
197. Chiang, C.-y. and C. Chen, *Toward characterizing extracellular vesicles at a single-particle level*. *Journal of biomedical science*, 2019. **26**(1): p. 1-10.
198. Hartjes, T.A., et al., *Extracellular vesicle quantification and characterization: common methods and emerging approaches*. *Bioengineering*, 2019. **6**(1): p. 7.

199. Théry, C., et al., *Proteomic analysis of dendritic cell-derived exosomes: a secreted subcellular compartment distinct from apoptotic vesicles*. The Journal of Immunology, 2001. **166**(12): p. 7309-7318.
200. Issman, L., et al., *Cryogenic transmission electron microscopy nanostructural study of shed microparticles*. PLoS One, 2013. **8**(12): p. e83680.
201. Melo, S.A., et al., *Cancer exosomes perform cell-independent microRNA biogenesis and promote tumorigenesis*. Cancer cell, 2014. **26**(5): p. 707-721.
202. Sharma, S., et al., *Structural-mechanical characterization of nanoparticle exosomes in human saliva, using correlative AFM, FESEM, and force spectroscopy*. ACS nano, 2010. **4**(4): p. 1921-1926.
203. Parisse, P., et al., *Atomic force microscopy analysis of extracellular vesicles*. European biophysics journal, 2017. **46**(8): p. 813-820.
204. Rikkert, L., et al., *Cancer-id: Toward identification of cancer by tumor-derived extracellular vesicles in blood*. Frontiers in oncology, 2020. **10**: p. 608.
205. Cheng, J., T. Nonaka, and D.T. Wong, *Salivary exosomes as nanocarriers for cancer biomarker delivery*. Materials, 2019. **12**(4): p. 654.
206. Yuana, Y., et al., *Atomic force microscopy: a novel approach to the detection of nanosized blood microparticles*. Journal of thrombosis and haemostasis, 2010. **8**(2): p. 315-323.
207. Hardij, J., et al., *Characterisation of tissue factor-bearing extracellular vesicles with AFM: comparison of air-tapping-mode AFM and liquid Peak Force AFM*. Journal of extracellular vesicles, 2013. **2**(1): p. 21045.
208. Zhu, L., et al., *Label-free quantitative detection of tumor-derived exosomes through surface plasmon resonance imaging*. Analytical chemistry, 2014. **86**(17): p. 8857-8864.
209. Rojalin, T., et al., *Nanoplasmonic approaches for sensitive detection and molecular characterization of extracellular vesicles*. Frontiers in chemistry, 2019. **7**: p. 279.
210. Liang, K., et al., *Nanoplasmonic quantification of tumour-derived extracellular vesicles in plasma microsamples for diagnosis and treatment monitoring*. Nature biomedical engineering, 2017. **1**(4): p. 1-11.
211. Woo, H.-K., et al., *Exodisc for rapid, size-selective, and efficient isolation and analysis of nanoscale extracellular vesicles from biological samples*. Acs Nano, 2017. **11**(2): p. 1360-1370.
212. Choi, D.S., et al., *Proteomics of extracellular vesicles: exosomes and ectosomes*. Mass spectrometry reviews, 2015. **34**(4): p. 474-490.
213. Kim, D.-K., et al., *EVpedia: an integrated database of high-throughput data for systemic analyses of extracellular vesicles*. Journal of extracellular vesicles, 2013. **2**(1): p. 20384.
214. Keerthikumar, S., et al., *ExoCarta: a web-based compendium of exosomal cargo*. Journal of molecular biology, 2016. **428**(4): p. 688-692.
215. Kalra, H., et al., *Vesiclepedia: a compendium for extracellular vesicles with continuous community annotation*. PLoS biology, 2012. **10**(12): p. e1001450.
216. Pocsfalvi, G., et al., *Mass spectrometry of extracellular vesicles*. Mass Spectrometry Reviews, 2016. **35**(1): p. 3-21.
217. Kreimer, S., et al., *Mass-spectrometry-based molecular characterization of extracellular vesicles: lipidomics and proteomics*. Journal of proteome research, 2015. **14**(6): p. 2367-2384.
218. Laurent, L.C., et al., *Meeting report: discussions and preliminary findings on extracellular RNA measurement methods from laboratories in the NIH Extracellular RNA Communication Consortium*. Journal of extracellular vesicles, 2015. **4**(1): p. 26533.
219. Williams, Z., et al., *Comprehensive profiling of circulating microRNA via small RNA sequencing of cDNA libraries reveals biomarker potential and limitations*. Proceedings of the National Academy of Sciences, 2013. **110**(11): p. 4255-4260.
220. Shao, H.L., et al., *New Technologies for Analysis of Extracellular Vesicles*. Chem. Rev., 2018. **118**(4): p. 1917-1950.

221. Meng, Y., et al., *Microfluidics for extracellular vesicle separation and mimetic synthesis: Recent advances and future perspectives*. Chemical Engineering Journal, 2021. **404**: p. 126110.
222. Chen, C., et al., *Microfluidic isolation and transcriptome analysis of serum microvesicles*. Lab on a Chip, 2010. **10**(4): p. 505-511.
223. Ashcroft, B.A., et al., *Determination of the size distribution of blood microparticles directly in plasma using atomic force microscopy and microfluidics*. Biomedical microdevices, 2012. **14**(4): p. 641-649.
224. Kanwar, S.S., et al., *Microfluidic device (ExoChip) for on-chip isolation, quantification and characterization of circulating exosomes*. Lab on a Chip, 2014. **14**(11): p. 1891-1900.
225. Vaidyanathan, R., et al., *Detecting Exosomes Specifically: A Multiplexed Device Based on Alternating Current Electrohydrodynamic Induced Nanoshearing*. Anal. Chem., 2014. **86**(22): p. 11125-11132.
226. Chen, C., et al., *based immunoaffinity devices for accessible isolation and characterization of extracellular vesicles*. Microfluidics and nanofluidics, 2014. **16**(5): p. 849-856.
227. He, M., et al., *Integrated immunoisolation and protein analysis of circulating exosomes using microfluidic technology*. Lab on a Chip, 2014. **14**(19): p. 3773-3780.
228. Dudani, J.S., et al., *Rapid inertial solution exchange for enrichment and flow cytometric detection of microvesicles*. Biomicrofluidics, 2015. **9**(1): p. 014112.
229. Shao, H., et al., *Chip-based analysis of exosomal mRNA mediating drug resistance in glioblastoma*. Nature communications, 2015. **6**(1): p. 1-9.
230. Zhao, Z., et al., *A microfluidic ExoSearch chip for multiplexed exosome detection towards blood-based ovarian cancer diagnosis*. Lab on a Chip, 2016. **16**(3): p. 489-496.
231. Zhang, P., M. He, and Y. Zeng, *Ultrasensitive microfluidic analysis of circulating exosomes using a nanostructured graphene oxide/polydopamine coating*. Lab on a Chip, 2016. **16**(16): p. 3033-3042.
232. Sina, A.A.I., et al., *Real time and label free profiling of clinically relevant exosomes*. Scientific reports, 2016. **6**(1): p. 1-9.
233. Fang, S., et al., *Clinical application of a microfluidic chip for immunocapture and quantification of circulating exosomes to assist breast cancer diagnosis and molecular classification*. PloS one, 2017. **12**(4): p. e0175050.
234. Hisey, C.L., et al., *Microfluidic affinity separation chip for selective capture and release of label-free ovarian cancer exosomes*. Lab on a Chip, 2018. **18**(20): p. 3144-3153.
235. Reátegui, E., et al., *Engineered nanointerfaces for microfluidic isolation and molecular profiling of tumor-specific extracellular vesicles*. Nature communications, 2018. **9**(1): p. 1-11.
236. Xu, H., et al., *Magnetic-based microfluidic device for on-chip isolation and detection of tumor-derived exosomes*. Analytical chemistry, 2018. **90**(22): p. 13451-13458.
237. Su, W.T., et al., *Microfluidic strategies for label-free exosomes isolation and analysis*. Trac-Trends Anal. Chem., 2019. **118**: p. 686-698.
238. Hassanpour Tamrin, S., A. Sanati Nezhad, and A. Sen, *Label-Free Isolation of Exosomes Using Microfluidic Technologies*. ACS Nano, 2021.
239. Liu, F., et al., *The exosome total isolation chip*. ACS nano, 2017. **11**(11): p. 10712-10723.
240. Liu, C., et al., *Field-free isolation of exosomes from extracellular vesicles by microfluidic viscoelastic flows*. ACS nano, 2017. **11**(7): p. 6968-6976.
241. Liu, C., et al., *λ -DNA-and aptamer-mediated sorting and analysis of extracellular vesicles*. Journal of the American Chemical Society, 2019. **141**(9): p. 3817-3821.
242. Huang, L.R., et al., *Continuous particle separation through deterministic lateral displacement*. Science, 2004. **304**(5673): p. 987-990.
243. Santana, S.M., et al., *Microfluidic isolation of cancer-cell-derived microvesicles from heterogeneous extracellular shed vesicle populations*. Biomedical microdevices, 2014. **16**(6): p. 869-877.

244. Wunsch, B.H., et al., *Nanoscale lateral displacement arrays for the separation of exosomes and colloids down to 20 nm*. Nature nanotechnology, 2016. **11**(11): p. 936-940.
245. Lee, K., et al., *Acoustic purification of extracellular microvesicles*. ACS nano, 2015. **9**(3): p. 2321-2327.
246. Wu, M., et al., *Isolation of exosomes from whole blood by integrating acoustics and microfluidics*. Proceedings of the National Academy of Sciences, 2017. **114**(40): p. 10584-10589.
247. Liu, C., et al., *Low-cost thermophoretic profiling of extracellular-vesicle surface proteins for the early detection and classification of cancers*. Nature biomedical engineering, 2019. **3**(3): p. 183-193.
248. Tian, F., et al., *Protein analysis of extracellular vesicles to monitor and predict therapeutic response in metastatic breast cancer*. Nature communications, 2021. **12**(1): p. 1-13.
249. Huang, M., et al., *Homogeneous, low-volume, efficient, and sensitive quantitation of circulating exosomal PD-L1 for cancer diagnosis and immunotherapy response prediction*. Angewandte Chemie, 2020. **132**(12): p. 4830-4835.
250. Midekessa, G., et al., *Zeta potential of extracellular vesicles: toward understanding the attributes that determine colloidal stability*. Acs Omega, 2020. **5**(27): p. 16701-16710.
251. Morani, M., et al., *Recent electrokinetic strategies for isolation, enrichment and separation of extracellular vesicles*. TrAC Trends in Analytical Chemistry, 2021: p. 116179.
252. El Ouahabi, O., et al., *A simple method for the analysis of extracellular vesicles enriched for exosomes from human serum by capillary electrophoresis with ultraviolet diode array detection*. Journal of Chromatography A, 2021. **1635**: p. 461752.
253. Dou, Y., et al., *Quantitative Capillary Electrophoresis for Analysis of Extracellular Vesicles (EVqCE)*. Separations, 2021. **8**(8): p. 110.
254. Zocco, D., et al., *Extracellular vesicles as shuttles of tumor biomarkers and anti-tumor drugs*. Frontiers in oncology, 2014. **4**: p. 267.
255. Piotrowska, M., et al., *Capillary zone electrophoresis of bacterial extracellular vesicles: A proof of concept*. J. Chromatogr. A, 2020: p. 461047.
256. Dawod, M., N.E. Arvin, and R.T. Kennedy, *Recent advances in protein analysis by capillary and microchip electrophoresis*. Analyst, 2017. **142**(11): p. 1847-1866.
257. Kaur, H., et al., *Capillary electrophoresis and the biopharmaceutical industry: Therapeutic protein analysis and characterization*. TrAC Trends in Analytical Chemistry, 2021. **144**: p. 116407.
258. Toseland, C.P., *Fluorescent labeling and modification of proteins*. Journal of chemical biology, 2013. **6**(3): p. 85-95.
259. Galievsky, V.A., A.S. Stasheuski, and S.N. Krylov, *"Getting the best sensitivity from on-capillary fluorescence detection in capillary electrophoresis"—A tutorial*. Analytica chimica acta, 2016. **935**: p. 58-81.
260. Martins, T.S., et al., *Exosome isolation from distinct biofluids using precipitation and column-based approaches*. Plos One, 2018. **13**(6).
261. Llorente, A., et al., *Molecular lipidomics of exosomes released by PC-3 prostate cancer cells*. Biochimica et Biophysica Acta (BBA)-Molecular and Cell Biology of Lipids, 2013. **1831**(7): p. 1302-1309.
262. Record, M., et al., *Exosomes as new vesicular lipid transporters involved in cell-cell communication and various pathophysiologicals*. Biochimica et Biophysica Acta (BBA)-Molecular and Cell Biology of Lipids, 2014. **1841**(1): p. 108-120.
263. Tani, Y. and T. Kaneta, *Indirect capillary electrophoresis immunoassay of membrane protein in extracellular vesicles*. J. Chromatogr. A, 2020. **1629**: p. 461513.
264. Kuhn, R. and S. Hoffstetter-Kuhn, *Capillary electrophoresis: principles and practice*. 2013: Springer Science & Business Media.

265. Khaledi, M.G., *High performance capillary electrophoresis*. John Wiley & Sons, Inc., New York, 1998. **146**: p. 303-401.
266. Landers, J.P., *Handbook of capillary and microchip electrophoresis and associated microtechniques*. 2007: CRC press.
267. Frenz, J. and W.S. Hancock, *High performance capillary electrophoresis*. Trends in biotechnology, 1991. **9**(1): p. 243-250.
268. Morani, M., M. Taverna, and T.D. Mai, *A fresh look into background electrolyte selection for capillary electrophoresis-laser induced fluorescence of peptides and proteins*. Electrophoresis, 2019. **40**(18-19): p. 2618-2624.
269. Dehghani, M. and T.R. Gaborski, *Fluorescent labeling of extracellular vesicles*. Methods in Enzymology, 2020. **645**: p. 15-42.
270. Morani, M., et al., *Electrokinetic characterization of extracellular vesicles with capillary electrophoresis: a new tool for their identification and quantification*. Anal. Chim. Acta, 2020.
271. Trapiella-Alfonso, L., et al., *Electromigration separation methodologies for the characterization of nanoparticles and the evaluation of their behaviour in biological systems*. Trac-Trends Anal. Chem., 2016. **84**: p. 121-130.
272. Overbeek, J.T.G., *Theory of electrophoresis—The relaxation effect*. Koll. Bith, 1943. **287**.
273. Booth, F., *The cataphoresis of spherical, solid non-conducting particles in a symmetrical electrolyte*. Proceedings of the Royal Society of London. Series A. Mathematical and Physical Sciences, 1950. **203**(1075): p. 514-533.
274. Wiersema, P., A. Loeb, and J.T.G. Overbeek, *Calculation of the electrophoretic mobility of a spherical colloid particle*. Journal of Colloid and Interface Science, 1966. **22**(1): p. 78-99.
275. Pyell, U., *Characterization of nanoparticles by capillary electromigration separation techniques*. Electrophoresis, 2010. **31**(5): p. 814-831.
276. d'Orlye, F., A. Varenne, and P. Gareil, *Size-based characterization of nanometric cationic maghemite particles using capillary zone electrophoresis*. Electrophoresis, 2008. **29**(18): p. 3768-3778.
277. d'Orlye, F., et al., *Charge-based characterization of nanometric cationic bifunctional maghemite/silica core/shell particles by capillary zone electrophoresis*. Electrophoresis, 2009. **30**(14): p. 2572-2582.
278. Liu, F.K., et al., *Studying the size/shape separation and optical properties of silver nanoparticles by capillary electrophoresis*. J. Chromatogr. A, 2005. **1062**(1): p. 139-145.
279. Vanifatova, N.G., et al., *Investigation of iron oxide nanoparticles by capillary zone electrophoresis*. Talanta, 2005. **66**(3): p. 605-610.
280. Parolini, I., et al., *Microenvironmental pH Is a Key Factor for Exosome Traffic in Tumor Cells*. J. Biol. Chem., 2009. **284**(49): p. 34211-34222.
281. Petersen, K.E., et al., *Exosome Isolation: Cyclical Electrical Field Flow Fractionation in Low-Ionic-Strength Fluids*. Anal. Chem., 2018. **90**(21): p. 12783-12790.
282. Šlampová, A., Z. Malá, and P. Gebauer, *Recent progress of sample stacking in capillary electrophoresis (2016–2018)*. Electrophoresis, 2019. **40**(1): p. 40-54.
283. Breadmore, M.C., et al., *Recent advances in enhancing the sensitivity of electrophoresis and electrochromatography in capillaries and microchips (2016–2018)*. Electrophoresis, 2019. **40**(1): p. 17-39.
284. Dziomba, S., K. Ciura, and M. Dawid, *The on-line preconcentration of nanoparticles in electromigration techniques*. J. Chromatogr. A, 2019. **1606**.
285. Cho, S., et al., *Isolation of extracellular vesicle from blood plasma using electrophoretic migration through porous membrane*. Sens. Actuators B, 2016. **233**: p. 289-297.
286. Bosch, S., et al., *Trehalose prevents aggregation of exosomes and cryodamage*. Scientific reports, 2016. **6**(1): p. 1-11.

287. Crosnier de Lassichère, C.d., et al., *Online preconcentration in capillaries by multiple large-volume sample stacking: an alternative to immunoassays for quantification of amyloid beta peptides biomarkers in cerebrospinal fluid*. Analytical chemistry, 2018. **90**(4): p. 2555-2563.
288. Margolis, L. and Y. Sadovskyz, *The biology of extracellular vesicles: The known unknowns*. Plos Biology, 2019. **17**(7): p. 12.
289. Taylor, G.I., *Dispersion of soluble matter in solvent flowing slowly through a tube*. Proceedings of the Royal Society of London. Series A. Mathematical and Physical Sciences, 1953. **219**(1137): p. 186-203.
290. Belongia, B. and J. Baygents, *Measurements on the diffusion coefficient of colloidal particles by Taylor–Aris dispersion*. Journal of colloid and interface science, 1997. **195**(1): p. 19-31.
291. d’Orlyé, F., A. Varenne, and P. Gareil, *Determination of nanoparticle diffusion coefficients by Taylor dispersion analysis using a capillary electrophoresis instrument*. Journal of Chromatography A, 2008. **1204**(2): p. 226-232.
292. Cipelletti, L., et al., *Measuring arbitrary diffusion coefficient distributions of Nano-Objects by Taylor dispersion analysis*. Analytical chemistry, 2015. **87**(16): p. 8489-8496.
293. Urban, D.A., et al., *Taylor dispersion of inorganic nanoparticles and comparison to dynamic light scattering and transmission electron microscopy*. Colloid and Interface Science Communications, 2018. **22**: p. 29-33.
294. Moser, M.R. and C.A. Baker, *Taylor dispersion analysis in fused silica capillaries: a tutorial review*. Analytical Methods, 2021.
295. Taylor, G.I., *The dispersion of matter in turbulent flow through a pipe*. Proceedings of the Royal Society of London. Series A. Mathematical and Physical Sciences, 1954. **223**(1155): p. 446-468.
296. Taylor, G.I., *Conditions under which dispersion of a solute in a stream of solvent can be used to measure molecular diffusion*. Proceedings of the Royal Society of London. Series A. Mathematical and Physical Sciences, 1954. **225**(1163): p. 473-477.
297. Sharma, U., N.J. Gleason, and J.D. Carbeck, *Diffusivity of solutes measured in glass capillaries using Taylor’s analysis of dispersion and a commercial CE instrument*. Analytical chemistry, 2005. **77**(3): p. 806-813.
298. Cottet, H., J.-P. Biron, and M. Martin, *On the optimization of operating conditions for Taylor dispersion analysis of mixtures*. Analyst, 2014. **139**(14): p. 3552-3562.
299. Chamieh, J., et al., *Limits in size of Taylor dispersion analysis: representation of the different hydrodynamic regimes and application to the size-characterization of cubosomes*. Analytical chemistry, 2017. **89**(24): p. 13487-13493.
300. Pyell, U., et al., *Characterization of gold nanoparticles with different hydrophilic coatings via capillary electrophoresis and Taylor dispersion analysis. Part I: Determination of the zeta potential employing a modified analytic approximation*. Journal of colloid and interface science, 2015. **450**: p. 288-300.
301. Pyell, U., et al., *Characterization of hydrophilic coated gold nanoparticles via capillary electrophoresis and Taylor dispersion analysis. Part II: Determination of the hydrodynamic radius distribution—Comparison with asymmetric flow field-flow fractionation*. Journal of colloid and interface science, 2015. **457**: p. 131-140.
302. Oukacine, F., et al., *Size-based characterization of nanoparticle mixtures by the inline coupling of capillary electrophoresis to Taylor dispersion analysis*. Journal of Chromatography A, 2015. **1426**: p. 220-225.
303. Oukacine, F., et al., *Inline Coupling of Electrokinetic Preconcentration Method to Taylor Dispersion Analysis for Size-Based Characterization of Low-UV-Absorbing Nanoparticles*. Analytical chemistry, 2018. **90**(4): p. 2493-2500.
304. Labied, L., et al., *Taylor Dispersion Analysis Coupled to Inductively Coupled Plasma-Mass Spectrometry for Ultrasmall Nanoparticle Size Measurement: From Drug Product to Biological Media Studies*. Analytical Chemistry, 2020. **93**(3): p. 1254-1259.

305. Kaminski, T.S., O. Scheler, and P. Garstecki, *Droplet microfluidics for microbiology: techniques, applications and challenges*. Lab on a Chip, 2016. **16**(12): p. 2168-2187.
306. Serra, M., et al., *The power of solid supports in multiphase and droplet-based microfluidics: towards clinical applications*. Lab Chip, 2017. DOI: **10.1039/C7LC00582B**.
307. Guo, M.T., et al., *Droplet microfluidics for high-throughput biological assays*. Lab on a Chip, 2012. **12**(12): p. 2146-2155.
308. Liu, C., et al., *Single-exosome-counting immunoassays for cancer diagnostics*. Nano letters, 2018. **18**(7): p. 4226-4232.
309. Ko, J., et al., *Sequencing-Based Protein Analysis of Single Extracellular Vesicles*. ACS Nano, 2021. **15**(3): p. 5631-5638.
310. Liénard-Mayor, T., et al., *Droplet-interfacing strategies in microscale electrophoresis for sample treatment, separation and quantification: A review*. Analytica Chimica Acta, 2020.
311. Mai, T.D., et al., *Single-step immunoassays and microfluidic droplet operation: Towards a versatile approach for detection of amyloid-beta peptide-based biomarkers of Alzheimer's disease*. Sens. Actuators B, 2018. **255**: p. 2126-2135.
312. Doufène, K., et al., *Microfluidic systems for droplet generation in aqueous continuous phases: A focus review*. Langmuir, 2019. **35**(39): p. 12597-12612.
313. Ali-Cherif, A., et al., *Programmable Magnetic Tweezers and Droplet Microfluidic Device for High-Throughput Nanoliter Multi-Step Assays*. Angew. Chem. Int. Ed., 2012. **51**(43): p. 10765-10769.
314. Lombardi, D. and P.S. Dittrich, *Droplet microfluidics with magnetic beads: a new tool to investigate drug-protein interactions*. Analytical and bioanalytical chemistry, 2011. **399**(1): p. 347-352.
315. Ferraro, D., et al., *Microfluidic platform combining droplets and magnetic tweezers: application to HER2 expression in cancer diagnosis*. Scientific reports, 2016. **6**(1): p. 1-11.
316. Wan, Y., et al., *Rapid magnetic isolation of extracellular vesicles via lipid-based nanoprobe*. Nature biomedical engineering, 2017. **1**(4): p. 1-11.
317. Kim, H. and S. Shin, *ExoCAS-2: Rapid and Pure Isolation of Exosomes by Anionic Exchange Using Magnetic Beads*. Biomedicines, 2021. **9**(1): p. 12.
318. Fang, X., et al., *A magnetic bead-mediated selective adsorption strategy for extracellular vesicle separation and purification*. Acta biomaterialia, 2021.

APPENDIX

Table A: Representative table showing a selection of completed and ongoing clinical trials with the term “exosome” (from <http://clinicaltrials.gov>, November 2021).

| NCT Number | Title | Status | Conditions | Interventions |
|-------------|--|------------------------|--|--|
| NCT05035134 | Application of Circulating Exosomes in Early Diagnosis and Prognosis Evaluation After Intracerebral Hemorrhage | Recruiting | •Intracerebral Hemorrhage#Circulating Exosomes | |
| NCT04894695 | Urine Exosomes to Identify Biomarkers for LN | Recruiting | •Lupus Nephritis | •Diagnostic Test: biomarkers detection in different groups |
| NCT04529915 | Multicenter Clinical Research for Early Diagnosis of Lung Cancer Using Blood Plasma Derived Exosome | Active, not recruiting | •Lung Cancer | •Diagnostic Test: Exosome sampling |
| NCT03800121 | Study of Exosomes in Monitoring Patients With Sarcoma (EXOSARC) | Recruiting | •Sarcoma | •Biological: Blood samples |
| NCT02702856 | Clinical Validation of a Urinary Exosome Gene Signature in Men Presenting for Suspicion of Prostate Cancer | Completed | •Prostate Cancer | •Other: ExoIntelliScore Prostate |
| NCT02393703 | Interrogation of Exosome-mediated Intercellular Signaling in Patients With Pancreatic Cancer | Recruiting | •Pancreatic Cancer •Benign Pancreatic Disease | |
| NCT04053855 | Evaluation of Urinary Exosomes Presence From Clear Cell Renal Cell Carcinoma | Recruiting | •Clear Cell Renal Cell Carcinoma | •Biological: Urinary sample |
| NCT03108677 | Circulating Exosome RNA in Lung Metastases of Primary High-Grade Osteosarcoma | Recruiting | •Lung Metastases •Osteosarcoma | •Other: Blood samples |
| NCT04154332 | Exosome Cargo From Preeclampsia Patients | Recruiting | •Preeclampsia | •Other: Sample collection |

| | | | | |
|-------------|---|------------|--|---|
| NCT03503461 | Major Activation Of NCC in Graft Urinary Exosomes | Completed | •Kidney Transplantation | •Other: exosomes analysis |
| NCT05058768 | Omics Sequencing of Exosomes in Body Fluids of Patients With Acute Lung Injury | Recruiting | •Acute Lung Injury | •Diagnostic Test: The lungs causes and extrapulmonary factors |
| NCT04499794 | The Study of Exosome EML4-ALK Fusion in NSCLC Clinical Diagnosis and Dynamic Monitoring | Recruiting | •Untreated Advanced NSCLC Patients •FISH Identified ALK Fusion Positive or Negative | •Drug: ALK inhibitor |
| NCT03032913 | Diagnostic Accuracy of Circulating Tumor Cells (CTCs) and Oncoexosome Quantification in the Diagnosis of Pancreatic Cancer - PANC-CTC | Completed | •Pancreatic Ductal Adenocarcinoma (PDAC) | •Procedure: Blood samples •Procedure: Portal vein blood sample |
| NCT03267160 | A Study of Exosome Proteomics and Hemodynamics in Sepsis | Completed | •Hemodynamic Instability •Autophagy | •Diagnostic Test: Hemodynamic parameters |
| NCT01860118 | LRRK2 and Other Novel Exosome Proteins in Parkinson's Disease | Completed | •Parkinson's Disease | |
| NCT03811600 | Exosomes Implication in PD1-PD-L1 Activation in OSAS | Recruiting | •Sleep Apnea Syndromes, Obstructive •Cancer | •Diagnostic Test: PD1/PD-L1 exosomal expression |
| NCT03895216 | Identification and Characterization of Predictive Factors of Onset of Bone Metastases in Cancer Patients | Recruiting | •Bone Metastases | |
| NCT02147418 | Exosome Testing as a Screening Modality for Human Papillomavirus-Positive Oropharyngeal Squamous Cell Carcinoma | Recruiting | •Oropharyngeal Cancer | |
| NCT04394572 | Identification of New Diagnostic Protein Markers for Colorectal Cancer | Recruiting | •Colorectal Cancer | •Biological: Blood sample |
| NCT03562715 | microRNAs Role in Pre-eclampsia Diagnosis | Completed | •Preeclampsia | |
| NCT03222986 | Sepsis-damaged Organs-double-markers Identification of Organ Failure Using Fluorescent Nanoparticle Tracking Analysis | Completed | •Sepsis With Multiple Organ Dysfunction (MOD) | |
| NCT03874559 | Exosomes in Rectal Cancer | Recruiting | •Rectal Cancer | •Diagnostic Test: Blood Draw |

| | | | | |
|-------------|--|------------------------|--|--|
| NCT04979767 | Function of Circulating Exosomes in Sepsis-induced Immunosuppression | Recruiting | <ul style="list-style-type: none"> •Sepsis •Septic Shock •Sepsis Syndrome •Sepsis Bacterial •Sepsis, Severe •Sepsis Bacteremia | |
| NCT04288141 | A Study to Measure the Expression of the HER2-HER3 Dimer in Tumour and Blood (Exosomes) Samples From Patients With HER2 Positive Breast Cancer Receiving HER2 Targeted Therapies | Recruiting | •HER2-positive Breast Cancer | •Other: Acquisition of blood samples and tumour tissue samples (biopsies) |
| NCT03236688 | Detection of ARv7 in the Plasma of Men With Advanced Metastatic Castrate Resistant Prostate Cancer (MCRP) | Active, not recruiting | •Metastatic Castrate Resistant Prostate Cancer | |
| NCT04155359 | Clinical Evaluation of the miR Sentinel BCa™ Test to Diagnose Bladder Cancer in Hematuria Patients | Recruiting | •Bladder Cancer | |
| NCT04523389 | Contents of Circulating Extracellular Vesicles: Biomarkers in Colorectal Cancer Patients | Recruiting | •Colorectal Cancer | <ul style="list-style-type: none"> •Biological: analysis (protein, lipid, RNA ...) of circulating exosomes, size and number •Other: Gathering additional information about the patient's cancer •Diagnostic Test: Diagnostic test |
| NCT04167722 | How Does Prostate Cancer Metastasize? Studying the Role of Secreted Packages (Exosomes) From Fat Tissue in Lean and Obese Patients | Recruiting | <ul style="list-style-type: none"> •Prostate Cancer •Obesity | •Procedure: Robotic Radical Prostatectomy |
| NCT04629079 | Improving the Early Detection of Lung Cancer by Combining Exosomal Analysis of Hypoxia With Standard of Care Imaging | Recruiting | •Lung Cancer | |

| | | | | |
|-------------|--|------------------------|---|---|
| NCT04720599 | Clinical Evaluation of ExoDx Prostate(IntelliScore) in Men Presenting for Initial Prostate Biopsy | Completed | •Urologic Cancer | •Diagnostic Test: ExoDx Prostate(IntelliScore) |
| NCT03236675 | Detection of Either the EML4-ALK Gene Rearrangements or the T790M EGFR Mutation in the Plasma of Advanced NSCLC Patients | Active, not recruiting | •Carcinoma, Non-Small-Cell Lung | |
| NCT04315753 | Circulating and Imaging Biomarkers to Improve Lung Cancer Management and Early Detection | Recruiting | •Lung Cancer | •Other: LDCT (Low Dose CT) |
| NCT04357717 | ExoDx Prostate Evaluation in Prior Negative Prostate Biopsy Setting | Recruiting | •Prostate Cancer | •Diagnostic Test: ExoDx Prostate |
| NCT04227886 | Study on Predictive Biomarkers of Neoadjuvant Chemoradiotherapy for Rectal Cancer | Recruiting | •Rectal Neoplasm Malignant Carcinoma •Chemoradiotherapy •Neoadjuvant Therapy •Predictive Biomarkers •Adenocarcinoma | •Radiation: Radiation •Drug: Capecitabine-Irinotecan Combination |
| NCT04120272 | Discovery for Biomarkers and Risk Factors for Postoperative Delirium in Elderly Patients With Spine Surgery | Recruiting | •Spinal Disease | •Procedure: Spine surgery |
| NCT03488134 | Predicting Prognosis and Recurrence of Thyroid Cancer Via New Biomarkers, Urinary Exosomal Thyroglobulin and Galectin-3 | Active, not recruiting | •Thyroid Cancer | |
| NCT04164966 | Development of Novel Biomarkers for the Early Diagnosis of Type 1 Diabetes | Recruiting | •Type 1 Diabetes | |
| NCT02226055 | An Investigation Into the Cardiovascular Risk and Aetiology of CKDu in Sri Lanka | Completed | •CKDu •Arterial Stiffness •Proteinuria •Serum Creatinine •Urinary Biomarkers •DNA Adducts | •Device: Arterial Stiffness Assessment |

| | | | | |
|-------------|--|------------|--|---|
| NCT04100811 | Identification of Clinically Insignificant or Significant Prostate Cancer With the miR Scientific Sentinel™ Platform | Recruiting | •Prostate Cancer | |
| NCT03694483 | Prostasomes as Diagnostic Tool for Prostate Cancer Detection | Recruiting | •Prostate Cancer | •Diagnostic Test: Genetic analysis for the detection of prostasomes |
| NCT04323579 | Validation of Multiparametric Models and Circulating and Imaging Biomarkers to Improve Lung Cancer EARLY Detection. | Recruiting | •Lung Cancer | |
| NCT03031418 | Clinical Evaluation of the 'ExoDx Prostate IntelliScore' (EPI) | Completed | •Cancer of Prostate | •Diagnostic Test: ExoDx Prostate Intelliscore |
| NCT04661176 | Evaluation of the Sentinel™ PCC4 Assay for Diagnosis, Prognosis and Monitoring of Prostate Cancer in Puerto Rico | Recruiting | •Prostate Cancer | •Diagnostic Test: miR Sentinel™ PCC4 Assay |
| NCT04924504 | Mechanisms Behind Severe Insulin Resistance During Pregnancy in Women With Glucose Metabolic Disorders (SIR-MET) | Recruiting | •Diabetes Mellitus, Type 2 •Gestational Diabetes •Overweight and Obesity •Pregnancy in Diabetic •Insulin Resistance •Insulin Sensitivity •Pregnancy, High Risk | •Other: No interventions |
| NCT03432806 | A Study of Imaging, Blood, and Tissue Samples to Guide Treatment of Colon Cancer and Related Liver Tumors | Recruiting | •Colon Cancer •Liver Tumors | •Other: blood draws •Procedure: colectomy or hepatectomy •Diagnostic Test: Fibroscan test |
| NCT03034265 | New Biomarkers and Difficult-to-treat Hypertension | Completed | •Hypertension | |
| NCT00331331 | The Vitreous Proteome and Inflammatory Mediators in Ocular Inflammatory Disease | Completed | •Uveitis •Vasculitis •Ocular Inflammatory Disease | |

| | | | | |
|-------------|--|------------|--|---|
| NCT03415984 | Prevalence of Age Related Macular Degeneration (ARMD) in Parkinson's Patients and Assesment of the Role of L-DOPA | Completed | <ul style="list-style-type: none"> •Parkinson Disease •Age Related Macular Degeneration | <ul style="list-style-type: none"> •Diagnostic Test: Color retinography •Diagnostic Test: Optical coherence tomography •Diagnostic Test: Fundus autofluorescence imaging |
| NCT03911999 | Exosomal microRNA in Predicting the Aggressiveness of Prostate Cancer in Chinese Patients | Completed | <ul style="list-style-type: none"> •Prostate Cancer | |
| NCT04617405 | Hormonal and Inflammatory Changes During Pregnancy in Women With Glucose Metabolic Disorders. | Recruiting | <ul style="list-style-type: none"> •Diabetes Mellitus, Type 2 •Gestational Diabetes •Overweight and Obesity •Pregnancy in Diabetic •Insulin Resistance •Insulin Sensitivity •Pregnancy, High Risk | <ul style="list-style-type: none"> •Other: No interventions |
| NCT04928534 | Cohort Study of Blood Biomarkers for TES | Recruiting | <ul style="list-style-type: none"> •Chronic Traumatic Encephalopathy •Traumatic Encephalopathy, Chronic •Traumatic; Encephalopathy, Postcontusional | <ul style="list-style-type: none"> •Diagnostic Test: Blood tests, Cognitive function tests, head MRI (plain scan and DTI sequence) examination and head PET (FDG-PET, Tau-PET and Amyloid-PET) examination |
| NCT03280576 | Validation of Progranulin as a Biomarker for Sepsis | Completed | <ul style="list-style-type: none"> •Sepsis | |
| NCT04534647 | Serological and Urinary Biomarkers in Latin American Patients With Systemic Lupus Erythematosus: GLADEL 2.0 Cohort | Recruiting | <ul style="list-style-type: none"> •Lupus Nephritis | <ul style="list-style-type: none"> •Diagnostic Test: different serum and urine biomarkers |
| NCT03870542 | Multicenter, Prospective Study for Urinary Exosomal Biomarkers of Kidney Allograft Tubulointerstitial Fibrosis | Recruiting | <ul style="list-style-type: none"> •Renal Fibrosis •Kidney Transplant Failure | <ul style="list-style-type: none"> •Procedure: kidney transplantation |

| | | | | |
|-------------|--|------------------------|--|---|
| NCT02862470 | Anaplastic Thyroid Cancer and Follicular Thyroid Cancer-derived Exosomal Analysis Via Treatment of Lovastatin and Vildagliptin and Pilot Prognostic Study Via Urine Exosomal Biological Markers in Thyroid Cancer Patients | Completed | •Thyroid Cancer | |
| NCT03791073 | New Biomarkers in Pancreatic Cancer Using EXPEL Concept | Active, not recruiting | •Oncology | |
| NCT02063464 | Blood Collection From People With Ovarian Cancer | Completed | •Ovarian Cancer •Cancer of the Ovary •Ovarian Neoplasms | |
| NCT03317080 | Dynamic Monitoring Circulating Tumor DNA in Surgical Patients With Lung Cancer | Active, not recruiting | •Lung Cancer | |
| NCT03049202 | BRONchoalveolar Investigations of Never-smokers With Chronic Obstruction From the Swedish CardioPulmonary bioImage Study | Recruiting | •Chronic Obstructive Pulmonary Disease •Emphysema •Chronic Bronchitis •Airway Obstruction •Smoking, Tobacco •Gender | |
| NCT03984006 | Early Detection of Autoimmune Thyroid Heart Disease Via Urinary Exosomal Proteins | Completed | •Thyroid Diseases •Heart Failure | |
| NCT03971955 | Characterlzation of Adult Onset Autoimmune Diabetes | Recruiting | •Diabetes | •Other: Mixed Meal Test •Other: Dual Energy X-Ray Absorptiometry (DEXA) •Procedure: Adipose Tissue Biopsy |

| | | | | |
|-------------|--|------------|--|--|
| NCT03995836 | Epigenetics Modifications in Morbid Obesity and Obstructive Sleep Apnea Patients: The EPIMOOSA Study | Completed | <ul style="list-style-type: none"> •Obstructive Sleep Apnea •Morbid Obesity •Epigenetic Disorder | <ul style="list-style-type: none"> •Device: CPAP •Procedure: Bariatric Surgery |
| NCT03941210 | Micro RNA as Prediction and/or Prognostic Markers of IRIS in TB-HIV Coinfected Patients | Recruiting | <ul style="list-style-type: none"> •HIV Infection •Tuberculosis Infection | <ul style="list-style-type: none"> •Other: Detection of molecular Biomarkers |
| NCT04921774 | Research on Patients With Heart Transplantation | Recruiting | <ul style="list-style-type: none"> •Heart Transplant Rejection | |
| NCT03250078 | A Pancreatic Cancer Screening Study in Hereditary High Risk Individuals | Recruiting | <ul style="list-style-type: none"> •Pancreatic Neoplasms | <ul style="list-style-type: none"> •Diagnostic Test: MRI/MRCP |
| NCT03334708 | A Study of Blood Based Biomarkers for Pancreas Adenocarcinoma | Recruiting | <ul style="list-style-type: none"> •Pancreatic Cancer •Pancreatic Diseases •Pancreatitis •Pancreatic Cyst | <ul style="list-style-type: none"> •Diagnostic Test: Blood Draw •Diagnostic Test: Tumor Tissue Collection •Diagnostic Test: Cyst Fluid |
| NCT04183530 | The Individualized Accurate Diagnosis and Treatment of Chronic Objective Pulmonary Disease(COPD) Patients Based on Multidimensional Data | Recruiting | <ul style="list-style-type: none"> •COPD •Acute Exacerbation of Chronic Obstructive Pulmonary Disease | |
| NCT04948437 | Urinary Exosomal Biomarkers of Thyroglobulin and Galectin-3 for Prognosis and Follow-up in Patients of Thyroid Cancer | Recruiting | <ul style="list-style-type: none"> •Thyroid Cancer •Papillary Thyroid Cancer •Follicular Thyroid Cancer | |
| NCT03944603 | Longitudinal Innate Immunity and Aging Study | Recruiting | <ul style="list-style-type: none"> •Healthy Older Adults Ages 60-89 | |
| NCT05004090 | Emotional Regulation in Children With ND: the Role of Genomic Variation, Proteomic Patterns, and Early Experience | Recruiting | <ul style="list-style-type: none"> •Neurodevelopmental Disabilities •Emotional Regulation •Epigenetics •Parental Factors | <ul style="list-style-type: none"> •Diagnostic Test: DNA methylation analysis •Diagnostic Test: Proteomics analysis •Diagnostic Test: Still Face Paradigm |

| | | | | |
|-------------|--|------------------------|---|---|
| NCT02890147 | Molecular Reclassification to Find Clinically Useful Biomarkers for Systemic Autoimmune Diseases: Case-control | Completed | •Healthy Subjects | |
| NCT02890134 | Molecular Reclassification to Find Clinically Useful Biomarkers for Systemic Autoimmune Diseases: Inception Cohort | Completed | •Systemic Autoimmune Diseases | |
| NCT02890121 | Molecular Reclassification to Find Clinically Useful Biomarkers for Systemic Autoimmune Diseases: | Completed | •Systemic Autoimmune Diseases | |
| NCT03275363 | The University of Hong Kong Neurocognitive Disorder Cohort | Recruiting | <ul style="list-style-type: none"> •Neurocognitive Disorder •Mild Cognitive Impairment •Alzheimer Dementia •Vascular Dementia •Age-related Cognitive Decline | <ul style="list-style-type: none"> •Diagnostic Test: Neurocognitive battery •Diagnostic Test: MRI •Biological: Blood tests •Diagnostic Test: EEG with event-related potential (ERP) •Diagnostic Test: Amyloid PET CT |
| NCT00578240 | Molecular Studies and Clinical Correlations in Human Prostatic Disease | Active, not recruiting | •Prostate Cancer | |

U.S. National Library of Medicine | U.S. National Institutes of Health | U.S. Department of Health & Human Services

Table B: Representative table showing a selection of completed and ongoing clinical trials with the term “extracellular vesicle” (from <http://clinicaltrials.gov>, November 2021).

| NCT Number | Title | Status | Conditions | Interventions |
|-------------|--|------------|---|--|
| NCT04653610 | Sequential Analysis Before and After Treatment Initiation to Unravel the Role of Naturally Occurring Extracellular Vesicles in HIV Infection | Recruiting | •Hiv | |
| NCT04523389 | Contents of Circulating Extracellular Vesicles: Biomarkers in Colorectal Cancer Patients | Recruiting | •Colorectal Cancer | <ul style="list-style-type: none"> •Biological: analysis (protein, lipid, RNA ...) of circulating exosomes, size and number •Other: Gathering additional information about the patient's cancer •Diagnostic Test: Diagnostic test |
| NCT04603326 | FoxBioNet: ECV (Extracellular Vesicle) 004 | Recruiting | •Parkinson Disease | •Procedure: Lumbar Puncture |
| NCT04742608 | Development of Liquid Biopsy Technologies for Noninvasive Cancer Diagnostics in Patients With Suspicious Thyroid Nodules or Thyroid Cancer | Recruiting | <ul style="list-style-type: none"> •Thyroid Gland Carcinoma •Thyroid Gland Nodule | <ul style="list-style-type: none"> •Procedure: Biospecimen Collection •Other: Electronic Health Record Review |
| NCT03381482 | Ectosomes, New Biomarkers of Tau Pathology? | Recruiting | •Alzheimer Disease | <ul style="list-style-type: none"> •Diagnostic Test: CSF drawing during spinal anaesthesia •Diagnostic Test: Fasting blood sample •Diagnostic Test: Lumbar puncture |
| NCT03775447 | Fox BioNet Project: ECV-003 | Completed | •Parkinson Disease | •Procedure: Lumbar Puncture |
| NCT04913545 | The Sensitivity and Specificity of Using Salivary miRNAs in Detection of Malignant Transformation of Oral Lesions. | Completed | •Oral Premalignant Lesions | •Diagnostic Test: using salivary miRNA (412,512) |
| NCT04578223 | Platelet Reactivity and Treatment With Prostacyclin Analogues in Pulmonary Arterial Hypertension | Completed | •Pulmonary Hypertension | |

| | | | | |
|-------------|--|------------------------|---|--|
| NCT04164134 | New Strategies to Detect Cancers in Carriers of Mutations in RB1 | Recruiting | <ul style="list-style-type: none"> •Retinoblastoma •Secondary Primary Malignancies After Retinoblastoma | •Other: blood draw |
| NCT03957252 | Validation of ClarityDX Prostate as a Reflex Test to Refine the Prediction of Clinically-significant Prostate Cancer | Recruiting | •Prostate Cancer | •Diagnostic Test: Blood test: ClarityDX Prostate |
| NCT04633109 | The Obese Taste Bud Study | Recruiting | •Obesity | <ul style="list-style-type: none"> •Procedure: taste bud biopsy •Diagnostic Test: oral glucose tolerance test •Diagnostic Test: Taste sensitivity •Diagnostic Test: olfactory function •Diagnostic Test: taste bud density •Diagnostic Test: anthropometry •Other: biospecimen collection •Other: questionnaires |
| NCT04349189 | Venous Thrombosis Biomarkers in Sickle Cell Disease and Sickle Cell Trait | Recruiting | <ul style="list-style-type: none"> •Sickle Cell Disease •Venous Thrombosis •Sickle Cell Trait •Hypercoagulable State •Venous Thromboembolism | |
| NCT04792983 | Cognition and the Immunology of Postoperative Outcomes | Recruiting | <ul style="list-style-type: none"> •Cognitive Impairment •Frail Elderly Syndrome •Delirium •Surgery | •Other: No intervention |
| NCT04529915 | Multicenter Clinical Research for Early Diagnosis of Lung Cancer Using Blood Plasma Derived Exosome | Active, not recruiting | •Lung Cancer | •Diagnostic Test: Exosome sampling |

| | | | | |
|-------------|--|------------|--|---------------------------|
| NCT04624997 | Coagulopathy and Vasculopathy Assessment as a Predictor of the Severity of SARS-CoV-2 / COVID-19 Infection | Recruiting | <ul style="list-style-type: none"> •COVID-19 •SARS-CoV-2 Infection | •Other: biological sample |
| NCT04993378 | Prospectively Predict the Efficacy of Treatment of Gastrointestinal Tumors Based on Peripheral Multi-omics Liquid Biopsy | Recruiting | <ul style="list-style-type: none"> •Advanced Gastric Adenocarcinoma •Immunotherapy | •Device: EV-array |
| NCT04892433 | Tissue Study in Patients Undergoing CAR-T Cell Therapy (CAR_21_01) | Recruiting | •CAR-T Therapy Complications | |
| NCT03944603 | Longitudinal Innate Immunity and Aging Study | Recruiting | •Healthy Older Adults Ages 60-89 | |
| NCT04305665 | HIV Study on MEasuring the Reservoir on Cellular Level to CUre Infection | Recruiting | •Hiv | |
| NCT03689257 | Study to Evaluate the Epidemiology and the Characteristics "Omics" in Patients Recently Diagnosed of Inflammatory Bowel Disease in Spain | Completed | •Inflammatory Bowel Diseases | |

U.S. National Library of Medicine | U.S. National Institutes of Health | U.S. Department of Health & Human Services

